Dehydrogenation of Isobutane using a Structured Adsorptive Reactor

by

Manal Ismail

August 2005

A thesis submitted for the degree of Doctor of Philosophy of the University of London and for the Diploma of Membership of the Imperial College

Department of Chemical Engineering and Chemical Technology,
Imperial College London, Prince Consort Road,
London SW7 2AZ, United Kingdom

This thesis is dedicated to my beloved parents, Ayahanda Tengku Ismail Tengku Sham and Bonda Madam Fadia Mohamed El-Sayed El-Khadragy. Their endless support, love, sacrifice and prayers have helped me immensely throughout my PhD course. May God Almighty bless them to the eternity.

Abstract

The advancement of adsorption technology has enabled the development of various types of adsorptive reactors, which incorporate periodic adsorption and regeneration steps for in-situ gas separation. When compared to conventional reactors, such reactors offer process intensification and, for equilibrium limited reactions, considerable improvement in conversion.

In this thesis, studies of the synergetic coupling of reaction and adsorption were conducted in a novel annular-type structured adsorptive reactor, SAR. The impetus for the work was to investigate the potential of employing a structured packing arrangement of adsorbent and catalyst, which could provide a low-pressure drop alternative to conventional packed bed arrangements. The system consisted of a central gas channel, surrounded by an annulus of admixed catalyst and adsorbent. This arrangement could be viewed as a hybrid between monolith-type and parallel-passage type structures. The reactor was operated with laminar flow in the central gas channel; reactant contact with admixed particles was achieved through diffusive transport in the direction perpendicular to convective gas flow. Thus, issues of channel size, gas space-time, diffusion, and adsorption reaction rates were central to the successful design of the reactor.

The work involved theoretical and experimental studies of the structured adsorptive reactor for the catalytic dehydrogenation of isobutane over an admixture of platinum-alumina catalyst and zeolite-KY adsorbent. A two-dimensional mathematical model was developed to help evaluate the benefits and limitations of such a design configuration. In evaluating the performance of annular-type reactor, studies on equivalent packed bed arrangement (PFR) were also carried out. Measured adsorbate (isobutene) and reactant breakthrough profiles were used to validate the mathematical model. Some key parameters such as adsorption equilibrium constants, isosteric heat of adsorption of adsorbed components, reaction rate constants as well as reaction activation energy were also obtained from experimental measurements.

Optimisation studies were also carried out for a range of key design parameters. This included the reactor temperature and the geometrical dimensions of the annular-type reactor. Overall, the SAR was found to lead to enhanced conversion relative to an equivalent PFR over a specified temperature range. However, the enhancement diminished as space time was reduced. In all cases, there was a significant reduction in pressure drop through the use of an SAR arrangement.

Acknowledgements

First, I would like to thank Universiti Kebangsaan Malaysia (UKM) for providing me with the financial support and funding providing the opportunity to pursue my PhD studies at Imperial College London. I am also grateful to my colleagues at the Department of Chemical Engineering and Process as well as the Dean of the Faculty of Engineering at UKM for their continuous support and motivation throughout my research.

I would like to express my deepest gratitude to my dear supervisor, Dr. Esat Alpay for his intellectual guidance and invaluable advice, as well as for the immeasurable help and support throughout my research endeavours. On a personal level, his unorthodox way of supervision has toughened me up, which leads to the mental reformation and paradigm shift. Nevertheless, his enthusiasm and determination in educating me in the many aspects of reaction engineering is undeniably inspiring.

I have been fortunate enough to meet so many helpful and friendly academic and non-academic staff in this department. Among those, I wish to thank are: Darren Palmer for his technical assistance, Prof. David Stuckey for believing in me, Sarah Everall, Jacque and Marie for their kind friendship, Jenny Huang for her assistance in our department library, Nam Ly and Gary Muhammad for their computer support and maintenance, Anna Dowden for sharing with me the gossips in the senior common room, Keith Walker and Peter Poggioli of the chemical engineering store for their friendly assistance and also the workshop team for their technical support.

I must also thank those people who have personally contributed to my well-being and sanity throughout the research: Abi Kolade who has been a confidante and a wonderful friend indeed, Vangelis and George for sticking with me through thick and thin, Siti Aslina, Suraya, Hekarl, Mikal and Zamri for the joyful memories, Natasha and Ming Fang for their encouragement during my writing-up period, Muhammad Dastgir, Michael Bajomo and the officemates at the rooms 518 and 517 for their sense of camaraderie, and to Azizah, Hasmawaty, Waheedah, Hanis and Rajesh who have been great neighbours at Du Cane Road. Their individual friendship is deeply appreciated.

I would also like to acknowledge Chong Kwang Hua for helping me set up the GC and Aamer Hussain for his comments on my technical writing skills. Many thanks to many of my department mates in general for making my stay in the college a truly memorable one.

Special dedication goes to my family: Baba, Mama, Amirah & Isa, Dr.Nahlah & Shahiran, Naglaa-Azam, Shuaib-Farah, Shihab, Hakeem, Sumaiyah and Samihah for their love, encouragement, utmost devotion, sacrifice and prayers. They have been my key motivation and inspiration throughout my studies and I am deeply indebted to them for their positive influence.

Last but never the least, I wish to express my humble gratitude to Arif for his loving companion and to those who have helped me indirectly towards achieving my pure ambition.

Table of Contents

Abstract i

Acknowledgements ii

Table of Contents iii

List of Figures ix

List of Tables xiii

Notations xvi

1 INTRODUCTION 1

2 BACKGROUND AND LITERATURE SURVEY 5

2.1 Introduction 5

2.2 Adsorption phenomena 6

2.2.1 Adsorbents 6

2.3 Periodic adsorption processes 8

2.3.1 Pressure swing adsorption 9

2.3.2 Thermal swing adsorption 15

2.4 Combined reaction-separation processes 16

2.4.1 Process review 17

2.4.2 Periodic adsorptive reactors 18

2.5 Structured packing reactors 26

2.5.1 PPR and monolith reactors overview 27

2.5.2 Structured adsorber packing 30

2.6 Annular packing reactors 31

2.6.1 Annular catalyst packing reactors 32

2.6.2 Annular packed bed adsorber 32

2.7 Research objective: Annular-type SAR overview 35

2.8 Concluding remarks 37

3 THEORETICAL BACKGROUND AND MODELLING 38

3.1 Introduction 38

3.2 Background theory 39

3.2.1 PPR underlying mass transfer theory 40

3.2.2 Isobutane dehydrogenation kinetic mechanism 42

3.3 SAR mathematical modelling 45

3.3.1 Model assumptions 45

3.3.2 Governing equations 46

3.3.3 Boundary conditions of the SAR model 56

3.4 PFR model 59

3.4.1 PFR boundary conditions 60

3.5 Performance indices 62

3.5.1 Reaction conversion 62

3.5.2 Conversion enhancement factor 64

3.5.3 Energy input 65

3.6 Concluding remarks 65

4 EXPERIMENTAL APPARATUS 66

4.1 Introduction 66

4.2 Ancillary lines 67

4.3 Reactor unit and configuration 70

4.3.1 PFR 70

4.3.2 SAR 70

4.4 Gas chromatography unit 74

4.5 Standard experimental procedures 76

4.5.1 Gas leak testing 76

4.5.2 Solid drying 77

4.5.3 Catalyst activation 77

4.5.4 GC Column conditioning 77

4.6 Concluding remarks 78

5 REACTION AND ADSORPTION KINETIC MEASUREMENTS 79

5.1 Introduction 79

5.2 Reaction kinetics determination 80

5.2.1 Pt-Al_2O_3 catalyst overview 81

5.2.2 Dehydrogenation of isobutane 82

5.2.3 Determination of reaction rate constants 84

5.2.4 PFR and SAR experiments 88

5.3 Adsorption kinetic determination 93

5.3.1 Synthetic zeolite KY overview 93

5.3.2 Adsorption equilibria parameters 95

5.3.3 Adsorption isotherms experiments 97

5.3.4 Chromatographic curves analysis 99

5.3.5 Mass transfer coefficient estimation 113

5.3.6 Diffusion coefficients 115

5.4 Error analysis 115

5.5 Concluding remarks 119

6 STRUCTURED ADSORPTIVE REACTOR INVESTIGATIONS 120

6.1 Introduction 120

6.2 SAR overview 121

6.3 Single-step process experimental study 124

6.3.1 PFR admixture experiments 124

6.3.2 SAR admixture experiments 131

6.4 Cyclic SAR studies 137

6.5 Concluding remarks 140

7 SAR THEORETICAL ANALYSIS 142

7.1 Introduction 142

7.2 Simulation strategy 143

7.2.1 Key variables and parameters 144

7.2.2 Spatial domain normalisation 150

7.2.3 Numerical method approach 151

7.3 Simulation results and discussions 152

7.3.1 SAR adsorption performance 153

7.3.2 Conversion enhancement effect 161

7.3.3 Cyclic process 167

7.4 Concluding remarks 174

8 CONCLUSIONS AND RECOMMENDATIONS FOR FUTURE WORK 177

8.1 Summary and conclusions of this work 178

8.2 Directions for future work 184

REFERENCES 186

APPENDICES

A GOVERNING DIFFUSION COEFFICIENTS 195

A.1 Molecular diffusion coefficient 195

A.2 Axial diffusion coefficient 197

B MASS TRANSFER COEFFICIENT FROM LDF APPROXIMATION 199

B.1 Effective intraparticle diffusion coefficient 199

B.2 Macropore diffusion 200

C GAS CHROMATOGRAPHY CALIBRATION 203

C.1 Gas Chromatography calibration results 203

D EXAMPLE OF CYCLIC STEADY STATE SAR MODEL 205

E EXAMPLE OF A SINGLE STEP SAR MODEL 216

F EXAMPLE OF A SINGLE STEP PFR MODEL 224

List of Figures

Fig. 2.1	Schematic diagram of an array of slabs of a PPR	27
Fig. 2.2	A typical monolith structure	28
Fig. 2.3	The novel annular-type SAR; AF = Axial Flow; RF = Radial Flow	36
Fig. 3.1	The six consecutive mass transfer steps in PPR	41
Fig. 3.2	Elementary diagram of a section of SAR for mathematical modelling purpose	47
Fig. 4.1	A schematic diagram of the experimental rig. NR= no-return valve; V1, V2 = 2-way valve; V3 = 3-way valve; V4 = one-way valve; MF1, MF2 = mass flow meter; PG = Pressure gauge; MA = Moisture Absorber; OS = Oxygen Scrubber; FC = Fume Cupboard	69
Fig. 4.2	The sintered tube	71
Fig. 4.3	The cross-sectional view of the sintered tube	71
Fig. 4.4	Schematic mechanical drawing of SAR	72
Fig. 4.5	Top and bottom view of Flange 1a, 1b and Flange 2	73
Fig. 5.1	Reaction rate constants plot at three temperatures	86
Fig. 5.2	Activation energy plot	87
Fig. 5.3	Catalytic isobutane dehydrogenation reaction for PFR and SAR	90
Fig. 5.4	Inert-only experiments for PFR and SAR conducted at minimum flow rate of each type of reactor, i.e. 0.050 l min^{-1} for PFR and 0.10 l min^{-1} for SAR.	100
Fig. 5.5	Isosteric heat of adsorption	103
Fig. 5.6	PFR breakthrough profile at T=600K for isobutane	104
Fig. 5.7	PFR breakthrough profile at T=650K for isobutane	105
Fig. 5.8	PFR breakthrough profile at T=700K for isobutane	105

Fig. 5.9	PFR breakthrough profile at T=600K for isobutene	106
Fig. 5.10	PFR breakthrough profile at T=650K for isobutene	106
Fig. 5.11	PFR breakthrough profile at T=700K for isobutene	107
Fig. 5.12	SAR breakthrough profile at T=600K for isobutane; flow rate = 0.10 l min^{-1}; sim = simulation	110
Fig. 5.13	SAR breakthrough profile at T=650K for isobutane; flow rate = 0.10 l min^{-1}; sim = simulation	111
Fig. 5.14	SAR breakthrough profile at T=700K for isobutane; flow rate = 0.10 l min^{-1}; sim = simulation	111
Fig. 5.15	SAR breakthrough profile for isobutene; flow rate = 0.10 l min^{-1}; sim = simulation	112
Fig. 6.1	PFR transient kinetic and adsorption response curves at T = 600K, flow rate = 0.050 l min^{-1}; admix= admixture; ads= adsorbent; sim = simulation; cat = catalyst	127
Fig. 6.2	PFR transient kinetic and adsorption response curves at T = 650K, flow rate = 0.050 l min^{-1}; admix= admixture; ads= adsorbent; sim = simulation; cat = catalyst	127
Fig. 6.3	PFR transient kinetic and adsorption response curves at T=700K, flow rate = 0.050 l min^{-1}; admix= admixture; ads= adsorbent; sim = simulation; cat = catalyst	127
Fig. 6.4	PFR conversion enhancement effect profile for three temperatures at constant flow rate = 0.050 l min^{-1}; sim = simulation	128
Fig. 6.5	PFR admixture breakthrough profiles at T=600K; sim = simulation	129
Fig. 6.6	PFR admixture breakthrough profiles at T=650K; sim = simulation	130
Fig. 6.7	PFR admixture breakthrough profiles at T=700K; sim = simulation	130
Fig. 6.8	The top cross-sectional view of the SAR reactor. R1 and R2 represent the radius of central gas channel and total SAR reactor radius respectively	131
Fig. 6.9	Breakthrough profile of SAR with or without the admixture of catalyst at T=600K, flow rate = 0.10 l min^{-1} . Pt and KY represents platinum-alumina catalyst and zeolite KY respectively; expt = experiment ; sim = simulation	134
Fig. 6.10	Breakthrough profile of SAR with or without the admixture of catalyst at T=650K, flow rate = 0.10 l min^{-1}. Pt and KY represent platinum-alumina catalyst and zeolite KY respectively; expt = experiment ; sim = simulation	135

Fig. 6.11	Breakthrough profile of SAR with or without the admixture of catalyst at T=700K, flow rate = 0.10 l min^{-1}. Pt and KY represent platinum-alumina catalyst and zeolite KY respectively; expt = experiment ; sim = simulation	135
Fig. 6.12	SAR adsorption enhancement effect at three different temperatures and constant flow rate of 0.10 l min^{-1}; sim = simulation	136
Fig. 6.13	Adsorption and desorption profile of SAR admixture process at T=600K and flow rate= 0.10 l min^{-1}; sim = simulation	138
Fig. 6.14	Adsorption and desorption profile of SAR admixture process at T=650 and flow rate= 0.10 l min^{-1}; sim = simulation	139
Fig. 6.15	Adsorption and desorption profile of SAR admixture process at T=700K and flow rate= 0.10 l min^{-1}; sim = simulation	139
Fig. 7.1	Isobutane adsorption breakthrough profile at T=600K, flow rate= 0.10 l min^{-1}, v= 0.067 ms^{-1}	155
Fig. 7.2	Isobutane adsorption breakthrough profile at T=650K, flow rate= 0.10 l min^{-1}, v= 0.072 ms^{-1}	155
Fig. 7.3	Isobutane adsorption breakthrough profile at T=700K, flow rate= 0.10 l min^{-1}, v= 0.078 ms^{-1}	156
Fig. 7.4	SAR isobutane adsorption breakthrough profiles at 4 different flow rates, T=600K	158
Fig. 7.5	SAR isobutane adsorption breakthrough profiles at 4 different flow rates, T=650K	158
Fig. 7.6	SAR isobutane adsorption breakthrough profiles at 4 different flow rates, T=700K	159
Fig. 7.7	Estimated pressure drop across the gas channel of SAR at increasing feed flow rates	160
Fig. 7.8	Estimated pressure drop across PFR bed at increasing feed flow rates	160
Fig. 7.9	Adsorption enhancement effect at three different temperatures; flow rate= 0.10 l min^{-1}	160
Fig. 7.10	Flow rate effect on adsorption enhancement; T=600K	163
Fig. 7.11	SAR axial effect on adsorption enhancement; T=600K, flow rate= 0.10 l min^{-1}, R1 and R2 are 0.004 m and 0.014 m respectively	165
Fig. 7.12	SAR annular thickness effect on adsorption enhancement; T=600K, flow rate= 0.10 l min^{-1}, reactor length, L= 0.14 m, d denotes δ, the annular thickness	165

Fig. 7.13	SAR isobutane dynamic cyclic process for adsorption only and combined reaction-separation process at T= 600K, flow rate= 0.10 l min^{-1}. Adsorption cycle time= 2000s; desorption cycle time=1500s; ads = adsorbent ; admix = admixture	169
Fig. 7.14	PFR isobutane dynamic cyclic process for adsorption only and combined reaction-separation process at T= 600K, flow rate= 0.10 l min^{-1}. Adsorption cycle time= 100s; desorption cycle time=100s; ads = adsorbent ; admix = admixture	170
Fig. 7.15	SAR isobutane dynamic cyclic process for adsorption only and combined reaction-separation process at T= 650K, flow rate= 0.10 l min^{-1}. Adsorption cycle time= 1200s; desorption cycle time=900s; ads = adsorbent ; admix = admixture	170
Fig. 7.16	PFR isobutane dynamic cyclic process for adsorption only and combined reaction-separation process at T= 650K, flow rate= 0.10 l min^{-1}. Adsorption cycle time= 60s; desorption cycle time=60s; ads = adsorbent ; admix = admixture	171
Fig. 7.17	SAR isobutane dynamic cyclic process for adsorption only and combined reaction-separation process at T= 700K, flow rate= 0.10 l min^{-1}. Adsorption cycle time= 800s; desorption cycle time=700s; ads = adsorbent ; admix = admixture	171
Fig. 7.18	PFR isobutane dynamic cyclic process for adsorption only and combined reaction-separation process at T= 700K, flow rate= 0.10 l min^{-1}. Adsorption cycle time= 30s; desorption cycle time=30s; ads = adsorbent ; admix = admixture	172
Fig. C.1	Methane calibration	203
Fig. C.2	Isobutane calibration	204
Fig. C.3	Isobutene calibration	204

List of Tables

Table 5.1	Summary of the particles bulk density	82
Table 5.2	Experimentally determined isobutane reaction rate constants at three temperatures.	86
Table 5.3	Volumetric flow rates used in the PFR and SAR experiments and their corresponding superficial velocities and space time. A_{PFR} and A_{gas} are the cross-sectional areas of PFR and SAR reactors. ε_t, the total bed voidage = 0.75. V_{sol} is SAR core gas channel volume	89
Table 5.4	Summary of reaction conversions of PFR and SAR, X_{PFR} and X_{SAR}, and the pressure drop calculated from the equations (5.6) and (5.7); SAR flow rate = 0.10 l min^{-1} ; PFR flow rate = 0.050 l min^{-1}	91
Table 5.5	Reynolds numbers of PFR and SAR	91
Table 5.6	Negligible convective transport test on the SAR annular packing; flow rate = 0.10 l min^{-1}; v'_{SAR} values change after forth decimal place	92
Table 5.7	Summary of the adsorbent bulk density	99
Table 5.8	Adsorption isotherm gradient values. The extrapolated values of butane and 1-butene are obtained from the work of Sheikh (1999).	102
Table 5.9	Adsorption equilibrium parameter values. The extrapolated values of butane and 1-butene are obtained from the work of Sheikh (1999)	102

Table 5.10	Isosteric heat of adsorption over zeolite KY	103
Table 5.11	Volumetric flow rates and the corresponding velocities, space times and Reynolds number of PFR	107
Table 5.12	Parameter used and estimated in this work; [a] Data from Sheikh (1999); [b] Data from Alpay et al (1996)	114
Table 5.13	Summary of molecular diffusion coefficient, D_m and axial dispersion coefficient, D_x used in this work; velocity, v for D_x corresponds to the estimated PFR gas velocity at given temperature	115
Table 5.14	Summary of the errors of the primary and secondary measurements	117
Table 5.15	Summary of the temperature difference, ΔT at three different temperatures	119
Table 6.1	Summary of parameters evaluated for SAR and PFR experiments at T = 600K; SAR flow rate = 0.10 l min^{-1}; PFR flow rate = 0.050 l min^{-1}; N_{Re} = Reynolds number; E = energy input; X = reaction conversion is obtained experimentally	133
Table 6.2	Summary of parameters evaluated for SAR experiment; SAR flow rate = 0.10 l min^{-1}; E = energy input. X = reaction conversion is obtained experimentally	136
Table 7.1	Base case parameters of SAR and its equivalent PFR	146
Table 7.2	Summary of flow rates at each temperature along with its Reynolds number, N_{Re} and estimated pressure drop, $\Delta P/L$	159

Table 7.3	Effect of varying reactor length on corresponding equilibrium conversion, X with (ad) and without incorporation of adsorbent (nad) for SAR at three different reactor lengths, T=600K, flow rate = 0.10 l min^{-1}	164
Table 7.4	Effect of increasing annular thickness on equilibrium conversion with (ad) or without (nad) incorporation of adsorbent for SAR at T = 600K, flow rate = 0.10 l min^{-1}	166
Table 7.5	Summary of energy input, cycle times and equilibrium conversion of SAR and PFR at flow rate = 0.10 l min^{-1}; t_{ads} and t_{des} are reaction-adsorption time and desorption time respectively; eqm = equilibrium; CSS = cyclic steady state	172
Table 7.6	Summary of the temperature dependent parameters and their respective Reynolds number, N_{Re}, at temperatures other than stated previously for an admixed process; feed flow rate= 0.10 litre min^{-1} at T=298K	174
Table 8.1	Summary of the SAR performances	182
Table 8.2	Major original contributions for this work	183
Table A.1	Summary of parameters used to calculate D_m	195
Table A.2	Summary of parameters for D_x calculation	197
Table B.1	Summary of parameters used to determine k_{mass}	201

Notations

a	Temperature dependent constant	-
A_{gas}	Central gas channel cross-sectional area	m^2
b	Langmuir adsorption constant	-
C	Gas phase molar concentration	mol m^{-3}
C_{gas}	Concentration accumulation at gas phase	mol s^{-1}
c_{pg}	Specific heat capacity	J kg^{-1} K^{-1}
C_{sol}	Concentration accumulation at solid phase	mol s^{-1}
d_c	Diameter of central gas channel	m
d_h	Hydraulic diameter	m
D_m	Molecular diffusion coefficient	m^2 s^{-1}
D_e	Effective diffusivity	m^2 s^{-1}
$\bar{D}_e$	Modified effective diffusivity	m^2 s^{-1}
D_k	Knudsen diffusivity	m^2 s^{-1}
D_p	Pore diffusivity	m^2 s^{-1}
d_{pore}	Particle pore diameter	m
d_p	Mean particle diameter	m
D_x	Axial diffusion coefficient	m^2 s^{-1}
E	Activation energy	J mol^{-1}
E (t)	Conversion enhancement factor	-
E_{input}	Energy input	J s^{-1}
f	Friction factor	-
G_{rxn}	Gibbs free energy	J mol^{-1}
H	Isosteric heat of adsorption	J mol^{-1}
H_T	Total enthalpy of reaction	J mol^{-1}
K	Effective adsorption equilibrium constant	-
k’	Reaction rate constant	m^3 kg^{-1} s^{-1}
k_1, k_{fwd}	Forward reaction rate constant	s^{-1}
k_2	Backward reaction rate constant	s^{-1}
K_{eq}	Reaction equilibrium constant	mol m^{-3}
K_P	Equilibrium constant based on partial pressure	-
K_{Po}	Equilibrium constant based on partial pressure at T_o	-
k_o	Pre-exponential factor/ frequency factor	-
L	Reactor length	m
m	Adsorption isotherm gradient	mol kg^{-1} Pa^{-1}
M_A	Molecular weight of species A	g mol^{-1}
M_B	Molecular weight of species B	g mol^{-1}
N_{AV}	Avogadro number	molecules mol^{-1}
P	Total pressure	Pa
P_{in}	Inlet pressure	Pa
P_{out}	Outlet pressure	Pa
Pe_∞	Limiting value of Peclet number	-

q	Average adsorbed phase concentration in a particle	mol kg^{-1}
q*	Equilibrium adsorbed phase concentration in a particle	mol kg^{-1}
q_{min}	Adsorption accumulation in solid phase	mol s^{-1}
q_s	Maximum amount of adsorbate loading onto a solid	mol kg^{-1}
r	Radial coordinate	m
R1	Central gas channel radius	m
R2	Total of R1 and annular thickness, δ	m
R_{gas}	Molar gas constant	J mol^{-1} K^{-1}
r_p	Mean particle radius	m
Re	Reynolds number	-
t	Temporal coordinate	s
t_{ads}	Adsorption cycle time	s
t_{es}	Desorption cycle time	s
t_c	Cycle half time	s
t_r	Adsorbate residence time / first moment	s
T	Operational temperature	K
T_o	Ambient temperaure	K
v	Superficial velocity	m s^{-1}
V	Reactor volume	m^3
v_{ave}	Average velocity	m s^{-1}
V_{gas}	Core channel reactor volume	m^3
V_{PFR}	PFR reactor volume	m^3
V_{sol}	Annular reactor volume	m^3
v_x	Axial velocity	m s^{-1}
W	Mass of the catalyst	kg
x	Axial coordinate	m
X_A	Reactant conversion	-
y	Component molar fraction	-

Greek letters

ρ_g	Bulk gas density	kg m^{-3}
σ^2_{AB}	Lennard-Jones collision diameter	m
$\sigma_A{}^2$	Lennard-Jones collision diameter for species A	m
Ω_{AB}	Collision integral	-
ρ^{ads}	Adsorbent bulk density	kg m^{-3}
ρ^{cat}	Catalyst bulk density	kg m^{-3}
θ_c	Cycle half time constant	-
υ^{stoich}	Stoichiometric coefficient	-
β_r	Radial dispersion factor	-
δ	Annular thickness	m
γ	Mean free path	m
ε_b	Intraparticle bed voidage	-

ε_p	Interparticle bed voidage	-
ε_t	Total bed voidage	-
μ	Bulk gas viscosity	Pa s
μ_r	First moment	s
ν_o	Volumetric flow rate	$m^3 s^{-1}$
τ	Space time	s
τ_p	Particle tortuosity factor	-
τ_x	Tortuosity factor	-
Γ	Pressure correction factor	-

Subscript

ad	With adsorbent
i	General component identifier
n	Total component identifier
nad	Without adsorbent

Chapter 1

Introduction

An adsorptive reactor involves a synergetic coupling of reaction and in situ separation process by adsorption using an adsorbent precursor. The concept is based on the Le Chatelier's principle in which the local removal of a product (or one of the products) results in a forward shift of the reaction equilibrium, hence increasing the reactant conversion and product yield. Early applications of such hybrid process involved the use of a pulse chromatographic reactor, with later extensions to real and simulated moving bed processes (Chatsiriwech *et al.,* 1994)

Due to its simplicity and practicality for large-scale continuous operation, a fixed bed adsorptive reactor is often employed. The periodic adsorbent regeneration and subsequent recovery of key adsorbates is accomplished using principles of pressure swing, rapid pressure swing or temperature swing adsorption, as well as inert purge gas stripping. Significant improvements of conversion, higher product yields, low energy input consumption due to low reaction temperature operation and effective periodic regeneration, characterise the efficiency of such a process. Despite the versatility, the high pressure drop is associated with packed beds. This limits the design and performance of such a reactor.

It is the aim of this study to incorporate the adsorptive reactor concept in a novel structured packing arrangement to tackle the problems associated with high pressure drop. It has been reported in the literature that employing monolithic and parallel passage type reactors could

substantially reduce the pressure drop, making them an attractive alternative to the conventional packing configuration. In addition, the transport limitation due to mass transfer resistance could be overcome in an annular packing configuration.

In this work, a theoretical and experimental study was carried out to investigate the potential of integrating the adsorptive reactor application in an annular-type structured packing configuration. A structured adsorptive reactor, SAR, can be viewed as a hybrid between a monolithic and a parallel passage structure integrated in an annular type packing arrangement. Such a novel configuration could provide a low pressure drop alternative to a fixed bed configuration.

The experimental works involved studies of the dehydrogenation of isobutane over an admixture of platinum-alumina catalyst and zeolite-KY adsorbent. Prior to reaction enhancement experiments, catalyst and adsorbent characterisations are carried out to obtain the key adsorption and kinetic parameters under isobaric condition at selected temperatures. A two-dimensional mathematical model has also been developed to assess the performance and viability of such process design configuration. The model equations are solved within the gPROMS simulation environment. For the computational validation purpose, design parameters are appropriately selected, which intrinsically affect the performance of the reaction-separation process. Equivalent conventional packed-bed reactor arrangements are compared as well for further validations.

The organisation of this thesis is presented as follows:

- Chapter 2: Background and literature survey

  This chapter presents a reviewed literature survey entailing the development of SAR. An overview of the novel annular-type SAR is also given.

- Chapter 3: Theoretical background and modelling

  A proposed mathematical model is presented. The equations are described in partial differential and algebraic equations to depict the transport phenomena as well as adsorption and reaction processes which are involved in the system. The theoretical background of an analogous diffusional mass transfer mechanism as well as the isobutane dehydrogenation reaction kinetic mechanism is also presented.

- Chapter 4: Experimental apparatus

  A description of the SAR rig is presented. Details on the unit operation is accompanied by a flowsheet. The standard experimental procedure for the combined reaction-adsorption process is also presented.

- Chapter 5:Reaction and adsorption kinetic measurements

  An overview of platinum-alumina catalyst and zeolite KY adsorbent selected to account for the dehydrogenation reaction and selective adsorption of isobutane and isobutene is given prior to the technical report. The performance of the SAR relative to the PFR-type reactor is also assessed which leads to the key adsorption parameter fitting in the simulation study.

- Chapter 6: Structured adsorptive reactor investigations

  The chapter begins with an overview of SAR configuration. The conversion enhancement studies of SAR and its equivalent packed bed adsorptive reactor configuration are presented. The chapter concludes with an account of cyclic SAR operations. All the results are compared with the simulation results to validate the study.

- Chapter 7: SAR theoretical analysis

  The viability of the SAR mathematical model is assessed, using a set of key variables and decision parameters, which include temperature and geometrical sizes to further justify the novel type system.

- Chapter 8: Conclusions and recommendations for future work

  The final chapter presents an overall conclusion of the research work with some suggestions for future work.

Chapter 2

Background and Literature Survey

2.1 Introduction

The motivation for developing the annular-type structured adsorptive reactor, SAR, is to develop a low pressure drop reactor configuration whilst maintaining the advantages of the packed bed. With reference to fig. 2.3, the SAR can be viewed as a hybrid between monolithic-type and parallel passage-type structures.

In this chapter, reviews entailing the development of the SAR are presented. These include:

- The process
  - An overview of the adsorption phenomena, the basic concepts underlying periodic adsorption processes, as well as adsorptive reactor technology
- The design
  - An account of the fundamental design in the context of parallel passage, monolithic and annular packing reactors

A general review of the underlying design concept of the SAR is also presented.

2.2 Adsorption phenomena

Fundamentally, adsorption phenomenon is a reversible process resulting from two types of interaction with atoms (or molecules) at the interface (i.e. solid-gas). The first type involves a degree of significant electron transfer and chemical reaction known as chemical adsorption (or chemisorption). The second one would be the relatively weak Van der Waal's forces and electrostatic interactions within the strength of the solid (adsorbent) surfaces forces and is known as physical adsorption (or physisorption). In the context of the periodic adsorption process development, physisorption is primarily preferred whereby the adsorbent has relatively weak (non-activated) and fully reversible nature which leads to regenerative properties (Alpay *et al.*, 1994).

The rate of adsorption is influenced by the presence of mass transfer resistances. In a simplified case where mass transfer limitations can be neglected at a specified temperature, linear adsorption isotherm will describe the instantaneous adsorption at low adsorbate concentration within Henry's law region. This is the underlying fundamental concept of the adsorption process where the quantity of the adsorbed component (i.e. adsorbate) per mass of adsorbent is in equilibrium with the pressure or concentration in the bulk phase at constant temperature.

2.2.1 Adsorbents

An effective adsorbent is specifically chosen for a given separation process. The properties of the adsorbent must complement the design of the adsorptive separation process for an efficient system (Sircar, 1994). The primary requirement is based on its selectivity,

capacity and stability such that it could contribute to better separation performances under different regeneration, chemical and physical conditions. Therefore, at a specified temperature and pressure, the regenerative properties of a selected adsorbent are determined by:

- Selectivity:
    - The ability of the adsorbent to selectively adsorb one or more adsorbates based on equilibrium selectivity (i.e. one component adhere better to the solid due to its equilibrium affinity) or kinetic selectivity (i.e. adsorbate may spend longer time within the pellet due to lower diffusion rate).

- Stability:
    - Economical aspect whereby high stability could minimise the process down-time and adsorbent replacement.

- Capacity:
    - The maximum loading of adsorbate possible on the adsorbent. This is associated with the micropore size and shape of the adsorbent particle.

There are many types of commercial adsorbents available, which vary in chemical form and geometrical surface structure. Of these, zeolites have seen many applications on an industrial scale. They are characterised not only by high selectivity, but also the ability to separate the components based on differences in the sizes and shapes of molecules (steric separation mechanism) (Dabrowski, 2001). They have a well-defined structure of porous, crystalline aluminosilicates of alkali and alkali earth metals. A zeolite type considered in this work is zeolite-KY. It is specifically chosen as it can retain its structure and crystallinity at reasonably high temperatures (see section 5.3.1).

2.3 Periodic adsorption processes

Periodic adsorption processes are intrinsically dynamic, operating in a periodic mode with a fixed cycle time. The adsorbent particles undergo two essential steps: adsorption and regeneration steps. Regeneration of the adsorbent involves removing of the adsorbate from the adsorbed phase into the gas phase. By doing so, the adsorbent can be reused in further cycles while enabling recovery of the adsorbate. This is usually accomplished by:

- Pressure Swing:
  - The gases are fed at high pressure during adsorption stage. The bed is then regenerated by reduction of the total pressure (depressurisation) to desorb the adsorbate from the adsorbent and eluded from the feed end of the bed.
- Thermal Swing:
  - The feed stream is fed at certain temperature. During regeneration, the bed is purged with a stream of hot inert gas to a temperature at which the adsorbates are desorbed.
- Purge gas stripping:
  - The inert, non-adsorbing gas is fed at the same operational temperature as the feed gas temperature to reduce the partial pressure of the adsorbate in the adsorbent.
- Displacement desorption:
  - A competitive adsorbing species displaces the main adsorbate; this requires additional separation steps for removing the displacement agent from the adsorbent.

The choice between possible modes of regeneration for a cyclic adsorption separation process depends on economic factors as well as technical considerations (Ruthven, 1984). Essentially, adsorption is favoured by low temperatures, high pressures, high enthalpies of adsorption and large adsorbent surface area (Sheikh, 1999), and the adsorption process may favour one component over another resulting in relative separation of the gas mixture. Examples of the common periodic adsorption process are pressure swing adsorption (PSA) and thermal swing adsorption (TSA).

2.3.1 Pressure swing adsorption

The pressure swing based process consists of two essential operations that of adsorption at high pressure and regeneration at reduced pressure. It can be divided into three groups:

a) Pressure swing adsorption (PSA)
b) Rapid pressure swing adsorption (RPSA)
c) Single and dual piston-driven PSA

PSA

Pressure swing adsorption (PSA) represents an important industrial operation for gas separation, and is widely favoured for drying, hydrogen purification and air separation processes (Doong and Yang, 1988). It is thought to be originally proposed and developed by Skarstrom as well as Montgareuil and Domine. The Skarstrom process consists of a two-bed four-step process, in which there is continuous product flow. The four operating steps involve:

1) Pressurisation step: A concentration gradient develops within the bed when it is pressurised and the product end is closed, the strongly adsorbed component is retained in the adsorbed phase
2) High pressure product release: The feed gas flows through the bed as the product end opens, eluding the weakly adsorbed components in the product stream
3) Depressurisation: The product end is closed and the exhaust valve at the feed end is opened. The strongly adsorbed component then desorbed as pressure drops and elute in a counter-current flow through the exhaust valve
4) Low pressure product purge: The exhaust and product end are open to enhance adsorbent regeneration, where the bed is purged in a counter-current gas flow until it becomes clean

Efficient utilisation of energy is essential for an economic PSA system. It generally operates at relatively low adsorbent loading and low temperature and is well suited for rapid cycling (Ruthven, 1984). Besides low maintenance, the readily automated operation, system flexibility during change of cycle time, high product purity, as well as long lifetime of vessels add to the advantages of the PSA process.

Nevertheless, the overall PSA process is fairly complex and requires large number of beds. For instance, a commercial multibed PSA process would involve two to ten bed configurations, operated according to complicated cycle sequences (Doong and Yang, 1988) to necessitate the adsorbent regeneration. Furthermore, additional steps become necessary such as purge or backfill to improve the productivity. These modifications among other things are developed to improve the purity of the product gas, increase the

working adsorption capacity of the selective adsorbate, as well as to minimise the loss of desired component(s) (Sircar, 1994).

Another way of improving the PSA process is through modifying the packed bed column configuration. This was strongly advocated by Rota and Wankat (1991) using scaling rules to observe the improvement of the existing PSA design whilst keeping its main performance constant. The mass transfer and heat transfer mechanism along with a set of algebraic equations relating to the cycle times and other auxiliary parameters were made dimensionless in order for the scaling method to remain valid. A better separation performance could be attained using smaller columns packed with smaller adsorbent particles sizes.

More comprehensive state-of-the-art reviews on PSA can be found from Ruthven (1984), Ruthven *et al.* (1994) and Suzuki (1990).

Rapid pressure swing adsorption

Turnock and Kadlec (1971) introduced a simple alternative to the two-bed four-cycle process by using much smaller particles and shorter cycle time for the periodic separation of nitrogen and methane. The development led to a single bed, 2-step process involving feed gas pressurisation and counter-current depressurisation. The rapid adsorption and desorption steps enabled the continuous withdrawal of product from the bed. Overall, RPSA can be deemed as the simplest PSA operation and still capable to offer relatively high adsorbent productivities at isothermal conditions for some separations (see Alpay *et al.*, 1994).

The work of Keller and Jones (1981) shed light on the potential of RPSA process. The modifications (on what is referred as pressure-swing parametric pumping) were made in terms of shorter pressurisation time, delay step after pressurisation, long depressurisation cycles, and installation of a product surge tank for the production of oxygen. Unlike a traditional PSA system, the flow resistance in bed is necessary for a successful RPSA process through utilisation of very small adsorbent particles sizes.

The RPSA can also be termed as pulsed PSA for an experimental study of the separation of a binary mixture of methane and carbon dioxide in a single isothermal column packed with an activated carbon adsorbent (Hart and Thomas, 1991). A comparable mathematical model to the one proposed by Turnock and Kadlec (1971) was shown to be in good agreement with the experimental results obtained.

RPSA has undergone a number of modifications in order to obtain higher productivity (see Alpay, 1992 and Sheikh, 1999). The drawback of RPSA however, is the large pressure drop across the bed (Kodde, 2001). Such a problem may be alleviated by implementing radial flow resistance distribution and considerably reduced adsorbent particle sizes in a radial flow RPSA configuration.

An experimental study pertaining to the radial flow RPSA concept has been investigated by Chiang and Hong (1995). They conducted the experiment using a 75 mm high annular basket of fine gauged stainless steel screen packed with three types of adsorbent particles sizes, and fitted into the disk-shape container as the replacement of adsorption column. Such a configuration was designed to incite the radial distribution of flow across the bed. Significantly lower pressure drop was obtained when compared to an axial flow RPSA

model. This was made possible due to the radial flow arrangement which provided a larger cross-sectional area for the same volume of bed packing. This arrangement also enables the use of a smaller particle size favourable for faster adsorption kinetics. Huang and Chou (2003) theoretically investigated such an arrangement whereby they predicted that at the same feed pressure and the same amount of adsorbents, the separation performance of the radial flow RPSA would be better by utilizing smaller adsorbent particles and longer effective lengths.

Single and dual piston-driven PSA

A single piston system was proposed for nitrogen and air separation by Eriksson (1979). In his patent, Eriksson (1979) stated that the dynamic of the system is achieved using a reciprocating moveable piston at each end of an adsorption column as the means of imposing cyclic gas flow and pressure variations on the gas mixture. This resulted in nitrogen to be adsorbed at high pressure. At this point, a non-adsorbing gaseous mixture having a high content of oxygen was passed through the adsorbent bed and exited. On expansion the bed was flushed with the non-adsorbed oxygen and subsequently, nitrogen was desorbed at a decreasing pressure. The patent claimed that the gas product, which was air, was far purer than that previously possible because part of the cycle was operated at partial vacuum (Rouse, 2004).

A dual piston-driven PSA concept was patented by Keller and Kuo (1982). Here, two driving pistons of unequal lengths were used to achieve high productivity separation of the components by gas volume displacement in the adsorption column at a reduced operating cost. Like the RPSA process, very rapid cycles were found to enhance the productivity of the process.

A piston-driven ultra-rapid PSA (URPSA) process for CO_2 recovery and high capacity oxygen enrichment was demonstrated by Suzuki *et al.* (1997). Although the moisture content in the model stack gas accumulated in the hydrophilic zeolite, it has drastically affected the CO_2 adsorption capacity. Nevertheless, the overall oxygen production capacity of the URPSA was found to be one order of magnitude higher than that of conventional PSA processes. In addition, the separation performance of this particular process strongly depended on the adsorbent particle size, which affected the overall pressure drop and production rate of the adsorption bed. They have also suggested the use of zeolites in honeycomb structures to counter the pressure drop problem across the bed.

Further experimental and theoretical studies on the exploitation of the dual piston-driven PSA system for CO_2 separation were carried out by Rouse (2004). Attempts were made in order to make the model more widely applicable for cyclic processes, through which a cycle time dependent parameter was introduced to modify the standard linear driving force (LDF) equation. Implementation of phase lags and amplitude difference enabled the use of two parameters, which ensure that both bulk and adsorbed concentration profiles can be accurately simulated. The selected activated carbon adsorbent extruded in a monolith form was characterised using chromatography and zero length column (ZLC) techniques. The experiment was conducted in two columns for CO_2 – N_2 separation, the first was configured in a honeycomb structure of the carbon monoliths. The second column housed rectangular shaped carbon monoliths within the aluminium tubular casing. From the parametric studies, employing a smaller monolith dimension can lead to better separation despite lower cycle times. The drawback of the experimental set-up on the other hand, was the significant pressure drop occurred due to small pipe work sections joining the composite sections of one of the columns. From the modelling aspects under adsorbing

total reflux conditions, there were reasonably good agreement of the pressure and cyclic steady state concentration profiles.

2.3.2 Thermal swing adsorption

Thermal swing regeneration processes are generally preferred for strongly adsorbed components as well as multicomponent adsorbates at widely different adsorption affinities. The simplest version of a TSA cycle operates with two beds: adsorption at low temperature (near or at ambient temperature) and regeneration at a higher temperature usually by passing a hot stream of inert gas. Of these, the regeneration step is the limiting factor in the design of the cyclic two-bed process. A long heating time could give rise to achieving a cyclic steady state condition (Yongsunthon, 1999) in which the concentration at all positions at any time in the cycle remain the same in all subsequent cycle (Ruthven, 1984).

The effectiveness of the regeneration step depends on the intensity between the purge gas flow rate and the regeneration temperature. The combination of either a higher regeneration temperature rise coupled with a smaller purge flow rate or a relatively low temperature at high purge flow rate will be the cost-determining factor of a TSA process. Implementing reverse-flow regeneration instead of a forward-flow could prevent incomplete adsorbate removal.

The TSA operation is not very feasible for short cycle time and repeated thermal swing cycling. While short cycles reduce the duration necessary for bed heating and cooling, increased frequency of thermal cycling tends to reduce the adsorbent life (Ruthven, 1984). There is also the need to have a large inventory of adsorbent, which is uneconomical.

More comprehensive reviews on TSA can be found from Ruthven (1984), Yang (1987), Suzuki (1990) and Yongsunthon (1999).

2.4 Combined reaction-separation processes

An innovation in recent years has been to create synergy through combined catalytic reaction-separation technologies (Gobina *et al.*, 1997). One aspect of this work is the use of permselective membranes for the gas-solid catalytic reaction. Membrane reactors have been applied to the dehydrogenation reactions by Shinji *et al.* (1982), Itoh (1987), Sun and Khang (1988), Champagnie *et al.* (1990), Matsuda *et al.* (1993), Ziaka *et al.* (1993), and the likes. Although such reactors enable lower reaction temperatures, higher conversion and increase in equilibrium yields of product, the continuous removal of hydrogen from a palladium-based membrane, for instance, may lead to increased catalyst fouling.

Owing to the great contribution towards effective dynamic and transient heterogeneous catalytic reaction coupled with the adsorptive reaction, adsorptive reactors have been an attractive choice in bulk separation and large-scale industrial process application. The developments as well as process intensifications of such unit operation have been widely investigated theoretically and experimentally for the past four decades.

More progress has been achieved through in situ reaction-separation combination in a single unit operation on a periodic basis. Basically, adsorbents are admixed into the catalyst particles to form a dual-operation in the same solid zone. It has been the more effective way in achieving higher conversions and yields in a catalysed reversible reaction (Xiu *et*

al., 2002). Kodde (2001) concluded the advantages of a combined reaction-separation process as follows:

- Increased conversion of reactants
- Improved selectivity and yield of desired product
- Reduced requirements for external energy supply or cooling capacity
- Reduced capital expenditure by process intensification
- More favourable reaction conditions may be possible

The control of mass transfer of the reaction species may be achieved significantly by incorporating the in situ separation technique. Most of the theoretical investigation and experimental works reported were conducted in the conventional random packing, fixed bed pressure swing reactor (PSR). This was due to its flexibility when compared to other reactors for example, the chromatographic-type reactor. Nevertheless, a high pressure drop occurred in such system.

2.4.1 Process review

Selective in situ removal of a strongly adsorbed product will shift the equilibrium of a catalytic reversible reaction towards further product formation. Subsequently, conversion enhancement is attainable in an equilibrium-limited reaction. This concept is based on Le Chatelier's principle which states that (Atkin, 2002):

"A system at equilibrium, when subjected to a disturbance, responds in a way that tends to minimize the effect of disturbance"

In the case of a highly endothermic catalytic dehydrogenation reaction of:

$$aA \rightleftharpoons bB + cC,$$

a selective adsorbent is introduced in an adsorption-enhanced separation system to favour the forward reaction by selectively adsorbing B leaving C to be purged from the system. During the regeneration step, B is desorbed and collected as product.

Adsorption is an exothermic process and favours low temperature operation. In order to achieve a considerable conversion enhancement effect of an endothermic dehydrogenation reaction, the choice of a suitable reaction temperature and pressure for the reaction and separation process has to represent a compromise between the equilibrium and kinetic factors (Han and Harrison, 1994).

2.4.2 Periodic adsorptive reactors

Periodic adsorptive reactors couple the chemical reaction and adsorption separation process into a single unit operation. The dynamics of the process requires insight into the interaction of local adsorption separation and the kinetics and thermodynamics of the chemical reaction over an admixture of (solid) catalyst and adsorbent packing. Upon equilibration of adsorbent, periodic regeneration is necessary to regenerate the adsorbent and subsequent recovery of key adsorbate(s) (Yongsunthon and Alpay, 1999). The choice of regeneration for such inherently transient operation depends on the strength of the adsorbates in order to ensure a complete desorption.

There are several types of these reactors in the literature. They range from pulse chromatographic reactors, countercurrent moving-bed and simulated countercurrent

moving-bed chromatographic reactors, pressure swing reactor (PSR), rapid pressure swing reactor (RPSR) to thermal swing reactor (TSR).

Pulse chromatographic reactor

Early applications focused on a pulse chromatographic reactor where pulses of reactant were fed to a chromatographic column packed with a catalyst as in the works of Roginskii *et al.* (1961), Magee (1963) and Chu and Tsang (1971). The course of a chemical reaction takes place in the pulse chromatographic reactor whereby the reaction products were separated by chromatographic action of the column, forcing a complete forward reaction. This particular configuration system is an example of a gas phase adsorptive reactor, which can be utilised to exceed the equilibrium limits.

Continuous countercurrent moving-bed and simulated countercurrent moving-bed chromatographic reactor

The pulse chromatographic reactor application has been expanded into a countercurrent moving-bed chromatographic reactor (CMCR). Here, the manipulation of the gas-and-solid continuous flows enables different velocities of the reactants and products. A stream of fine catalyst particles is fed from the top of the reactor and falls countercurrently to the upward flowing current of reactant gas (contained in an inert gas carrier). Such an operation is capable of producing a significant increase in the conversion as well as high product purity (see Petroulas *et al.*, 1985, Fish *et al.*, 1986).

The major drawback of the CMCR is that of solid handling (Bjorklund and Carr 1995). Such a problem could be rectified using a simulated countercurrent moving-bed

chromatographic reactor (SCMCR). This is achieved by simulating the countercurrent operation in a single (or multi) column configuration. The countercurrent movement is simulated by successively switching the time interval between the feed and product through a series of feed point inlets and product removal outlets.

Pressure swing reactor

A pressure swing reactor (PSR) uses the principles of PSA for adsorbent regeneration. One practical significance of conversion enhancement by PSA is a lower temperature operation which leads to energy saving and minimum degree of catalyst deactivation (Chatsiriwech *et al.*, 1994). In addition, the separation properties of the process can be utilised to give a high purity recovery of a key product (Sheikh, 1999).

The simplest configuration consists of two reactors; each packed with an admixture of catalyst and adsorbent, and involves three steps (see Yongsunthon, 1999, Sheikh, 1999):

1) Pressurisation:
    - Simultaneous reaction and adsorption takes place at high pressure. The local removal of a strongly adsorbed component by adsorption at high pressure may favourably shift the reaction equilibrium towards further product formation
2) Product release step:
    - Enriched stream of weakly adsorbed components are withdrawn out of the product end
3) Depressurisation:
    - Reduction of total pressure resulting in the desorption of the adsorbate, which is subsequently eluded as exhaust from the bed

Alpay *et al.* (1994) applied the PSR concept for the industrially important reaction schemes of isomerisation ($A \rightleftharpoons B$), dissociation/disproportionation ($2A \rightleftharpoons B + C$), and dehydrogenation ($A \rightleftharpoons B + H_2$ and $A \rightleftharpoons B + 3H_2$). Possible improvements in equilibrium yields have been theoretically predicted for the isomerisation and dissociation/disproportionation reaction schemes. Although there was rather low or no improvement of equilibrium yield observed for the dehydrogenation reactions, possible conversion enhancement improvements were indicated.

Chatsiriwech *et al.* (1994) also theoretically studied the reversible dissociation reaction, $2A \rightleftharpoons B + C$. The conversion enhancement effect was found to be improved with the inclusion of a purge step in the PSR system. As well as achieving low temperature operation, potential advantages of the PSR include a higher reactor productivity which led to energy savings and prolonged catalyst activity.

Carvill *et al.* (1996) introduced the term SERP (sorption enhanced reaction process) for the study of the reverse water-gas shift reaction for the production of carbon monoxide. Two parallel fixed bed PSR reactors were packed with adsorbent-catalyst admixture and involved five operational steps: countercurent pressurisation, sorption-reaction, countercurrent depressurisation, purge (1) and purge (2). In contrast to a conventional reactor, direct production of carbon monoxide, enhanced conversion, increased forward reaction rate as well as efficient in situ adsorbent regeneration was rendered possible when applying the periodic SERP scheme. Subsequently, a lower temperature, energy-saving operation could be achieved.

Hufton *et al.* (1999) continued the work of Carvill *et al.* (1996) by experimentally investigating the production of H_2 by steam-methane reforming (SMR) in a bench-scale PSA system. A selective chemisorbent (potassium carbonate promoted hydrotalcite) was admixed with the Ni-based catalyst, for the selective removal of CO_2 product. The adsorbent was regenerated periodically by using the principles of PSA (Hufton *et al.*, 1999). This was found attractive as the PSA operation made the SERP concept very efficient by:

1. Direct production of desired reaction product at high purity (> 95mol% H_2) with up to 82% of hydrogen produced
2. Low operating temperature could be employed throughout the reaction and regeneration steps
3. Subsequent hydrogen purification step could be eliminated for hydrogen production

Since then, a number of studies relating to the SERP concept for the SMR process operated in the PSR have been carried out. Modifications were made to the adsorbent through use of different precursors and a diverse range of operating conditions explored. Examples include the works of Ding and Alpay (2000), Xiu *et al.* (2002) and the authors reviewed by them.

Rapid pressure swing reactor

Rapid pressure swing reactor (RPSR) incorporates the advantages of RPSA using a single bed, commonly operates with two to three cycle step process: pressurisation (simultaneous reaction and adsorption separation), exhaust step and countercurrent depressurisation (adsorbent regeneration). It is an attractive alternative to the PSR in which higher

adsorbent/productivity is attainable due to continuous product stream throughout the cycle as a result of rapid-cycling and low permeability of the bed packing (Sheikh, 1999).

Vaporciyan and Kadlec (1987) first published a theoretical study of the RPSR system for three reaction schemes: $A \rightleftharpoons 2C$; $2A \rightleftharpoons C$; and $A \rightleftharpoons \frac{1}{2} B + C$. Intrinsically, the reaction conversion and separation accomplished depend upon the manner in which the pressure and reactant concentrations are controlled at the feed boundary. Of all the reaction schemes, the third one gave rise to the conversion enhancement effect in the RPSR through preferential in situ adsorption of component B over component C. In conjunction with rapid cycle operation, cycle time period has been considered as the main design parameter. This was because too short cycle times gave rise to considerable bed attenuation that it would affect the delivery flow rate while long cycle times would lead to long exhaust times. Subsequently, this implied a reasonable cycle time which would be sufficient to increase the conversion for the reactions which produce higher product moles (i.e. $A \rightleftharpoons 2C$ and $A \rightleftharpoons \frac{1}{2} B + C$).

A theoretical and experimental study of RPSR has also been conducted by Vaporciyan and Kadlec (1989) to account for conversion and selectivity improvements. The experimental work involved carbon monoxide oxidation over an admixture of platinum-alumina catalyst and 5 Å molecular sieve adsorbent. Due to high adsorbent capacity and selectivity for the strongly adsorbed product, i.e. carbon dioxide, resulted in sharp increase of forward reaction, which approached irreversible reaction behaviour. Consequently, carbon monoxide conversion enhancement and higher carbon dioxide production over the steady state plug flow operation could be achieved. For the theoretical study of three reversible

reaction schemes: A ⇌ ½ B + ½ C; A ⇌ B; and C ⇌ A ⇌ B, selectivity and conversion improvements could also be achieved when incorporating RPSR model. Apart from the manipulation of the reaction phenomena in terms of residence time distribution, the nature of the reaction law and equilibrium shifts, the common underlying cause to the improvements was due to the opposing concentration gradients created by the reaction and separation components of the process.

Lee and Kadlec (1989) presented a theoretical study of RPSR based on the fixed bed tubular reactor model, packed with adsorbent and catalyst for a parallel reaction of B ⇌ A ⇌ C. They assigned the boundary condition at the end of the reactor as a periodic function. In the parallel reaction, the selectivity of B was maximized by the optimal distributions of the adsorbent capacity and catalyst activity.

Cheng *et al.* (1998) performed a study of a general dynamic model of the RPSR for a case study of a reversible dissociation reaction, 2A ⇌ B + C. The model was described by a set of partial differential and algebraic equations to account for the dynamic variation and spatial distributions of properties within the bed. Both the successive substitution (SS) and simultaneous discretisation (SD) schemes have been applied to obtain a cyclic steady state solution. Orthogonal collocation of finite elements method, OCFEM was employed for the discretisation of both spatial and temporal domains. The SD approach was employed for the optimisation study of the RPSR to maximize the yield of C as it was found to be more robust and efficient than SS approach. A 32% increase over the equilibrium yield indicated the significant improvement on employing the optimisation solution.

The RPSR performance has also been theoretically and experimentally investigated for the in situ reaction-separation of 1-butene dehydrogenation as reported in the work of Sheikh *et al.* (2001). Two types of operation considered in the experimental work: countercurrent and cocurrent exhaust gas flow arrangements. Each of the flow arrangement performance was compared to an equivalent packed bed PFR. The dehydrogenation reaction scheme, represented in the form of $A \rightleftharpoons B + C$, was theoretically analysed with emphasis on relative effects of adsorption and reaction parameters on conversion enhancement. Most of the simulation results were in good agreement with the experimental results with exceptions to few cases like the inability to observe the predicted conversion enhancement of 1-butene due to the cracking of butadiene. There was a decrease in 1-butene conversion and butadiene yield when operated using the countercurrent arrangement due to lower gas-phase residence time of the adsorbing reactant (Sheikh, 1999). With a cocurrent arrangement, higher 1-butene conversion was achieved but at the loss of bulk separation (Sheikh *et al.*, 2001).

Thermal swing reactor

The thermal swing reactor (TSR) basically incorporates thermal and concentration swing operations. The cyclic single-stage configuration process consists of a single bed, 2-steps of isobaric operation which included: feeding step (in situ reaction-separation step at reaction temperature) and regeneration step (the adsorbent is regenerated by passing a stream of hot inert gas purge and subsequent key adsorbate recovery).

Yongsunthon and Alpay (1999) conducted a theoretical investigation using the TSR process for the endothermic dehydrogenation of methylcyclohexane to toluene (represented as $A \rightleftharpoons B + 3C$) over an admixture of platinum-alumina catalyst and zeolite 5A adsorbent.

Two types of process configuration were considered: single-stage and multi-stage configurations. Preferential adsorption of product component B (i.e. toluene) increased as the temperature decreased, which subsequently increased the overall reaction rate due to favourable shift of the reaction equilibrium. In the second step of the single-stage configuration, adsorbent regeneration occurred on feeding the hot inert gas stream operated in either unidirectional or reverse-flow arrangement. This hot purge gas also supplied the reaction heat by means of bed reheat. Two multistage reactor configurations employed series and mixed series-parallel connections and operated with either one of the flow arrangements. Optimal results were observed using the multistage configuration involving mixed series-parallel connections of the stages, and the disproportional splitting of feed streams to each stage. Substantial conversion enhancement as well as bulk gas separation could also be achieved at no additional energy input.

2.5 Structured packing reactors

Due to their simplicity and relatively low investment cost, fixed bed reactors have been used for solid-gas reaction and separation processes (or a combination of these) at the expense of high pressure drop. This has called for the development of a structured packing system with a capability of achieving a low pressure drop whilst maintaining the advantages of the packed bed configuration. Two of the main interests are parallel passage reactor (PPR) and monolithic (honeycomb) reactor which have found a wide application for catalytic processes.

2.5.1 PPR and monolith reactors overview

The PPR is a continuous flow reactor, partly filled with equal arrays of wire screen gauze envelopes loosely packed with solid (usually catalyst) particles parallel to gas flow (see Fig. 2.1). The fine apertures of the screen provide an unobstructed access of gas to diffuse towards the solid particles allowing mass transfer between them.

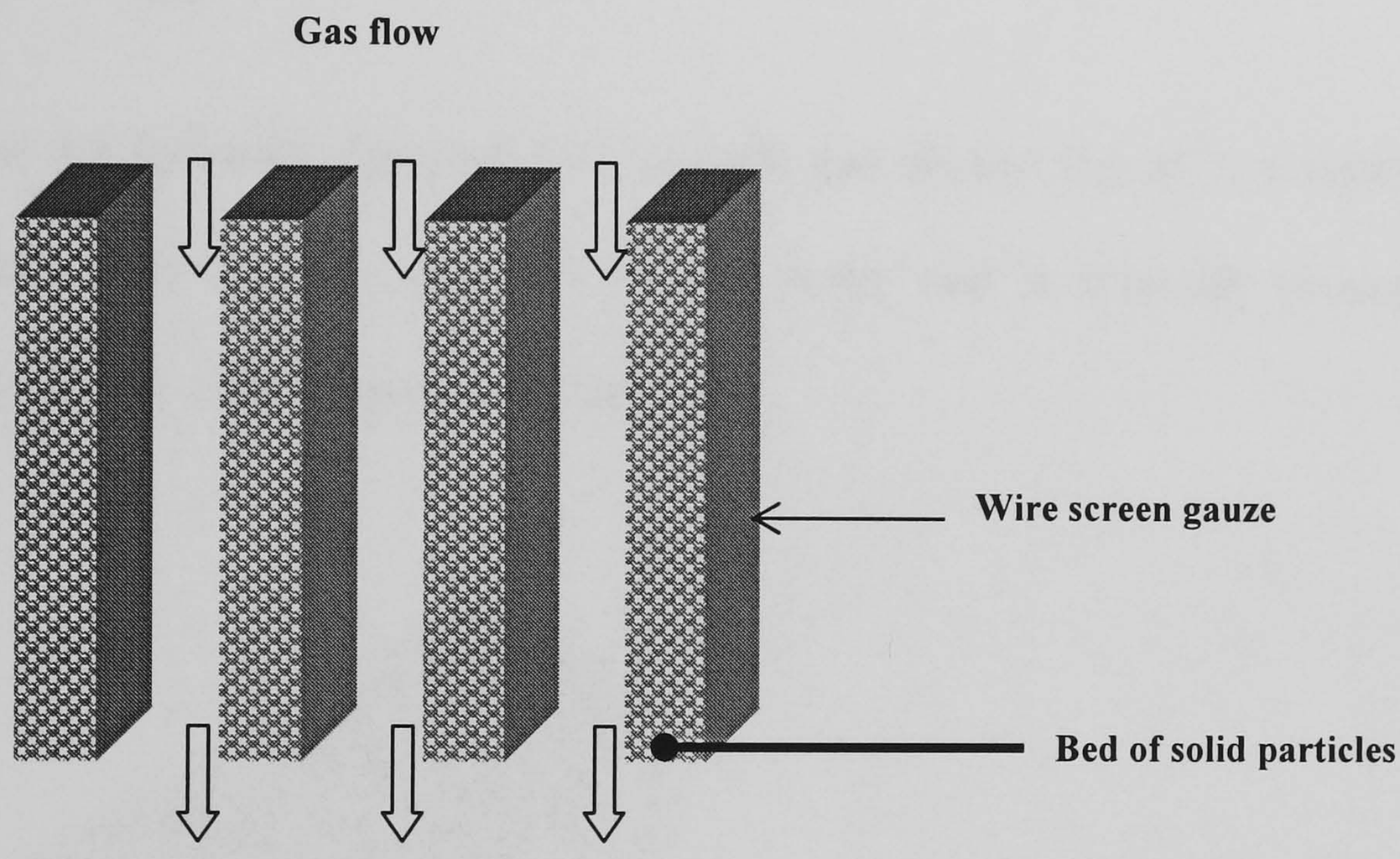


Fig.2.1 Schematic diagram of an array of slabs of a PPR

PPR is characterised by low mass transfer resistance, laminar flow operation, flexible solid packing and low pressure drop. The momentum transport through the slabs involves the dispersion and molecular diffusion of the feed gas along the straight parallel solid layer channels. The solid particles are essentially surrounded by stagnant gas, suggesting the absence of convective transport in the bed packing. Therefore, during a chemical reaction, the catalytic conversion is highly dependent upon molecular diffusion transport where the reactant products have to diffuse from the catalyst bed towards the gas stream via the screen gauze.

Unlike the conventional fixed bed packing, the PPR configuration would allow a low mass transfer resistance operation due to the relatively low friction of gas flow between the empty channel and the solid slabs. Substantial reduction in pressure drop therefore occurs and can be determined using the Hagen-Poisuille correlation:

$$\frac{\Delta P}{L} = 4 f \frac{1}{d_h} \rho_g v^2 \qquad (2.1)$$

where d_h is the hydraulic diameter (m), ρ_g bulk gas density (kg m^{-3}), v superficial velocity in the channel (m s^{-1}), and f is the friction factor and is inversely proportional to the superficial velocity at low Reynolds numbers.

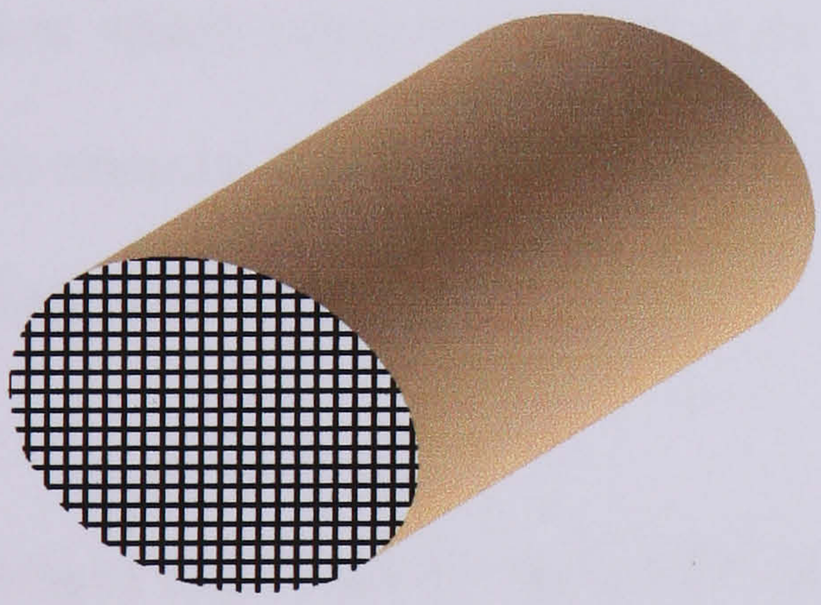


Fig.2.2 A typical monolith structure

A large stack of catalyst element of uniform structure with small passages describes the monolithic reactors, and a well-known example is the honeycomb reactor. It comprises a ceramic or metal honeycomb structure manufactured through extrusion, where a thin layer of material with a large surface has been bonded in a so-called washcoat catalyst. The use of structured wires, gauze or thin plates to which the catalyst particles have been deposited using an adhesive (Van den Bleek *et al.*, 1996) would improve the mechanical strength and thermal stability of the monolith structure.

Monolithic reactor is characterised by small internal diffusion resistance, laminar operation and of course, low pressure drop. However, it does possess drawbacks in terms of high manufacturing cost and the malleability of the structure. It can only be applied to certain processes in which the catalyst is reasonably stable and/or the ease to regenerate is feasible (Cybulski and Moulijn, 1998). The washcoat are less wear resistant and could give rise to rapid loss of catalyst activity. Another disadvantage is that only small catalyst particles can be deposited.

With regards to the structured arrangement of solid packing, PPR would be an attractive alternative to the monolithic reactors (Sie and Calis, 1998). Besides more flexible solid packing utilising relatively small catalyst particles, it can withstand thermal stresses in application where rapid temperature rises or drops occur during start-up and shut down. This is in contrast to the washcoat layers in the monoliths, which need special devices to avoid crack or detachments.

One common drawback for both PPR and monolithic reactor is the poor heat and mass lateral transport. In a PPR, the most effective method is to alternately shut off the inlets and outlets of the channel in order to enable the gas to flow laterally through the beds (Van den Bleek et al, 1996), which leads to the lateral flow reactor configuration (Seijger *et al.*, 2001). The disadvantages of lateral flow for monolith reactors on the other hand, include poor radial and axial heat transport. To counter such problems, the monolith structure would comprise a continuous, binderless washcoat material to improve the transport mechanism.

Industrial applications of PPR can be found in: the Shell Flue Gas Desulphurization (SFGD) process to remove sulphur oxide and nitrogen oxide from flue gas using copper oxide on alumina catalyst as the regenerative chemisorbent; and the Shell low temperature NO_x reduction process using vanadium and titania catalyst on a silica support. Monolith catalysts on the other hand, are applied in automotive catalytic converters as well as in organic components and carbon monoxide incinerators.

Overall, the structured packing arrangements offer an attractive alternative to the traditional packed bed configuration. To date, there have been a number of publications associated with the use of catalyst incorporated in the structured packing development. In conjunction with the adsorption technology, the adsorbent packing performance could also be exploited in a parallel passage or monolithic type structure as reviewed in the following section.

2.5.2 Structured adsorber packing

The advantages of utilising a structured bed packing arrangement are equally relevant to adsorption processes. Pioneering this concept, Ruthven and Thaeron (1997) have conducted a theoretical and experimental study of a so-called parallel passage adsorbent contactor. This consists of two sheets of activated carbon fibre adsorbent layers which are attached to the top and bottom of a very narrow column. Separation studies were conducted by passing gas in laminar flow through the narrow straight channels between equally spaced parallel sheets. The ease of the flow resulted in significantly reduced pressure drop at a lower mass transfer resistance. Ruthven and Thaeron (1997) also predicted that similar advantage were to be expected for a monolithic adsorber consisting of small cylindrical passages through a solid structure of adsorbent.

Structured adsorber packing has also been gaining its significance for various adsorption applications through the fabrication of adsorbent into honeycomb structures and packed in monolithic forms with controlled adsorption properties. In the case of an activated carbon adsorbent, the open structure carbon honeycomb has shown to provide relatively high mechanical strength, thermal stability, relatively uniform porosity and a low pressure drop characteristic. The honeycomb shape also offers a relatively high surface area to volume ratio. A continuous carbon structure which eliminates the use of polymeric binders further enhances the mechanical strength and durability of the carbon honeycombs (see Gadkaree, 1998; Yates *et al.,* 2000; Valdes-Solis *et al.*, 2001).

The monolithic configuration has also been employed in the case of zeolite 5A adsorbent (see Li *et al.*, 1998a, 1998b, 2001). Such a configuration was demonstrated to yield lower pressure drop and faster pressurisation time (i.e. three to five times faster) than that of conventional packed bed. In spite of these advantages, the separation performance throughout the pressure swing cycle was found to be lower than that of the packed bed. This was attributed to the poorer film mass transfer between the gas and the monolith surface. Nonetheless, these experimental findings suggest scope for using monolith-based structures for relatively compact, power saving design.

2.6 Annular packing reactors

The use of annular packing configuration leads to a potential reduction in pressure drop. An overview on the advantages of catalyst and adsorbent packing in an annular-type configuration is given in the following sections.

2.6.1 Annular catalyst packing reactor

The performance of such annular configuration as a reliable design, which is analogous to a monolithic reactor, was studied by Beretta (1998), Beretta *et al.* (1999), Groppi *et al.* (2001) and Papadias *et al.* (2001). Their main objective was to achieve a minimal pressure drop throughout the solid-gas catalytic process relative to the performance of a conventional fixed bed reactor. Beretta (1998) has found out that even at a very high space velocity, the performance of a layer of a small amount of catalyst, which was deposited onto a ceramic tubular support and contacted longitudinally by the gas stream, was considerable at the absence of pressure drop. This implied a fully controlled diffusion regime; with minimal impact of mass transfer limitation at high temperature condition. Continual investigations were also conducted in 1999 where analysis of such a reactor configuration could well be expanded for very short contact times while maintaining the advantages of such reactor.

Further theoretical and experimental studies were then carried out by Groppi *et al.* (2001) who extended the annular configuration to a parallel flow pattern. Such an arrangement ensured negligible pressure drop at high flow rates. Small thermal gradient using such an annular reactor could also be achieved as reported by Papadias *et al.* (2001) and thus, kinetic studies could be carried out isothermally under laminar flow conditions.

2.6.2 Annular packed bed adsorber

An early account of the concept of an annular packed bed adsorber was found in the application of sulphur oxide and nitrogen separation over 5A molecular sieve adsorbent

using PSA process. Kehat *et al.* (1988) reported an increase in sulphur oxide adsorption could be achieved by increasing its feed concentration and bed total pressure while keeping the temperature and feed flow rate at a minimum during the pressurisation step. In their experimental study, the possibility of achieving low resistance to flow during the desorption step was the only advantage of utilising the annular packing configuration over the conventional packed bed system. No account on pressure drop is given.

The development of the annular packed bed adsorber configuration has since been extended to offer a larger mean cross-sectional area, and a reduced distance of travel for flow which give rise to substantial reduction of pressure drop. Subsequently, a faster mass transfer rate could be achieved for kinetically controlled adsorption process. Tierney *et al.* (1998) have reported the theoretical results on the application of computational fluid dynamics (CFD) codes to an annular geometry along with the experimental validation within the annular packed bed. Both the numerical and physical experiments were made on the basis of the gas movement through such configuration, where unobstructed distributors bound the annular bed on two sides at isothermal conditions.

Tierney *et al.* (1999) have further continued their previous work by conducting both 1-D simulation and experimental studies for the purification of dilute CO_2/air using a proprietary zeolite 4A as the adsorbent within an annular bed adsorber. Orthogonal collocation and first-order finite difference methods were applied in the model for discretization in the spatial and temporal directions respectively. These studies indicated that the annular beds did not have a major influence on the dynamics of adsorption. They also implied numerically that, at the absence of axial dispersion, the performances of annular and conventional fixed bed reactor were expected to be similar. Nonetheless, the

predicted and measured data were consistent with each other, therefore suggested a good agreement between numerical and experimental investigations.

Based on the TSA process, a non-isothermal annular-type adsorber was recently proposed by Yoshida *et al.* (2003), where the investigations have been carried out both theoretically as well as experimentally over a controlled temperature distribution. This was intended for a simultaneous separation of multi-components solutes compared to only one from a gaseous mixture in a conventional TSA process. The annular configuration was designed through which the gases were fed upward along the coaxial circular tubes, with the adsorbents filled in the annular region in between. The underlying separation principle was on the basis of a high temperature dependence and hence, the adsorption equilibrium have to be sustained in such a way that the adsorption and desorption were repeated as the thermal waves travelled slowly along the column. They have concluded that the control of the temperature distribution in the adsorber was essential in order to achieve effective separation.

2.7 Research objective: Annular-type SAR overview

Tackling the pressure drop problem has been of particular concern when it comes to an adsorptive reactor. Essentially, by creating a new means of reactor configuration, the separation performance and conversion may be enhanced significantly whilst maintaining a low pressure drop.

In this work, a 2-dimensional 2-zone model has been developed based on a monolithic model by Hoebink and Marin (1998) but with some modifications to match the assumptions associated with simultaneous adsorption and reaction. The reactor is an annular, parallel-flow type reactor such that the reactant gas flows through a parallel passage of the core gas channel, and is separated from the particles by fine wire screen gauze (see Fig.2.3). Employing the PPR principle, the gas disperses radially along the axial direction, and intraparticle molecular diffusion governs the flow in the solid zone. Instead of the PPR non-circular geometry-arrangement, which uses slabs of loosely packed catalyst that might increase mass transfer limitation bound by the bed thickness, the novel configuration will have a monolith-like constructed rigid wall channel.

This hybrid type reactor utilises the adsorptive reactor application, where it incorporates the combination of catalyst and adsorbent particles admixture, creating in situ reaction-separation process for the dehydrogenation of isobutane. Operated at isothermal and isobaric conditions, the reaction conversion performance of such a design largely depends on the geometrical design as well as the flow rates of the feed gas and intraparticle diffusion. The circular channel provides a good radial mixing, which could predominantly outweigh the performance of the square slab arrangement of PPR. The feed gas will flow in

a radial diffusive manner with presumably better convective transport. Governed by molecular diffusion inwards and outwards into the core channel, the gas stream could still be able to achieve low pressure drop characteristic relative to the randomly packed bed reactor. This system operates on inert, non-adsorbing gas purge stripping as its main adsorbent regeneration technique. The underlying mass transfer mechanism of PPR could be applied due to its analogous bed packing distribution.

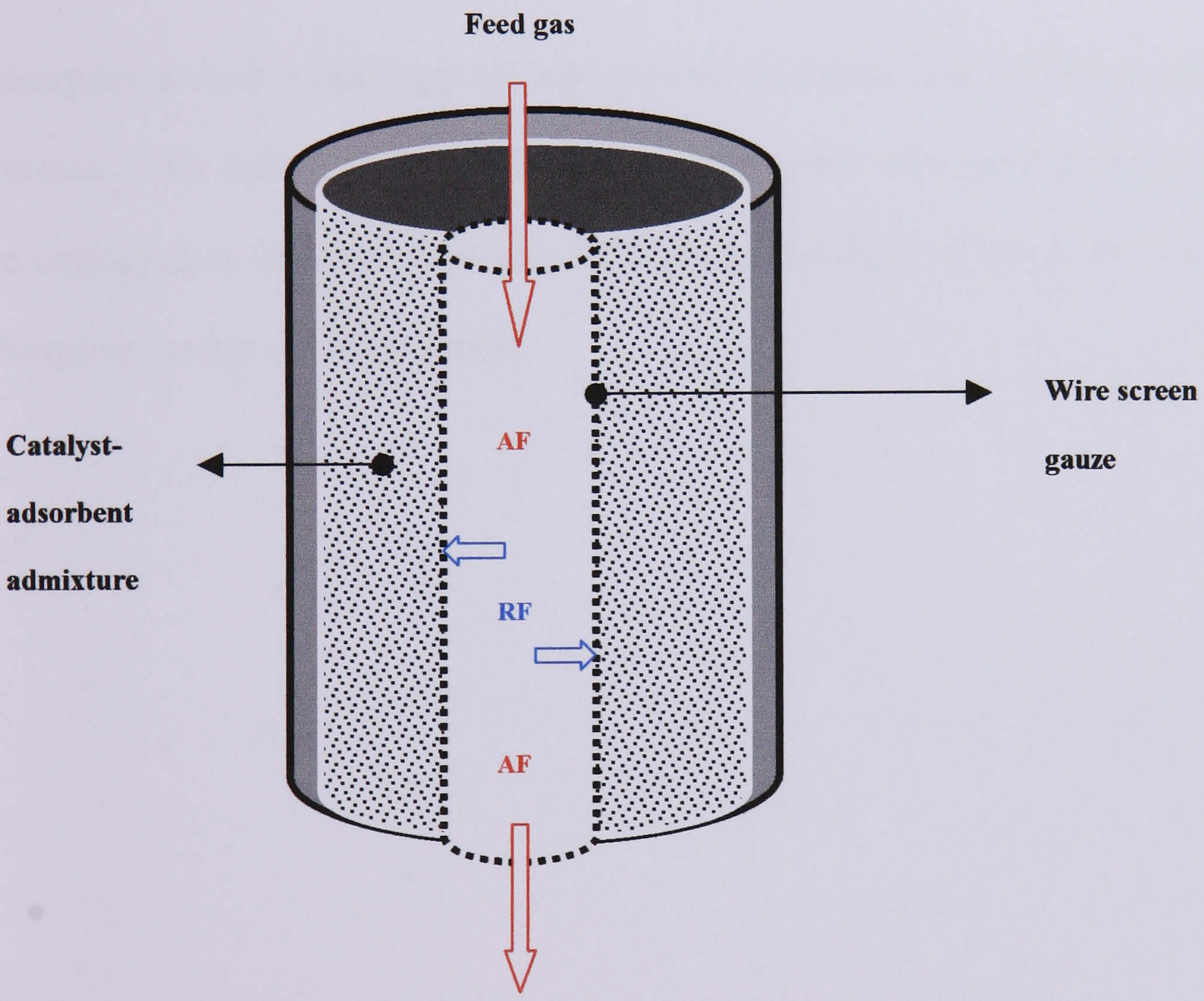


Fig.2.3 The novel annular-type SAR; AF = Axial Flow; RF = Radial Flow

2.8 Concluding remarks

The development of structured catalyst/adsorbent packing configurations, particularly in the parallel passage and monolithic type arrangement, has generated much interest due to their low pressure drop characteristic. Employing an annular type solid packing configuration has also contributed to a major improvement for catalytic and adsorption processes.

Adsorptive reactor technology to date employs traditional packed bed configuration. The potential of the hybrid reactor could well be enhanced if structured packing configurations are employed to alleviate relatively high pressure drops. In this work, an annular flow adsorptive reactor will be explored.

Chapter 3

Theoretical Background and Modelling

3.1 Introduction

In this chapter, the theoretical basis of the SAR process is presented. In particular, the theoretical background for modelling and simulation of an isothermal and isobaric, annular-type structured adsorptive reactor process is described. Discussions on the adsorption theory as well as governing intraparticle diffusions, reaction kinetic for the isobutane dehydrogenation reaction and on gas flow in the core gas channel are given.

Initially, the governing partial differential equations to model the 2-zone, 2-dimensional annular type SAR are derived. It is based on a monolithic model, where it distinguishes the process behaviour in both solid and gas phase of the reactor. To a certain extent, the solid phase equation could be compared to a PFR-like model, where the catalyst and adsorbent particles are randomly packed in an annular region of the SAR. In other words, this illustrates certain similarities to a packed bed system where both adsorption and reaction takes place in the solid phase, yet in a defined structural configuration. Contrary to the 1-dimensional model that simplifies most of the mechanistic process, this particular SAR model is chosen to depict the idea of the novel configuration by considering an

empty central gas channel where the reactant gas diffuses radially along axial direction towards the wire screen gauze by means of diffusion.

The simulation is carried out under dynamic circumstances. This will take into account the accumulation effect of each channel of the structured reactor packing, i.e. for both solid and gas phase. Both adsorption and kinetic rate expression are included in modelling the solid phase to describe the occurrence of the main reaction process. Each of the SAR and PFR performance is presented in cyclic steady state as well as single step process depending to the boundary conditions imposed to each model. The design parameters for the SAR model are either experimentally determined or evaluated using semi-empirical correlations.

This chapter begins with the background theory of the parallel passage reactor (PPR) analogous diffusion mechanism followed by isobutane dehydrogenation kinetic mechanism overview. These are presented under section 3.2. Model assumptions, governing equations and the corresponding boundary conditions are presented under section 3.3. For the reactor configuration performance comparison, a 1-dimensional PFR model is described in section 3.4 along with its corresponding boundary conditions. Section 3.5 describes the performance indices relevant for further reactor configuration assessment.

3.2 Background theory

The first part of this section focuses on the underlying mass transfer theory of the PPR which may be regarded as analogous to the diffusive transport of the SAR model. This section continues with an

account of the kinetic mechanism of isobutane dehydrogenation, which includes the proposed Horiuti-Polanyi four-step mechanism over the platinum-alumina catalyst. Although zeolite KY has been selected as the adsorbent for the conversion enhancement of the catalytic process, there is little published work describing isobutane adsorption over such adsorbent. The reasons behind the choice of employing zeolite KY is presented in Chapter 5 (see section 5.3).

3.2.1 PPR underlying mass transfer theory

In order to understand the diffusive mechanism in the SAR, the mass transfer theory of the PPR is applied to depict the likely transport phenomena in which the former geometrical configuration is analogous in terms of bed packing. Essentially, the solid material in each of the reactor type is separated from the gas channel by fine wire screen gauze.

The reactant contact with admixed particles is achieved through diffusive transport in the direction perpendicular to the convective flow in the central gas channel (see fig. 3.2). Molecular diffusion predominates in the solid zone. This governing transport mechanism becomes evident as the particles are mainly surrounded by stagnant gas and are not in direct contact with the gas stream in the central gas channel. Therefore, the catalytic reaction and adsorption that will take place will particularly be the result of intraparticle diffusion of the reactant gas across the annular bed packing.

Calis, *et al.* (1994), and Sie and Calis (1998) have outlined six consecutive steps to depict the mechanism of the mass transfer from the gas channel to the solid zone in a PPR. Neglecting the mass transfer resistance in the gas channel, the proposed steps are (see fig.3.1):

1. From the bulk flow in the gas channel to the stationary gas film at the outer surface of the wire gauze screen
2. Through the screen
3. To the edge of the bed of the particles through the stationary film at the inner surface of the bed
4. Through the interstitial channels of the bed
5. Through the stationary film around the particles
6. Through the intraparticle pores of the particles

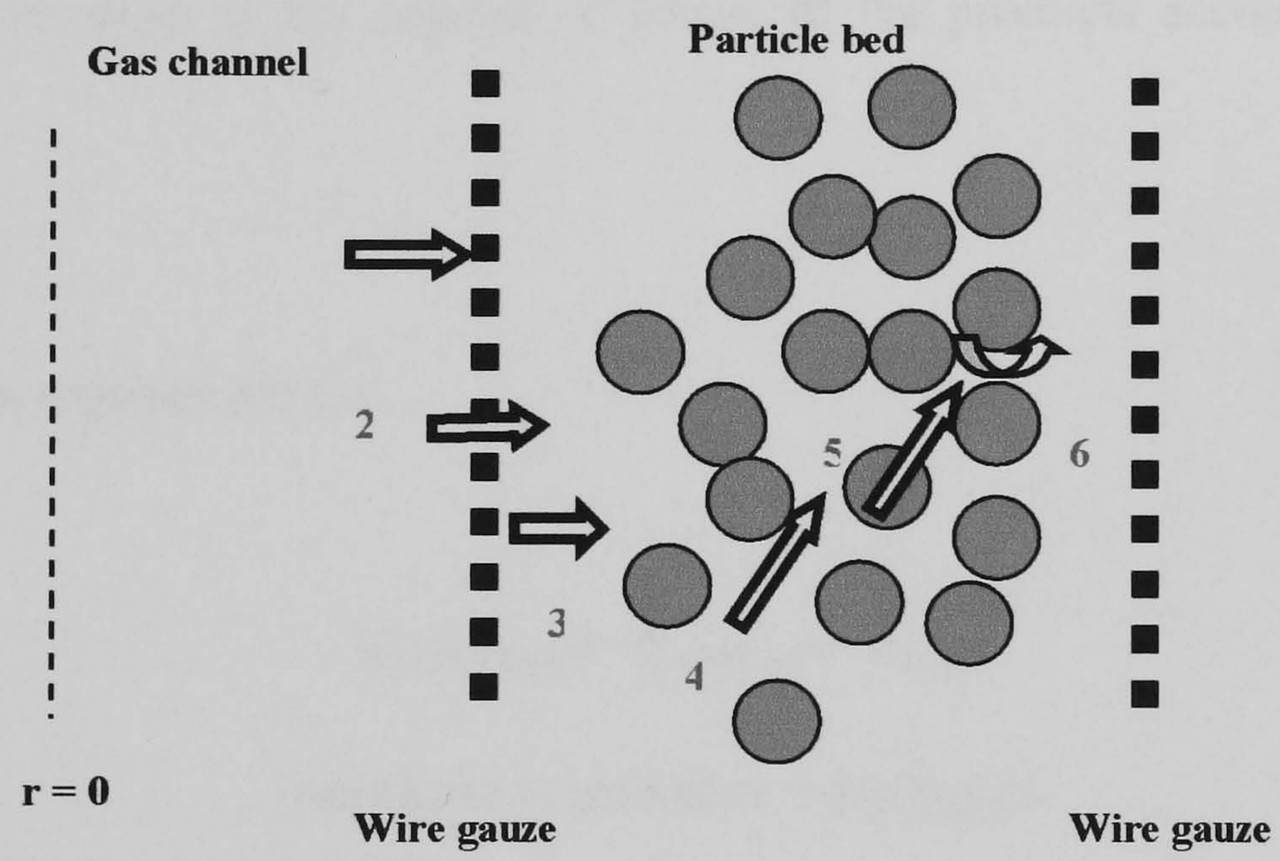


Fig.3.1 The six consecutive mass transfer steps in PPR

With reference to fig. 3.1, the diffusive transport in Step (1) may be limited by the geometry factor of the PPR gas channel. Steps (2) and (3) were deemed much faster than the other steps and therefore the mass transfer resistance at that particular positions could be neglected. The intraparticle diffusion at step (4) and step (5) are hardly distinguishable at very low gas velocities since there is an absence

of any convective transport in the bed packing. Here, the gas transport is essentially governed by molecular diffusion. In Step (6), the overall mass transfer would only be limited by temperature at isobaric condition where the governing molecular diffusion coefficient is described by Chapman-Enskog kinetic theory (see equation 3.17).

3.2.2 Isobutane dehydrogenation kinetic mechanism

The catalytic reversible dehydrogenation of isobutane is highly endothermic and therefore requires a high reaction temperature to achieve significant conversion. In addition, low pressure operation is favoured due to the increase in the number of moles of the products according to Le Chatelier's principle.

The overall reaction is represented as:

$$iC_4H_{10\,(g)} \rightleftharpoons iC_4H_{8\,(g)} + H_{2\,(g)}$$

$$\text{isobutane} \rightleftharpoons \text{isobutene} + \text{hydrogen}$$

In order to depict the kinetic mechanism of isobutane dehydrogenation, a four-step Horiuti-Polanyi mechanism is considered (see Loc *et al.*, 1987, Cortright *et al.,* 1998, and Casanave *et al.,* 1999). The four-step kinetic mechanism is thus depicted as follows:

- Dissociative adsorption of isobutane at the surface of the catalyst

$iC_4H_{10} + 2^* \rightleftharpoons iC4H_9^* + H^*$ -------- step (1) rate determining step

- Surface reaction of the adsorbed isobutane

$iC_4H_9^{*} + 2^* \rightleftharpoons iC4H_8^{**} + H^*$ -------- step (2)

- Desorption of isobutene

$iC_4H_8^{**} \rightleftharpoons iC_4H_8 + 2^*$ -------- step (3)

- Desorption of the adsorbed hydrogen

$H_2 + 2^* \rightleftharpoons 2H^*$ -------- step (4)

The symbol * represents the active surface site.

Cortright *et al.* (1998) assumed that steps (2)-(4) were quasi-equilibrated for the experimental conditions of their study, which has led to the following rate expression for the hydrogenation-dehydrogenation reactions:

$$r_{DH} = k_1 \theta_*^{\,2} \left[P_{iC_4H_{10}} - \frac{P_{iC_4H_8} P_{H_2}}{K_{eq}} \right]$$

where r_{DH} was the net dehydrogenation rate, k_1 the rate constant for the dissociative adsorption of isobutane, step (1), K_{eq} the overall equilibrium constant for isobutane dehydrogenation, and θ_* is the fraction of sites that was free of the adsorbed species which was less than 10^{-5} at the reaction conditions. That value of θ_* was dependent on the adsorption/desorption equilibria for hydrogen and isobutene and could be determined from the following expression:

$$\theta_* = \frac{-K_3}{4P_{iC_4H_8}}\left[1+\sqrt{K_4P_{H_2}}-\sqrt{1+K_4P_{H_2}+\frac{8P_{iC_4H_8}}{K_3}+2\sqrt{K_4P_{H_2}}}\right]$$

where K_3 was the equilibrium constant for isobutene desorption in step (3), and K_4 the equilibrium constant for hydrogen adsorption in step (4).

In terms of choice of catalyst, platinum-alumina came as the prime one as platinum itself is considered a highly active catalytic element and is not required in large quantities to catalyze the dehydrogenation reaction (Bhasin et al, 2001). Combined with its alumina support, it has excellent thermal stability and mechanical strength under processing, transport and catalyst regeneration conditions. In addition, such alumina support possesses the superior capability to maintain a high degree of platinum dispersion, which is essential for achieving high dehydrogenation activity and selectivity. Prior to the introduction of isobutane into the catalytic reaction zone, it is necessary to feed certain amount of hydrogen upon the platinum-alumina catalyst, such that it could suppress the formation of hydrogen-deficient carbonaceous deposits (Dyroff, 2002).

3.3 SAR mathematical modelling

The monolith reactor mathematical model is applied to describe the adsorption and reaction kinetic properties as well as the transport phenomena of the SAR. It is based on the concept where flow along the monolithic channel wall corresponds to fully developed laminar flow profile due to molecular diffusion. The classical problems due to the gas flow behaviour in a fixed bed reactor could be resolved, hence the great reduction of the pressure drop across the reactor. Nonetheless, the modelling still requires an understanding of the theoretical basis of the intraparticle diffusion limitation as well as adsorption and reaction kinetics in the annular section of the reactor. In the following discussion, the assumptions of the general model are first given followed by the governing process equations.

3.3.1 Model assumptions

Model assumptions are divided into two sections to account for the gas and bed properties, and the process operation. Where applicable, additional assumptions for specific applications or extensions of the model will be given in the text.

a) Assumption for the gas channel and annular packed bed properties

- Negligible radial convective velocity
- Fully developed, incompressible laminar flow in the channel
- Constant voidage, temperature and particle size, uniformly packed with adsorbent and catalyst
- The axial velocity along radial distance obeys Newton's Law of Viscosity at maximum shear stress

- Ideal gas behaviour
- Adsorption rate described by a linear driving force approximation
- Adsorption equilibrium described by a linear isotherm
- Reaction rate expressed in simple power-law
- Axial and radial diffusion in the fluid phase are included because of the reasonably low convective transport
- Negligible convective transport in the solid phase

b) Assumptions for Process Operation

- Constant temperature and composition of feed gas
- Isothermal, isobaric and adiabatic operation
- Absences of pressure gradient in the cross-sectional area at the entrance and exit points
- Negligible dead volumes in the feed and product outlet sections of the reactor
- Negligible pressure drop across the inlet and outlet of the bed

3.3.2 Governing equations

Based upon the above assumptions, the component material balances for the annular-type SAR can be described as:

General material balance:

$$\begin{bmatrix}\text{Rate of}\\ \text{accumulati on}\\ \text{of component i,}\\ \text{in elemental}\\ \text{volume}\end{bmatrix} = \begin{bmatrix}\text{Flowrate of}\\ \text{component i,}\\ \text{IN of elemental}\\ \text{volume}\end{bmatrix} - \begin{bmatrix}\text{Flowrate of}\\ \text{component i,}\\ \text{OUT of elemental}\\ \text{volume}\end{bmatrix} + \begin{bmatrix}\text{Rate of}\\ \text{generation}\\ \text{of component i,}\\ \text{in elemental}\\ \text{volume}\end{bmatrix} \quad 46$$

General material balance:

$$\begin{bmatrix}\text{Rate of accumulati on of component i, in elemental volume}\end{bmatrix} = \begin{bmatrix}\text{Flowrate of component i, IN of elemental volume}\end{bmatrix} - \begin{bmatrix}\text{Flowrate of component i, OUT of elemental volume}\end{bmatrix} + \begin{bmatrix}\text{Rate of generation of component i, in elemental volume}\end{bmatrix} \quad (3.1)$$

This general balance equation is applied for both gas and solid phases.

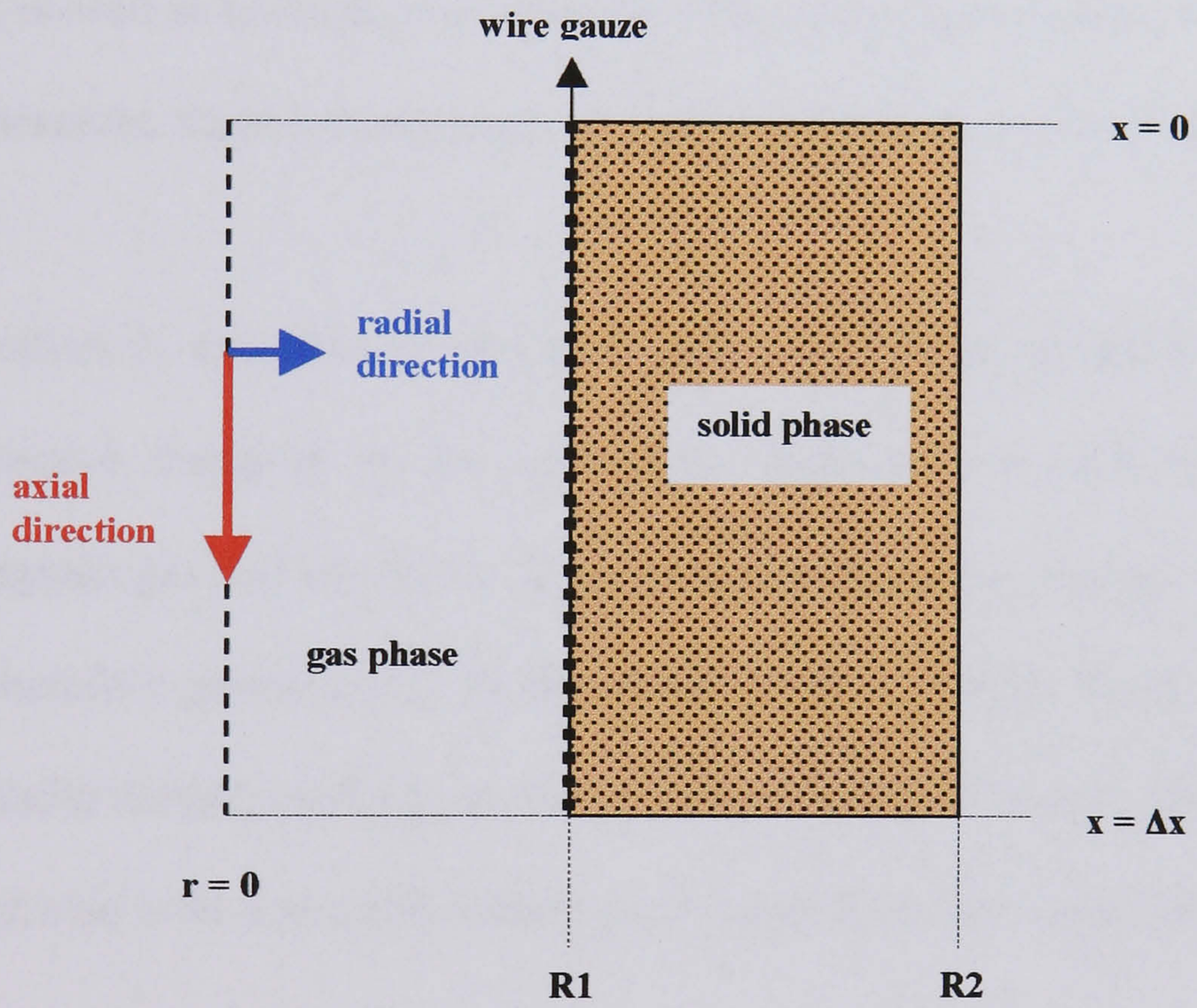


Fig.3.2 Elementary diagram of a section of SAR for mathematical modelling purpose

The mathematical model presented in this work distinguishes the two zones in the SAR reactor, i.e. the gas phase and solid phase (see fig.3.2). The mass transfer and flow mechanism are subject to the boundary conditions described in section 3.3.3.

(3.2)

where x, r and t are the axial, radial and temporal coordinates respectively, C_i is the gas phase molar concentration of component i (mol m^{-3}), v_x is the axial superficial velocity (m s^{-1}),and D_i is the molecular diffusion coefficient (or also denoted as D_m) for both axial and radial directions of component i (m^2 s^{-1}). This equation describes the mass transport phenomena in an empty core gas channel where only feed and reacted gas flows across the channel in both axial and radial directions towards its outlet as well as towards and outwards of the wire screen gauze, which separates the solid and gas phase. Therefore, there is no reaction or separation process occurs in this section.

The convective effect is excluded in the solid phase component material balance to signify the absence of convective transport in the solid phase annulus. The solid particles are essentially surrounded by stagnant gas and are not in direct contact with the gas stream. The mass transfer of the component i is therefore governed by molecular diffusion. Catalytic reaction and separation takes place in this particular annular packing section and hence, reaction and adsorption kinetic expressions are included which also infer a possible admixture of catalyst and adsorbent packing in this region.

Extending and modifying equation (3.2) yields

$$\varepsilon_t \frac{\partial C_i}{\partial t} = D_i \frac{\partial}{\partial x}\left(\frac{\partial C_i}{\partial x}\right) + \frac{D_i}{r}\frac{\partial}{\partial r}\left(r\frac{\partial C_i}{\partial r}\right) + \left(\rho_{bed}^{cat} \bullet R_1\right) - \left(\rho_{bed}^{ads} \bullet R_2\right) \qquad (3.3)$$

ε_t is the total bed voidage defined by

$$\varepsilon_t = \varepsilon_b + \varepsilon_p\left(1 - \varepsilon_b\right)$$

(3.4)

where ε_p and ε_b are the bed intraparticle and interparticle void fractions respectively. Assuming ideal gas behaviour, the component gas phase concentration is related to the total pressure P by

$$\frac{P}{R_{gas}\ T} = \sum_{i=1}^{n} C_i \qquad (3.5)$$

where P is the total pressure (Pa), R_{gas} the universal gas constant (J mol^{-1} K^{-1}), T the operational temperature of the reactor (K) and n the total number of components. The component gas phase concentration is also related to the component mole fraction, y_i , i.e.

$$C_i = y_i \sum_{i=1}^{n} C_i \qquad (3.6)$$

R_1 represents the overall reaction rate for component i (mol m^{-3} s^{-1}) while R_2 is the adsorption rate of component i (mol kg^{-1} s^{-1}) expressed in LDF form. The bulk density of catalyst and adsorbent denoted by ρ^{cat} and ρ^{ads} (kg m^{-3}) respectively.

Velocity Profile

B.U.C. LOUVAIN-LA-NEUVE

Essentially, the axial velocity profile in the radial direction is a simplified continuity equation of momentum balance based on the Newton's Law of viscosity taking into account the maximum velocity, average velocity and the maximum shear stress at the wall surface. Therefore, for a fully developed laminar flow, the velocity profile considered in this work is expressed as

$$v_x(r) = 2\,v_{x,ave}\left[1-\left(\frac{r}{R1}\right)^2\right] \tag{3.7}$$

where $v_{x,ave}$ ($m\ s^{-1}$) represents the average inlet velocity along the fully developed velocity profile across the core gas channel. Assuming incompressibility, the velocity is inversely proportional to R1, which is the radius of the core gas channel. In addition, the kinetic contribution to pressure loss becomes negligible due to laminar flow along a smooth wall.

The Reaction Kinetic Model

The overall isobutane dehydrogenation reaction expressed in section 3.2.2 is represented in the following reaction scheme:

$$A \underset{k_2}{\overset{k_1}{\Leftrightarrow}} B + C \tag{3.8}$$

where A, B and C denote isobutane, isobutene and hydrogen correspondingly and k_1 and k_2 are the forward and backward reaction rate constants respectively (s^{-1}) related by the equilibrium constant

$$K_{eq} = \frac{k_1}{k_2} \tag{3.9}$$

where K_{eq} is the reaction equilibrium constant (mol m^{-3}). Cortright *et al.* (1998) reported that at reaction temperature of 673-773K, the rate of isobutane dehydrogenation is nearly first order, suggesting that the surface coverage by adsorbed isobutyl species is low. Therefore, simple power-law kinetics is considered for a pseudo-first order reaction and the overall reaction rate, R_1 from equation (3.3) can be written as

$$R_1 = \upsilon_i^{stoich} \bullet k_1 \bullet \left(C_A - \frac{C_B C_C}{K_{eq}} \right) \tag{3.10}$$

K_{eq} is evaluated by the thermodynamics of the reaction at equilibrium and k_{fwd} (i.e. forward rate constant k_1) is determined experimentally. The stoichiometric coefficient, υ_i^{stoich} defined as

$\upsilon_i = -1$ for reactant;

$\upsilon_i = +1$ for product

Adsorption kinetic

Gas-solid mass transfer resistances determine the rate of adsorption of a molecule onto an adsorbent particle. These may be either due to internal particle structure i.e. intraparticle resistance, or due to an external fluid film surrounding a particle, i.e. extraparticle resistance, or due to a combination of both resistances.

In the case of intraparticle mass transfer limitations, they mainly arise from microporous structure of adsorbents and are dependent on the adsorbent pore diameter distribution. Four transport mechanisms may be identified within a pore of an adsorbent as proposed by Ruthven (1984):

- Knudsen diffusion
- Surface diffusion
- Molecular diffusion
- Poiseuille flow

To distinguish the dominating mechanisms, three criteria are involved in the diffusion process:

- The relative magnitudes of the pore diameter, d_{pore} (m) to the mean free path, γ (m), of the diffusing molecules
- The nature of the physical interactions between the pore walls and the diffusing molecules
- The magnitude of the pressure drop within the pore for larger pores

The first criterion distinguishes between a molecular and Knudsen flow regime. Therefore, when there are negligible interactions between gas molecules and pore walls, i.e. $d_{pore} >> \gamma$, molecular diffusion predominates. Knudsen diffusion on the other hand is more dominant when there are

substantial molecular collisions with the pore wall, i.e. $d_{pore} << \gamma$. The second criterion describes surface diffusion where there is strong adsorption through the physical adsorbed layer. Poiseuille diffusion falls under the third criteria in the case when there is a large pressure drop across a single particle.

From previous assumption, the rate of adsorption in a particle, R_2, (mol kg^{-1} s^{-1}) from equation (3.3) is expressed in terms of the linear driving force (LDF) model of Glueckauf and Coates (1947),

$$R_2 = \frac{\partial q_i}{\partial t} = k_{mass,i}\left(q_i^* - q_i\right) \tag{3.11}$$

where q_i is the average adsorbed phase concentration of component i in a particle (mol kg^{-1}), q^*_i equilibrium adsorbed phase concentration of component i in a particle (mol kg^{-1}), and k_{mass} the mass transfer coefficient, for a component i (s^{-1}) can be expressed as

$$k_{mass,i} = \frac{15\,\bar{D}_{e,i}}{r_p^{\,2}} \tag{3.12}$$

where $\bar{D}_{e,i}$ is the modified effective diffusivity of D_e from equation B.3 (see Appendix B) and r_p the mean particle radius (m). This modified effective diffusivity coefficient, $\bar{D}_e$ (m^2 s^{-1}), is often dependent on contributions from more than one of these diffusional transport mechanisms. This will then determine the mass transfer coefficient, k_{mass} (s^{-1}), which can be treated as a fitting parameter for mass transfer where a large value of k_{mass} indicating the instantaneous local equilibrium model.

Detailed calculations for the determination of $k_{mass,i}$ values for the adsorption of C_4 components on zeolite KY are presented in Appendix B.

Adsorption Isotherm

At a specific temperature T (K), the adsorption isotherm relates the equilibrium adsorbed q^*_i (mol kg^{-1}) to the local gas phase concentration, C_i (mol m^{-3}) in this expression:

$$q_i^* = f(C_i, T) \tag{3.13}$$

Ruthven (1984) and Yang (1987) have presented reviews as well as proposed several models to predict pure and multicomponent isotherms. Langmuir type models have been considered amongst the simplest form of isotherms in which they are deemed adequate in predicting both physical and chemical adsorption. For adsorption of a pure adsorbate i, the Langmuir isotherm is given as

$$\frac{q_i^*}{q_{si}} = \frac{b_i C_i}{1 + b_i C_i} \tag{3.14}$$

where q_{si} denotes the maximum (saturation) amount which can be adsorbed onto a solid at equilibrium (mol kg^{-1}) , b_i is the Langmuir adsorption constant for the specific adsorption process (m^3 mol^{-1}) and C_i the gas-phase molar concentration of component i (mol m^{-3}). For a gas mixture of n components, equation (3.14) can be extended to

$$\frac{q_i^*}{q_{si}} = \frac{b_i C_i}{1 + \sum_{i=1}^{n} b_i C_i}$$

(3.15)

The extended Langmuir equation could be simplified to a linear form in the case of low adsorbate concentrations and it is expressed as

$$q_i^* = q_{si} b_i C_i = m_i C_i R_{gas} T \tag{3.16}$$

where m_i is usually referred to as the adsorption isotherm gradient (mol kg^{-1} Pa^{-1}), and its values are determined experimentally.

Governing diffusion transport

Molecular diffusion, D_i (m^2 s^{-1}) is inversely proportional to the pressure for a binary gas mixture at a low pressure and increases with the increasing temperature. At high pressure however, it no longer varies inversely with pressure. In this work, the diffusivity is a simplified derivation using the Chapman-Enskog kinetic theory. Therefore for ideal gas condition, D_{AB} (m^2 s^{-1}) (see Bird *et al.*, 1960):

$$D_{AB} = 1.8583 \times 10^{-7} \frac{\sqrt{T^3\left(\frac{1}{M_A} + \frac{1}{M_B}\right)}}{P\,\sigma_{AB}^2\,\Omega_{AB}} \tag{3.17}$$

where T is the reactor temperature (K), M_A , M_B are the molecular weight of species A and B, which in this work represents isobutane (58.124 g mol^{-1}) and nitrogen (28.00 g mol^{-1}), P is the total pressure (atm), σ^2_{AB} is Lennard-Jones collision diameter for A and B (m) and Ω_{AB} is the corresponding dimensionless collision integral. Details of the calculation are presented in Appendix A.

3.3.3 Boundary conditions of the SAR model

The initial conditions for both solid and gas phase at all position of axial and radial domains are set experimentally where the beds only contain nitrogen, which is the inert diluent gas at atmospheric pressure, and the adsorbent is free of adsorbates.

Initial conditions:

$\forall x$, $\forall r$, $t=0$

$$y_i = 0 \, , \forall \, i \neq 1 \tag{3.18}$$

$$y_{nitrogen} = \frac{P}{R_{gas} T} = \sum_{i=1}^{n} C_i \tag{3.19}$$

$$P = P_{atm} \tag{3.20}$$

$$q_i = 0 \tag{3.21}$$

Gas phase:

i) At the entrance,

$$x = 0, \quad C = C_i^{in} \quad \text{for} \quad 0 < r \leq R1 \tag{3.22}$$

ii) At the maximum centre,

$$r = 0, \quad \frac{\partial C_i}{\partial r} = 0 \quad \text{for } \forall x \tag{3.23}$$

iii) At the core channel end,

$$x = L, \quad \frac{\partial C_i}{\partial x} = 0 \quad \text{for} \quad 0 \leq r \leq R1 \tag{3.24}$$

Solid phase:

i) At the top and bottom loading,

$$\text{for} \quad R1 < r \leq R2$$

$$x = 0, \quad \frac{\partial C_i}{\partial x} = 0 \quad \text{and} \quad x = L, \quad \frac{\partial C_i}{\partial x} = 0 \tag{3.25}$$

ii) At the wall of the packing side,

$$r = R2, \quad \frac{\partial C_i}{\partial r} = 0 \quad \text{for} \quad 0 < x < L \tag{3.26}$$

iii) Linear Adsorption rate and Equilibrium Adsorption Isotherm:

$$\text{for} \quad 0 \le r < R1 \;, \quad \forall x$$
$$\frac{\partial q_i}{\partial t} = 0 \quad ; \quad q_i^* = 0 \tag{3.27}$$

Velocity profile boundary conditions:

$$\text{for} \quad R1 < r \le R2$$
$$v_x(r) = 0 \tag{3.28}$$

Extended Cyclic Steady State Boundary Conditions of SAR

At gas phase and solid phase, the boundary conditions follow exactly as in the single-step model.

Therefore, the modification is made in the desorption step:

Gas phase:

At the entrance,

$$x = 0 \;, \; \sum_{i=1}^{n} C_i = \frac{P}{R_{gas}\, T} \quad \text{for} \quad 0 < r \le R1 \tag{3.29}$$

3.4 PFR model

The PFR model is a 1-D model describing the conventional packing configuration of catalyst-adsorbent particles. From equation (3.3), it is modified to:

$$\varepsilon_t \frac{\partial C_i}{\partial t} = -v_{ave} \frac{\partial C_i}{\partial x} + D_x \frac{\partial}{\partial x}\left(\frac{\partial C_i}{\partial x}\right) + \left(\rho_{bed}^{cat} \bullet R_1\right) - \left(\rho_{bed}^{ads} \bullet R_2\right)$$

(3.30)

where v_{ave} is the superficial velocity throughout the bed and D_x is the axial bed dispersion ($m^2\ s^{-1}$).

Axial Dispersion

For gas flow in a packed bed, some degree of backmixing or intermixing will result in a deviation from plug flow regime. This mixing phenomenon arises from local fluctuations in flow velocities and molecular and turbulent (eddy) diffusion within the packed bed. Such effects predominate in the axial direction, where bed diameters much greater than the particle diameter, and the flow is said to be axially dispersed plug flow. A statistically random manner of the axial mixing in a repeated mixing distribution is expressed as Fickian-type diffusion in the form of

$$\frac{\partial C}{\partial t} = \frac{\partial}{\partial x}\left[D_x \frac{\partial C}{\partial x}\right] \tag{3.31}$$

where D_x , the axial dispersion coefficient is a lumped parameter accounting for all mechanisms responsible for axial mixing effect. In this work, D_x is a simplified form of the Langer *et al.* (1978) correlation (see Alpay, 1992, Sheikh, 1999):

$$D_x = \frac{\varepsilon_b D_i}{\tau_x} + \frac{(v d_p)^2}{Pe_\infty\left(v d_p + \beta_r \varepsilon_b \frac{D_i}{\tau_x}\right)}$$

(3.32)

where ε_b is the bed particle voidage, τ_x the axial bed tortuosity factor, v the interstitial inert gas velocity (m s^{-1}), d_p the mean particle diameter (m), D_i the molecular diffusion for binary system derived from Chapman-Enskog kinetic theory (m^2 s^{-1}), Pe_∞ is the limiting value of the dimensionless Peclet number and β_r is the radial dispersion factor. Further details on D_x calculation are presented in Appendix A.

3.4.1 PFR Boundary conditions

Initial conditions:

$\forall x$, t=0

$$y_i = 0 \, , \forall \, i \neq 1 \tag{3.33}$$

$$y_{nitrogen} = \frac{P}{R_{gas} \, T} = \sum_{i=1}^{n} C_i \tag{3.34}$$

$$P = P_{atm} \tag{3.35}$$

$$q_i = 0 \tag{3.36}$$

At the entrance:

- For single step PFR model

$$x = 0\,, \quad C = C_i^{in} \tag{3.37}$$

- For cyclic steady state, desorption step

$$x = 0\,, \quad \sum_{i=1}^{n} C_i = \frac{P}{R_{gas}\,T} \tag{3.38}$$

At the channel end,

$$x = L\,, \quad \frac{\partial C_i}{\partial x} = 0 \tag{3.39}$$

3.5 Performance indices

The reactor configuration performance is assessed in terms of the reaction conversion, conversion enhancement effect and energy input consumption. Each of the stated indices would determine the effectiveness of using SAR packing arrangement relative to the conventional packed bed adsorptive reactor.

3.5.1 Reaction conversion

In general, the reaction conversion can be defined as:

$$X_A = \frac{\text{Total inlet molar flowrate of A in gas phase} - \text{Total outlet molar flowrate of A in gas phase}}{\text{Total inlet molar flowrate of A in gas phase}} \quad (3.40)$$

In the case of SAR model, it is mathematically expressed as

$$X_{i=1} = \frac{\left(\int_{r=0}^{R1} C_{i=1,x=0,r}\, v_x\, dr\right) - \left(\int_{r=0}^{R1} C_{i=1,x=L,r}\, v_x\, dr\right)}{\left(\int_{r=0}^{R1} C_{i=1,x=0,r}\, v_x\, dr\right)} \quad (3.41)$$

For single-step SAR model, isobutane accumulation effects in both gas and solid phase as well as adsorption accumulation in the solid phase are taken into consideration.

Thus, this is extended to:

$$X_{i=1} = \frac{\left(A_{gas}\int_{r=0}^{R1} C_{i=1,x=0,r}\, v_x\, dr\right) - \left(A_{gas}\int_{r=0}^{R1} C_{i=1,x=L,r}\, v_x\, dr\right) - \left(V_{gas}.C_{gas}\right) - \left(V_{sol}.\varepsilon.C_{sol}\right) - \left(V_{sol}.\rho_b.q_{min}\right)}{\left(A_{gas}\int_{r=0}^{R1} C_{i=1,x=0,r}\, v_x\, dr\right)} \quad (3.42)$$

and C_{gas} (t), C_{sol} (t) are defined as concentration accumulation at gas and solid phase respectively, and q_{min} (t) is the adsorption accumulation at solid phase of reactant component, i.e.

$$C_{gas} = \frac{2}{R1^2 L} \int_{x=0}^{L} \int_{r=0}^{R1} r\, C_{i=1,x,r}\, dr\, dx \tag{3.43}$$

$$C_{sol} = \frac{2}{L\left[R2 - R1\right]^2} \int_{x=0}^{L} \int_{R1}^{R2} r\, C_{i=1,x,r}\, dr\, dx \tag{3.44}$$

$$q_{min} = \frac{2}{L\left[R2 - R1\right]^2} \int_{x=0}^{L} \int_{R1}^{R2} r\, q_{i=1,x,r}\, dr\, dx \tag{3.45}$$

A_{gas} is the cross-sectional area of the gas channel (m^2), V_{sol} the total volume occupied in the annular section of SAR (m^3), V_{gas} the core gas channel volume of SAR (m^3), L the SAR length (m), R1 and R2 the radii of gas channel and total reactor radius (m). On the other hand, the continuous cyclic operation eliminates the reactant concentration and adsorption accumulation effects and so the standard conversion equation (3.41) applies.

The reaction conversion in both cyclic steady state and single-step 1-D PFR model is expressed as

$$X_{i=1} = \frac{\left(C_{i=1,x=0}\, v_{ave}\right) - \left(C_{i=1,x=L}\, v_{ave}\right)}{\left(C_{i=1,x=0}\, v_{ave}\right)} \tag{3.46}$$

3.5.2 Conversion enhancement factor

Prior to adsorbent equilibration, the effect of in situ adsorption during the catalytic dehydrogenation reaction is observed at the step changes of the transient response curve. The conversion enhancement effect resulting from in situ adsorption at any time is investigated by calculating the normalised conversion of isobutane in the presence (ad) and absence (nad) of adsorbent and is expressed by:

$$E(t) = \frac{(X_{i=1})_{ad} - (X_{i=1})_{nad}}{(X_{i=1})_{nad}} \times 100 \qquad (3.47)$$

where E (t) is the conversion enhancement factor. E (t) > 0 implies conversion enhancement in the presence of adsorbent. On adsorbent equilibration, E (t) approaches zero (see Ding and Alpay, 2000). The enhancement effect is predicted to be more pronounced at lower temperature reaction operation due to the exothermic behaviour of adsorption.

This equation (3.47) applies to both SAR and PFR model.

3.5.3 Energy input

The energy input, E_{input} (J s^{-1}) is defined as the cycle average rate of heat supply to raise an inlet stream from ambient temperature, T_o (298K) to the reactor isothermal temperature, T and is expressed as

$$E_{input} = \frac{P}{R_{gas}\, T} A_{gas}\, v_{ave}\, c_{Pg} (T - T_o)$$

(3.48)

where c_{Pg} is the specific heat capacity of bulk gas (i.e. nitrogen) (J mol^{-1} K^{-1}) and A_{gas} of SAR is equivalent to the cross-sectional area of the PFR reactor model for simulation and optimisation studies in Chapter 7.

3.6 Concluding remarks

The SAR mathematical modelling was developed based on the monolith reactor model developed by Hoebink and Marin (1998). The design concept intended to incorporate the favourable characteristics of a monolith and parallel passage type designs.

The inclusion of adsorption and reaction kinetics expression in the solid phase material balance enabled the reaction enhancement assessment using the novel reactor configuration at specific design parameters and operating conditions. Tests on the validity of the model are presented in Chapter 5.

Chapter 4

Experimental Apparatus

4.1 Introduction

The validity of the mathematical model described in Chapter 3 can be verified by conducting a series of experiments using pilot scale SAR and PFR reactors. Prior to conducting the experimental work, the rig needs to be constructed and assembled. In this Chapter, the description of the experimental apparatus and standard experimental procedures are presented. The rig in this work comprises three main sections: ancillary lines, reactor unit and gas chromatography (GC) unit.

The next section describes the ancillary lines of the rig, which consists of feed gas supply and product delivery. Section 4.3 deals with the design aspect of the reactors studied with more emphasis given to the SAR design. While the PFR is a simple stainless steel tube, the SAR design is more complex. It is constructed in such a way that it could house a fine sintered gauze tube inside the main shell tube in order to ensure complete separation of the solid material from the feed gas. More details on this reactor design and accompanying mechanical drawing is presented in section 4.3.

Section 4.4 focuses on the GC unit and the related commissioning work, which include GC carrier gas and feed gas calibrations. Section 4.5 presents the standard experimental procedures: gas leak testing solid drying, catalyst activation, as well as GC column conditioning.

4.2 Ancillary lines

The ancillary line of the rig can be divided into two main sections: feed gas supply and product delivery and vent line. Fig.4.1 shows the arrangement of each section. Each line is constructed using ¼" OD stainless steel tube and connected using Swagelok fittings.

The gas pressure of each feed gas supply is manually controlled using the regulator valve. A pressure gauge is located on the main feed line towards the reactor unit to give indication that there is sufficient gas pressure to be fed into the reactor. A 2-way valve, V1 in which the valve opens at only one direction at a time, connects the 10% H_2 in N_2 carrier and pure N_2 line. The main feed line is operated by manually switching from one feed stream to another via a 3-way valve. This is purposely for simulating a cyclic process whereby it allows the user to immediately switch from the feed gas stream to N_2 stream for regeneration step. Each feed gas line is fitted with a no-return valve as a safety measure to prevent any back flow of the gas when the system is in operation. The feed flow rates at STP are measured using two calibrated mass flow controller of model Brooks 5850E and the flow rates are manually set and monitored using an Aalborg GFM-17 mass flow meter.

The product delivery line is insulated to achieve a near isothermal condition. Here, the product gases are collected by bypassing a product exhaust connector. A one way valve, V4 on the vent line is closed to direct the gases from the connector into the 1/16" product sample line. During solid drying (as well as during analysing time for a single step process), V4 is switched open and the 1/16" sample line is connected to Vent line 2 (see fig.4.1). This allows removal of any trapped reacted gas to be purged towards the fume cupboard through Vent line 1 and Vent line 2.

Three types of feed gas mixtures were employed in this work:

- Stream 1 is subdivided into two feed gas supplies:
  - Pure N_2 (99.995% v/v)
  - 10% H_2 in N_2 carrier

- Stream 2
  - Premixed reaction gas consisting of 95% (v/v) nitrogen, 4.8% (v/v) isobutane, and 0.1% (v/v) of each of isobutene, methane, and hydrogen

Pure N_2 is mainly fed during the adsorbent drying and regeneration step. It does not react with the catalyst. The dilute H_2 is used for catalyst activation only. All the feed gases are fed at ambient temperature and obtained in certified pressurised cylinders supplied by BOC Gas Ltd.

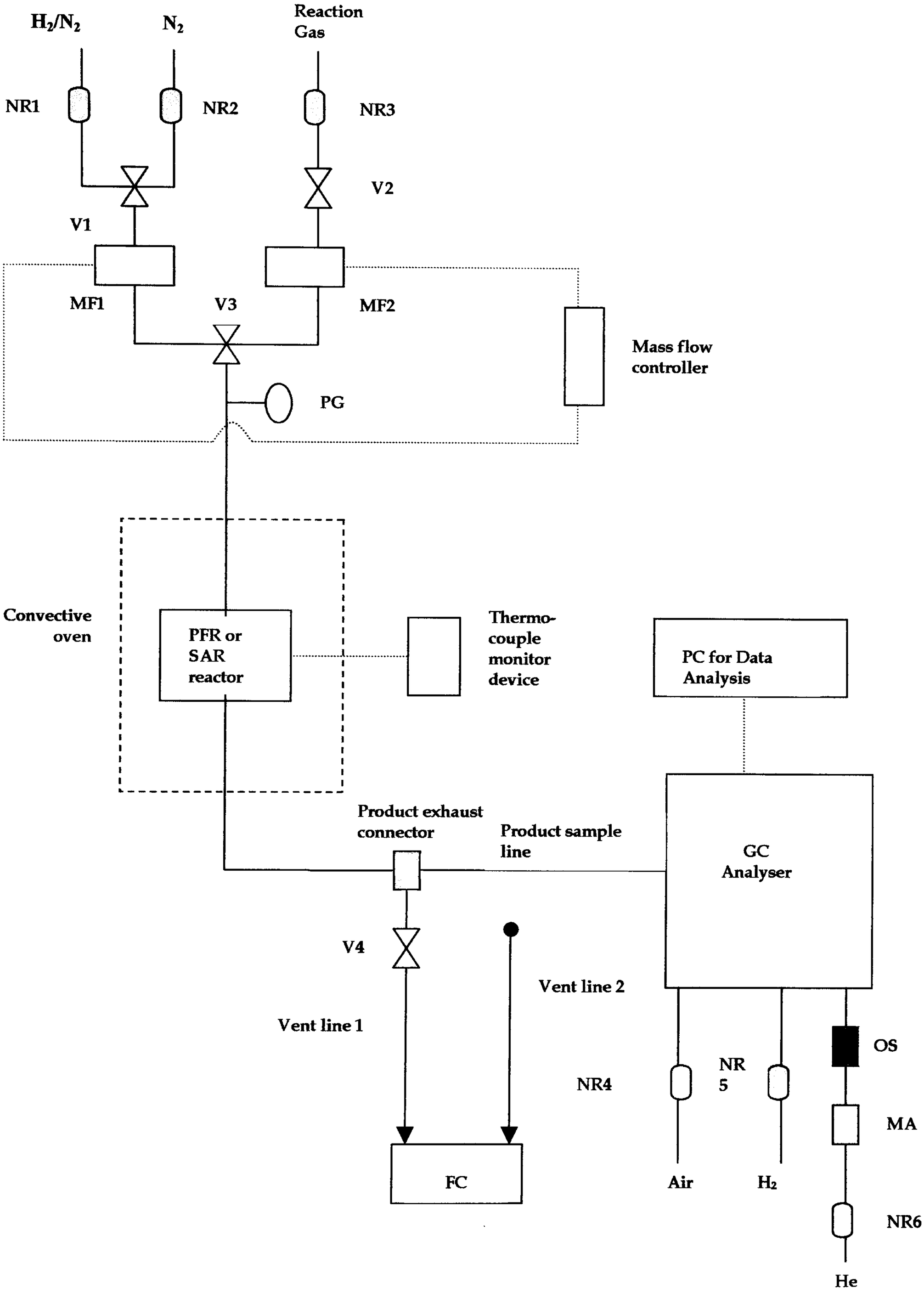


Fig.4.1 A schematic diagram of the experimental rig. NR= no-return valve; V1, V2 = 2-way valve; V3 = 3-way valve; V4 = one-way valve; MF1, MF2 = mass flow meter; PG = Pressure gauge; MA = Moisture Absorber; OS = Oxygen Scrubber; FC = Fume Cupboard

4.3 Reactor unit and configuration

The reactor unit consists of a reactor column, a convective oven, and three type-K thermocouples system. The column is fitted inside the convective oven using Swagelok connections. Each of the type-K thermocouples are connected to the outer reactor wall using a thin piece of stainless steel wire. The thermocouples are placed along the inlet, middle and outlet section of the column. The reaction temperature is set and monitored at the control box of the convective oven.

There are two reactor configurations used in the experimental work: SAR and PFR. Descriptions of each reactor are now presented.

4.3.1 PFR

The PFR is simply a stainless steel (type 316) tube of 0.00452m ID and 0.14m length. Swagelok fittings are used to connect the reactor to the feed and product lines. Particles retention within the tube is achieved by use of glass-wool plugs.

4.3.2 SAR

The SAR reactor was constructed within the Chemical Engineering department workshop. It consists of a sintered stainless steel central gas channel (10.5mm O.D. and ~0.008m ID) and fitted inside a stainless steel outer shell tube of ~0.014m ID. The total length of the reactor is 0.14m. The sintered tube is made of a roll of multi-layered, very fine wire mesh of 1 micrometer (μm) and is manufactured and supplied by Plastok Ltd while the outer shell tube is supplied by TW Steel. The reactor arrangement as illustrated in fig.4.4 can be viewed as a hybrid between monolith, parallel passage and annular reactor type structures.

Figs 4.2 and 4.3 show snapshots of the sintered stainless steel tube used.



Fig.4.2 The sintered tube

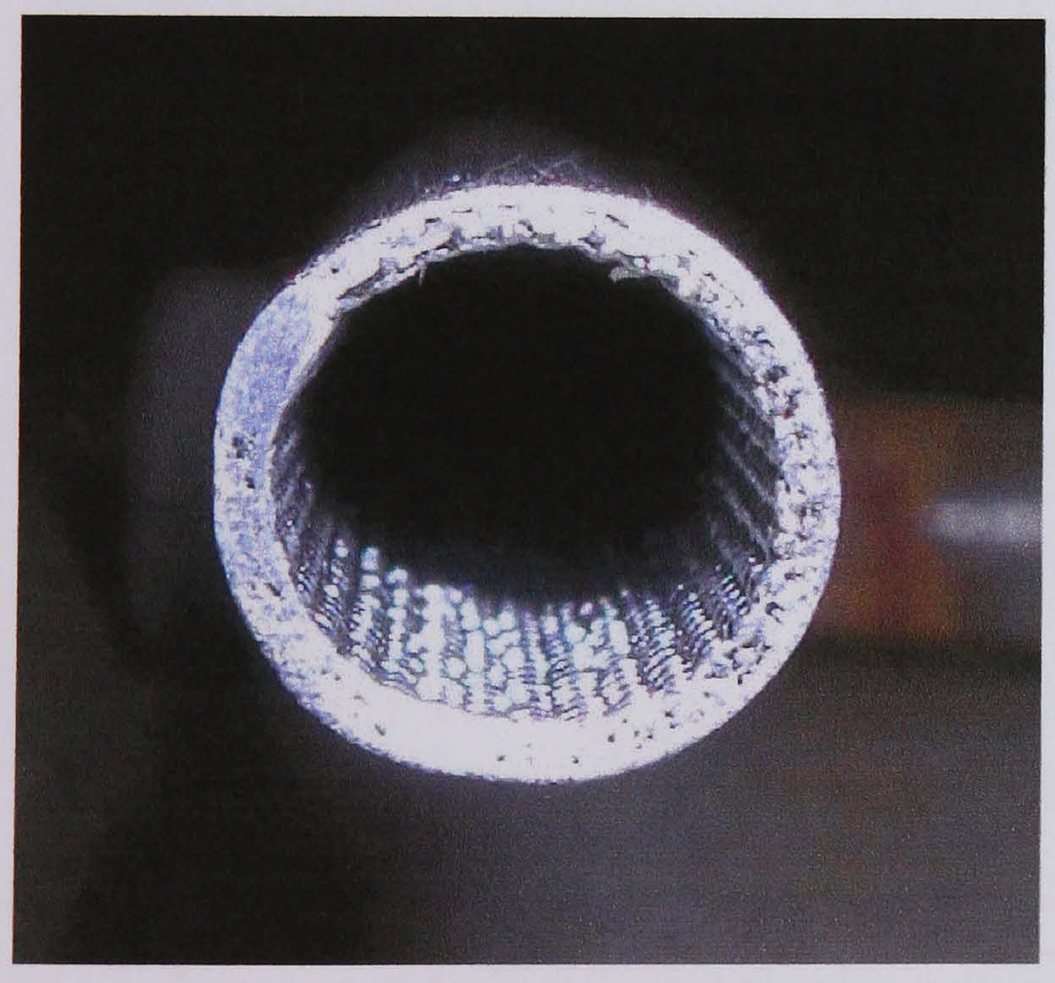
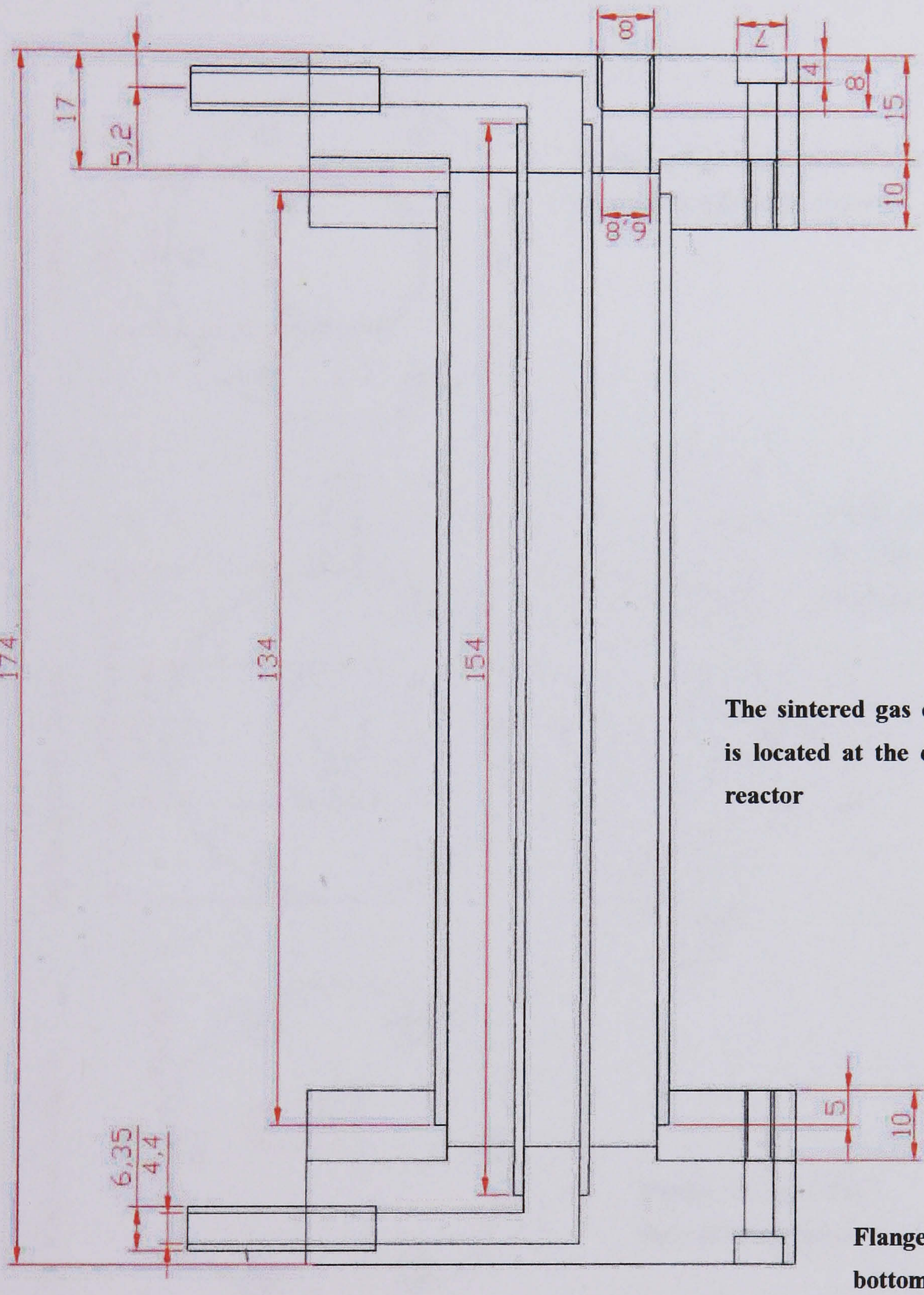


Fig.4.3 The cross-sectional view of the sintered tube



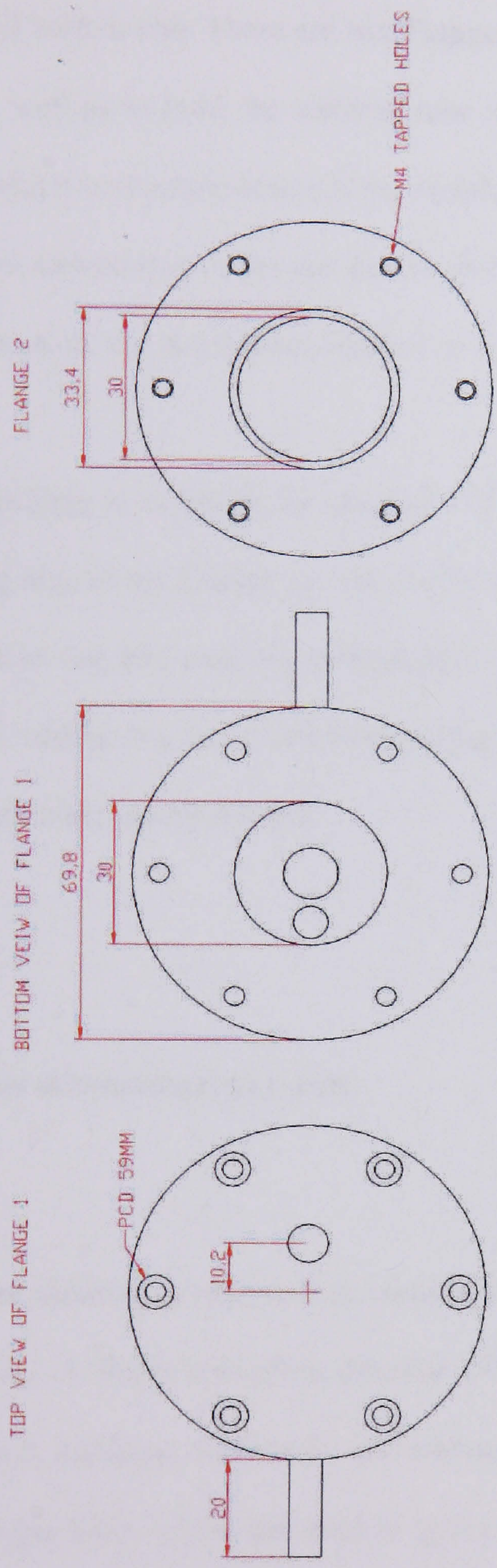
Flange 1a (top) and 1b

The sintered gas channel tube is located at the centre of the reactor

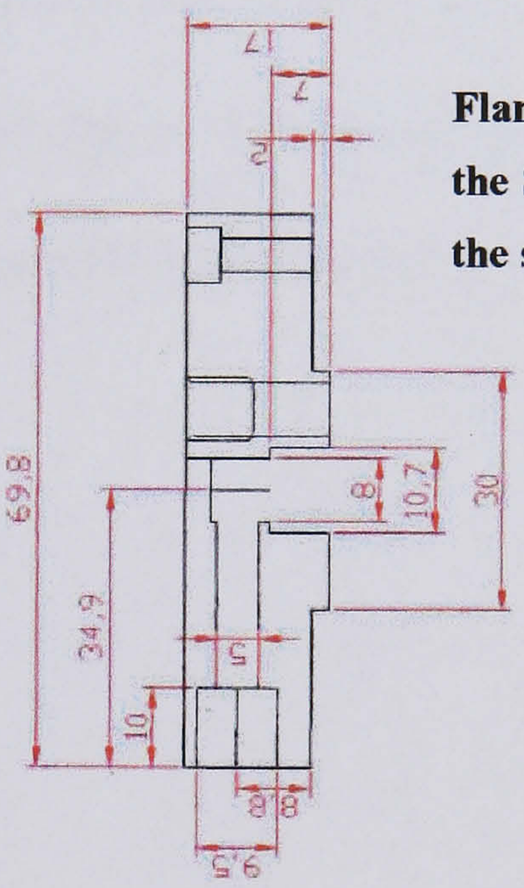
Flange 2

Flange 1a bottom

Fig.4.4 Schematic mechanical drawing of SAR



Flange 2, the flange attached to the bottom side of the reactor



Flange 1b, top side of the SAR, connected to the shell tube

Flange 1a top with the solid loading hole

Fig.4.5 Top and bottom view of Flange 1a, 1b and Flange 2

The outer shell tube is permanently attached to Flange 2 and Flange 1b (see fig.4.3) at the top side and bottom end. There are two Flanges 1a, one of each end of the reactor, which act as the cap as well as to hold the sintered tube in position. Only top Flange 1a has a solid loading hole, which is directed towards the annulus section of the reactor. The gas flows through the top inlet and bottom outlet gas line in each of the Flange 1a. A copper disc washer is inserted between each top and bottom Flanges 1a-1b and Flanges 1a-2 to ensure pressure sealing.

Bed packing is achieved by pouring the solid particles into the annulus through the solid loading hole of top Flange 1a. The SAR column is placed vertically inside the convective oven to sustain the bed packing arrangement throughout the operation. In addition, it may help prevent adding any unwanted strain on the sintered tube structure, which could be the case if it is placed horizontally instead.

4.4 Gas chromatography unit

This gas chromatography unit consists of a Valco multiposition valve mounted on a Shimadzu 14-B GC. A flame ionisation detector (FID) is used to detect the combustible hydrocarbon gases (i.e. methane, isobutane, and isobutene in this work). The GC is connected to pure H_2 and air gas lines, which are used to ignite the FID; helium is used as the GC carrier gas. The latter is connected to a moisture absorber and oxygen scrubber to prevent any presence of moisture and oxygen during chromatography analysis. A PC for data acquisition and the control of the multiposition valve containing Shimadzu software is used.

The GC is equipped with a stainless steel Graphpac column of ~2.0 m length and 1/8" outer diameter (OD) packed with 0.19% picric acid of 80-100 mesh size supplied by Alltech Ltd. The maximum operating temperature for this column is 120 °C. To obtain a significant peak separation of each of the hydrocarbon components, the column temperature is fixed at 30 °C as proposed by the supplier. Both injector and detector temperatures are set at 100°C and 120°C to avoid condensation in the column. Using the FID, only the hydrocarbon gases i.e. isobutane, isobutene and methane were detected. Methane has the same adsorption affinity as hydrogen (Sheikh, 1999), and acted as the internal standard to obtain the initial response factor of isobutane and isobutene during GC calibration. In other words, there was negligible adsorption of methane over zeolite KY (Alpay *et al.*, 1996).

The GC was calibrated using constant delivery of 40 ml min^{-1} or 360kPa helium gas carrier. By doing so, the retention times of methane, isobutane, and isobutene are maintained at 0.57 min, 3.65 min, and 6.00 min respectively. A range of volume fractions of each of methane (used as an internal standard), isobutane, and isobutene are then fed via the sampling loop into the GC at ambient temperature. In this work, two premixed gas mixtures used are obtained from BOC Ltd: the first cylinder contains 0.1 % (v/v) of isobutene, methane, hydrogen, and 4.8% of isobutane in a nitrogen balance; and the second contains 0.5 % of hydrogen, 1 % of methane, 1.5 % of isobutylene and 2.4 % of isobutane in a nitrogen balance. These gases thus allow the GC to be calibrated for the whole range of mole fractions employed in this work (Sheikh, 1999). The results of the GC calibrations are presented in Appendix C.

4.5 Standard experimental procedures

The SAR and PFR studies were carried out for four packing materials:

1) Inert diluent (carborundum) only

2) Platinum-alumina catalyst + inert diluent

3) Zeolite KY + inert diluent

4) Platinum-alumina + zeolite KY + inert diluent

In all cases, the gas leak testing and solids drying were carried out; see section 4.5.1 and 4.5.2. Where catalyst was present, a catalyst activation step was necessary. The GC column was also conditioned before use to remove any water vapour and impurities in the column adsorbent packing. The standard experimental procedures are now given.

4.5.1 Gas leak testing

Before the start of the experiment, the feed line, reactor column and product delivery line undergo gas leak testing. The equipment was tested for gas leaks at ambient temperature. The product line was disconnected from the product exhaust connector and replaced by a pressure cap, which was tightly bolted. The one-way vent valve was also fully closed. Pure N_2 was then fed at 0.10 l min^{-1} (in the case of PFR, at 0.050 l min^{-1}) and the pressure gauge is monitored. The moment the feed gas reached a significantly high pressure of ~60psi, the supply was cut off by closing the 2-way valve on Stream 1 and immediately closing the nitrogen cylinder regulator valve. The pressurised rig is left for about ten minutes and any change of pressure was monitored. Any gradual decrease of pressure indicated gas leakage.

The procedure was then repeated at the highest reactor operating temperature (i.e. T = 700K). A constant pressure reading over a 10-minute was considered as leak-free.

4.5.2 Solid drying

Solid drying in the packing region of each reactor is necessary to remove any moisture present. This is achieved by purging it with a constant feed of N_2 at a flow rate of 0.05 l min^{-1} for PFR (in the case of SAR, at 0.10 l min^{-1}) at 600K. The one-way valve, V4 is left fully open whilst the 1/16" product line is disconnected from the Valco loops and connected to the Vent line 2 (see fig.4.1), which is also directed towards the fume cupboard. This N_2 purge is maintained for approximately 5 hours prior to running the experiment.

4.5.3 Catalyst activation

The reactor column is fed with 10% H_2 in N_2 carrier at the same temperature (i.e. 600K) for another 12 hours whenever catalyst is present. The activation step over hydrogen addition ensures the catalyst activity throughout the process.

4.5.4 GC column conditioning

It is a good practice to condition the GC column before running any GC analysis. This is to remove any water or other impurities in the adsorbent packing. The column, injector and detector temperatures are fixed at 30 °C, 100 °C and 120 °C correspondingly and the helium carrier gas is fed into the sample loop at 360kPa for approximately one hour.

4.6 Concluding remarks

The experimental apparatus for the SAR and PFR experiments has been described. This consisted of ancillary lines, reactor unit and GC unit. Particular attention was given to the design of the SAR reactor. Also described were the standard procedures used for leak-testing, solid drying and catalyst activation.

Chapter 5

Reaction and Adsorption Kinetic Measurements

5.1 Introduction

Thermodynamically, the catalytic dehydrogenation of isobutane requires a reasonably high temperature and low pressure to overcome equilibrium limitations. Therefore, there is much interest in achieving lower reaction temperatures and hence, an overall lower energy consumption and a possible alleviation of catalyst fouling (Alpay *et al.,* 1994). One of the ways to achieve this is by combining reaction with in situ separation process. Based on its material tolerance to high temperatures and pressures, the reversible nature of the adsorbent has been an attractive choice for gas separation under reaction conditions (Ding and Alpay, 2000). Nevertheless, characterisation of the adsorbent and catalyst are essential prior to designing a process to achieve the reaction enhancement effect.

In this study, general criteria for selecting the catalyst depends on its ability to selectively convert the reactants into desired products at a specific set of reaction conditions to ensure high catalytic activity and stability whilst minimising any unwanted side reactions such as hydrogenolysis, isomerisation, and coking. On the other hand, the adsorbent is chosen based on its preferential adsorption to the desired adsorbate due to equilibrium or kinetic selectivity properties. In addition, it has to maintain a separation capacity as well as chemical and physical stability under reaction conditions.

In this chapter, studies on platinum-alumina (Pt-Al_2O_3) catalyst and zeolite KY adsorbent for the isobutane dehydrogenation process are presented. The reaction kinetic and adsorption characterisation studies were initially carried out in a conventional fixed bed tubular reactor to obtain key parameters such as reaction rate constants, activation energy, adsorption isotherm values, and the isosteric heat of adsorption.

The performance of the novel SAR is also presented in this chapter. Results for the catalytic dehydrogenation process are analysed and compared to an equivalent PFR reactor. The predicted significant improvement to achieve low pressure drop characteristic using this structured reactor in comparison with the traditional packed bed reactor is also presented. A low pressure drop operation will lead to significant reduction of energy consumption and thus, a better reactor packing configuration alternative in the development of industrial adsorption process (Rouse, 2004).

5.2 Reaction kinetic determination

This section begins with an overview of Pt-Al_2O_3 catalyst considered for the reversible catalytic dehydrogenation of isobutane in this work. The experimental setup for the dehydrogenation reaction is given prior to the measurements of reaction rate constant. This section concludes with an account on PFR and SAR dehydrogenation reaction experiments to investigate the performance of the structured packing configuration relative to the conventional bed packing arrangement.

5.2.1 Pt-Al_2O_3 catalyst overview

Commercial isobutane dehydrogenation reaction is conventionally catalysed by chromia-alumina catalyst. The production of isobutene from isobutane is based on Catofin process in which it extends the Houdry Catadiene process using chromia-alumina catalyst (see Bhasin et al, 2001). Although reasonable reaction selectivity to isobutene is achieved, chromia-alumina deactivates rapidly on-stream and has to be operated at relatively high temperature (> 823K) (see Hill *et al.,* 1998, Cortright, 1998).

The dehydrogenation of light (low molecular weight) paraffins is endothermic and generally requires a higher temperature than that of the heavy paraffins. Lower operating pressures are preferred to favourably shift the equilibrium conversion according to Le Chatelier's principle (see Bhasin *et al.,* 2001, Hill *et al.,* 1998). Nevertheless, reasonable per-pass conversion levels as well as high olefin selectivity needs to be maintained (Bhasin *et al.,* 2001). Therefore, the catalytic dehydrogenation reaction has to be operated at high temperature sufficient to achieve high equilibrium conversion and high isobutene yields whilst preventing side reactions, coke formation, catalyst deactivation as well as high energy consumption.

Pt-Al_2O_3 is also reported to achieve more than twice the activity at temperatures from 623K to 673K than the chromia-alumina catalyst and thus it is a suitable catalyst for low-temperature dehydrogenation of isobutane in a conventional reactor (Matsuda *et al.,* 1993). Furthermore, it has relatively low coke yields and can typically be used for 10-12 days on-stream without regeneration with only a minor decrease in activity (Pujado and Vora, 1984).

It is necessary to feed and maintain a small amount of hydrogen in the reaction section to help maintain the platinum-alumina stability. The hydrogen diluent also acts as an extra heat carrier for the endothermic dehydrogenation reaction. Its alumina support is non-acidic and provides excellent thermal stability and mechanical strength under processing, transport, and catalyst regeneration conditions (Bhasin *et al.*, 2001).

Typical temperatures for a commercial isobutane dehydrogenation process would be above 873K to achieve economically attractive conversions (see Bhasin *et al.*, 2001, Hill *et al.*, 1998). However, in this work, experimental studies are carried out at temperatures from 600K to 700K to prevent unwanted side reactions and facilitate higher adsorbent capacities.

5.2.2 Dehydrogenation of isobutane

The kinetic studies of dehydrogenation of isobutane were conducted in a packed bed tubular reactor. These experiments utilise commercial 0.5% platinum on alumina catalyst supplied by Johnson Matthey PLC . The platinum-alumina catalyst is crushed and sieved into the particle size of 106-250 μm. The bulk density is estimated by weighing the mass of the sieved particles that can be filled in a 1.0 ml volume. This is repeated three times and the average reading of the bulk density is presented in Table 5.1. In this work, the total bed voidage, $\varepsilon_{T,}$, is assumed constant.

Compound	Particle size range, μm	Bulk density, kg m^{-3}
Platinum-alumina	106-250	1000 ±5%
Carborundum	106-250	1640 ±5%

Table 5.1 Summary of the particles bulk density

The tubular reactor consists of a cylindrical stainless steel tubular column of length 0.14m and internal diameter 0.00452 m, packed with an admixture of catalyst and inert diluent particles (carborundum) of the same particle size (i.e. 106-250 μm). As a precaution, the admixing of the particles was initially carried out in a small glass tube where it was shaken and left to settle to ensure even particle distribution prior to filling into the reactor column. Glass wool was packed at the ends of the column in order to retain the particles. The reactor was connected to the gas lines with Swagelok fittings and fitted inside the Perkin-Elmer 8500 GC convective oven. Further details of the basic experimental set-up has been described in section 4.2 and 4.3 of Chapter 4.

Two main feed streams were employed in the experiment. The first consisted of the reaction gas feed with five premixed feed gases of 95% (v/v) nitrogen, 4.8% (v/v(isobutane, and 0.1% (v/v) of each of isobutene, methane (used as the internal standard), and hydrogen. The hydrogen diluent was added to give higher resistance to coking and to also maintain the catalyst activity throughout the process. A mass flow meter was used to set and monitor the feed gas flow rates during the experiment. The second stream consisted of either the purge gas or activation gas stream. The former consists of pure nitrogen (99.995% v/v) and the latter consists of 10% (v/v) hydrogen in nitrogen carrier. A 2-way valve enabled manual switching from one stream to the next.

The feed gases were fed via a preheat section, consisting of a long tubular line within the convective oven and directly upstream of the reactor inlet. Three type-K thermocouples were tied by thin piece of stainless steel wire around the inlet, middle and outlet section of the outer wall of the reactor to detect the temperature distribution. Samples of the product gas from the reactor outlet were fed via the 1/16 inch vent line to the 16-loop Valco valve. The gas

sampling line arrangement was such that dead volumes were minimised (Ding and Alpay, 2000). Each of the samples were injected at computer-controlled time intervals into Shimadzu 14-B GC analyser equipped with an FID detector and a Graphpac column. See fig.4.1 of Chapter 4 for the schematic layout of the experimental setup.

This bench-scale equipment set-up was used for measuring the reaction rate constant and evaluating the PFR-type performance.

5.2.3 Determination of reaction rate constants

Isobutane dehydrogenation reaction is a reversible process but at low pressure operation and reasonably high reaction temperature, a pseudo-first order reaction is assumed where it is carried out in a constant reactor volume and at constant volumetric flow rate. The forward reaction rate constant will be measured at three different temperatures at isobaric condition. Therefore, for a tubular reactor, the forward rate constant, k_{fwd} (s^{-1}) of A for the pseudo-first order reaction of

$$A \rightarrow B + C$$

is obtained from this equation

$$\ln\frac{C_A}{C_{A0}} = -k_{fwd}\tau \qquad (5.1)$$

In the case of plug-flow operation, the time it takes for the reactant feed gas to enter the reactor completely is called the space-time, τ (s) (Fogler, 1992). It is obtained by dividing the reactor volume, V (m^3), by the constant volumetric flow rate entering the reactor, ν_o ($m^3\ s^{-1}$)

$$\tau = \frac{V}{\nu_o} \tag{5.2}$$

Equation (5.1) is represented as a straight-line plot of ln (C_A/C_{Ao}) versus different values of τ at zero y-intercept. The space-time values are obtained by varying the volumetric flow rates at a given temperature. The negative gradient of the slope is the forward reaction rate constant, k_{fwd}.

Experimental procedure

The admixture of catalyst and inert diluent particles (106-250 μm sizes) was packed in the reactor column as described in section 5.2.2. The mass of the catalyst employed, W, is 5.0 x 10^{-4} kg. Prior to running this experiment, the fresh catalyst was first dried by passing nitrogen gas at 600K for 2 hours. The catalyst was then activated with 10% (v/v) of hydrogen in nitrogen carrier at the same temperature for approximately 12 hours. The feed gases were fed at ambient temperature. The first set of experiment was carried out at a constant oven temperature of 600K for different feed gas volumetric flow rates. Experiments were then repeated at temperature 650K and 700K. All the product samples were injected to the 16-loop Valco valve via the 1/16 inches product line and analysed using a Shimadzu 14-B GC equipped with an FID detector and a Graphpac column.

Reaction rate constant results

The linearity of the plots of ln (C_A/C_{Ao}) versus τ are shown in Figure 5.1 confirms the pseudo first order kinetics for low equilibrium conversions. In order to include the effect of the

reactor volume, V and the mass of the catalyst employed, W, the forward reaction rate constant can also be expressed as k' ($m^3\ kg^{-1}\ s^{-1}$) and it is represented by

$$k' = \frac{k_{fwd}\, V}{W} \qquad (5.3)$$

The values of k_{fwd} and k' are tabulated in Table 5.2. At each of the temperatures given, the values of the equilibrium constant, K_{eqm}, were predetermined by thermodynamic calculations.

T, K	K_{eqm} , mol m^{-3}	k_{fwd} , s^{-1}	k' , $m^3\ kg^{-1}\ s^{-1}$
600	**0.0131**	**0.0982 ± 0.015**	**4.419×10^{-4}**
650	**0.0810**	**0.2120 ± 0.006**	**9.540×10^{-4}**
700	**0.3870**	**0.2633 ± 0.0057**	**1.185×10^{-3}**

Table 5.2 Experimentally determined isobutane reaction rate constants at three temperatures

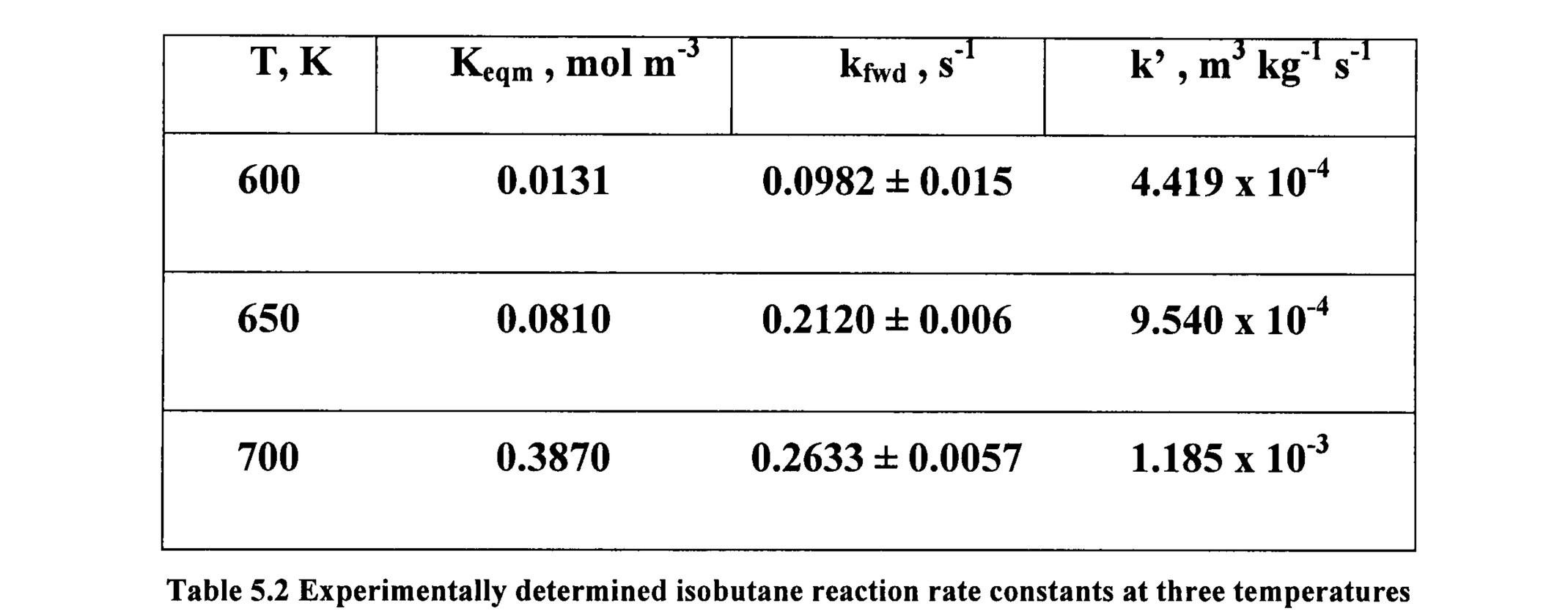


Fig. 5.1 Reaction rate constants plot at three temperatures

The higher the reaction temperature, the faster the rate of reaction and this temperature dependence behaviour can be empirically correlated in terms of Arrhenius equation. Therefore, at any specific reaction temperature, the reaction rate constant, k' (see Hartley, 1991, Fogler, 1992) can be expressed as:

$$k'(T) = k_o \exp\left(\frac{-E}{R_{gas}\,T}\right) \tag{5.4}$$

where k_o is the dimensionless pre-exponential factor or frequency factor, E ,the activation energy, J mol^{-1} , R_{gas} , the molar gas constant, J mol^{-1} K^{-1} and T the reaction temperature, K.

It can then be rearranged as

$$\ln k' = \ln k_o - \frac{E}{R_{gas}}\left(\frac{1}{T}\right) \tag{5.5}$$

Thus, the activation energy, E, can be determined from a straight-line plot of ln k' versus 1/T.

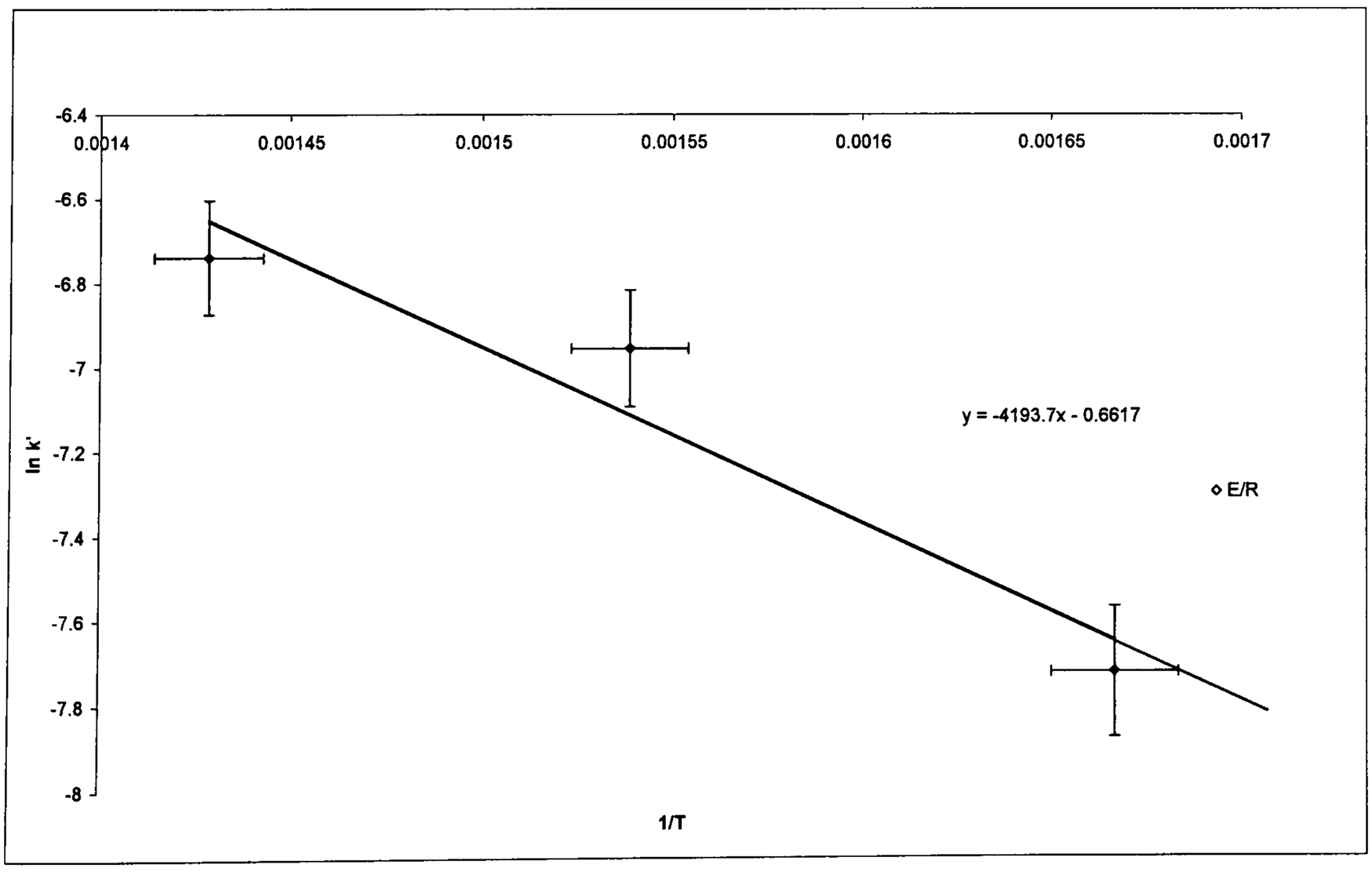


Fig. 5.2 Activation energy plot

With reference to fig.5.2, the Arrhenius equation 5.4 of the catalytic isobutane dehydrogenation reaction can be represented as

$$k'(T) = 0.517\exp\left(\frac{-34900}{R_{gas}T}\right)$$

where the activation energy, E = 34.9 ± 8.0 kJ mol^{-1}. (*see footnote)

5.2.4 PFR and SAR experiments

The PFR experiments for the packed bed tubular reactor were conducted at three different temperatures. The performance was then compared to an SAR. At a minimum flow rate of 0.05 l min^{-1}, very slow pressure building up in the SAR occurred as the results of the mass transfer of feed gas diffusing radially from the core gas channel towards the fine screen gauze wall. In addition, there was an apparent difference of the amount of solid particles used (larger amount of inert diluent particles added in SAR) due to the different bed packing volumes between the PFR and SAR. Therefore, different minimum gas flow rates were selected for each type of reactor such that the reaction performance could be investigated at highest possible space time for different reactor packing configurations. As shown in table 5.3, the following volumetric flow rate, ν_o, of reactant gas fed at ambient temperatures was modified in terms of gas law whereby gas volume increases with increasing temperature. The corresponding superficial velocities of the modified ν_o were determined based on the cross-sectional area of each reactor studied. The reaction conversions were observed under the chosen operating conditions.

---

* The error is the average deviation from the activation value

	PFR ; $A_{PFR} = 1.605 \times 10^{-5}$ m^2 ; $V_{PFR} = 2.26 \times 10^{-6} \varepsilon_t$ m^3				SAR ; $A_{gas} = 5.027 \times 10^{-5}$ m^2 ; $V_{sol} = 7.04 \times 10^{-6}$ m^3			
T, K	ν (298K), l min^{-1}	ν (T) x 10^{-6}, m^3 s^{-1}	v_{PFR}, m s^{-1}	τ_{PFR}, s	ν (298K), l min^{-1}	ν (T) x 10^{-6}, m^3 s^{-1}	v_{SAR}, ms^{-1}	τ_{SAR}, s
600	0.05	1.68	0.105	1.00	0.10	3.36	0.067	2.10
650	0.05	1.82	0.113	0.93	0.10	3.64	0.072	1.94
700	0.05	1.96	0.122	0.86	0.10	3.91	0.078	1.80

Table 5.3 Volumetric flow rates used in the PFR and SAR experiments and their corresponding superficial velocities and space time. A_{PFR} and A_{gas} are the cross-sectional areas of PFR and SAR reactors. ε_t, the total bed voidage = 0.75. V_{sol} is SAR core gas channel volume

Experimental procedure

The general PFR packing conditions are similar to the one in previous rate constant experiment but this time, 1.0×10^{-3} kg of catalyst was used and the remaining reactor volume was occupied with inert diluent particles. The same amount of catalyst was loaded inside the annular region of the SAR reactor. The geometrical layout of the SAR has been described in section 4.3.2 of Chapter 4.

The PFR reactor was first fitted into the oven, and the experiments were carried out at the constant volumetric flow rate of 0.05 l min^{-1}. The product samples were injected to the Shimadzu 14-B GC analyser via the 16-loop Valco valve. Injection time intervals were predetermined from the simulation results. The packed bed column was then removed from the oven and was replaced by the SAR reactor. In this case, the minimum feed gas flow rate of 0.1 l min^{-1} was used.

PFR and SAR experiments results

From Figure 5.3, it can be seen that the equilibrium conversion of isobutane increases at higher temperature. There was also a marginal difference of equilibrium conversions for both SAR and PFR reactors at any given reaction temperatures, despite the fact that gas-solid contact was mainly achieved by the diffusion of gas rather than any convective mechanism in the SAR. This indicates that the SAR packing configuration has the possibility to achieve a similar catalytic reaction performance to a PFR configuration but at the same time overcoming pressure drop problems. The conversion measurements and corresponding calculated pressure drop are presented in Table 5.4.

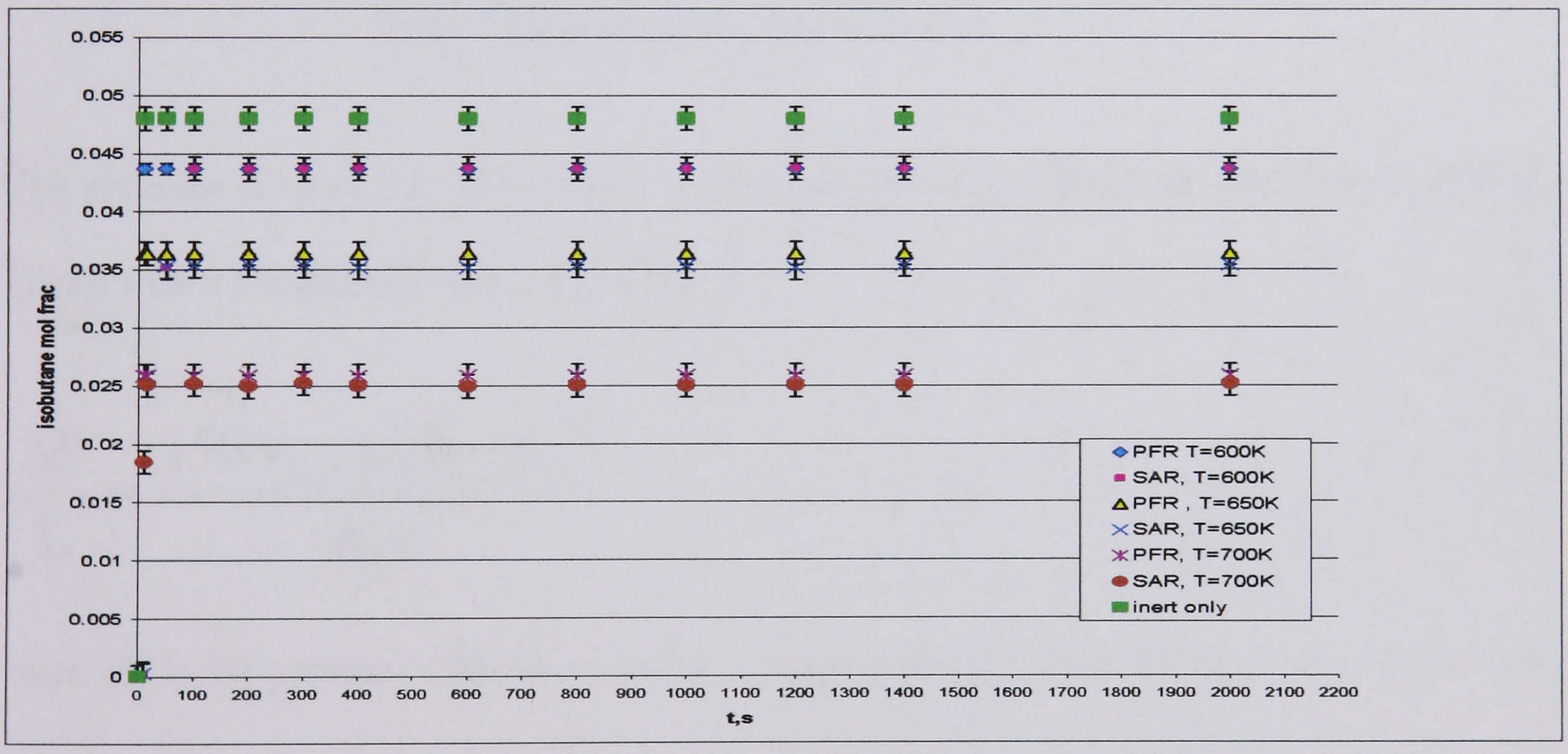


Fig. 5.3 Catalytic isobutane dehydrogenation reaction for PFR and SAR

T, K	PFR		SAR	
	$X_{PFR} \pm 5\%$	Pressure drop, Pa m^{-1}	$X_{SAR} \pm 5\%$	Pressure drop, Pa m^{-1}
600	0.090	2.17×10^3	0.090	2.71
650	0.24	2.48×10^3	0.26	2.86
700	0.46	2.80×10^3	0.48	3.00

Table 5.4 Summary of reaction conversions of PFR and SAR, X_{PFR} and X_{SAR}, and the pressure drop calculated from the equations (5.6) and (5.7); SAR flow rate = 0.10 l min^{-1} ; PFR flow rate = 0.050 l min^{-1} († see footnote)

T, K	Re_{PFR}	Re_{SAR}
600	1.71	24.84
650	1.91	27.64
700	2.11	30.52

Table 5.5 Reynolds numbers of PFR and SAR

The pressure drop in the PFR reactor was calculated using the Ergun equation according to Darcy's Law for laminar flow condition, i.e.

$$\frac{\Delta P}{L} = \frac{150\, v_{ave}\, \mu (1-\varepsilon_t)^2}{d_p^2\, \varepsilon_t^3} \qquad (5.6)$$

were ΔP is the pressure difference at the reactor input and output (Pa), L the reactor length (m), v_{ave} the bed superficial velocity (m s^{-1}), μ the inert gas (nitrogen) viscosity (Pa s), ε_t the total bed voidage and d_p the mean particle (catalyst or adsorbent) diameter (m).

† The errors correspond to the absolute error, which were obtained experimentally

The SAR pressure drop was calculated using Hagen-Poisuille equation (Coulson *et al.*, 1990), resulting from the momentum transfer of the flowing gas across the gas channel, i.e.,

$$\frac{\Delta P}{L} = 4 f \frac{1}{d_c} \rho_g \, v_{ave}^{\,2} \qquad (5.7)$$

where ρ_g is the inert gas density (kg m^{-3}), d_c is the diameter of the gas channel (m) and the f, the friction factor, is inversely proportional to the bed superficial velocity (Sie and Calis, 1998):

$$f = \frac{8}{Re} \qquad (5.8)$$

and

$$Re = \frac{\rho_g \, v_{ave} \, d_c}{\mu} \qquad (5.9)$$

For packed bed, laminar flow condition, the Reynolds number was calculated by substituting d_c for d_p in equation (5.6). The Reynolds numbers for each reactor are tabulated in Table 5.5.

T, K	v_{SAR}, m s^{-1}	v'_{SAR}, m s^{-1}
600	0.067	1.31×10^{-4}
650	0.072	1.31×10^{-4}
700	0.078	1.31×10^{-4}

Table 5.6 Negligible convective transport test on the SAR annular packing; flow rate = 0.10 l min^{-1} ; v'_{SAR} values change after forth decimal place

In order to verify the assumption of negligible convective transport in the annular packing system, the pressure drop values estimated using the Hagen-Poisuille equation (i.e. equation (5.7)) are substituted into the Ergun equation for laminar flow (i.e. equation (5.6)) where v_{ave}, the superficial velocity becomes the unknown. By referring to Table 5.6, considerably small v'_{SAR} values in the order of 10^{-4} m s^{-1} support such an assumption as described above.

5.3 Adsorption kinetic determination

A proprietary adsorbent is chosen based on either its selective adsorption properties or its selective mass transfer (Alpay *et al.,* 1994). In this section, the physical and adsorptive properties of zeolite KY are presented. Initially, the conventional packed bed tubular reactor experiment is carried out. It employs the step chromatography method and is presented by means of breakthrough curves. A similar method is subsequently employed in the case of SAR and its performance aspects are investigated relative to the equivalent PFR configuration.

5.3.1 Synthetic Zeolite KY Overview

In general, zeolites are crystalline, hydrated aluminosilicates of group I and group II elements, based on infinitely extending 3-D networks of AlO_4 and SiO_4 tetrahedra linked to each other by oxygen-sharing (Breck, 1974). They are available both in naturally occurring forms as well as in synthesized forms, and a letter or group of letters (see Yang, 1987) designates the latter. One important type is zeolite type Y with potassium cation, K.

Zeolite KY type is related to faujasite and is represented in this form: K_{56} $[(AlO_2)_{56}$ $(SiO_2)_{136}]$. It has an effective channel aperture (or kinetic diameter) of 8.0 Å which is deemed large enough to admit quite large molecules such as naphthalene and neopentane and its lattice is

much more open than that of zeolite type A (Ruthven, 1984). The framework consists of diamond-like array of linked octahedra, joined tetrahedrally through six rings containing 12 (Si Al)O_4 tetrahedra (Breck, 1974). Zeolite KY exhibits a stable and reversible dehydration effect, retaining its structure up to 760° C (Breck, 1974). This has made it possible for zeolite KY to be utilised for high temperature hydrocarbon separations.

Zeolite KY not only exhibits steric behaviour at high temperatures, but is also employed for its potential as a catalyst support material. This was reported in the work of Sheikh (1999) whereby the significant separation of butadiene (product) and methane was observed but the zeolite its chemical inertness at 763 K. Alpay and his co-workers (1996) also studied the hydrocarbon separation performance of zeolite KY at relatively high temperatures. The measurements of the adsorption equilibria parameters of methylcyclohexane (MCH) and toluene were carried out at temperatures ranging from 423 K to 683 K. Adsorption of MCH over zeolite KY was first observed at 523 K while toluene was observed at a higher temperature of 673K. Higher adsorption affinities were measured relative to other zeolites such as 3A, 4A, 5A, ZSM-5, 10X, 13X and Na-Y.

In this work, the adsorption characterisation of isobutane and isobutene were investigated at temperature of 600K, 650K and 700 K. Zeolite KY particles were supplied in a pellet form by Bayer.

5.3.2 Adsorption equilibria parameters

For a particular adsorption column, various characterisation techniques can be employed to obtain the key adsorption parameters such as:

- Gravimetric and pulse or step chromatographic methods to measure adsorption response curve
- Zero length column (ZLC) to measure matching desorption curves

In this work, step chromatographic method was employed for both PFR and SAR analyses. The dynamic step response was measured at the column outlet and interpreted in the breakthrough curve form. The step response was carried for an initially sorbate free column (Ruthven, 1984) and the adsorption equilibrium parameters determined based on following the assumptions (see Ruthven, 1984) as follows:

- Linear isotherm
- Isothermal bed, therefore neglecting the heat transfer resistance across the bed
- Isobaric operation
- Dilute adsorbate
- Constant gas flow rate
- Axially dispersed plug flow model for the PFR
- LDF model for the adsorption kinetic
- Uniform particle size distribution

For an ideal case whereby the assumptions of isothermal operation at isobaric condition and linear isotherm are considered, the adsorbate residence time (or first moment), t_r (s), can be written as (see Alpay and Kershenbaum, 1995, Alpay *et al.,* 1996):

$$t_r = \frac{K_i L}{u_e} \tag{5.10}$$

where K_i is the dimensionless effective adsorption equilibrium constant parameter for adsorbate i, L is the reactor column length (m), and u_e is the superficial gas velocity at the exit condition. The temperature dependence of m_i (mol kg^{-1} Pa^{-1}) is first obtained from a linear adsorption equilibrium parameter equation:

$$K_i = \varepsilon_t + \rho_b m_i R_{gas} T \tag{5.11}$$

where ε_t is the total bed voidage, ρ_b ,the bulk adsorbent density (kg m^{-3}), R_{gas} the molar gas constant (J mol^{-1} K^{-1}) and T the adsorption column temperature (K).

In order to obtain the isosteric heat of adsorption of component i, H_i (J mol^{-1}), m_i can be expressed in terms of a van't Hoff type equation and this yield:

$$m_i = a_i \frac{\exp\left(\frac{-H_i}{R_{gas} T}\right)}{T^{1/2}} \tag{5.12}$$

where a_i is the temperature independent constant for a given combination of adsorbate and adsorbent. Rearranging equation (5.12) by the substitution of equation (5.11) gives

$$\ln(\kappa_i) = c_i - \frac{H_i}{R_{gas}}\left(\frac{1}{T}\right) \tag{5.13}$$

where

$$\kappa_i = \frac{(K_i - \varepsilon_t)}{T^{1/2}} \tag{5.14}$$

and

$$c_i = \ln(a_i \rho_b R_{gas}) \tag{5.15}$$

A plot of ln (κ_i) versus 1/T will yield a straight line of gradient proportional to H_i after obtaining K_i values at different temperatures. Such van't Hoff type equation will enable the estimation of K_i at any operating temperature, thus acts as a test for the validity of the van't Hoff relationship (Alpay *et al.*, 1996).

5.3.3 Adsorption isotherm experiments

Adsorption equilibria parameters were initially obtained using the conventional packed bed configuration. The basic set-up was similar to that which was described in Section 5.2.2 whereby the reactor consisted of stainless steel of ¼ inches OD and 0.14 m length tubular reactor fitted inside the oven. Three temperatures were chosen for the investigation: 600 K, 650 K and 700 K. The FID was used as the detector in the GC.

The first part of the PFR experiment was conducted using only inert diluent packing inside the column. This acted as the control experiment to be compared with the adsorbent-inert diluent

admixture experiments. Prior to running the experiment, the GC column underwent conditioning by purging with helium 368K and at a steady flow rate of 0.040 l min^{-1} for 30 minutes. This was vital in order to remove any trace of contaminants, such as water. The injector and detector temperatures of the GC analyser were set at 373 K and 393 K respectively to avoid any water condensation. Meanwhile, the oven temperature was set at 600 K, and the reactor was purged with nitrogen at a flow rate of 0.050 l min^{-1}.

The purge gas stream was closed using a manually operated 2-way valve. A 3-way valve on the feed line was opened to feed in the premixed gases mentioned in section 5.2.2 at the same flow rate of 0.050 l min^{-1}. The product samples were fed through the 1/16 inches vent line and injected into the 16-loop Valco valve at programmed time intervals. When the last sample was injected to the 16^{th} loop, the feed gas stream was switched back to nitrogen purge stream and maintained at the same temperature and flow rate. At this stage , the sample vent line was disconnected from the Valco valve input port and immediately connected to the exhaust line connected to the fume cupboard. Similar procedure were carried out for the other two temperatures.

In the second part of the PFR experiment, the zeolite KY adsorbent was first crushed and sieved to give constant particle size range of 106-250 μm. Bulk density measurement was conducted again by employing the same technique as was described in section 5.2.2 (see Table 5.7). A new adsorption column was then packed with admixture of (5.0×10^{-4} kg) zeolite KY and inert diluent particles and fitted inside the oven. Once again, the GC column underwent conditioning by a steady flow of helium carrier gas at column temperature of 303 K. At 600 K, the adsorbent bed was purged with hot nitrogen at 0.050 l min^{-1}. As the purge stream was switched to the feed stream, sampling commenced. When the adsorption was completed, the

outlet vent line was disconnected and the feed stream was instantly switched to purge stream. Subsequently, the reactor bed underwent a purge stripping cycle to regenerate the adsorbent. The regenerated step proceeded until the end of the GC analysing time (~ 160 minutes). At the same adsorbate temperature, experiments were repeated for different flow rates. The above procedures were then repeated for other adsorbate temperatures.

Compound	Particle size range, μm	Bulk density, kg m^{-3}
Zeolite KY	**106-250**	**500 ±5%**

Table 5.7 Summary of the adsorbent bulk density

For the SAR experiments, similar experiments were carried out using admixture of 0.030 kg of each particle distributed evenly in the annular region. The feed gas flow rate was kept constant at 0.10 l min^{-1} (see section 5.2.4).

5.3.4 Chromatographic curves analysis

Repeated experiments have been carried out for both SAR and PFR-like reactors in order to check reproducibility. The adsorption kinetic and equilibrium parameters are determined by matching the breakthrough response curves obtained from the experiments to the breakthrough curves obtained from the mathematical representation under the identical experimental conditions. The assumption of LDF is a valid approximation in which concentration change is sufficiently small when fitted to the theoretical response (Ruthven, 1984). Peak elutions obtained from the step chromatography method are analysed using Trapezoidal rule for unequal segments.

Due to the significant difference of the amount of adsorbent used in each of the reactor investigated as well as the relatively smaller volume of the PFR reactor, it is not possible to directly compare the adsorption breakthrough performance of the two reactor types. Thus, the adsorption performance analyses are presented in separate subsections.

Inert only experiment

Initially, there is a good agreement between the two reactors in the inert-only experiments, whereby the very fast breakthrough of isobutane and isobutene is expected. This behaviour can be seen in Figure 5.4. Nevertheless, there is an approximately one second time lag at the initial step responses of the SAR. This is due to relatively higher residence time in SAR resulting in relatively longer contact time between diffusing gas and solid in the annular region.

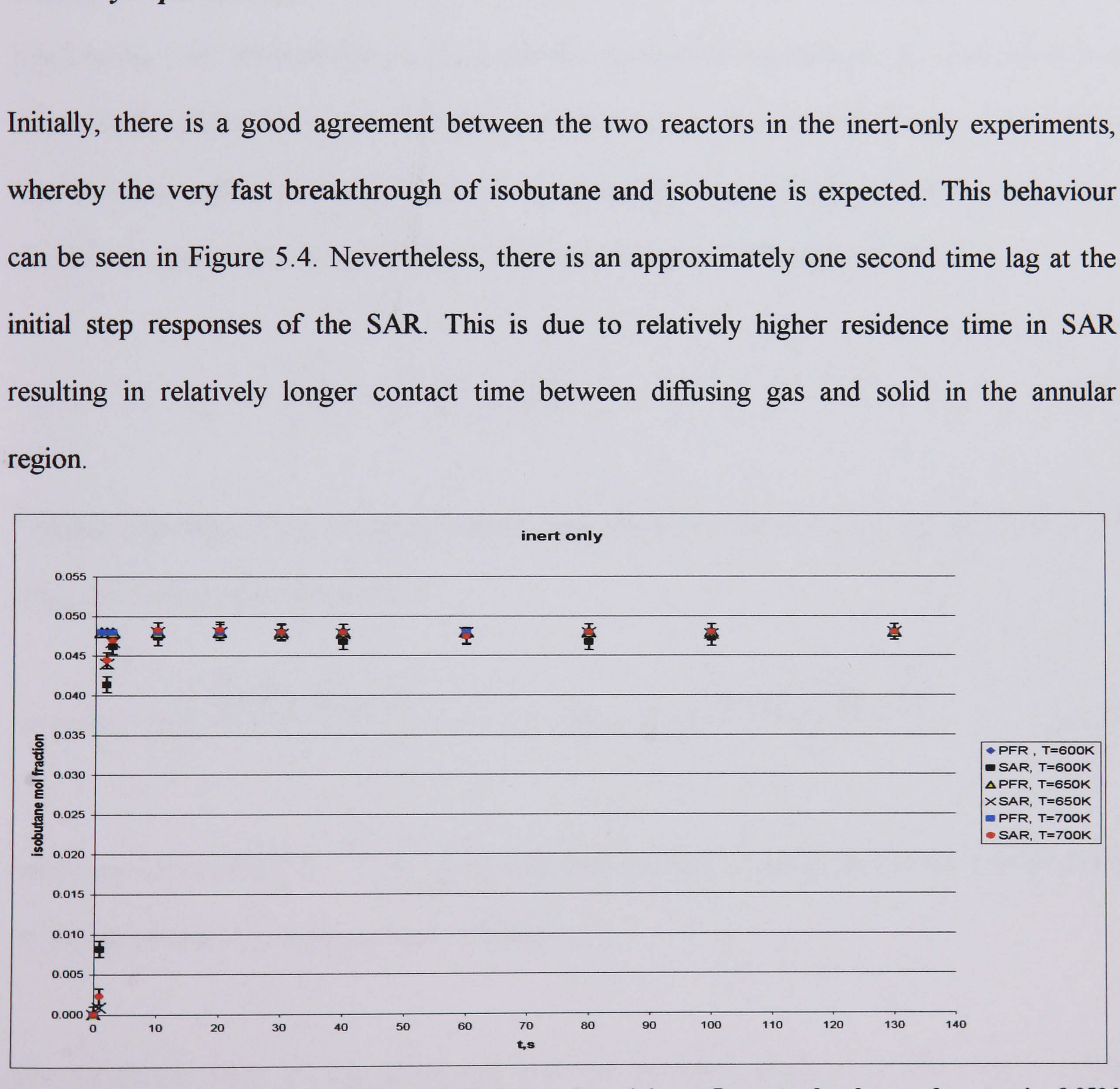


Fig. 5.4 Inert-only experiments for PFR and SAR conducted at minimum flow rate of each type of reactor, i.e. 0.050 l min^{-1} for PFR and 0.10 l min^{-1} for SAR.

Adsorption equilibria parameter results

The adsorption equilibria parameters initially obtained using the first moment analysis to estimate K_i, adsorption equilibrium constant values at a selected range of temperatures and gas velocities. The response plots represented the step changes of the adsorbates from initial zero loading to complete stepped concentration input (where the concentration of the adsorbates is equal to the feed concentrations). From the theory, the first moment of the eluted peak was shown to be equivalent to the adsorbate residence time within the bed (Alpay *et al.,* 1996). The transient uptake rate was obtained by using the first moment numerical integration through the application of van der Laan's theorem (Karger and Ruthven, 1992), i.e.

$$\mu_r \equiv t_r = \int_0^\infty \left(1 - C/C_o\right)dt \qquad (5.16)$$

Unequal segments of the chromatographic response were treated by solving equation (5.16) using the Trapezoidal rule method:

$$t_r = (t_2 - t_1)\left(\frac{f(\alpha_1)+f(\alpha_o)}{2}\right) + \ldots\ldots + (t_n - t_{n-1})\left(\frac{f(\alpha_n)+f(\alpha_{n-1})}{2}\right) \qquad (5.17)$$

where α_n represented $\left(1 - C_n/C_o\right)$ at each time interval, t, and C_o is the inlet concentration of the adsorbates (i.e. isobutane and isobutene).

The parameters (i.e. m_i, the adsorption isotherm gradient) obtained at this stage are then adjusted until the theoretical response curves match with the experimental curves. These new m_i values are then used to estimate the isosteric heat of adsorption as well as mass transfer coefficient values (see Table 5.8). In this work, the adjusted breakthrough response results for

both reactors are shown in Figure 5.6 to Figure 5.15. Subsequently, the K_i values are quantified using equations (5.11) and tabulated in Table 5.9.

Figure 5.5 represents the plot of ln (κ_i) versus 1/T where the gradient is proportional to H_i. With reference to equation (5.13), the H_i values for isobutane and isobutene could be determined (see Table 5.10). As a comparison, extrapolated m_i, K_i as well as the H_i values obtained from the work of Sheikh (1999) based on the van't Hoff type equation for butane and 1-butene adsorption over zeolite KY are also shown in each corresponding table. This is due to their similar relative molecular weights to isobutane and isobutene respectively.

T, K	$m_{isobutane} \pm 0.01$ mol kg^{-1} Pa^{-1}	$m_{butane} \pm 0.01$ mol kg^{-1} Pa^{-1}	$m_{isobutene} \pm 0.01$ mol kg^{-1} Pa^{-1}	$m_{1\text{-butene}} \pm 0.01$ mol kg^{-1} Pa^{-1}
600	3.523×10^{-6}	1.804×10^{-6}	7.882×10^{-6}	2.730×10^{-6}
650	2.196×10^{-6}	8.882×10^{-7}	3.469×10^{-6}	1.180×10^{-6}
700	1.031×10^{-6}	6.529×10^{-7}	2.105×10^{-6}	8.590×10^{-7}

Table 5.8 Adsorption isotherm gradient values. The extrapolated values of butane and 1-butene are obtained from the work of Sheikh (1999)

T, K	$K_{isobutane}$	K_{butane}	$K_{isobutene}$	$K_{1\text{-butene}}$
600	9.54	4.8	20.41	7.1
650	6.68	2.7	10.12	3.5
700	3.75	2.2	6.88	2.8

Table 5.9 Adsorption equilibrium parameter values. The extrapolated values of butane and 1-butene are obtained from the work of Sheikh (1999)

Isosteric heat of adsorption, $-H_i$, kJ mol^{-1}			
isobutane	**butane**	**isobutene**	**1-butene**
42.57 ± 0.75	**35.78 ± 0.75**	**46.30 ± 0.75**	**40.70 ± 0.75**

Table 5.10 Isosteric heat of adsorption over zeolite KY

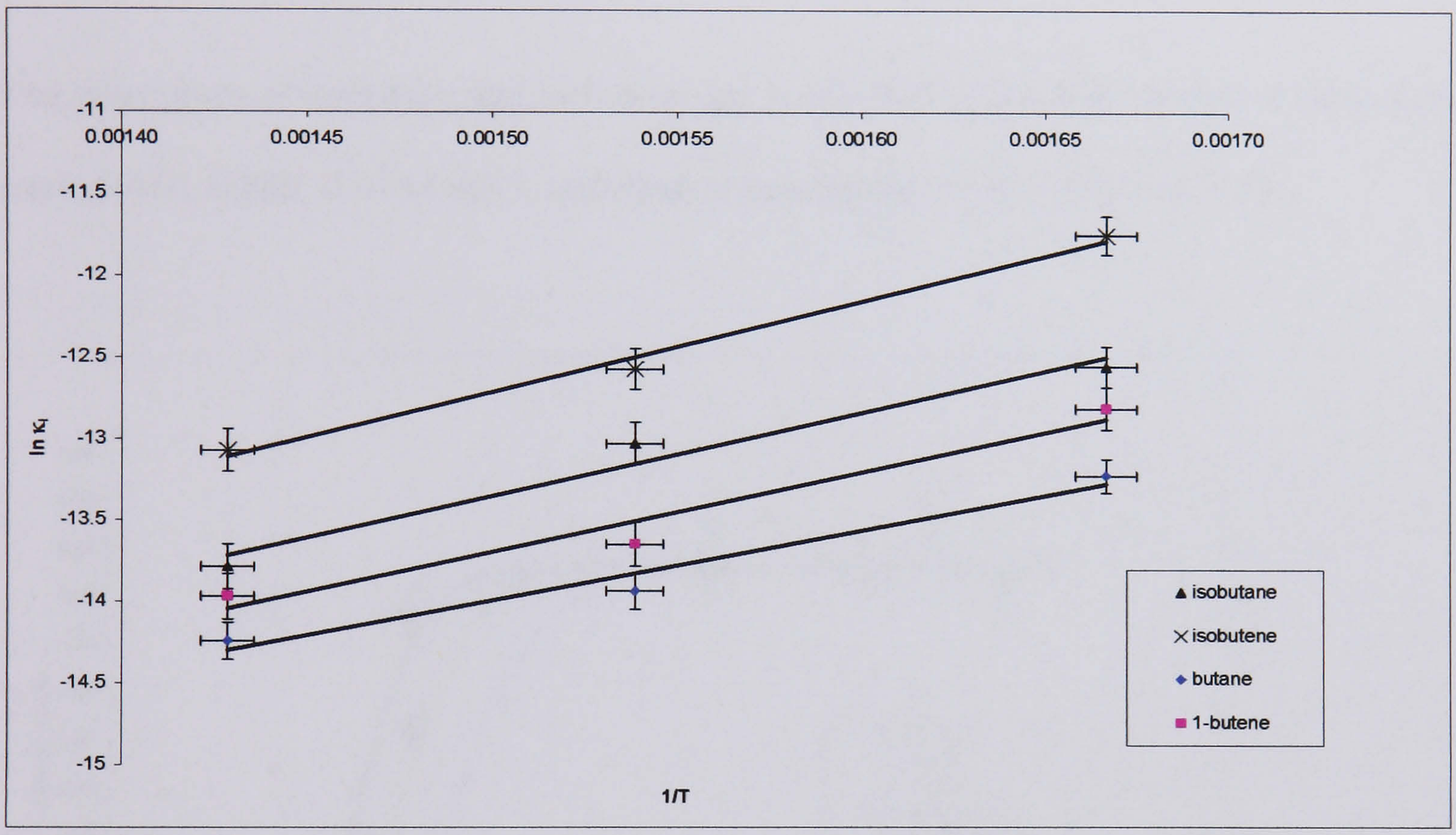


Fig. 5.5 Isosteric heat of adsorption

From Table 5.10, the isosteric heat of adsorption of isobutene and 1-butene are found to be 8.76% and 13.76% higher than isobutane and butane respectively. This is due to the presence of double bonds or polar bonds in the molecule, which gave rise to an additional electrostatic contribution to the heat of adsorption (Ruthven, 1984). Isobutane is also found to have a higher heat of adsorption than butane. The former exhibits different chemical behaviour due to the presence of a tertiary carbon atom and to the stability of the associated free radical (Kroschwitz *et al.*, 1991). In addition to the exothermic characteristic of the physical adsorption observed, information concerning the magnitude of the isosteric heat of adsorption and their level of adsorbate loading is useful. This enables the determination of the degree of

homogeneity of the interior surface of the zeolite relative to the adsorbate concerned (Breck, 1974).

PFR adsorption analysis

The adsorption of isobutane and isobutene are conducted in the PFR reactor at three gas flow rates: 0.050, 0.060, 0.070 l min^{-1}, and three temperatures i.e. 600, 650 and 700K.

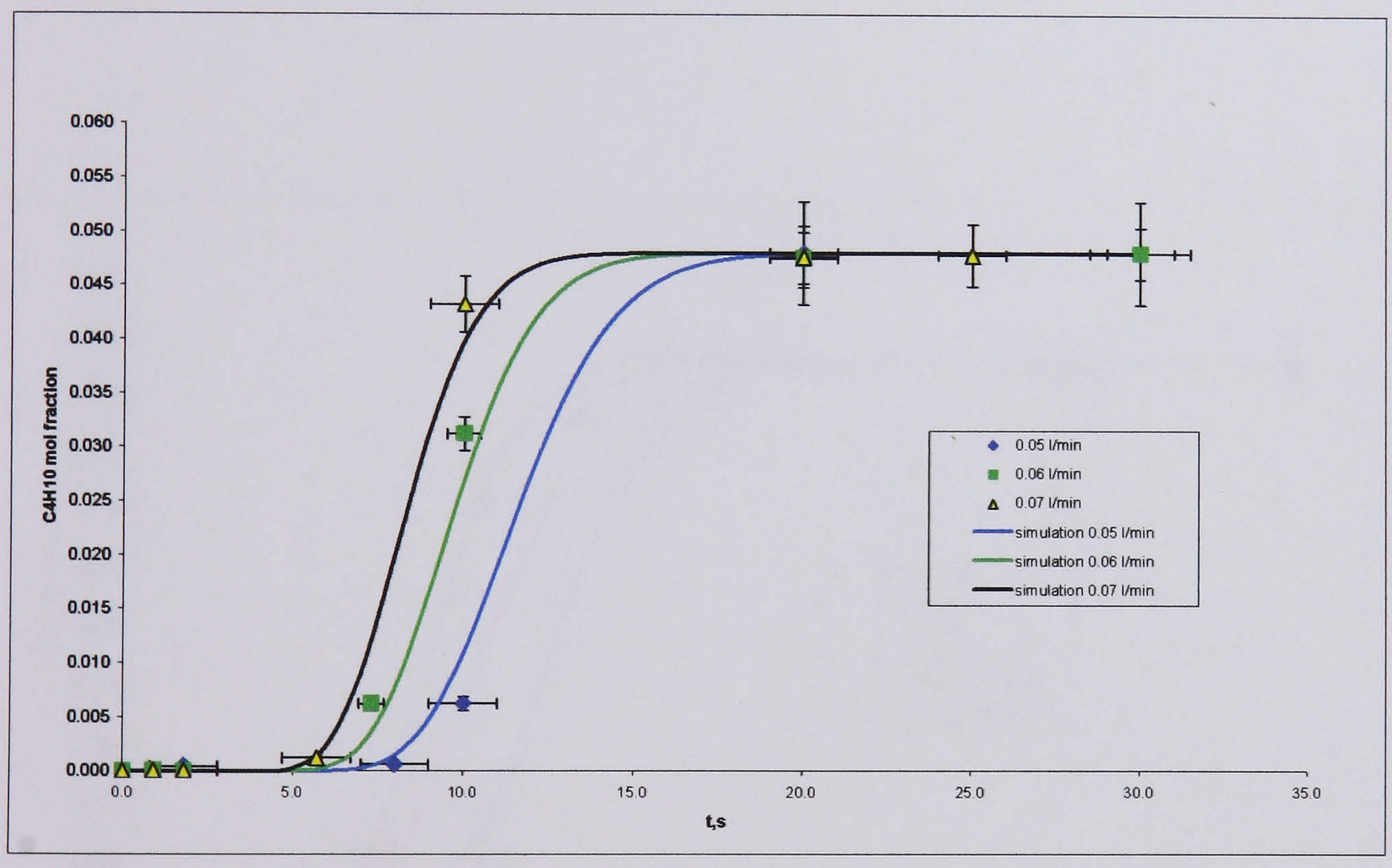


Fig. 5.6 PFR breakthrough profile at T=600K for isobutene (‡ see footnote)

‡ the error bars in each figure (i.e. figs 5.6 to 5.11 are based on 95% confidence interval

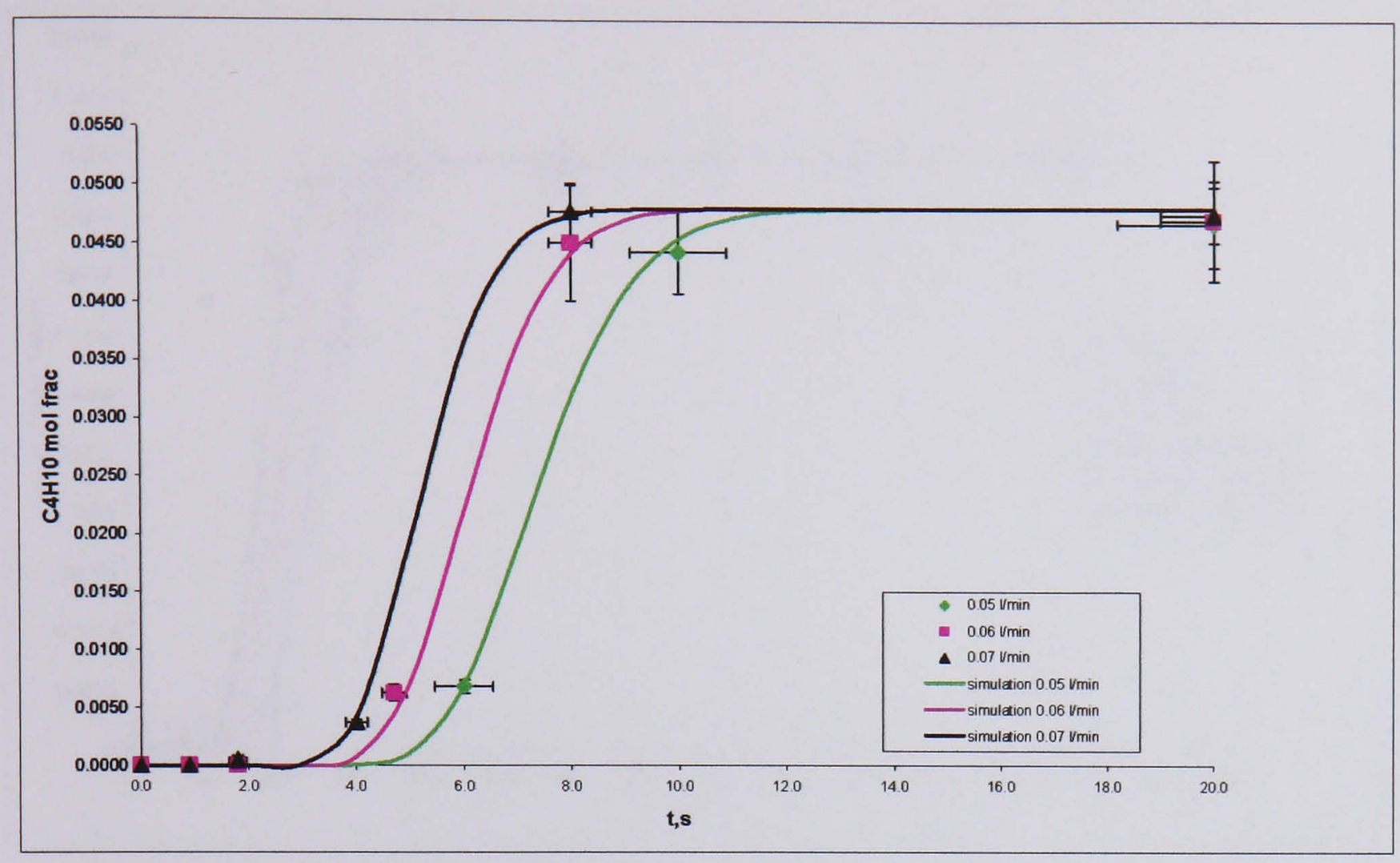


Fig. 5.7 PFR breakthrough profile at T=650K for isobutane

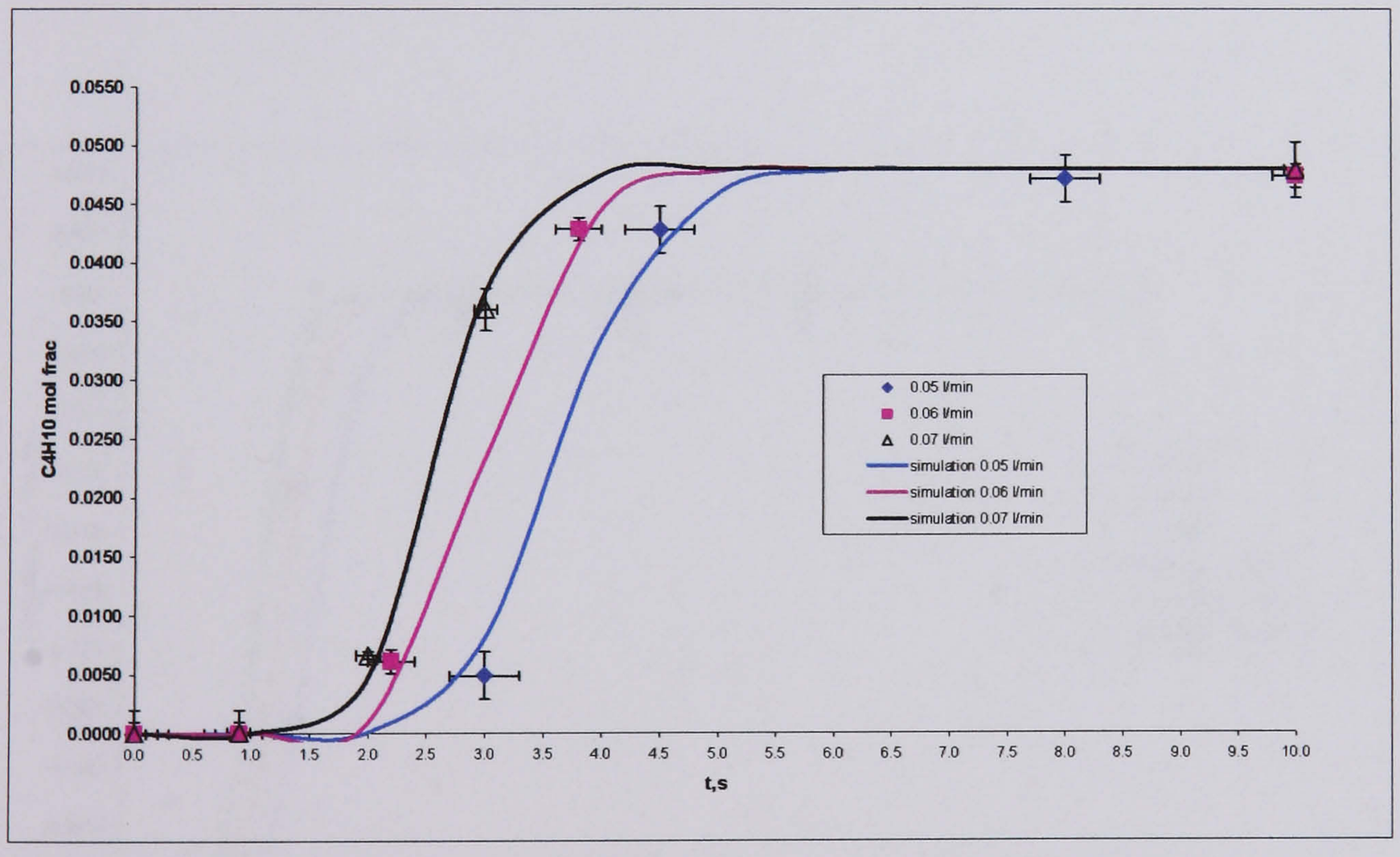


Fig. 5.8 PFR breakthrough profile at T=700K for isobutane

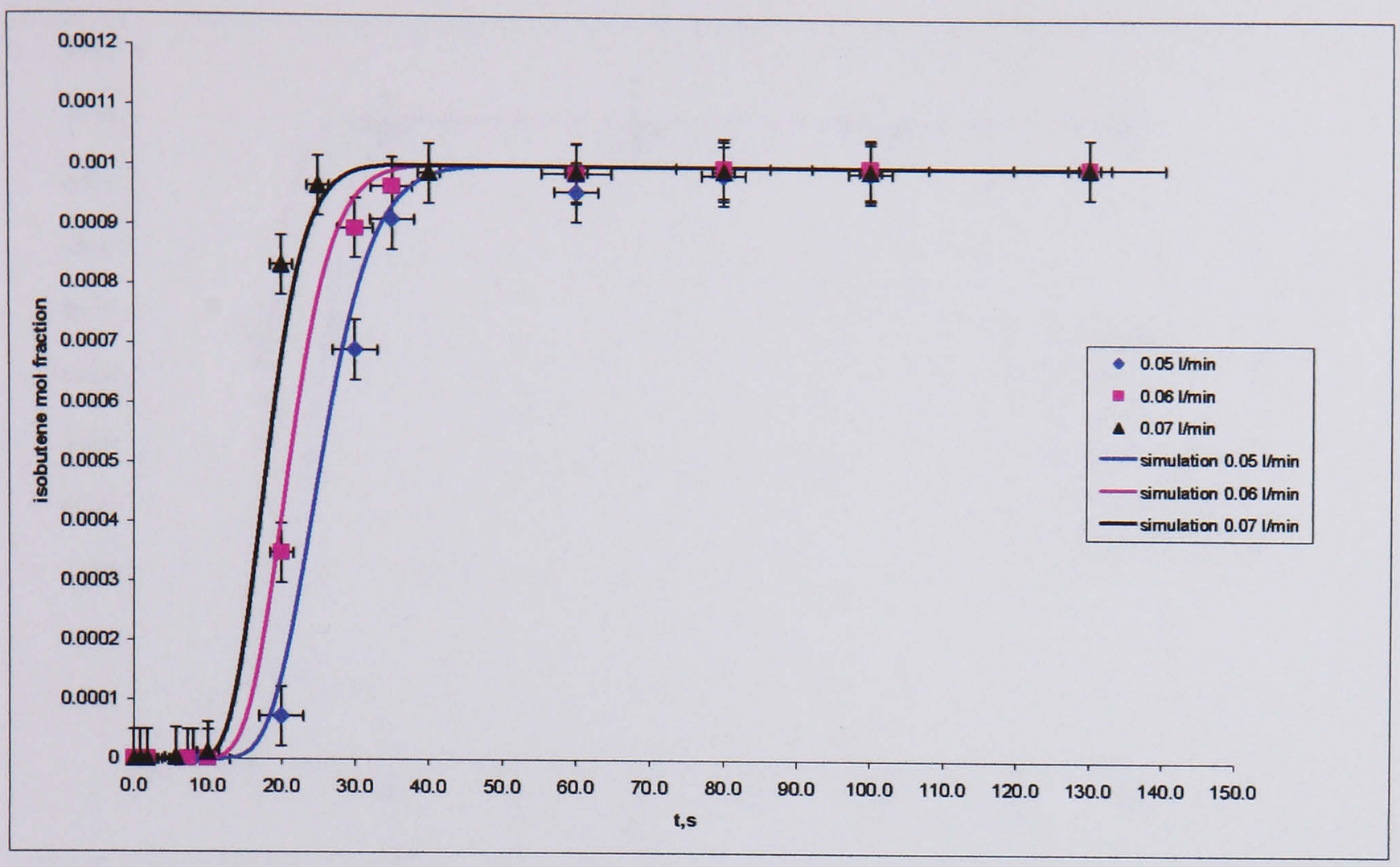


Fig. 5.9 PFR breakthrough profile at T=600K for isobutene

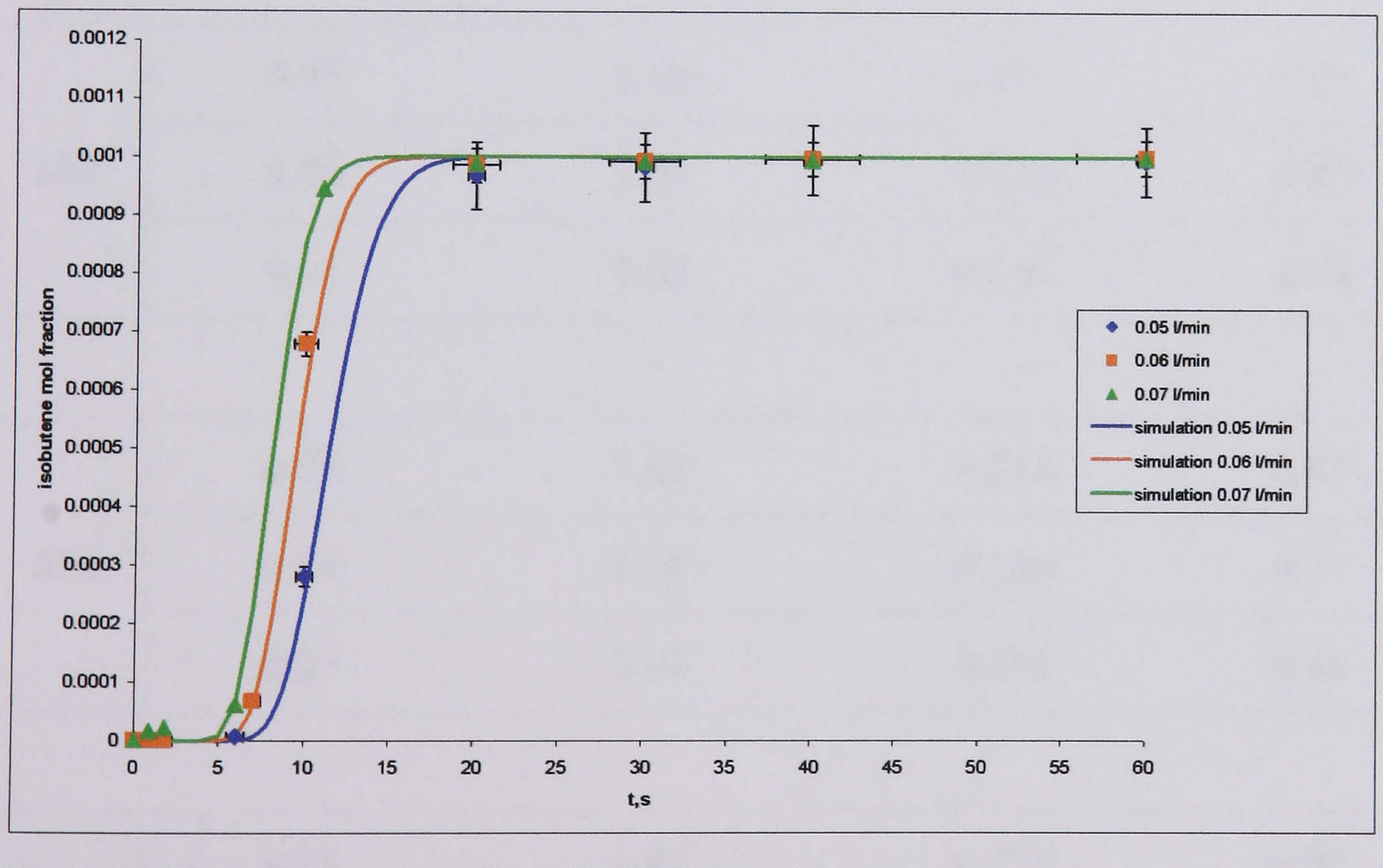


Fig. 5.10 PFR breakthrough profile at T=650K for isobutene

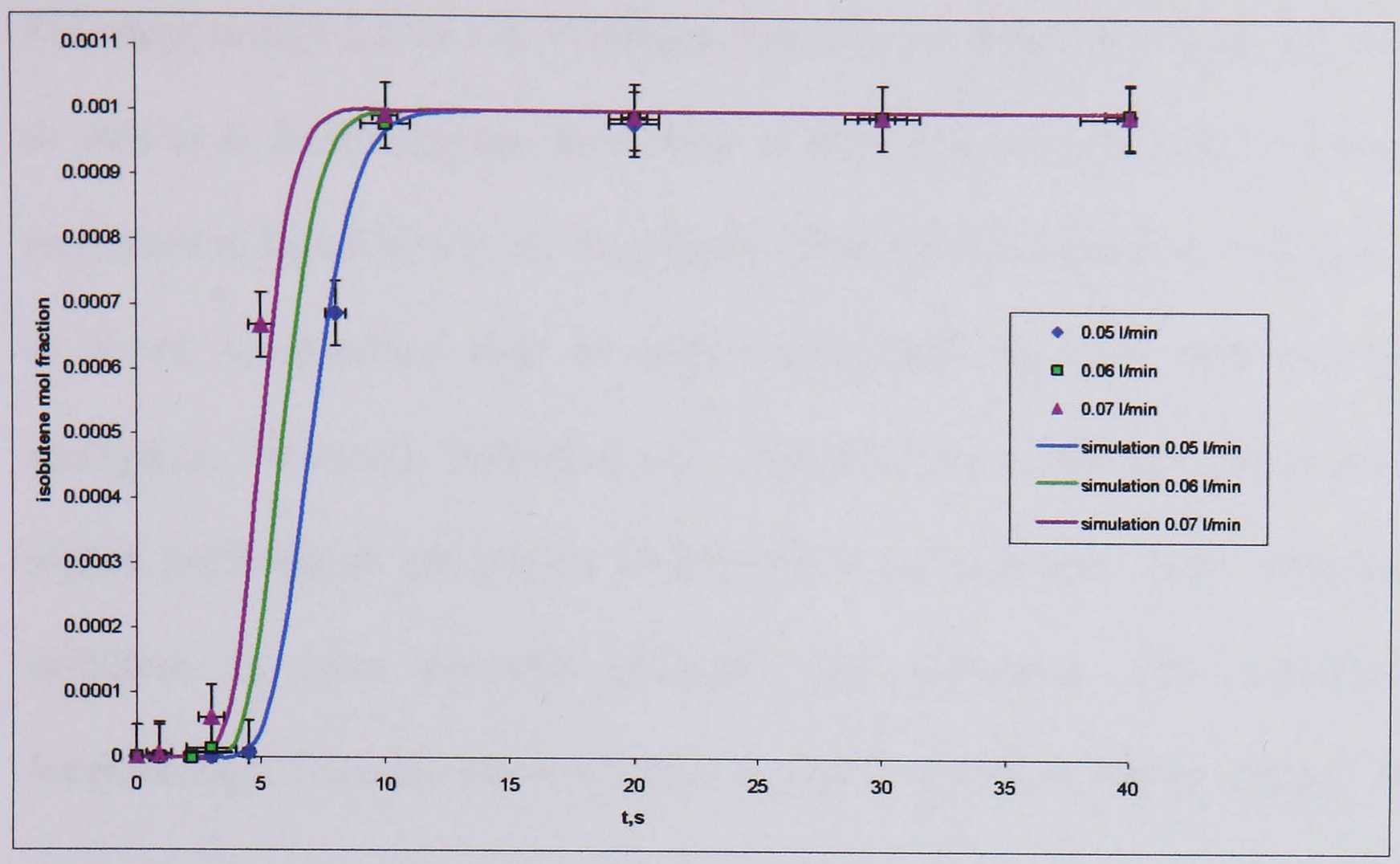


Fig. 5.11 PFR breakthrough profile at T=700K for isobutene

T,K	ν (298K), l min^{-1}	ν(T) x 10^{-6} , m^3 s^{-1}	v, m s^{-1}	τ_{PFR}, s	Reynolds number, Re_p
600	0.05	1.68	0.105	1.00	1.72
	0.06	2.01	0.125	0.84	2.10
	0.07	2.35	0.146	0.72	2.42
650	0.05	1.82	0.113	0.93	1.93
	0.06	2.18	0.136	0.77	2.31
	0.07	2.54	0.159	0.66	2.70
700	0.05	1.96	0.122	0.86	2.13
	0.06	2.35	0.146	0.72	2.55
	0.07	2.74	0.171	0.61	2.98

Table 5.11 Volumetric flow rates and the corresponding velocities, space times and Reynolds number of PFR

Referring to figs.5.6 to 5.8, isobutane step responses become faster at increasing temperatures as well as at increasing gas flow rates. Similar trends could also be seen from isobutene step responses in figs.5.9 to 5.11. In general, isobutane and isobutene adsorption affinities increase at lower temperature due to higher adsorbent capacity and exothermic behaviour of adsorption. However, isobutene step responses are relatively longer in each case indicating higher preferential adsorption characteristic of isobutene over isobutane. In other words, isobutene is more strongly adsorbed than isobutane. The relatively longer isobutene breakthrough time also reflects higher m_i and K_i values as shown in table 5.8 and 5.9.

As flow rate increases, gas-solid contact time reduces considerably and this effect corresponds to the decreasing space time, τ_{PFR} tabulated in table 5.11. Consequently, this reduces the local retention of the adsorbates. Such phenomena are represented by the shorter step response as well as shorter equilibration time as shown in figs. 5.6 to 5.11. The flow rate effect becomes more significant when the bed is operated at higher temperatures due to the fact that bulk gas physical properties (i.e. gas density and viscosity) are temperature dependent.

Another important aspect when analysing the PFR step response curves is the effect of axial dispersion. There is substantial interstitial gas velocity across the traditional packed bed configuration. Consequently, there is some degree of backmixing or intermixing, which resulted in the deviation from plug flow (Alpay, 1992). Therefore, the axial dispersion effect in the packed bed tubular reactor cannot be neglected.

For a gas flow in a packed bed, axial dispersion effect is more dominant in the bed of porous particles than molecular diffusion. The significant axial dispersion from the direct transport

through the solid at low Reynolds number contributes to the step response profiles shape. Such intraparticle diffusion depended on the effective intraparticle diffusivity and the magnitude of the concentration gradient through the particle (Ruthven, 1984). The increasing axial dispersion diffusivity at higher temperatures may attenuate the adsorptive effect in the PFR. This is indicated by the considerably steeper breakthrough curves when adsorption process is conducted at 700K (see figs.5.8 and 5.11).

SAR adsorption analysis

There is considerably longer step response and hence, longer breakthrough time when adsorption process is conducted using the SAR (see figs.5.12 to 5.15). Higher adsorbent-inert diluent particles admixture loading, which also implies higher amount of isobutane and isobutene adsorbed per mass of zeolite KY, give rise to the longer adsorbates retention time. In addition, the radial and axial mixing due to molecular diffusion in the core gas channel as well as in the solid packing region suggests that the adsorption in the SAR is mass transfer controlled. Here, adsorbates may spend relatively longer time within the adsorbent particles due to increasing adsorbent capacity at lower temperature. This in fact is in accordance with the prediction made by Karger and Ruthven (1992) where the slower uptake of the SAR system could be affected by zeolite KY intracrystalline diffusion prior to the intraparticle molecular diffusion.

By referring to table 5.3, the SAR residence time, τ_{SAR} decreases at increasing temperature albeit imposing similar feed gas flow rate (i.e. 0.10 l min^{-1}). This effect coupled with decreasing adsorbent capacity at higher temperatures has led to faster equilibration time of

each adsorbed component. Nevertheless, τ_{SAR} is relatively higher than that of PFR, indicating higher gas-solid contact time and relatively lower feed flow rate bypass in the gas channel. In the absence of convective flow in the annular packed bed region in the SAR, molecular diffusion predominates. At minimum pressure drop estimated in bed, such diffusivity transport is directly proportional to the temperature. This also gives rise to the decrease in breakthrough time whereby at higher temperature, the diffusion flux increases and as a result, the intraparticle diffusion effect is minimised.

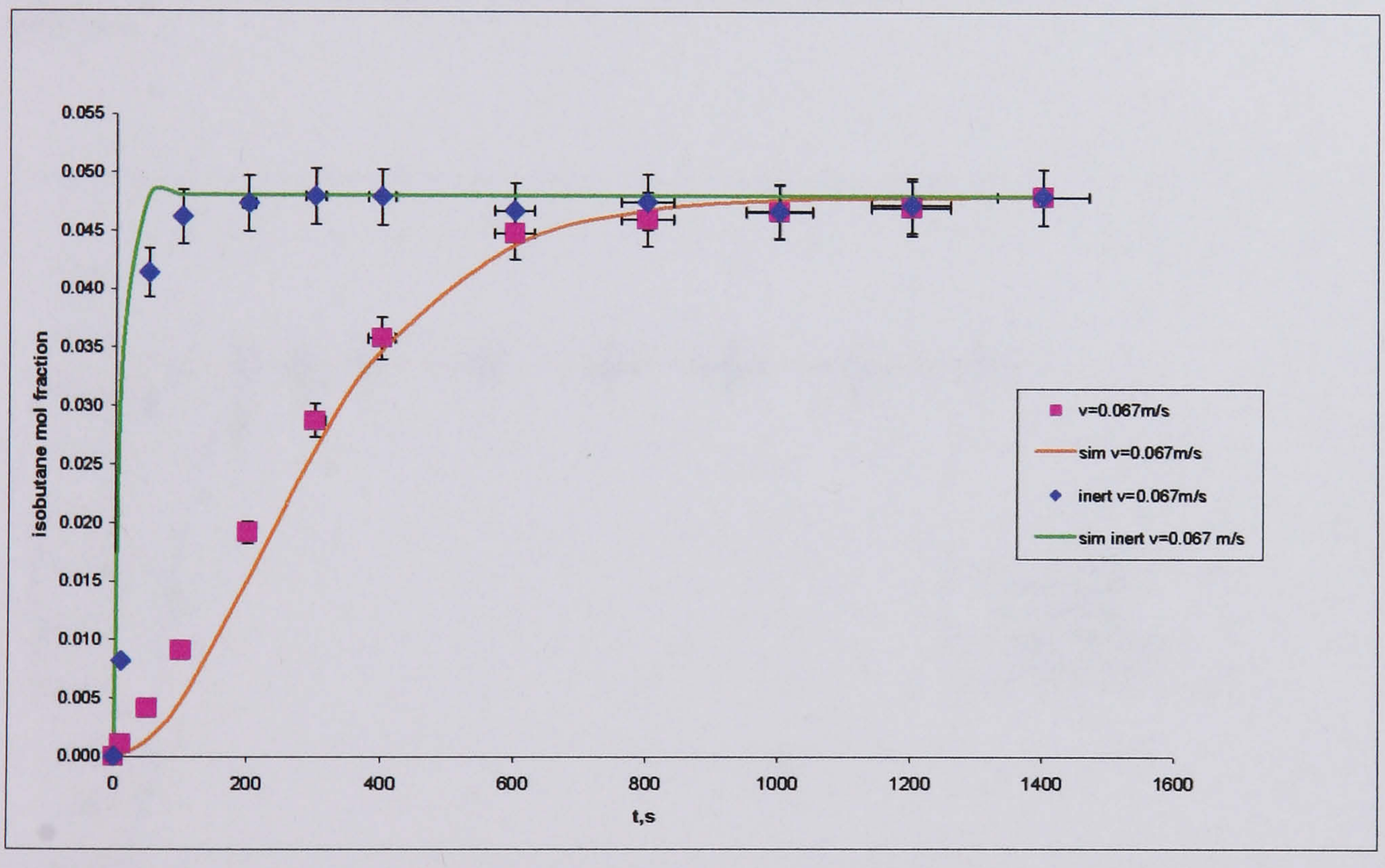


Fig. 5.12 SAR breakthrough profile at T=600K for isobutane; flow rate = 0.10 l min^{-1}; sim = simulation

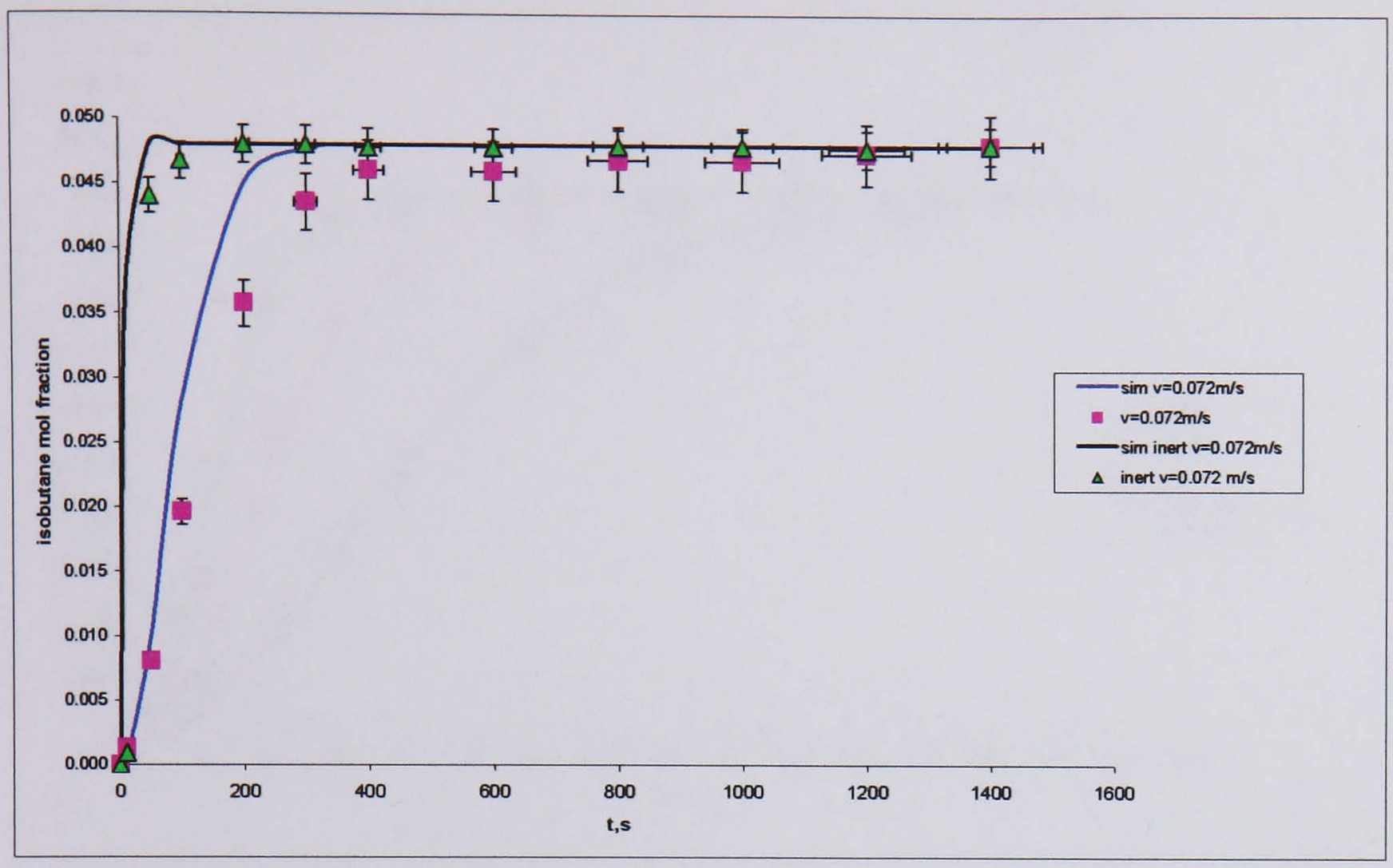


Fig. 5.13 SAR breakthrough profile at T=650K for isobutane; flow rate = 0.10 l min^{-1}; sim = simulation ([§] see footnote)

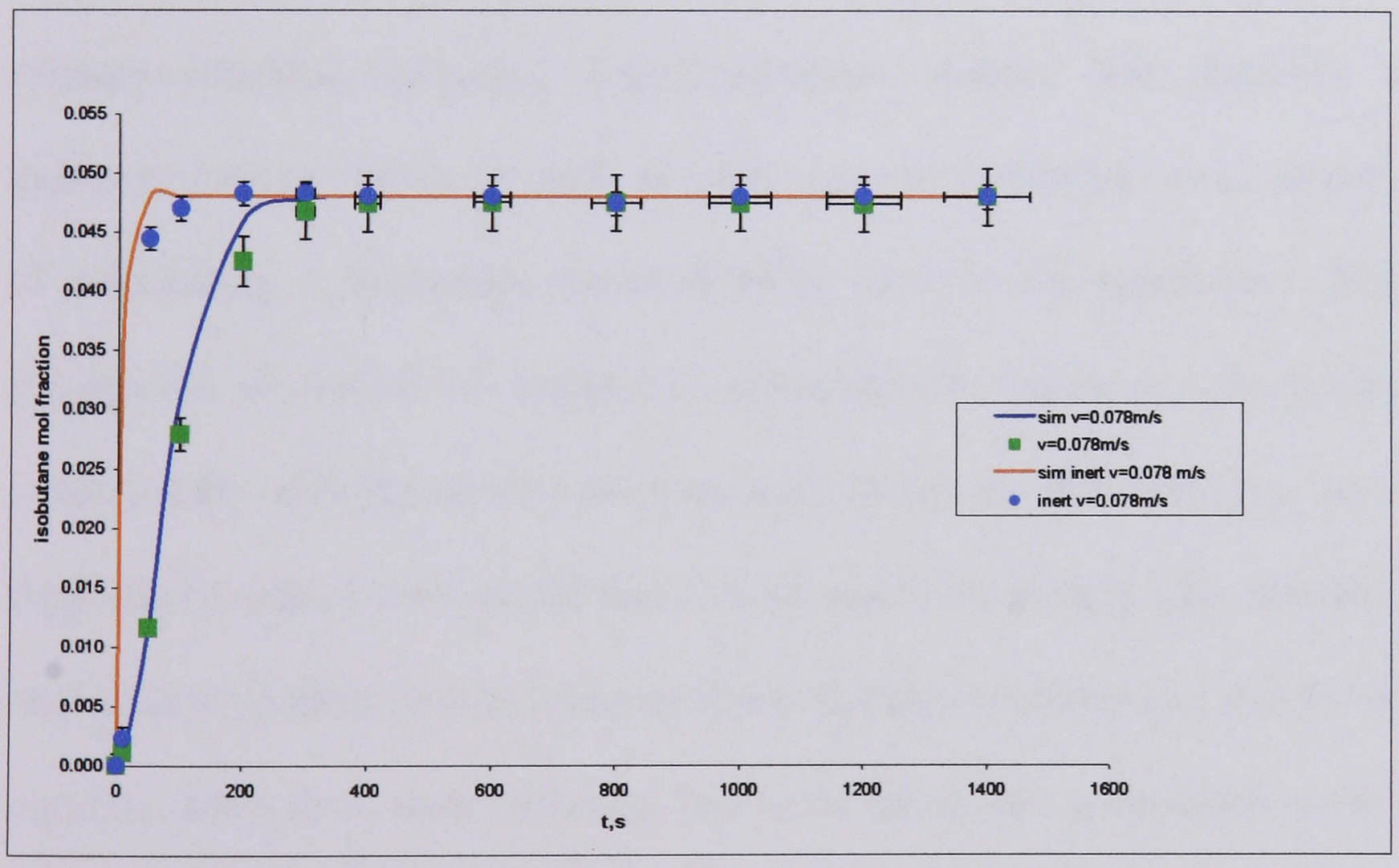


Fig. 5.14 SAR breakthrough profile at T=700K for isobutane; flow rate = 0.10 l min^{-1}; sim = simulation

---

[§] error bars in each figure (i.e. figs 5.12 to 5.15 are based on 95% confidence interval

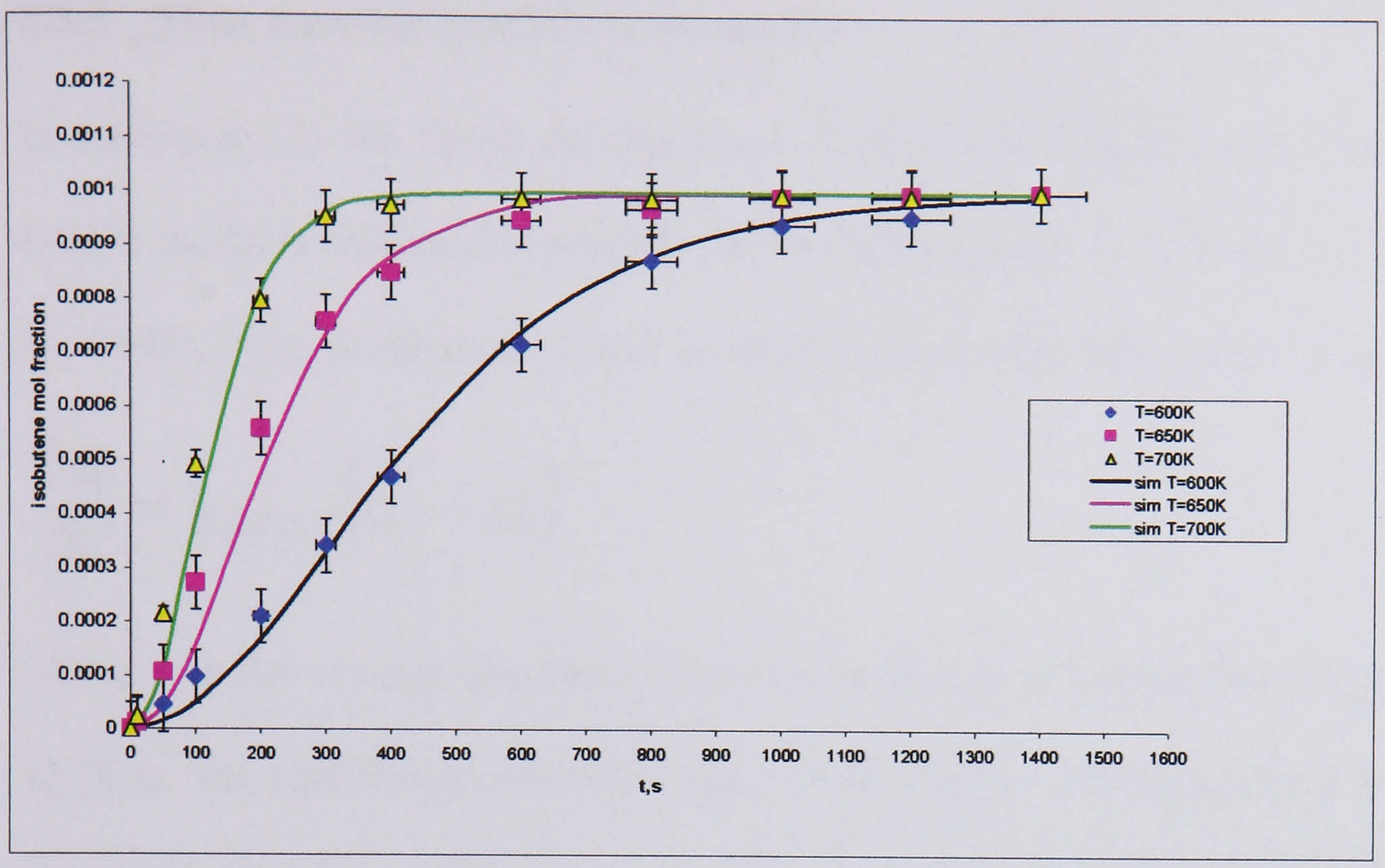


Fig. 5.15 SAR breakthrough profile for isobutene; flow rate = 0.10 l min^{-1}; sim = simulation

The adsorption characterisation would acquiesce with the necessary information to the sorption-enhanced isobutane dehydrogenation studies. The disparity of the adsorption isotherm gradient values of each of isobutane and isobutene would accentuate the possibility of establishing a favourable thermodynamic shift in the equilibrium. Since there would be preferential adsorption for isobutene, represented by higher m_i values, the equilibrium would consecutively shift forward to produce more isobutene and hydrogen. As a result, this would significantly improve the equilibrium conversion of isobutane. Nevertheless, higher adsorption enhancement effects tend to occur at lower reaction temperatures due to increasing adsorption capacity. Therefore, such limitation has to be taken into consideration when dealing with the combined in situ reaction and separation process.

5.3.5 Mass transfer coefficient estimation

In section 5.3.2, the linear driving force (LDF) model based on the Glueckauf and Coates (1947) model is assumed to account for the mass transfer or diffusional resistances (Cheng *et al.,* 1998). Thus, at dilute adsorbate concentration, the adsorption rate is given by

$$\frac{\partial q_i}{\partial t} = k_{mass,i}\left(q_i^* - q_i\right) \tag{5.19}$$

where q_i is the average adsorbed phase concentration of component i in an adsorbent (mol kg^{-1}), q_i^* the equilibrium adsorbed phase concentration of component i (mol kg^{-1}) and $k_{mass,i}$ the mass transfer coefficient (s^{-1}). This model is the simplest and most widely used approximation and it is based on the simplification of Fick's second law of diffusion (Jain *et al.,* 2003). The mass transfer coefficient, $k_{mass,i}$ for a spherical particle was further described according to Glueckauf and Coates (1947) as

$$k_{mass,i} = \frac{15\,\bar{D}_{e,i}}{r_p^2} \tag{5.20}$$

where $\bar{D}_{e,i}$ is the modified effective diffusivity ($m^2\ s^{-1}$) and r_p is the mean adsorbent particle radius (m). The validity of such equation is that it should satisfy the limit in the following expression as described by Glueckauf (1955) (see Alpay, 1992, Alpay *et al.,* 1993, Cheng *et al.,* 1998, Sheikh, 1999)

$$\theta_{c,i} \equiv \frac{\bar{D}_{e,i}\,t_c'}{r_p^2} > 0.1 \tag{5.21}$$

where $\theta_{c,i}$ is the dimensionless cycle half time, t'_c the cycle half time (Glueckauf, 1955) for the cyclic adsorption and desorption process (s) (Alpay, 1992) . The detailed calculations of $k_{mass,i}$ for the adsorption of C_4 species on zeolite KY are presented in Appendix B. The factor 15 in equation 5.20 is incorporated in the definition of dimensionless time and bed length parameters for the diffusional model, thus making these quantities numerically equivalent to the corresponding quantities for the linear rate model (Ruthven, 1984).

Parameters	**Operating Conditions**			**units**
d_p	**$1.78\ 10^{-4}$**			**m**
ε_b [b]	**0.35**			**-**
ε_t [b]	**0.75**			**-**
ε_p	**0.615**			**-**
P	**1.0×10^5**			**Pa**
T	**600**	**650**	**700**	**K**
$k_{mass,\ isobutane}$	**215.47**	**343.81**	**727.03**	**s^{-1}**
$k_{mass,\ isobutene}$	**100.97**	**228.17**	**373.32**	**s^{-1}**
ρ_g	**2.76**	**2.98**	**3.21**	**kg m^{-3}**
μ	**2.95×10^{-5}**	**3.12×10^{-5}**	**3.27×10^{-5}**	**Pa s**

Table 5.12 Parameter used and estimated in this work; [a] Data from Sheikh (1999); [b] Data from Alpay et al (1996)

The instantaneous degree of the adsorption rate were estimated based on the $k_{mass,i}$ values. Sheikh (1999) stated that high values of $k_{mass,i}$ signifies instantaneous adsorption rates, whereas low values of $k_{mass,i}$ indicates that the process would be limited by mass transfer resistance. By referring to table 5.12, considerably high $k_{mass,i}$ values imply instantaneous rate of adsorption for isobutane and isobutene and hence, maximum possible separation at

negligible diffusional limitations. Such information would be necessary to predict the outcome of the adsorption-enhanced isobutane dehydrogenation process.

5.3.6 Diffusion coefficients

Table 5.13 provides a summary of molecular diffusion coefficient, D_m (or D_{AB}) and axial diffusion coefficient, D_x used in this work. The corresponding equation for each type of diffusion coefficients have been presented in Chapter 3 (see sections 3.32 and 3.4). More details of the diffusion coefficients calculations are given in Appendix A.

T,K	D_m , $m^2 s^{-1}$	D_x , $m^2 s^{-1}$
600	3.35×10^{-5}	$1.83 \times 10^{-5} + \frac{v^2}{670(v + 0.052)}$
650	3.86×10^{-5}	$2.11 \times 10^{-5} + \frac{v^2}{670(v + 0.060)}$
700	4.39×10^{-5}	$2.40 \times 10^{-5} + \frac{v^2}{670(v + 0.067)}$

Table 5.13 Summary of molecular diffusion coefficient, D_m and axial dispersion coefficient, D_x used in this work; velocity, v for D_x corresponds to the estimated PFR gas velocity at given temperature

5.4 Error analysis

Errors in this work can be divided into primary and secondary measurements. The primary measurements include: temperature and gas flow rates (where the errors are measured using bubble column), which are obtained directly during the experimental work; and pressure

gradient by theoretical estimation. These are represented in percentage of absolute errors. On the other hand, approximate maximum errors for the secondary measurements are as a result of the primary measurements errors and they include: adsorption isotherm measurement and reactant conversion and bulk density.

With reference to Table 5.14, the secondary measurement errors are most probably due to the significant inequality in reactor volume as well as the amount of the admixed adsorbent + inert or catalyst + inert particles used in each of the reactors investigated. According to the work of Alpay and Kershenbaum (1995), if the pressure drop across the bed is substantial (i.e. the ratio of inlet pressure over outlet pressure, $P_{in} / P_{out} \gg 1$), equation (5.10) would be modified to include the pressure correction factor, Γ, and this is expressed as:

$$t_r = \frac{\Gamma K_i L}{u_e} \tag{5.22}$$

where

$$\Gamma = \frac{2}{3}\left[\frac{(1+\gamma)^{3/2} - 1}{\gamma}\right] \tag{5.23}$$

and

$$\gamma = \left(\frac{P_{in}}{P_{out}}\right)^2 - 1 \tag{5.24}$$

In this work, the pressure difference estimated is minimal for the PFR and zero for the SAR (i.e. the ratio of inlet pressure over outlet pressure, $P_{in} / P_{out} \approx 1$). Thus, the isobaric ideal case condition as described in Section 5.3.2 to calculate the first moment could be applied (i.e. by using equation (5.10)). Nevertheless, the axial dispersion effect in the PFR cannot be neglected and therefore, the discrepancies on fitting the corresponding theoretical response to the PFR breakthrough curves are relatively higher than that of the SAR breakthrough curves.

Also, from Table 5.14, the reactant conversion maximum errors are determined from three repeated experiments at each flow rate and/or temperature investigated. Calculated errors are higher at T = 700K ($\geq$ 2.0%) due to the temperature influence on the physical properties of the bulk gas, which causes the gas to expand when heated hence, reduced space time.

Primary measurements	**Absolute errors**
Time measurement (bubble column)	**± 0.1 s**
Reactor temperature based on the K-thermocouple readings at inlet, middle and outlet wall of the reactor (*)	**600 ± 5K** **650 ± 10K** **700 ± 10K**
Secondary measurements	**Approximate maximum errors**
Bulk density	**0.05**
Adsorption isotherm (PFR)	**0.75**
Reactant conversion	**0.05**

Table 5.14 Summary of the errors of the primary and secondary measurements

*** The temperature errors represent the maximum possible fluctuation before the reactor temperatures approach isothermal, i.e. minimum temperature difference between each point detected on the outer reactor wall.**

In Chapter 3, both reactors (i.e. PFR and SAR) are assumed to be operated isothermally throughout the reaction and adsorption process. This assumption in fact, could be a true case when the experiments are carried out at reasonably low temperatures. In this work, the isobutane conversions at selected temperatures of 600K, 650K and 700K are relatively small suggesting a considerably small occurrence of heat loss. In this case, the isothermal assumption could be tested in terms of an adiabatic operation.

Thus, for an adiabatic process, the average heat supplied into the reactor by the bulk gas to raise an inlet stream from ambient temperature, T_o (298K) to the reactor isothermal temperature, T is equivalent to the total heat output during the dehydrogenation and adsorption process at corresponding T, i.e.,

$$n_{bulk} c_{Pg} \Delta T = X_A y_A \frac{P}{R_{gas} T} A_{gas} v_{ave} \Delta H_{rxn} - q_{A,T} \rho_{ads}^{bulk} \nu_T \Delta H_A \qquad (5.25)$$

where c_{Pg} the specific heat capacity of the bulk gas (J mol^{-1} K^{-1}), n_{bulk} the molar flow rate of the bulk gas (mol s^{-1}), y_A the isobutane mole fraction, X_A the reaction conversion, q_A the amount of isobutane adsorbed (mol kg^{-1}), ρ_{ads} the bulk density of the adsorbent, ν_T the volumetric flow rate (m^3 s^{-1}), ΔH_A the isosteric heat of adsorption of isobutane (J mol^{-1}) (see Table 5.10) and ΔH_{rxn} is the total enthalpy of reaction (J mol^{-1}) and was determined from thermodynamic calculations..

T, K	$\Delta H_{rxn}(T)$ x 10^5 J mol^{-1}	q_A, mol kg^{-1}	ΔT, K
600	1.223	0.016	0.04
650	1.228	0.007	0.02
700	1.232	0.003	0.01

Table 5.15 Summary of the temperature difference, ΔT at three different temperatures; ΔH_A= 42570 J mol^{-1}

At c_{Pg} = 28.44 J mol^{-1} K^{-1} for nitrogen, the temperature difference, ΔT for each of the selected temperatures are summarised in Table 5.15. Where higher temperature is naturally favoured by the endothermic dehydrogenation reaction, operating at such condition would further reduce the adsorbent capacity leading to faster equilibration time. As a result, sorbate adsorption becomes more difficult and this temperature effect will be investigated in Chapter 6 and 7 respectively for the conversion enhancement effect of in situ reaction-separation process. Nevertheless, the isothermal assumption in this work is valid based on the infinitesimal ΔT in Table 5.15.

5.5 Concluding remarks

The forward rate constant for the isobutane dehydrogenation reaction was determined based on the assumptions of constant reactor volume and constant volumetric flow rates at isobaric conditions. Platinum-alumina catalyst was selected for the catalytic reversible dehydrogenation process because it was possible to achieve good selectivity, stability and activity at given operating conditions. The adsorption kinetics of isobutane and isobutene were investigated over zeolite KY. The adsorption equilibria parameters were estimated by matching the theoretical response curves to that of the experimental curves such that adequate comparisons could be made between the performance of SAR and traditional packed bed reactor.

Chapter 6

Structured Adsorptive Reactor Investigations

6.1 Introduction

In most cases reported, the catalytic reversible dehydrogenation of isobutane over a platinum-alumina catalyst has been conducted in a traditional packed bed, plug flow reactor at high temperatures. The choice of reactor design has also been without doubt critical to the success of the catalytic process. Nevertheless, existing product recovery processes have added to the overall cost of the manufacturing and thus, an economic appeal exists in the integration of the reaction and separation stage.

One of the attractive ways of attaining a high equilibrium conversion and production yield is by combining the chemical reaction with some form of in situ separation step in a single unit operation. Such operation utilises Le Chatelier's principle whereby the removal of one of the reaction products result in a forward shift of equilibrium, hence increasing the rate of the forward reaction. This in situ separation method has led to designs based on chromatographic reactors, membrane reactors and pressure, thermal, and concentration swing type reactors.

In this chapter, the study of combined reaction and separation process involving two types of reactor configurations is presented. In this case, the separation performance of the fixed bed adsorptive reactor and the novel annular-type SAR are investigated. The general experimental

set up and procedure of both the SAR and PFR reactors are similar to those described in previous chapters (see chapter 4 and 5). The in situ reaction and adsorption process, which involves an admixture of platinum-alumina catalyst and zeolite KY adsorbent, is conducted at isothermal temperatures and atmospheric pressure. The periodic regeneration of adsorbent involves purging the reactor with an inert gas, which may also be used to supply the necessary reaction heat to the catalyst and to prevent any moisture build-up.

In this work, the adsorption-enhanced dehydrogenation reaction was theoretically studied by incorporating the adjusted kinetic and adsorption parameters obtained from Chapter 5 within the gPROMS simulation environment. The experimental validations, which are presented in the forms of breakthrough and conversion enhancement profiles, are observed by comparing the experimental data to results obtained from the theoretical model.

6.2 SAR overview

Basically, adsorptive reactors couple the operations of adsorption and catalytic reversible reactions into a single process (Alpay *et al.,* 1993). Reaction enhancement can therefore be achieved through limitation of the backward reaction by the removal of the adsorbable product. Adsorptive reactor technology has been applied to chromatographic type system and extensions of this include real and simulated moving bed processes (Chatsiriwech *et al.,* 1994). Due to its non-continuous and relatively complex operation, especially in the case of moving bed processes, chromatographic reactors are often unsuitable for large-scale operations.

The general configuration of the adsorption-enhanced reaction process can then be traditionally described in such a way that it comprises a fixed bed column packed with an admixture of a catalyst and an adsorbent that selectively removes a reaction by-product from the reaction zone (Carvill *et al.,* 1996). In conjunction with the adsorption technology, the reactor bed has to be periodically or continuously regenerated using principles such as pressure swing, thermal swing and concentration swing adsorption as well as inert gas purge stripping. The periodic regeneration necessitates in the selective removal of the reaction by-product (adsorbate) upon equilibration of the adsorbent (Ding and Alpay, 2000).

The advantages of adsorption-enhanced, packed-bed adsorptive reactors have thus far shown potential in achieving high equilibrium conversion and product yield at lower reaction temperatures. This in turn enables minimum sensible heat losses, efficient in situ regeneration of adsorbent, improved selectivity, and lower overall energy consumption while reducing the degree of catalyst deactivation (see Alpay *et al.,* 1993, Alpay *et al.,* 1994, Chatsiriwech *et al.,* 1994, Carvill *et al.,* 1996, Yongsunthon and Alpay, 1999, Sheikh, 1999, Ding and Alpay, 2000).

However, conventional random packed, fixed bed reactors have one obvious disadvantage, considerably high pressure drop across the bed even though it may be offset by the versatility to overcome mass transfer limitations at a lower operating cost (Ruthven and Thaeron, 1997). Where overall effectiveness and the efficiency, and hence the financial aspects of the conversion process are of great importance (Van den Bleek *et al.,* 1996), the pressure drop has to be maintained as low as possible. One of the possible attractive means of achieving this is to provide a certain arrangement or structure in the solid packing (Van den Bleek *et al.,* 1996).

In this work, the novel annular-type, structured adsorptive reactor, SAR, is chosen specifically to provide an alternative means of adsorptive reactor whilst achieving a low pressure drop requirement across the reactor. It combines the advantages of an annular bed adsorber (see Kehat *et al.,* 1988, Tierney *et al.,* 1999, Yoshida *et al.,* 2003) as well as an annular structured catalyst-packing reactor (Beretta, *et al.,* 1998). The fluid flow mechanism may thus be compared to a parallel passage reactor (see Calis *et al.,* 1994, Sie and Calis, 1998). Almost invariably, the feed gas flow rate is assumed to be uniformly distributed along the entire bed length (Heggs *et al.,* 1994), and the reactor is operated within laminar flow region. Further details on the mechanical design and configuration of SAR have been described in Chapter 2, 3 and 4.

In this chapter, focus is given on the admixture studies for both the PFR and SAR type reactor configurations. Conversion enhancement profiles are used to evaluate the overall performance of the dehydrogenation reaction for both configurations.

The key objectives of this work are:

- To investigate the potential of admixed platinum-alumina catalyst and zeolite KY adsorbent in achieving adsorption-enhanced dehydrogenation reaction. This will be the key step to establishing a reaction-separation process.
- To advocate and verify the theoretical studies of SAR and PFR by comparing the mathematical model results with the experimental findings, thus making the theoretical model viable for further simulation investigations
- To further exploit the potential of SAR through theoretical and experimental investigations of a complete adsorption and desorption cycle at isothermal and isobaric conditions

6.3 Single-step process experimental study

The emphasis of this study is to validate the theoretical studies regarding the adsorption-enhanced isobutane dehydrogenation reaction through the SAR system, while making some comparisons to the conventional PFR system. In Chapter 3, modelling of the system has been undertaken but with the addition of introducing the conversion enhancement factor, E (t). The primary evidence of the catalyst-adsorbent admixture potential is investigated through PFR experiments at three temperatures: 600K, 650K and 700K at constant feed gas flow rates. The results are presented in the form of breakthrough curves and conversion enhancement effect profiles.

6.3.1 PFR admixture experiments

As described in Chapter 5, two main feed streams: the reaction gas stream and purge gas/activation gas stream were employed in the experiment. The former consists of the reaction gases with five premixed feed gases of 95% v/v nitrogen, 4.8% v/v isobutane (the reactant gas), and 0.1% v/v of each of isobutene, methane and hydrogen. The latter consists of the purge gas- activation gas stream of pure nitrogen (99.995% v/v) and 10% hydrogen/nitrogen v/v and was interconnected via a 2-way valve. These gases are fed during the experimental investigations and the flow rates controlled at the inlet gas stream by the mass flow meter. The feed streams are operated by manually switching from one feed stream to another via a 3-way valve.

Methodology

The admixture of catalyst and adsorbent particles (~106-250 μm) was packed in the reactor column as described in section 5.2.2. The mass of each platinum-alumina catalyst and zeolite KY adsorbent employed, W, is 5.0 x 10^{-4} kg (admixture ratio = 1:1). The remaining space of the reactor volume is filled with the equivalent inert diluent particle sizes to create a dense environment. Prior to running this experiment, the fresh catalyst and adsorbent are first dried by passing 99.995% nitrogen purge at 600K for 2 hours at a flow rate of 0.05 litre min^{-1} to remove any water vapour in the bed. Catalyst activation is carried out by purging the column with 10% hydrogen in nitrogen carrier at the same temperature and this is maintained for another 12 hours. The feed gases are fed at atmospheric pressure and ambient temperature and fed via the preheat section before entering the reactor. The volumetric flow rates are varied using the mass flow meter control device. The first experiment is carried out at a constant oven temperature of 600K and is repeated at different constant volumetric flow rates. The whole procedure is then repeated at two other different sets of temperatures i.e. 650K and 700K. All the product samples are injected to the 16-loop Valco valve via the 1/16 inches product line and analysed in the Shimadzu 14-B GC equipped with an FID detector and a Graphpac column. During the sample analysis, the reactor bed is purged by nitrogen at the same reaction temperature to remove the adsorbates and thus, subsequently preparing a clean bed operation (i.e. adsorbent free of adsorbates) for the next experiment.

Results and Discussions

This section discusses the effect of varying the bed temperature at constant flow rate and the effect of varying flow rates at constant bed temperature for the PFR system. Reproducibility is

obtained by repeating the same experiment for each parameter set. The PFR conversion enhancement factor is assessed by applying equation (3.47).

i) Effect of varying temperatures

The admixture feasibility potential is first investigated by varying bed temperatures at a constant feed gas flow rate of 0.05 l min^{-1}. The adsorption-only and catalyst-only breakthrough curve results from Chapter 5 are included on each of the relevant admixture plots. This is to show that reaction with in situ separation does take place and hence, the feasibility of the catalyst and adsorbent admixture.

Figs 6.1 to 6.3 illustrate the adsorption enhanced effect in the presence of zeolite KY adsorbent where the transient period is longer than that of the catalyst-only run. This indicates the occurrence of in situ separation whereby isobutene, which is the stronger adsorbable product component, is selectively adsorbed throughout the dehydrogenation reaction process. In as much as having the desirable effect of the retention of isobutene due to the interaction between the adsorption and reaction process, the conversion enhancement effect is found to decrease as reaction temperature increases. While the adsorption of isobutene increases the net rate of forward reaction, the adsorption affinity decreases resulting in noticeably lower E (t) at higher temperatures (see fig.6.4). Nonetheless, for each case, the absence of adsorbent gives shorter breakthrough time, suggesting that the transient kinetic response of the catalysed isobutane dehydrogenation is only thermodynamically limited.

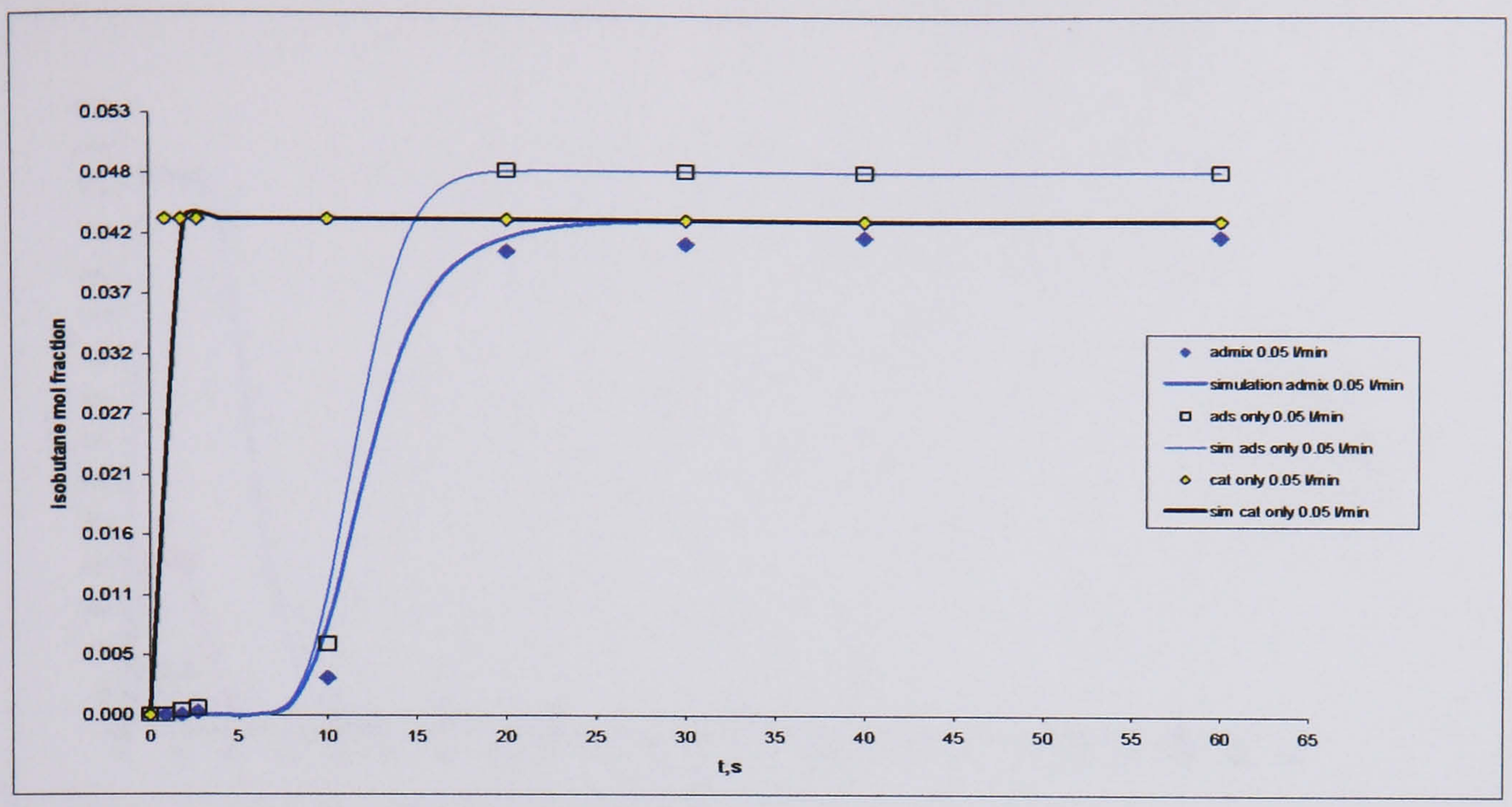


Fig. 6.1 PFR transient kinetic and adsorption response curves at T=600K, flow rate=0.050 l min^{-1}; admix= admixture; ads= adsorbent; sim = simulation; cat = catalyst

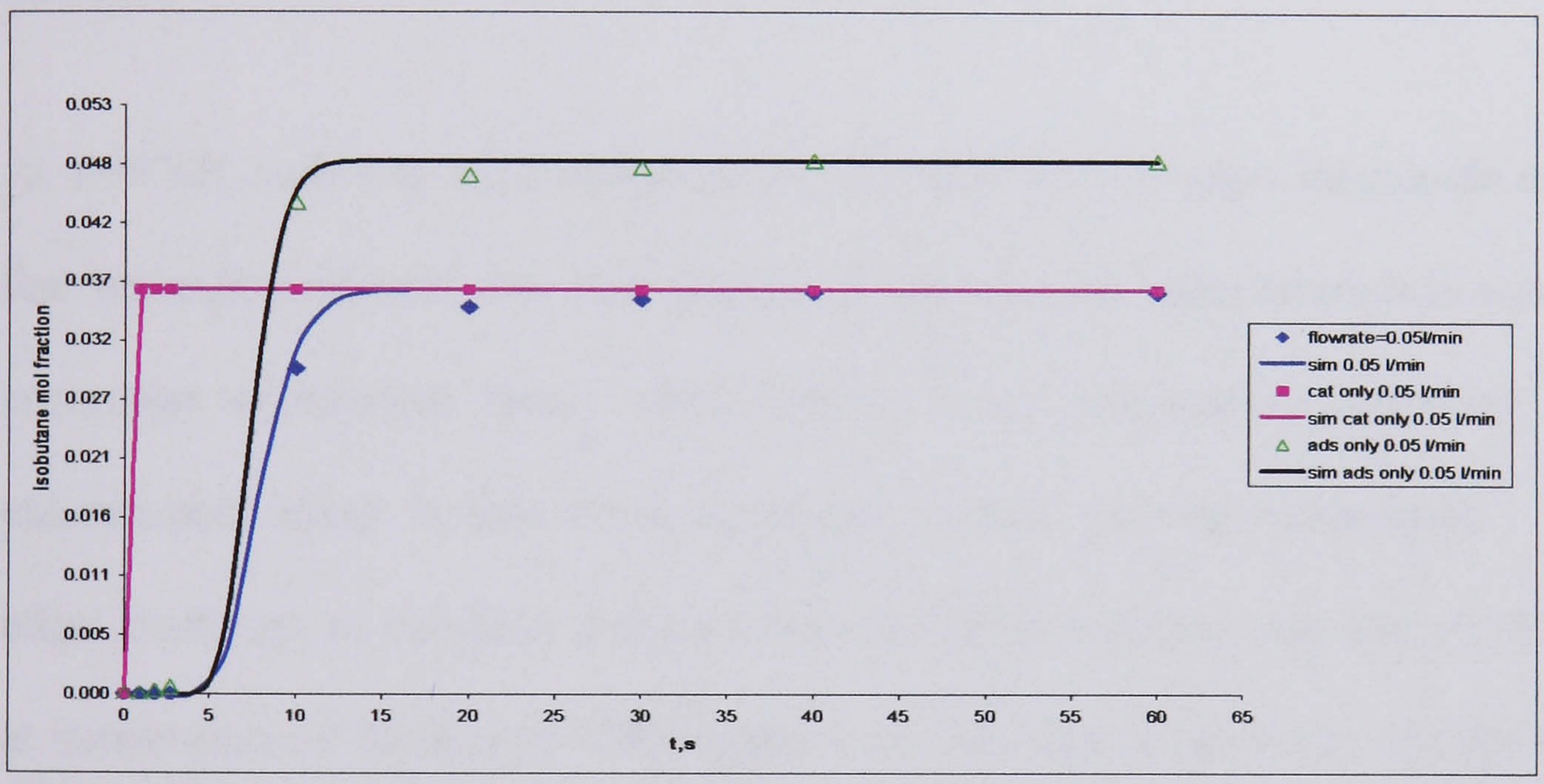


Fig. 6.2 PFR transient kinetic and adsorption response curves at T=650K, flow rate=0.050 l min^{-1}; admix= admixture; ads= adsorbent; sim = simulation; cat = catalyst

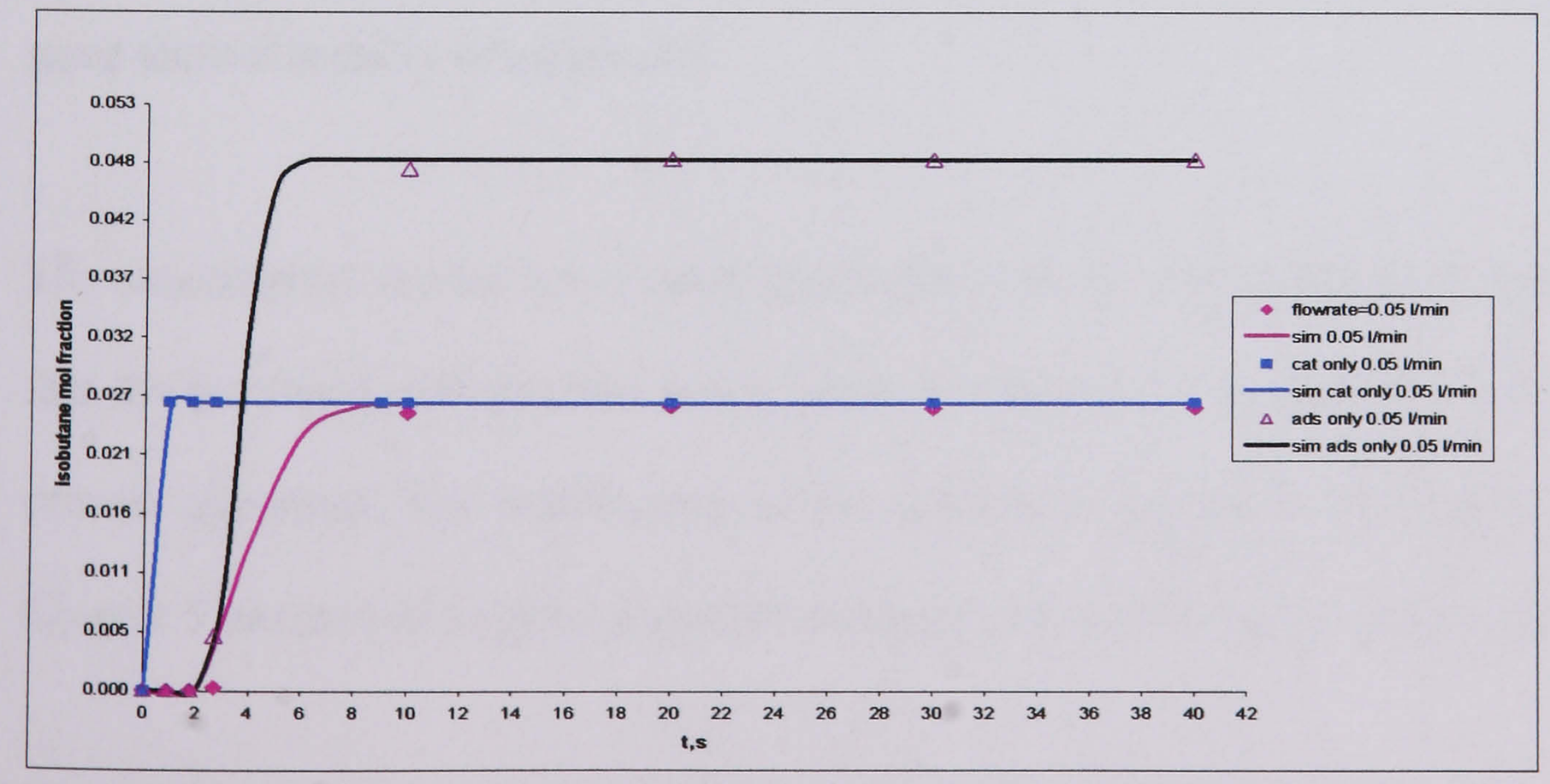


Fig. 6.3 PFR transient kinetic and adsorption response curves at T=700K, flow rate=0.050 l min^{-1}; admix= admixture; ads= adsorbent; sim = simulation; cat = catalyst

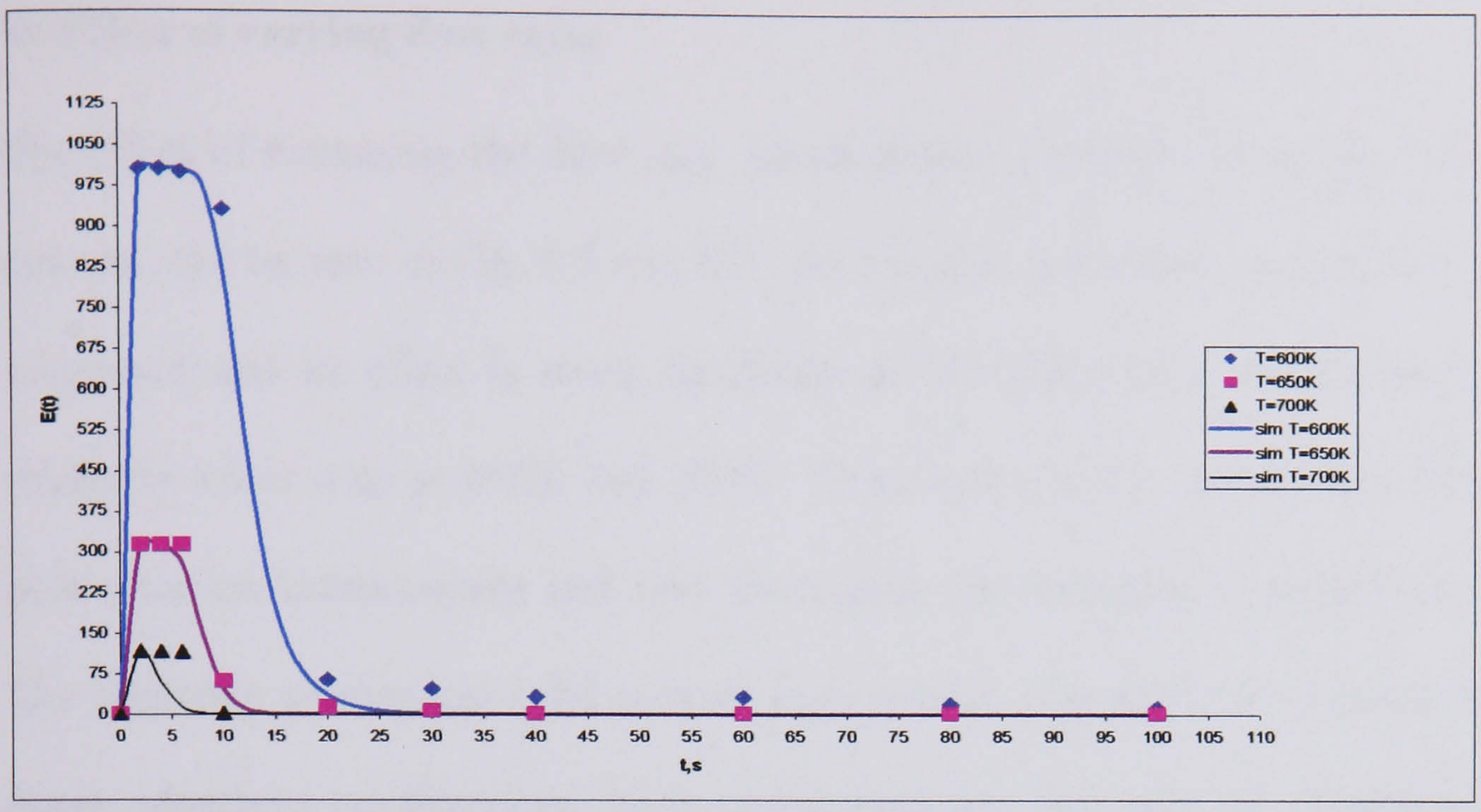


Fig. 6.4 PFR conversion enhancement effect profile for three temperatures at constant flow rate= 0.050 l min^{-1}; sim = simulation

At T=600K, only 9.0 % of isobutane is converted but the larger magnitude of E (t) indicates that separation effect in the PFR system at this reaction temperature is in accordance with the adsorption equilibrium factor which favours lower temperature operation. The conversion enhancement effect is thus more significant at low reaction temperature. The separation effect continues to decrease despite achieving higher reaction conversions of 24.5% and 47% at temperature of 650K and 700K respectively (see figs.6.2 and 6.3). Nevertheless, reasonable magnitude of adsorption separation effects were obtained at these two temperatures implying good thermal stability of zeolite KY.

The experimental results are in good agreement with the PFR theoretical responses indicating that the proposed mathematical model given in Chapter 3 is suitable for transient, single-step process operation. The modification of the adsorption parameters as shown and discussed in Chapter 5 has proven to give adequate theoretical outcome at each reaction temperature.

ii) Effect of varying flow rates

The effect of increasing the flow rate, which implies relatively lower space time in the reactor column, can be seen in Fig. 6.5 and 6.7. At a higher space time, the backward reaction rate is minimised and its effect is more significant at T=600K where the equilibrium conversion is relatively lower than at 650K and 700K. In all cases, a low space time will generally lead to poor reaction enhancement and thus decreasing the retention of adsorbate in the adsorbent. The relatively shorter gas-solid contact time reduces efficient bed utilisation and this leads to faster adsorbent equilibration. Such phenomena are indicated by relatively shorter transient time and relatively steeper breakthrough curve at each increment of feed flow rates.

Higher space times however may lead to poor heat transfer (Ding and Alpay, 2000), and this may deviate from a nearly isothermal condition across the reactor. Nevertheless, the cross-sectional area of the PFR column (i.e. at 1.605×10^{-5} m^2) is relatively small such that it may reduce such an effect throughout the process and thus, more efficient heat transport.

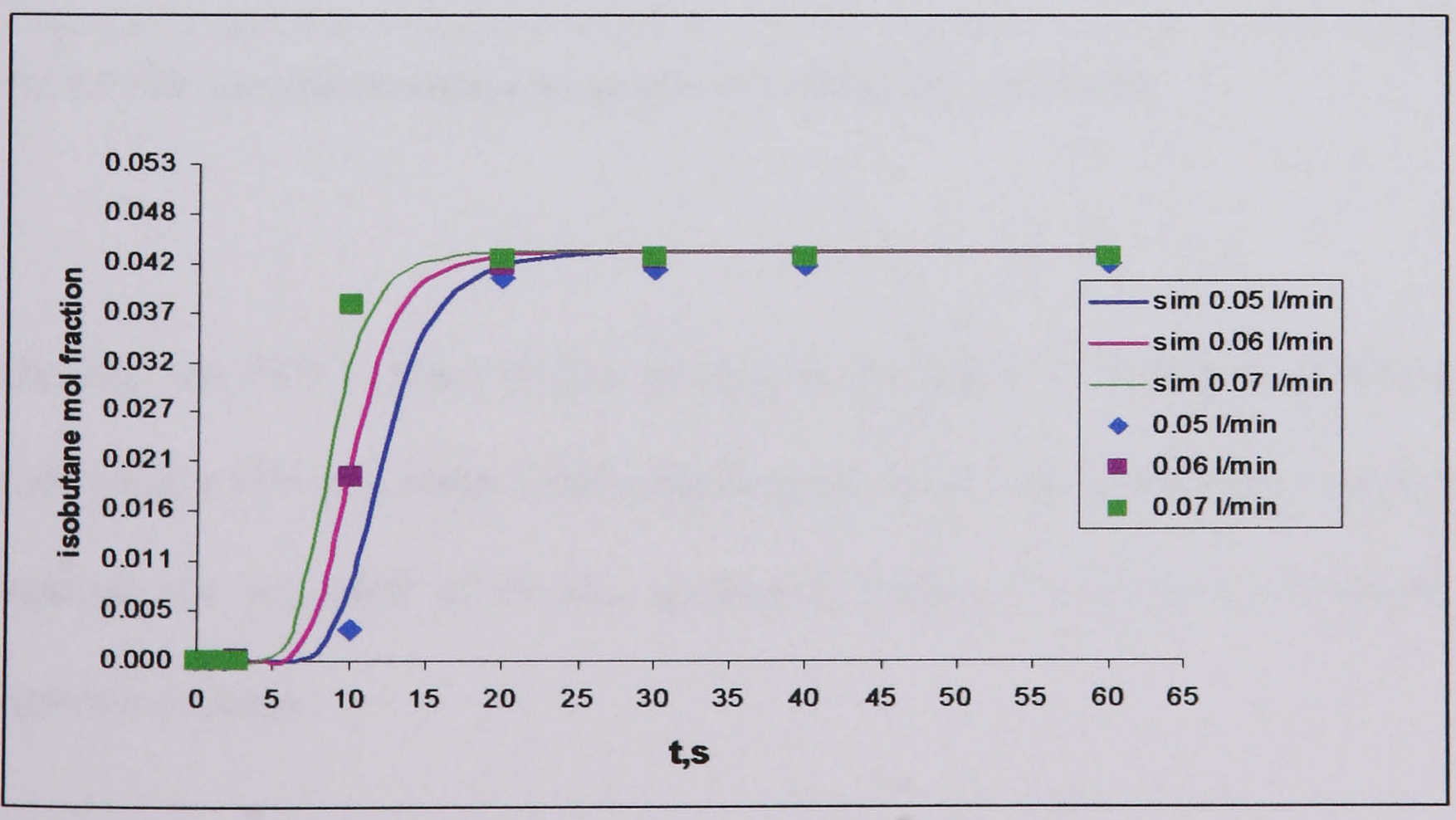


Fig. 6.5 PFR admixture breakthrough profiles at T=600K; sim = simulation

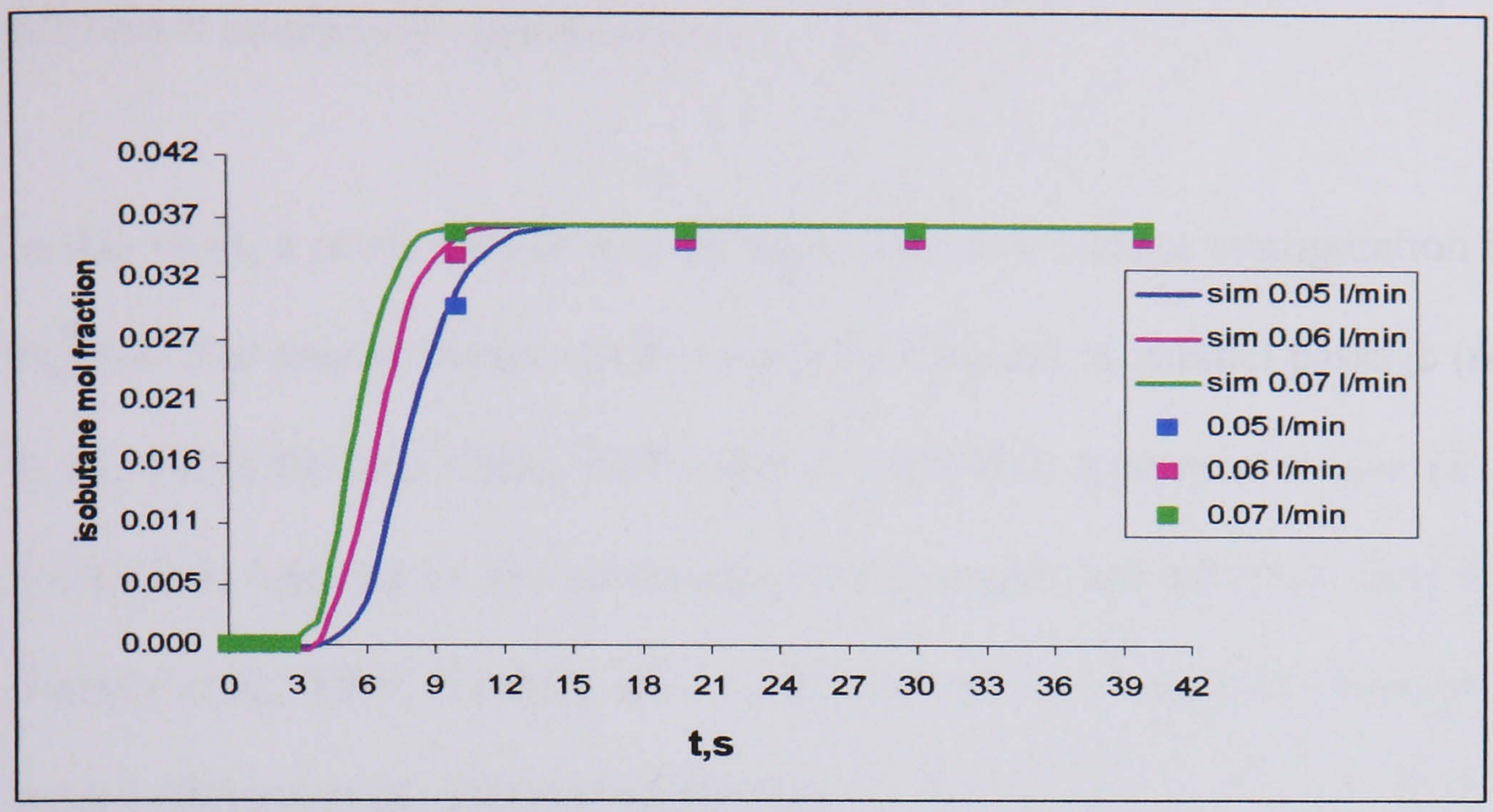


Fig. 6.6 PFR admixture breakthrough profiles at T=650K; sim = simulation

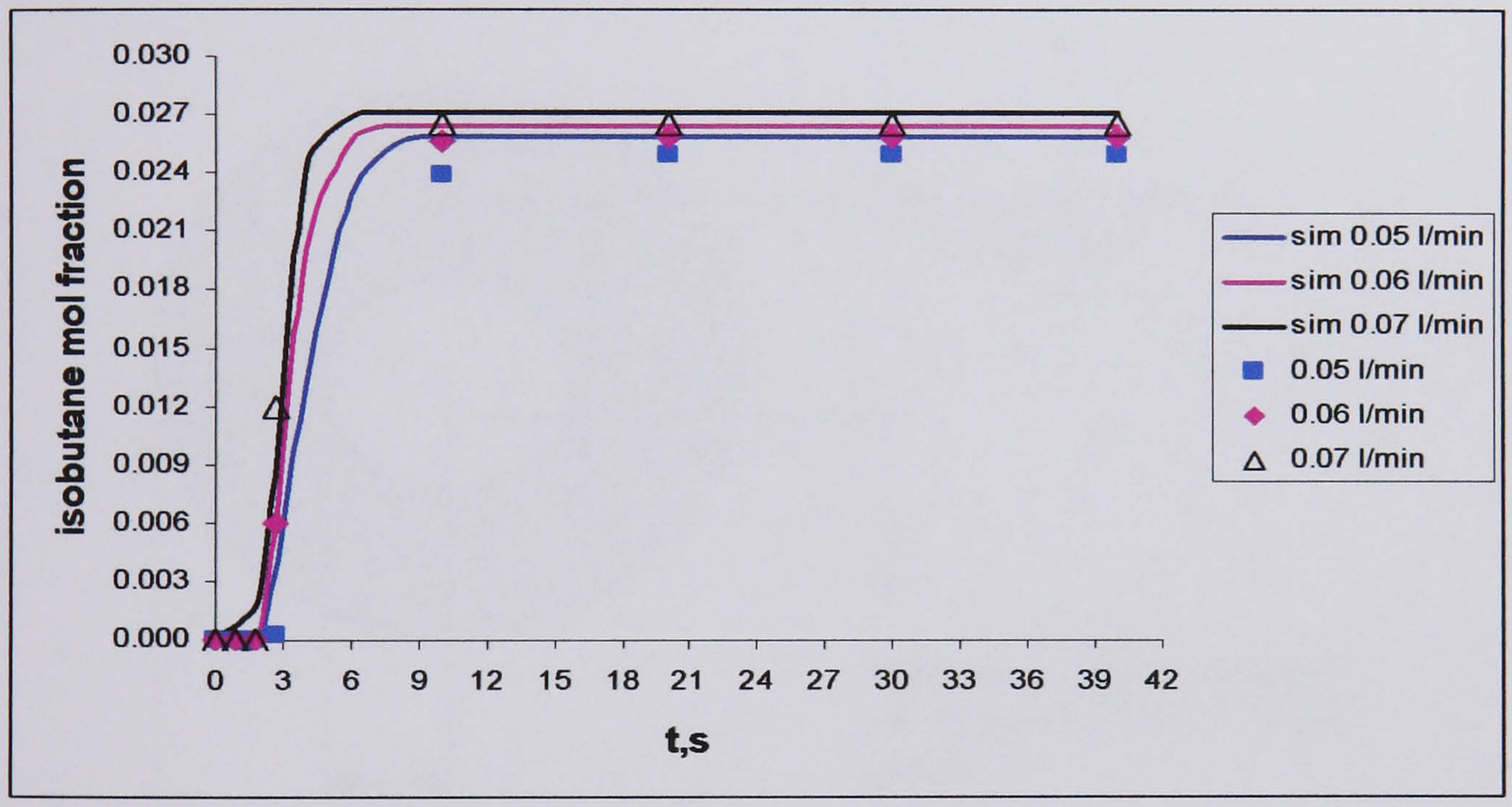


Fig. 6.7 PFR admixture breakthrough profiles at T=700K; sim = simulation

Overall, the PFR system shows promising feasibility of admixing platinum-alumina catalyst with zeolite KY adsorbent. The experimental results along with the computational validations indicate the potential of in situ separation during the catalytic reversible dehydrogenation reaction process.

6.3.2 SAR admixture experiments

In this work, a novel 2-zone annular-type adsorptive reactor configuration is considered; see Fig. 6.8. The reactor model can be viewed as a hybrid of parallel passage (see Van den Bleek *et al.,* 1996, Sie and Calis, 1998) and a monolithic type reactor (see Hoebink and Marin, 1998). It is inspired by the advantages of an annular bed adsorber (see Kehat *et al.,* 1988, Tierney *et al.,* 1999, Yoshida *et al.,* 2003) as well as an annular structured catalyst-packing reactor (Beretta *et al.,* 1998) configuration.

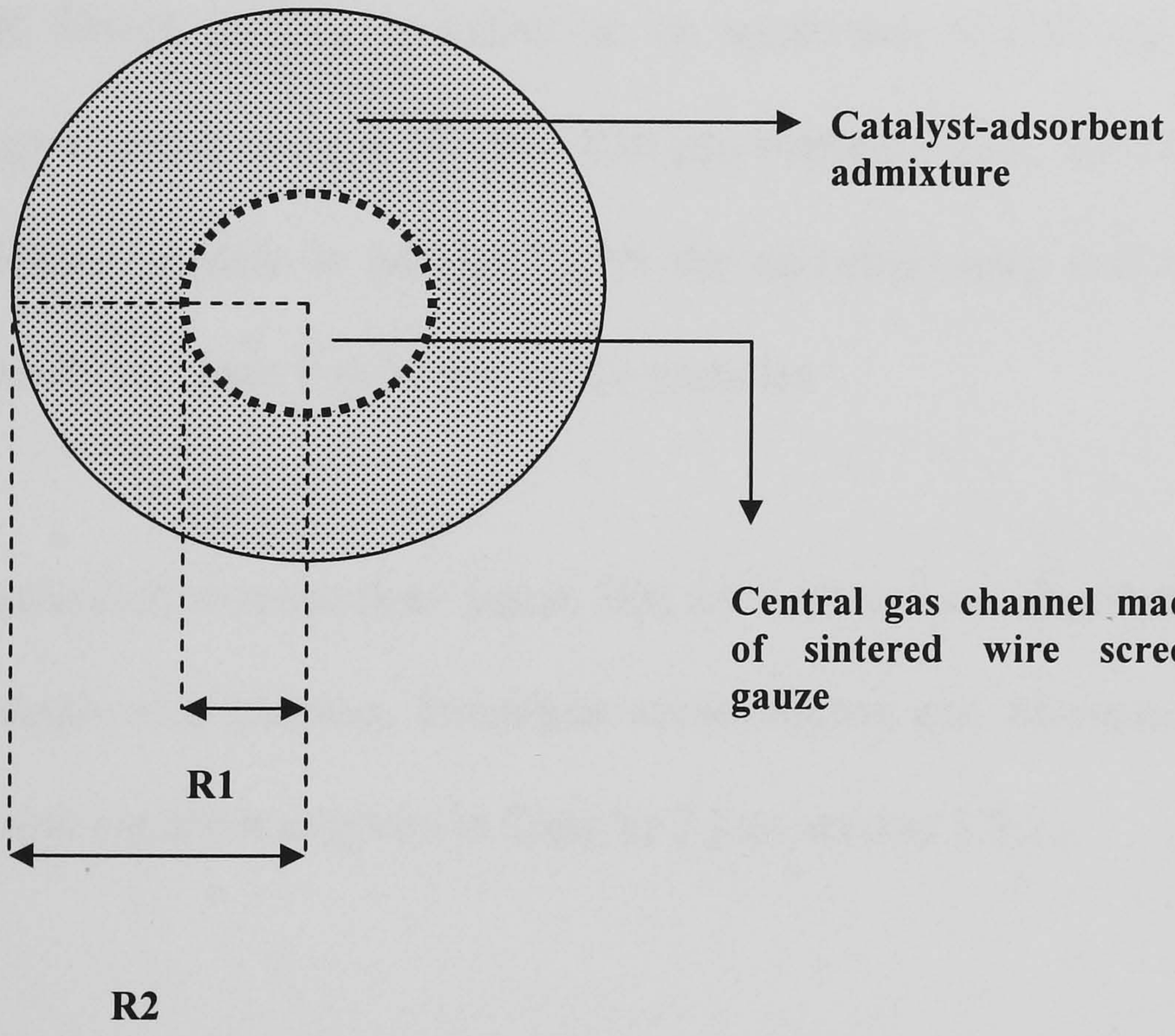


Fig.6.8 The top cross-sectional view of the SAR reactor. R1 and R2 represent the radius of central gas channel and total SAR reactor radius respectively

This novel adsorptive reactor consists of a central gas channel, made of sintered wire screen gauze, surrounded by an annulus of admixed catalyst and adsorbent. The feed gas diffuses perpendicular to the feed flow, while interparticle diffusion governs the flow in the catalyst-adsorbent admixture zone. Since the main flux of gas into the particle zone is through

diffusion and not convection, relatively small particle sizes can be employed. Thus, mass transfer resistances within the adsorbent and catalyst particles can be minimised.

An almost similar experimental procedure and set up of PFR is applied to the SAR system from the admixture drying and catalyst activation steps to the catalytic dehydrogenation reaction experiments. Its feed gas flow rate however, is kept constant at 0.1 litre min^{-1} throughout the drying and activation operations. In each case, particle drying by hot nitrogen purge is carried out for at least 3 hours prior to running the reaction-separation process to ensure absolute removal of water vapour especially from zeolite KY. Approximately 0.092 kg of inert diluent particle is added on an admixture of 0.01 kg zeolite KY and 0.0025 kg platinum-alumina catalyst of 106– 250 μm particle sizes. In Chapter 5, an extra amount of inert diluent particle is admixed with the adsorbent-only and catalyst-only experiments to compensate the mass left by one of the particles.

The conversion enhancement factor, E(t) for SAR can also be obtained using equation (3.47). For a single step process, isobutane accumulation and adsorption are incorporated into the conversion equation as given in Chapter 3 (see section 3.5.1).

Results and discussions

The transient response profiles of catalyst-adsorbent admixed SAR system are shown in Fig. 6.9 to Fig. 6.11 for different reaction temperatures at constant flow rate of 0.10 l min^{-1}. As can be seen, in general, it takes a longer time for the adsorbate to break through when operated in the SAR system relative to that of the PFR (see figs 6.1 to 6.3).

SAR		PFR	
A_{gas} , m^2	5.027×10^{-5}	A_{PFR} , m^2	1.605×10^{-5}
L, m	0.14	L, m	0.14
v , m s^{-1}	0.067	v , m s^{-1}	0.105
τ , s	2.10	τ , s	1.00
N_{Re}	49.68	N_{Re}	1.73
$\Delta P/L$, Pa m^{-1}	2.71	$\Delta P/L$, Pa m^{-1}	2.17×10^{3}
E , J s^{-1}	0.58	E , J s^{-1}	0.96
X	0.090	X	0.090

Table 6.1 Summary of parameters evaluated for SAR and PFR experiments at T = 600K; SAR flow rate = 0.10 l min^{-1}; PFR flow rate = 0.050 l min^{-1}; N_{Re} = Reynolds number; E = energy input; X = reaction conversion is obtained experimentally

By referring to table 6.1, it is apparent that both reactors investigated are operated well within laminar flow region, indicated by low Reynolds numbers. In addition, similar reaction conversion is attained at considerably low energy input. Therefore, three major factors that give rise to the different transient response profiles for the two reactors are the amount of solid loading, bed packing arrangement and gas-solid contact time.

The amount of zeolite KY adsorbent particles loaded in the SAR is twenty times higher than that in the PFR. Consequently, this permits greater amount of adsorbate retained per mass of adsorbent and hence, longer adsorbate breakthrough. The second factor signifies the diffusivity transport mechanism arises as the result of employing parallel passage type configuration. Thus, the flow transport in the annular packing of the SAR occurs only by molecular diffusion. The efficiency of in situ adsorption may well be enhanced due to negligible axial dispersion effect since there is an absence of convective transport in the annular bed. Conversely, the flow through the interstices in the packed bed PFR is somewhat

tortuous and this encourages the occurrence of axial dispersion effect. As the result, the separation efficiency may deviate from an ideal plug flow characteristic.

There is also relatively higher space time, τ in the SAR compared to the PFR as shown in table 6.1. This third factor arises from the relatively bigger gas channel volume to PFR reactor volume (~ 3:1 ratio). At relatively lower gas velocity, the flow diffuses perpendicularly towards the annular region via fine screen gauze wall. Once again, molecular diffusion predominates in the annular bed and thus allowing higher gas-solid contact time, which also means higher residence time and higher isobutene retention and its subsequent influence in the local reaction kinetics and equilibria in the reactor.

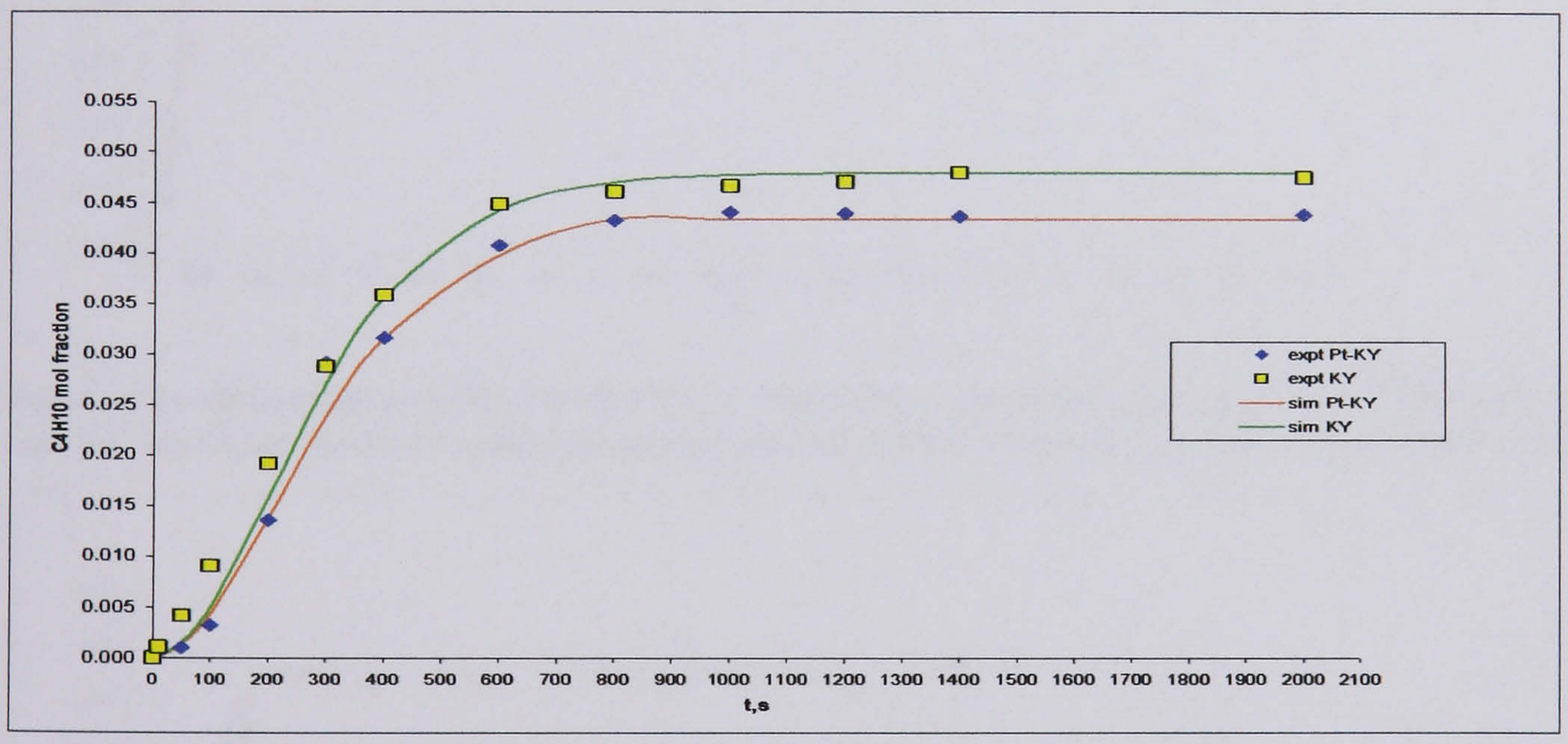


Fig. 6.9 Breakthrough profile of SAR with or without the admixture of catalyst at T=600K, flow rate= 0.10 l min^{-1}. Pt and KY represents platinum-alumina catalyst and zeolite KY respectively; expt = experiment ; sim = simulation

There is also tendency for the experimental breakthrough curve to deviate slightly from the simulation prediction at higher temperature i.e. at 650K and 700K (see figs. 6.10 and 6.11). Such discrepancy may be caused by relatively higher adsorption of isobutene experimentally than as predicted in the model. The forward rate of reaction, k' (m^3 kg^{-1} s^{-1}) significantly increases which in turn increases the isobutane equilibrium conversion. Consequently, a higher amount of isobutene is produced and adsorbed at the same time during the reaction-

adsorption process. The relatively faster adsorbent equilibration is thus caused by local retention of both the unreacted isobutane and higher amount of isobutene at somewhat decreasing adsorbent utilisation. This is owing to the fact that the adsorption equilibria are temperature dependent and so, the decreasing adsorbent capacity at higher temperature has led to the shorter adsorbate breakthrough and higher intraparticle diffusion resistance.

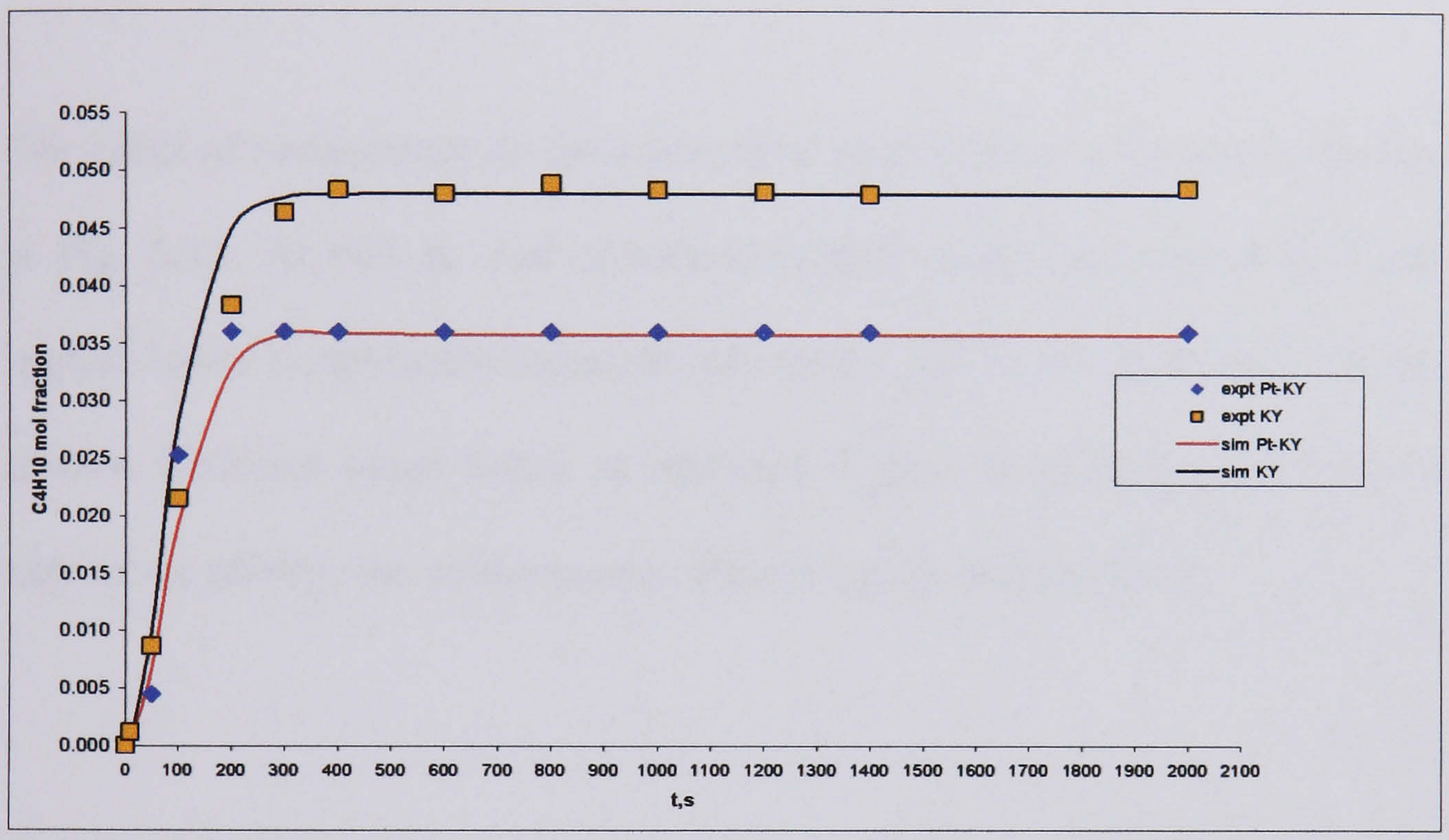


Fig. 6.10 Breakthrough profile of SAR with or without the admixture of catalyst at T=650K, flow rate= 0.10 l min^{-1}. Pt and KY represent platinum-alumina catalyst and zeolite KY respectively; expt = experiment ; sim = simulation

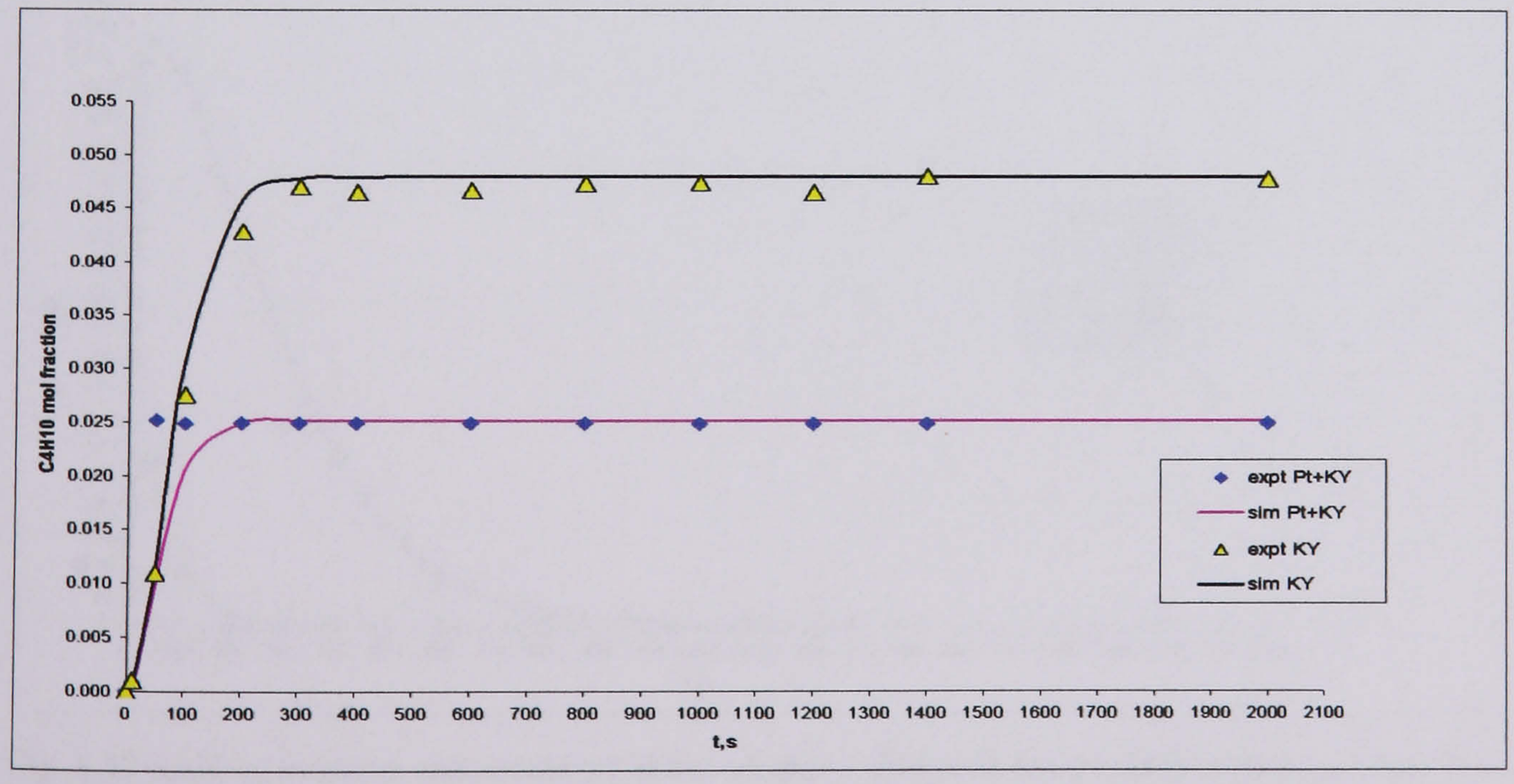


Fig. 6.11 Breakthrough profile of SAR with or without the admixture of catalyst at T=700K, flow rate= 0.10 l min^{-1}. Pt and KY represent platinum-alumina catalyst and zeolite KY respectively; expt = experiment ; sim = simulation

T, K	v, m s^{-1}	τ , s	N_{Re}	E, J s^{-1}	ΔP/L, Pa m^{-1}	X
650	0.072	1.94	55.28	0.67	2.86	0.26
700	0.078	1.80	61.05	0.77	3.00	0.48

Table 6.2 Summary of parameters evaluated for SAR experiment; SAR flow rate = 0.10 l min^{-1}; E = energy input. X = reaction conversion is obtained experimentally

The effect of temperature on the conversion enhancement isobutane dehydrogenation is shown in Fig. 6.12. At 600 K, and considerably high space time, isobutane yield is low, but the relative lower temperature increases adsorption affinity for isobutane. On the other hand, the catalyst performs much better at relatively higher temperature, but because of the reduced adsorption affinity, the enhancement effect is significantly reduced.

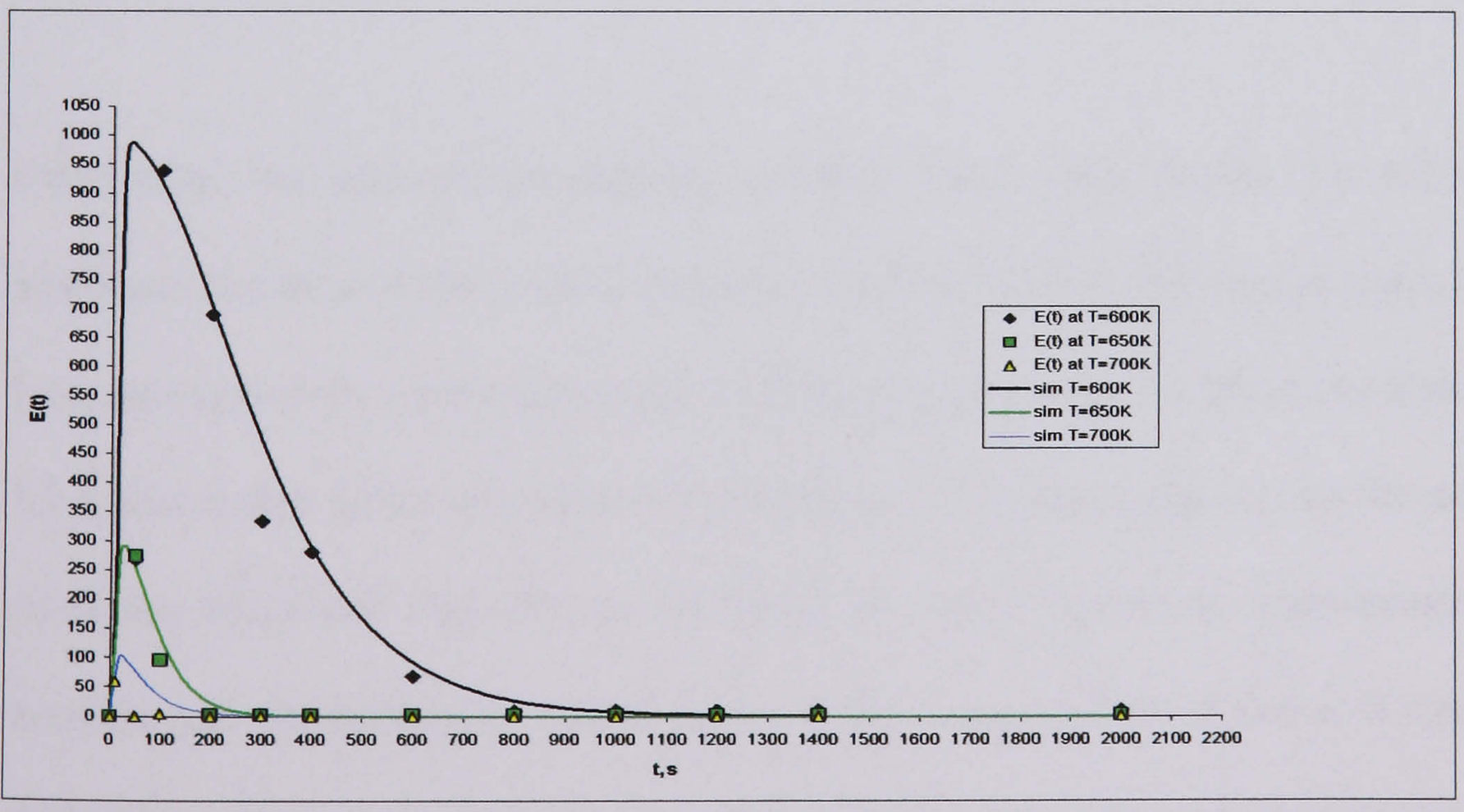


Fig. 6.12 SAR adsorption enhancement effect at three different temperatures and constant flow rate of 0.10 l min^{-1}; sim = simulation

Apart from low coke yields in platinum-alumina catalyst, a possible lower catalyst deactivation effect may also be achieved at lower reaction temperature. This has led to the search for an optimal reaction temperature for a maximum possible enhancement (Ding and Alpay, 2000) of the in situ reaction and separation process. The choice would have to be such that it is a compromise between adsorption equilibria and kinetic factors (Han and Harrison, 1994). Therefore, it is necessary to make a careful selection of the adsorbent and catalyst such that the kinetics of reaction and capacity of the adsorbent are in accord (Ding and Alpay, 2000).

6.4 Cyclic SAR studies

One of the key advantages of the synergetic coupling of catalytic reversible reaction with in situ separation is the ability to attain efficient in situ regeneration of the adsorbent (Carvill *et al.,* 1996). This is due to the fact that adsorption-enhanced reaction processes are intrinsically dynamic in operation.

Essentially, the adsorption-enhanced reaction takes place during the adsorption step. The adsorbate can be desorbed and collected as product during the regeneration (desorption) step. Hot, non-adsorbable inert gas purge isothermal regeneration method is employed in this work for a reasonably dilute adsorbate concentration. The purge gas carries the adsorbate removed from the adsorbent bed (Breck, 1974) at the same operating temperature as the reaction temperature. Subsequently, cyclic steady state is approached in the first cycle (Yang, 1987). This allows for the concentrations at all positions at any time in the cycle to be in consistent in all subsequent cycle (Ruthven, 1984).

In terms of energy requirement, purge stripping (or partial pressure reduction) using the inert gas as the carrier in the desorption step proves to be economical regeneration method. By referring to tables 6.1 and 6.2 and figs 6.13 to 6.15, the low energy input required to supply the heat during reaction-adsorption step is also sufficient for desorption step thus allowing complete adsorbate removal and to prepare for a clean bed for subsequent cycles. In addition, the adsorption process is carried out within Henry's law region whereby the adsorbate concentration is considerably dilute and thus, purge stripping is applicable.

At higher operating temperature, the desorption rate increases considerably and this is seen in figs. 6.13 to 6.15. Since there is no reaction takes place during this step, continuous hot nitrogen purging into the reactor bed results in faster removal of dilute adsorbates from the solid annular region. Inherently, desorption is an endothermic process and requires more heat in order to completely regenerate the bed and hence, it is more efficient at higher temperatures. The experimental data is in good agreement with the equilibrium theory, which further validates the two-dimensional, dynamic cyclic mathematical modelling developed for such process design configuration.

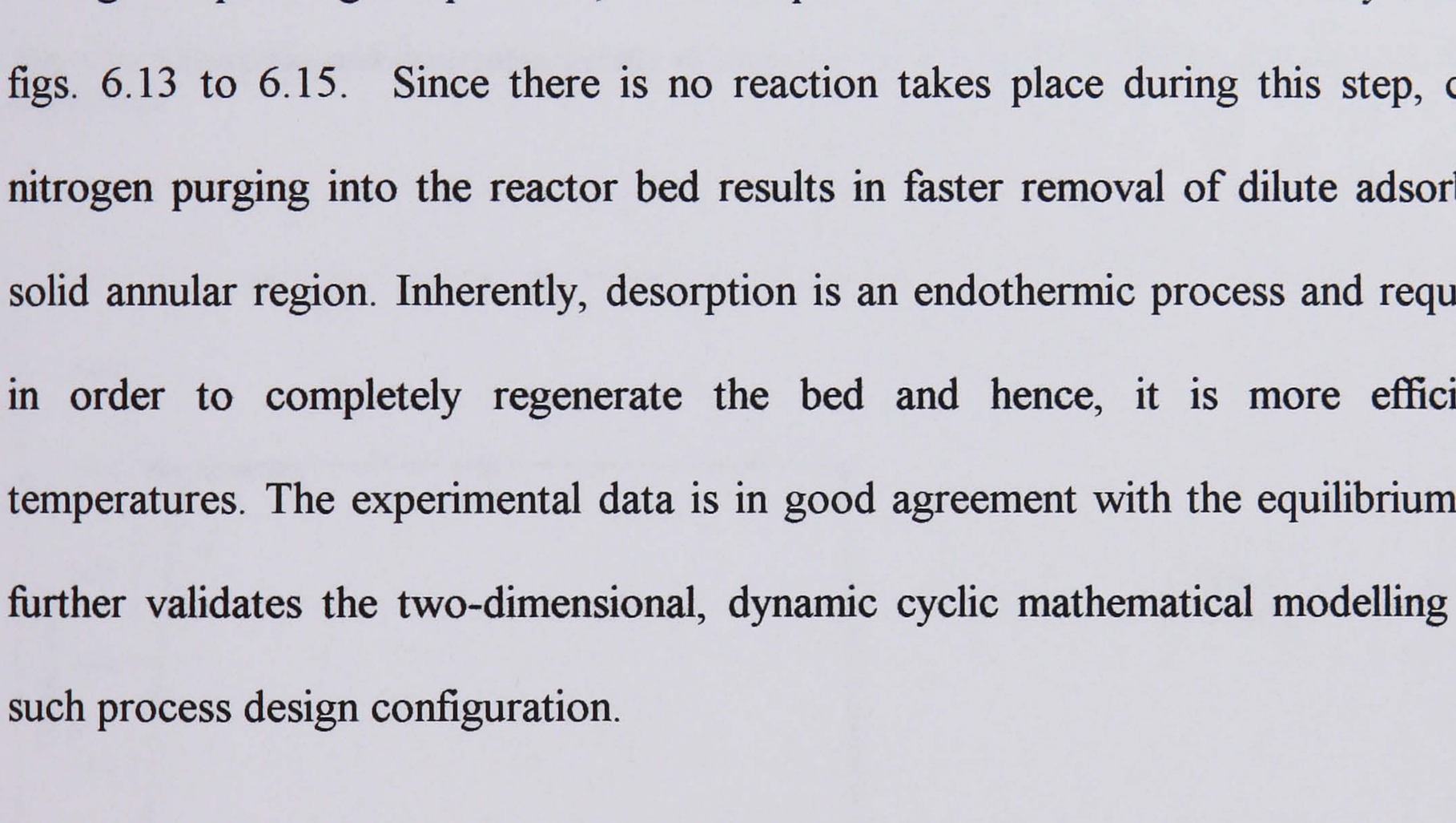


Fig. 6.13 Adsorption and desorption profile of SAR admixture process at T=600K and flow rate= 0.10 l min^{-1}; sim = simulation

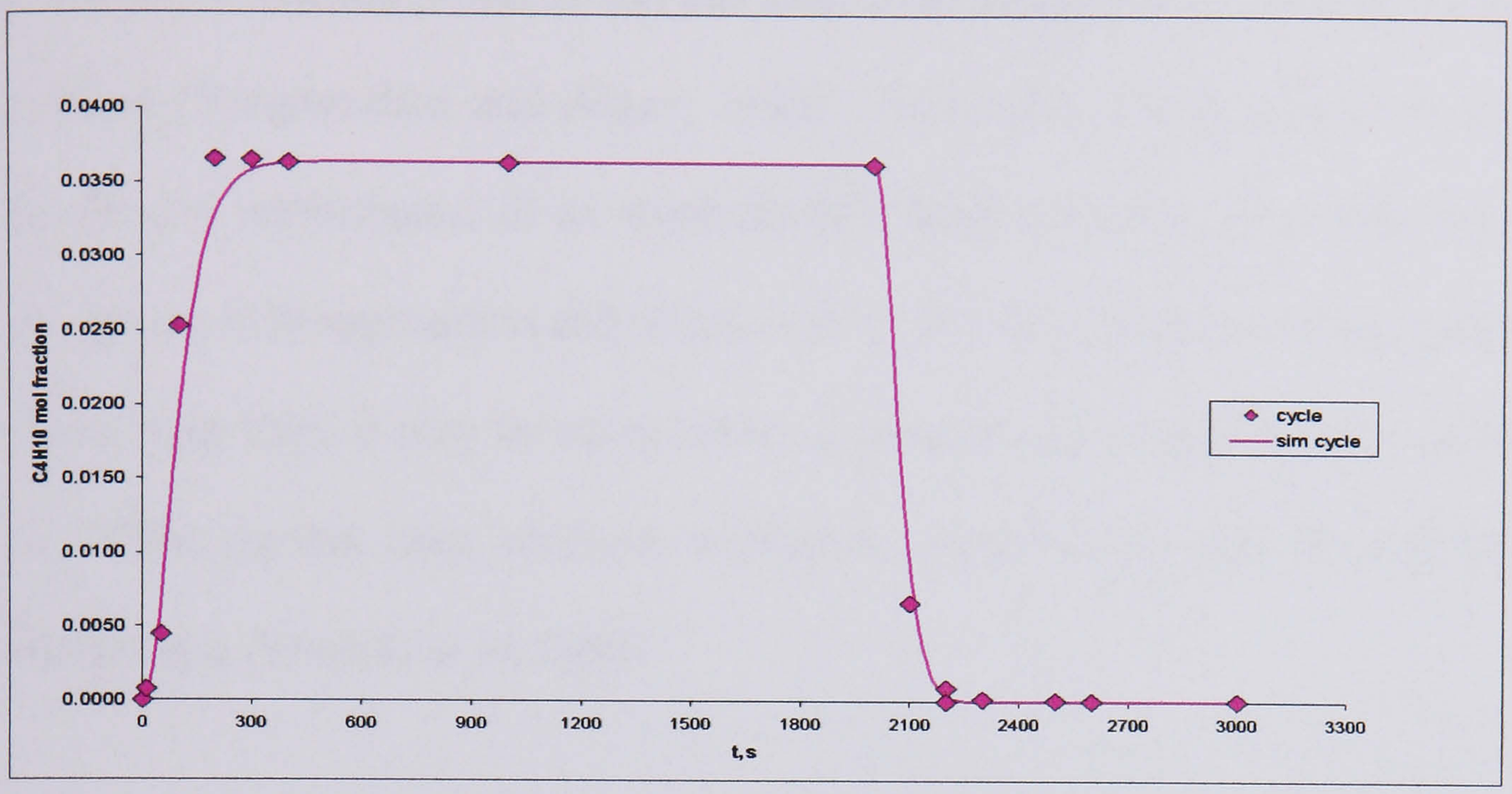


Fig. 6.14 Adsorption and desorption profile of SAR admixture process at T=650 and flow rate= 0.10 l min^{-1}; sim = simulation

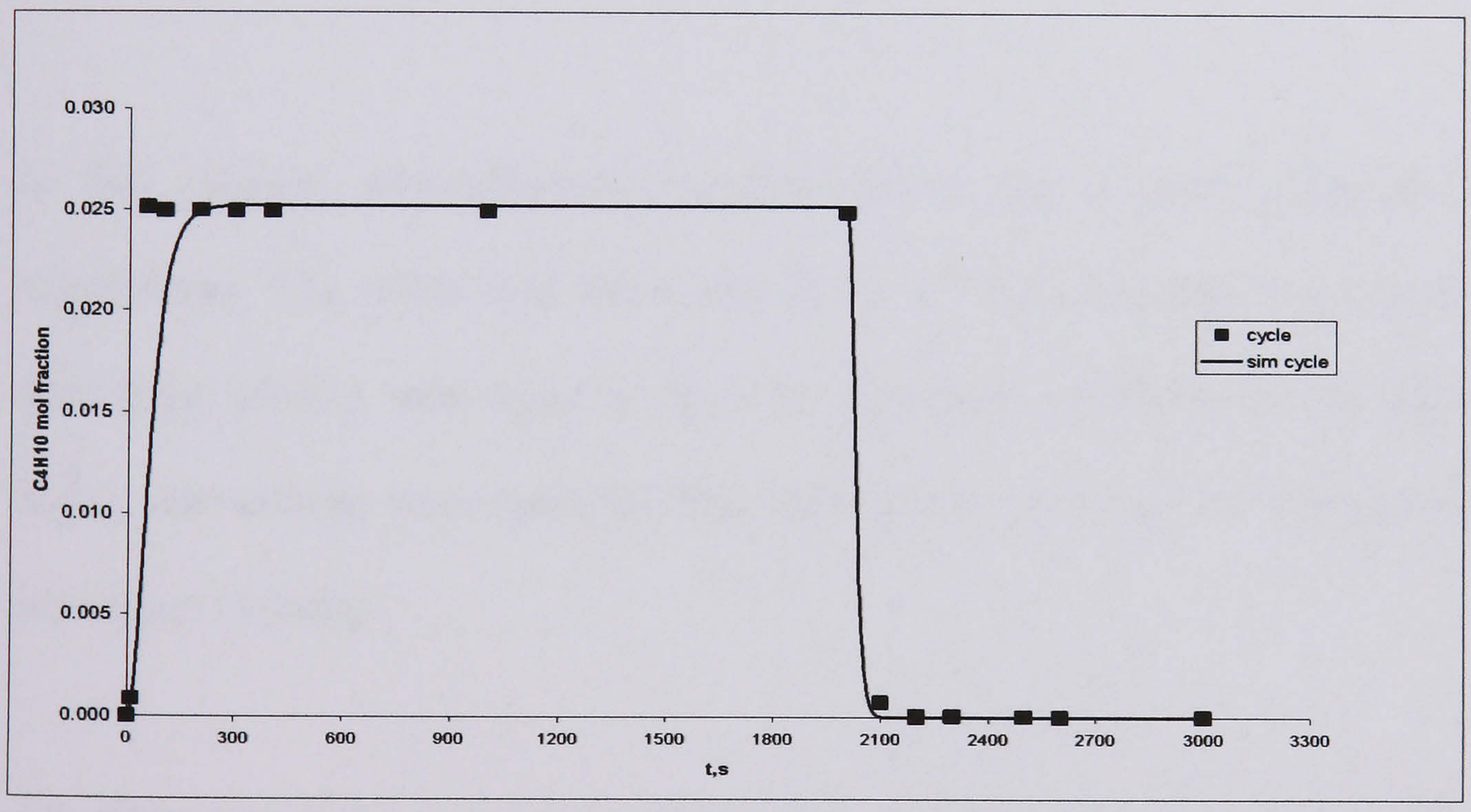


Fig. 6.15 Adsorption and desorption profile of SAR admixture process at T=700K and flow rate= 0.10 l min^{-1}; sim = simulation

At isobaric condition, a thermal swing adsorption (TSA) method could also be applied as an alternative to the inert gas purge stripping method. Periodic regeneration by nitrogen purge at elevated temperature at presumably uniform bed saturation may also generate favourable

catalyst activity profiles (Yongsunthon and Alpay, 1999). During the adsorption step, the bed cools as the reaction proceeds and this leads to an increase in adsorption affinity of adsorbable product (Yongsunthon and Alpay, 1999). Substantial improvements over the equilibrium conversion performance of an adiabatic PFR have reportedly been attained at no additional energy input (Yongsunthon and Alpay, 1999). It is also postulated that given the flexibility of conducting TSA, it may be extended in an annular-type non-isothermal adsorber (Yoshida *et al.,* 2003). In that case, effective separation is realised through the control of temperature distribution (Yoshida *et al,* 2003).

6.5 Concluding remarks

In this chapter, adsorption-enhancement effect was observed through PFR and SAR experiments. The effect was more significant at lower reaction temperatures due to higher adsorption affinity and capacity prior to adsorbent equilibration. At higher temperatures, higher conversions were achieved thus reducing the potential for enhancement due to lower adsorption capacity.

The difference of the amount of solid loading, bed packing configuration and reactor residence time have contributed to the higher conversion enhancement effect using the SAR. It may be deduced that longer interaction between adsorption and reaction processes was due to possibly higher isobutene retention at relatively higher solid loading amount (i.e. adsorbent particles packed in the SAR was twenty times higher than that in the PFR). This factor, along with molecular diffusive transport mechanism in the bed packing configuration and relatively

higher residence time, had significant influence to the local reaction kinetics and adsorption equilibria and hence, substantial improvement in reaction enhancement in the SAR. The cyclical aspect of reaction-separation process of SAR has also been discussed whereby inert purge stripping was deemed a reasonable regeneration technique.

In all respect, good agreement between the experimental data and the simulation results was achieved. Thus, further model-based evaluation of the SAR process was possible.

Chapter 7

SAR Theoretical Analysis

7.1 Introduction

The emphasis of theoretical investigation is on exploring, and thus exploiting the potential and capabilities of an adapted technology for a particular process. The generalised, well-structured concepts are examined in the light of the real experimental studies in order to compare the methodologies with practical features (Elsner *et al.,* 2002). Nevertheless, the choice of an appropriate model to account for the dynamic of such process is essential. Mathematical approximations together with the choice of adsorption equilibria and kinetic model would determine the viability and feasibility of the unit operation design thus bridging the gap between the theoretical concepts and real chemical system.

In this chapter, the theoretical studies of the SAR based on the two-dimensional mathematical model described in Chapter 3 are presented. The model equations are solved within the gPROMS simulation environment. Measured reaction kinetics and adsorption parameters (see Chapter 5) are used in the model. The simulations thus provide a method to further predict the outcome of the reaction-separation process without recourse to experimentation. Reactor performance comparisons relative to an equivalent packed bed reactor are made in terms of conversion enhancement. Numerical studies are also carried out to explore the optimal selection of the design and operating parameters.

Therefore, a simulation strategy describing methodology of the theoretical study is presented in the next section. Here, the mathematical approach to simultaneously solving the SAR and PFR models include identifying the key input and dependent variables as well as decision parameters. The numerical method of the model involves simulating the intrinsically periodic nature of the adsorptive reactor process by implementing the backward finite difference method in the single step process as well as for cyclic steady state approach.

Section 7.3 presents the simulation results analysis for both the novel SAR and its equivalent packed bed reactor by referring to the breakthrough curves as well as conversion enhancement profiles at given operating conditions. Cyclic steady states profiles are also presented in which conditions at all positions of the first cycle remain the same for subsequent cycle in both solid and gas phases.

7.2 Simulation strategy

The design and overall performance of the SAR is assessed in terms of concentration profiles, conversion enhancement effects, pressure drop characteristics and energy requirement. The theoretical investigations of the SAR are thus intended as a means of exploring its potential as a possible alternative to a conventional packed bed tubular reactor.

This novel adsorptive reactor configuration integrates the catalytic and adsorption functions in the annular region. It allows the feed gas to flow along the empty central core of the reactor, which subsequently gives rise to a low-pressure drop operation. For laminar flow, pressure drop can be estimated from the Hagen-Poisuille correlation.

Of course, for tortuous interstitial flow through the traditional packed bed configuration, the greater interphase momentum resistance (Dautzenberg and Mukherjee, 2001) leads to a large increase in pressure drop for equivalent feed flow rates. High pressure drop is often the major disadvantage of a conventional packed bed configuration relative to the structured packing arrangement. Hence, it is interesting to compare the synergetic performance of the SAR with the equivalent packed bed configuration based on the model assumptions addressed in Chapter 3 (see section 3.3.1).

The adsorption-only and adsorptive reactor performances are conducted within Henry's law region where very low adsorbate concentration is taken into consideration.

7.2.1 Key variables and parameters

Essentially, key input variables and hence, numerical aspects of the simulation of the governing mathematical model discussed in Chapter 3 have to be identified. A set of decision parameters and operating condition values are subsequently assigned to find the optimal conditions of the key dependent variables while satisfying all of the important constraints (Nilchan, 1997).

The key input variables for the SAR and PFR systems include (see Waldron and Sircar, 2000):

a) Multicomponent adsorption equilibria and kinetic parameters which cover the entire range of conditions i.e. temperature, T, gas phase mole fraction of each component, i, y_i , operating at atmospheric pressure, P

b) Physical properties of the bulk gas as a function of T, in this case, nitrogen. These include gas density, ρ_{gas}, gas viscosity, μ, and specific heat capacity, c_{pg}.

c) Fluid dynamics and mass transfer characteristics

d) Sequence of the cycle steps and their durations

These key input variables are predetermined by the decision parameters, which include:

a) Isothermal temperature, T for the entire reaction-separation and regeneration cycles

b) Feed gas conditions

c) Superficial velocity, v, as a function of temperature

d) Reactor geometrical parameters:

- Central gas channel radius, R1 (which is equivalent to the PFR radius, R_{PFR}
- Total reactor radius, R2
- Annular thickness, δ ($\delta = R2 - R1$)
- Reactor length, L

The decision parameters and key input variables will then determine the performance of the key dependent variables of the system:

a) Energy input supplied to the reactor

b) Equilibrium conversion

Each of the simulation results will be compared to the base case values as shown in Table 7.1.

base case parameters	value	unit
SAR gas channel radius, R1	0.004	m
SAR total reactor radius, R2	0.014	m
PFR radius, R_{PFR}	0.004	m
SAR and PFR length, L_{SAR}, L_{PFR}	0.14	m
Operating temperature, T	600	K
Feed flow rate, ν, from experiment	0.10	l min^{-1}
Superficial velocity, v	0.067	m s^{-1}
$y_{i=isobutane}$	0.048	-
$y_{i=isobutene}$	0.001	-
$y_{i=hydrogen}$	0.001	-

Table 7.1 Base case parameters of SAR and its equivalent PFR

With reference to table 7.1, the PFR dimensions are equivalent to the central gas channel of the SAR. As described in Chapter 3 (see section 3.4), the PFR mathematical model is a 1-D model whereby only the change in axial direction is described and radial direction is excluded. At similar amount of admixture loading, the adsorption-only as well as conversion enhancement effect performances of the structured annular reactor are compared with the conventional tubular reactor in section 7.3.

All the variables and decision parameters that are temperature dependent are written in algebraic equations, whereby the only unknown is the temperature itself. For the nitrogen carrier:

1. The gas viscosity, μ (Pa s), is determined from the following correlation (Watson, 1972):

$$\mu = \left(\frac{T^{1/2}}{A_0 + A_1 s + A_2 s^2 + A_3 s^3 + A_4 s^4}\right) \times 1 \times 10^{-6} \quad ,$$
$$s = \frac{100}{T} \qquad (7.1)$$

$A_0 = 0.57956129$; $A_1 = 2.8474859$; $A_2 = -13.232490$; $A_3 = 37.106107$; $A_4 = -37.549675$

2. The gas density, ρ_{gas} (kg m^{-3}), is estimated based on its value of 1.25 kg m^3 at 273K (see Perry, 1997).

The actual feed gas flow rates in the reactor are adjusted based on the flow rate value at room temperature, T_o = 298K. These modified flow rates values are used to estimate the superficial velocities by dividing them with the cross-sectional area of the reactor. The gas phase component concentration, C_i (mol m^{-3}) is represented as

$$C_i = y_i \sum_{i=1}^{n} C_i \qquad (7.2)$$

where yi is the component mole fraction (see table 7.1). The total gas phase concentration is derived based on the ideal gas law equation:

$$\sum_{i=1}^{n} C_i = \frac{P}{R_{gas}\, T} \qquad (7.3)$$

where P is the total pressure (Pa), R_{gas} is the universal gas constant (J mol^{-1} K^{-1}), T is the reactor temperature (K) and n is the total number of components. For the dehydrogenation of isobutane to isobutene over a uniform admixture of platinum-alumina catalyst, Pt-Al_2 O_3 and

zeolite-KY adsorbent, the adsorption equilibria parameters for isobutene and isobutane, which have been previously obtained by matching the experimental response curve to the theoretical ones (see section 5.3.4),are represented by a van't Hoff type equation, i.e.

$$m_{isobutene} = 7.1\times10^{-10}\ \exp\left(\frac{46298.17}{R_{mol}T}\right) \tag{7.4}$$

$$m_{isobutane} = 7.3\times10^{-10}\ \exp\left(\frac{42570.17}{R_{mol}T}\right) \tag{7.5}$$

Hydrogen is assumed as non-adsorbable. The pseudo-first order reaction rate constant, k' (m^3 kg^{-1} s^{-1}) of the catalytic dehydrogenation reaction is described by an Arrhenius-type equation:

$$k'(T) = 0.517\exp\left(\frac{-34900}{R_{gas}T}\right) \tag{7.6}$$

where the activation energy, E = 34.9 kJ mol^{-1} is also obtained experimentally (see Chapter 5, section 5.2.3).

For an endothermic reaction, the equilibrium constant, K_{eq}, and equilibrium conversion, X_e, increase as the reaction temperatures increase. K_{eq} is related to K_p by:

$$K_{eq} = K_p\frac{P}{R_{gas}T} \tag{7.7}$$

K_p may be obtained using the van't Hoff correlation (see Fogler, 1992),

$$\frac{d \ln K_P}{d T} = \frac{\Delta H_T}{R_{mol} T^2} \tag{7.8}$$

where Kp is pressure equilibrium constant based on partial pressure and ΔH_T, the total enthalpy of reaction is calculated from the heats of formation. Integration of equation (7.8) then yields:

$$K_P = K_{Po} \exp\left[\begin{array}{l} -13118\left(\frac{1}{T}-\frac{1}{T_o}\right)+5.39\ln\left(\frac{T}{T_o}\right)-0.0057145\left(T-T_o\right)+ \\ 1.327\times10^{-6}\left(T^2-T_o^2\right)-1.223\times10^{-10}\left(T^3-T_o^3\right) \end{array}\right] \tag{7.9}$$

and $K_{Po} = 1.472 \times 10^{-14}$, obtained from the change in the Gibbs free energy:

$$-R\,T\,\ln K_{p_o} = \Delta G_{rxn}\left(T_o\right) \tag{7.10}$$

The molecular diffusion coefficient, D_m ($m^2\ s^{-1}$) based on the Chapman-Enskog correlation can be written as:

$$D_m = 2.28 \times 10^{-9}\left(\sqrt{T^3}\right) \tag{7.11}$$

In the case of PFR, axial dispersion coefficient, D_x ($m^2\ s^{-1}$) at any T based on the correlation of Langer *et al.* (1978) is given as:

$$D_x = 0.55 D_m + \frac{v^2}{670\left(v + 1536\ D_m\right)} \tag{7.12}$$

The adsorption mass transfer coefficient, $k_{mass,i}$ (s^{-1}) of isobutane and isobutane derived based on the approximation of LDF model of Glueckauf and Coates (1947) and represented as:

$$k_{mass,i} = 1.894 \times 10^{9} \left(\frac{0.083 \left[\frac{1}{\beta} \right]}{\rho_{ads} R_{gas} T m_i} \right) \tag{7.13}$$

where ρ_{ads} is bulk density of adsorbent (kg m^{-3}) (see table 5.9, Chapter 5) and β is written as:

$$\beta = \frac{1}{D_m} + \frac{1}{7.63 \times 10^{-7} T^{1/2}} \tag{7.14}$$

7.2.2 Spatial domain normalisation

The underlying 2-D model is optimised by defining normalised space co-ordinates as follows:

- For axial- co-ordinates:

$$\lambda = \frac{x}{L} \quad ; \quad x = \{0 : L\}$$

All the partial derivatives are then expressed in terms of these new independent variables:

$$\frac{\partial}{\partial x} = \frac{1}{L} \frac{\partial}{\partial \lambda} \quad ; \quad \frac{\partial^2}{\partial x^2} = \frac{1}{L^2} \frac{\partial^2}{\partial \lambda^2} \tag{7.15}$$

- For radial- co-ordinates:

$$\xi = \frac{r}{R2} \quad ; \quad r = \{0 : R2\}$$

The new radial partial derivatives then become:

$$\frac{\partial}{\partial r} = \frac{1}{R2}\frac{\partial}{\partial \xi} \quad ; \quad \frac{\partial^2}{\partial r^2} = \frac{1}{R2^2}\frac{\partial^2}{\partial \xi^2} \tag{7.16}$$

7.2.3 Numerical method approach

The model is expressed by a set of partial differential equations (PDEs) describing the physical laws of conservation of material and momentum. Another set of algebraic equations (AEs) describe the auxiliary relationships such as the equation of state and the adsorption isotherms (Yongsunthon, 1999). In other words, the model is a combination of distributed and lumped parameter systems to account for the differentiation of axial and radial dimensions, which vary with time. The PDEs are solved by applying the method of lines, whereby the PDEs are converted into sets of ordinary differential equations, ODEs, with respect to time (Oh, 1995).

Due to its ability to solve problems involving a strong convective component (Oh, 1995), finite difference method is applied in this work. The discretisation involves a fixed number of points to the left and right of the integral approximation point (Oh, 1995). The finite difference method is solved using backward grid position with respect to the spatial domains: axial and

radial. It is therefore known as backward finite difference method, BFDM. In the gPROMS environment, BFDM method allows a user to specify the tolerance level by adjusting automatically the step size and integration order to maintain the desired integration error. This method transforms the PDEs to ODEs over a small interval of time and thus, convergence is assured for specific size of increments of interval length.

More details on the numerical method approaches can be referred from the works of Oh (1995), Nilchan (1997), and Yongsunthon (1999).

7.3 Simulation results and discussions

The mathematical model described in Chapter 3 along with the temperature-dependent equations described above was coded in gPROMS modelling environment. BFDM was applied for spatial discretisation i.e. 50 grid points for axial and 24 grid points for radial.

The adsorption and combined reaction-separation studies of SAR are initially analysed at three different temperatures, which were used in the experimental work. The SAR performance is compared to the equivalent packed bed system in which the latter shares similar geometrical sizes as the SAR central gas channel. These assessments of the reactors involved a single-step process, where adsorption and adsorption-enhanced reaction take place in the reaction step of the cycle. Breakthrough profiles then lead to information of the conversion enhancement effect.

Adsorption beds are intrinsically transient, spatially distributed systems, in which the properties of the solid and fluid phases vary over time (Nilchan, 1997). Periodic regeneration is thus inevitable as the periodic removal of adsorbate from the adsorbent is needed. The cyclic steady state operation of adsorption and desorption of SAR as well as its equivalent PFR is herein investigated over three different temperatures utilising inert gas purge stripping regeneration method.

7.3.1 SAR Adsorption performance

The transient adsorption profiles of PFR and SAR at three different temperatures are shown in figs. 7.1 to 7.3. The PFR here is of the same diameter and length as the core gas channel of the SAR.

With reference to fig.7.1, it takes a longer time for adsorbate breakthrough in the SAR than the PFR. In addition to the increasing adsorbent capacity since adsorption is favoured by low temperature operation, the equilibration time is prolonged in the SAR compared to the PFR due to the molecular diffusive transport mechanism and relatively higher space time (see table 7.2). This is attributed to the structured packing arrangement of the SAR in which the gases are principally transported inwards and outwards of the bed by molecular diffusion at relatively higher gas-solid contact time. In the absence of a convective effect in the annular packing, faster mass transfer due to almost negligible intraparticle diffusion limitation resulting in effective adsorption throughout the bed. The annular packing arrangement also offers a larger mean cross-sectional area and reduced distance of travel for flow which further overcome the mass transfer resistance. This is in contrast to the transport phenomena in the

PFR where the mass transfer resistance in the bed increases primarily due to axial dispersion effect. Even though it provides direct gas-solid contact, the feed gas undergoes somewhat tortuous flow as it diffuses and disperses directly towards the solid surface along the random bed packing. Consequently, this reduces the gas-solid contact time indicated by relatively lower space time (see table 7.2) at similar operating temperature. Such adverse effects account for the shorter breakthrough time. It is also interesting to note the initial time lag at zero loading of the PFR curve, which may be due to the intrusion of some intracrystalline diffusional resistance of the adsorbent as the result of the random orientation of the pores (see Ruthven, 1984). This gives rise to a longer diffusional path and a reduced concentration gradient in the direction of flow.

In terms of change in temperatures, the higher it gets, the faster the rate of adsorbent equilibration represented by shorter breakthrough curves (see figs 7.2 and 7.3). Adsorption is intrinsically an exothermic process. Consequently, the adsorbent capacity decreases due to the inherently temperature dependent adsorption kinetic property where the amount of gas physically adsorbed decreases rapidly with increasing temperature. In addition to that, there is a marked increase of gas velocity albeit having similar feed flow rate. This is due to the temperature influence on the physical properties of the bulk gas such as density and viscosity causing the gas to expand when heated. As a result, the gas-solid contact time is further reduced in both SAR and PFR reactor, represented by lower space time in table 7.2.

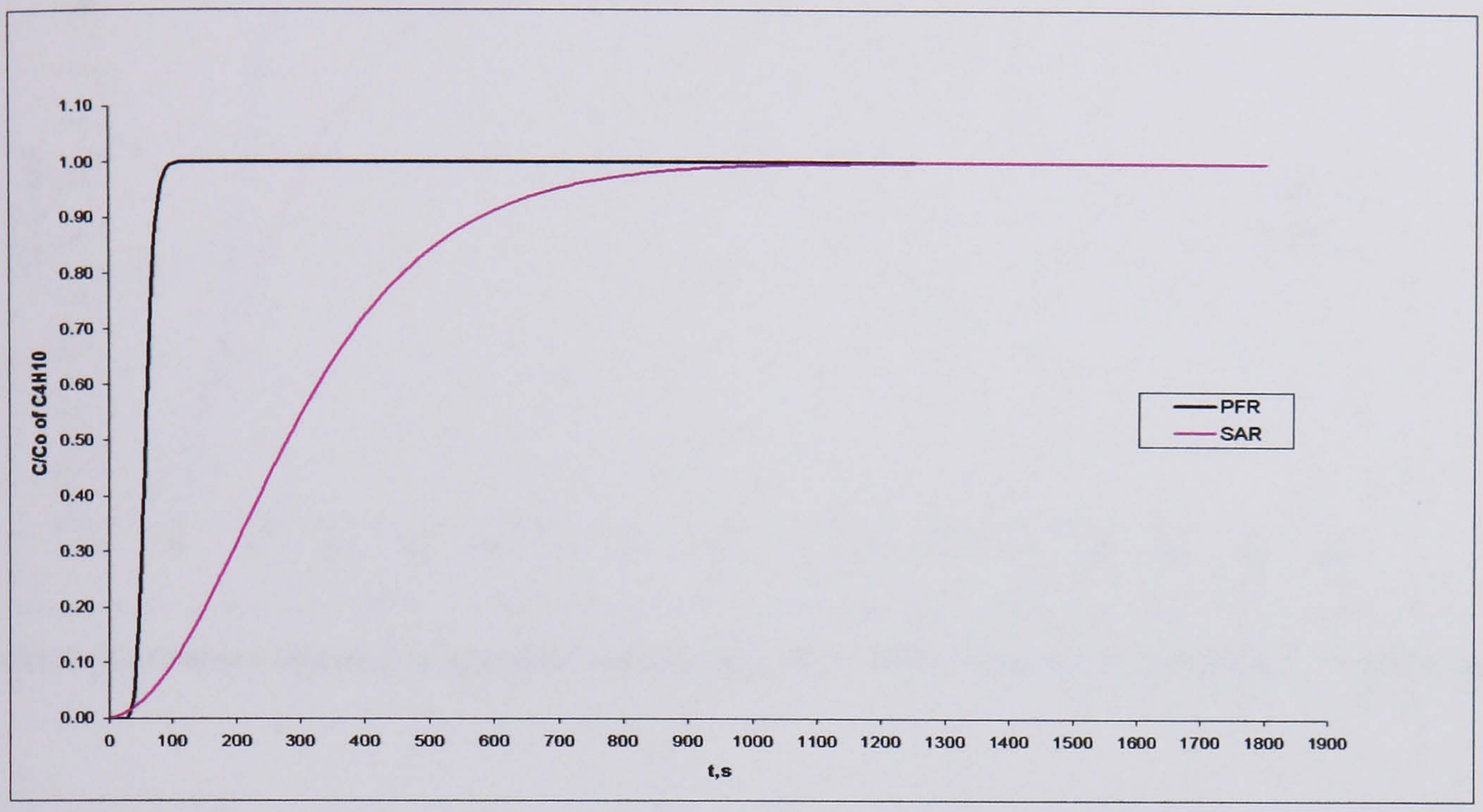


Fig. 7.1 Isobutane adsorption breakthrough profile at T=600K, flow rate= 0.10 l min^{-1}, v= 0.067 ms^{-1}

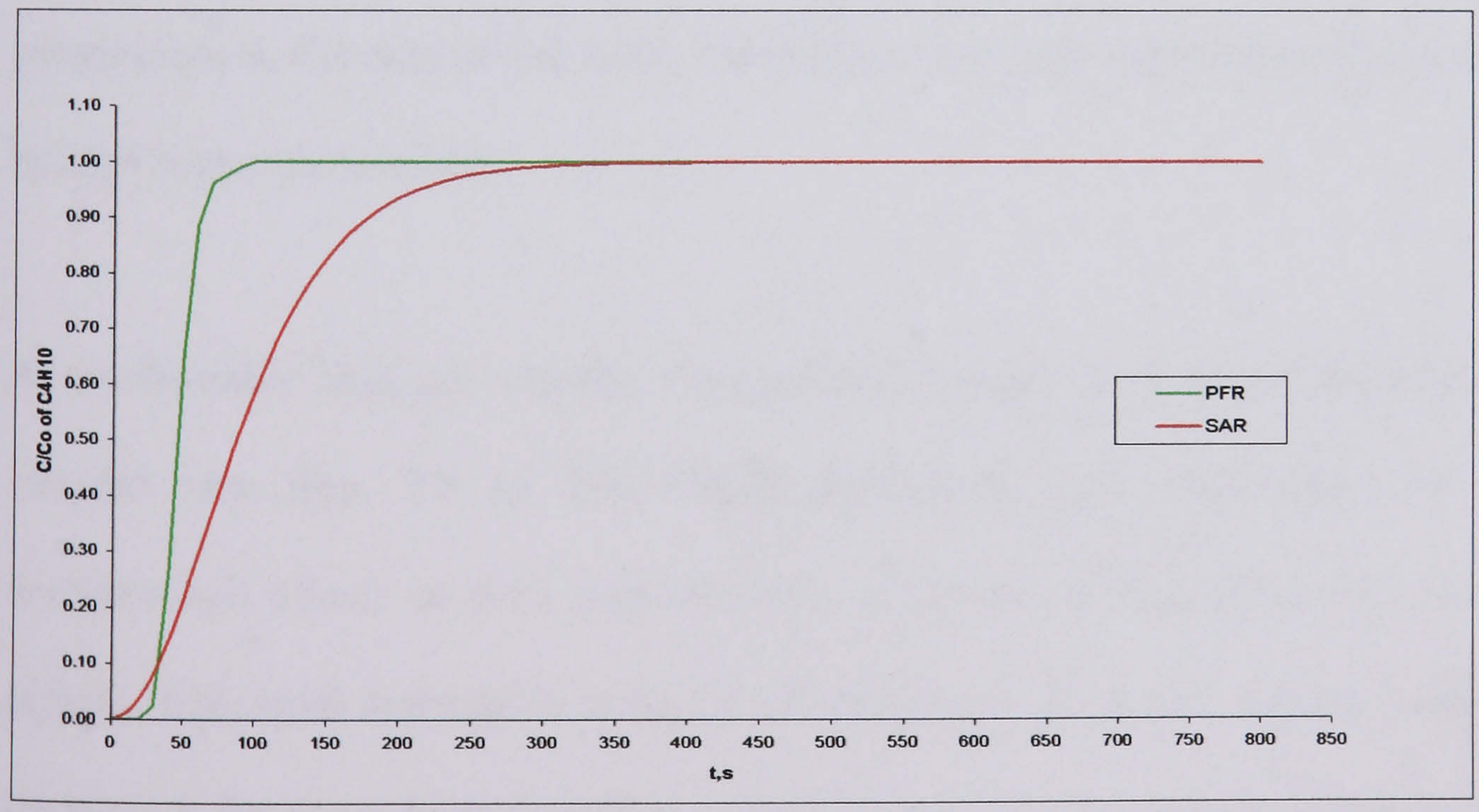


Fig. 7.2 Isobutane adsorption breakthrough profile at T=650K, flow rate= 0.10 l min^{-1}, v= 0.072 ms^{-1}

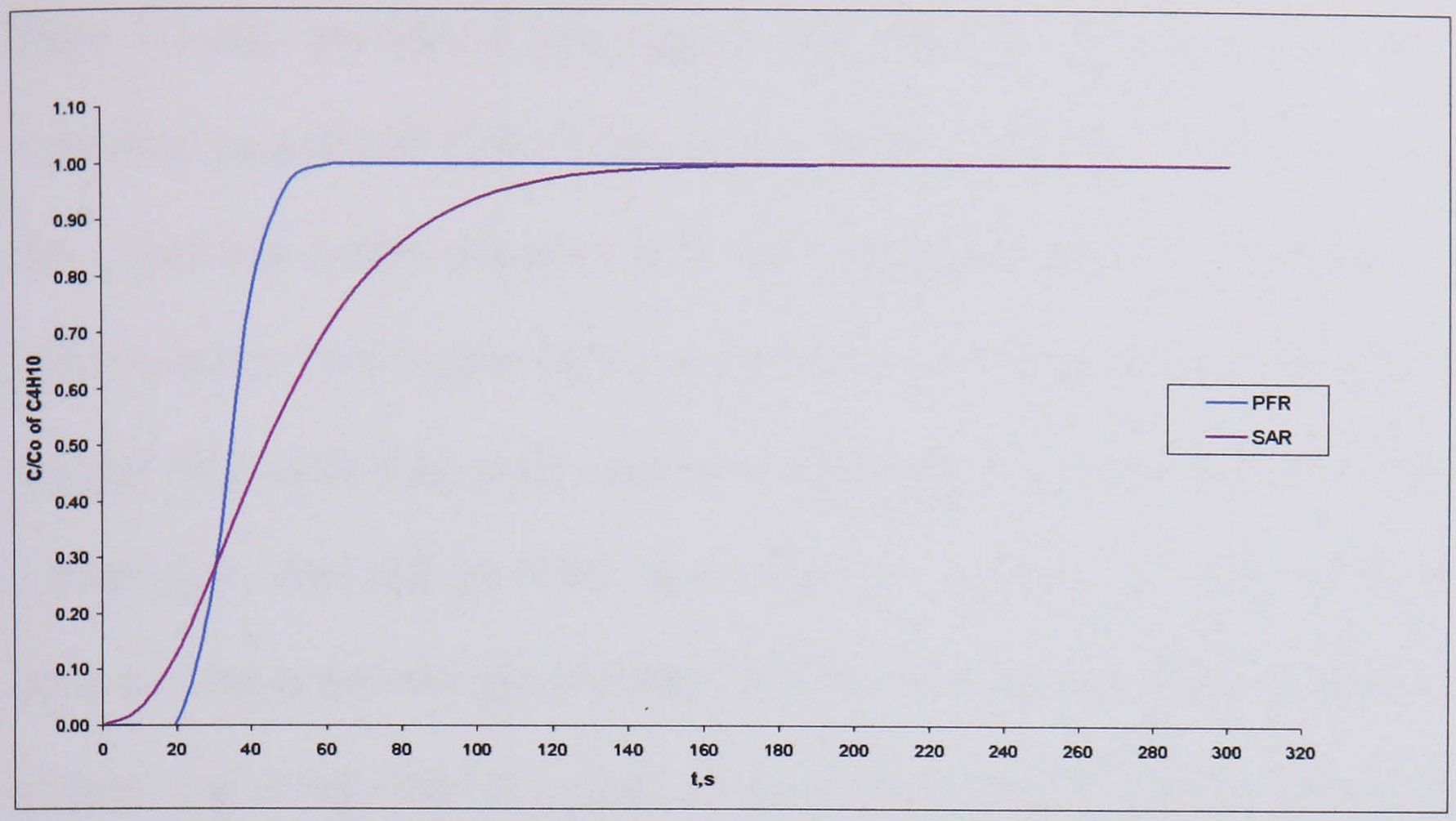


Fig.7.3 Isobutane adsorption breakthrough profile at T=700K, flow rate= 0.10 l min^{-1}, v= 0.078 ms^{-1}

The effect of feed gas flow rates on adsorption are measured at three temperatures. For the first three flow rates selected (see table 7.2), the fluid dynamics is well within the laminar region, depicted by low Reynolds numbers. For the fourth flow rate value of each operating temperature in the case of the SAR, the laminar flow approaches the transition region depicted by high Reynolds numbers.

At considerably high gas velocity, the gas-solid contact time on the adsorbent is significantly reduced (see figs. 7.4 to 7.6). Such phenomena are represented by the diminishing breakthrough effects as flow rate increases. In terms of fluid distribution across the annular reactor, high axial convective transport of momentum (and thus greater superficial velocities) leads to an apparent decrease of the amount of gas diffusing perpendicular to the flow towards the solid zone. The substantial loss of adsorbate from the flow in the SAR affects the adsorption capability of the adsorbent to the extent where only a relatively small fraction of adsorbate is retained. This subsequently adds more constraint for the adsorption to occur.

Table 7.2 also provides a summary of the effect of increasing feed flow rates across the equivalent packed bed PFR. There is a substantial increase in pressure drop estimated across the packed bed system at higher flow rates, especially at higher temperature despite operating within laminar flow region (see also fig7.8). The change in the bulk gas physical properties coupled with increasing axial dispersion effect across the bed renders a much lower gas-solid contact time, depicted by lower space time. In contrast, an obviously minimum (estimated) pressure drop across the gas channel of SAR would provide some insights into the possibility of operating at high feed flow rates for lower temperature catalytic reaction and/or exothermic process as well as adsorption process (see fig.7.7). The radial and axial mixing of the flow at low velocity could be incited using static mixers, which is also quite effective in attenuating input fluctuation and radial variations in flow composition and temperature without needs for moving parts (see Nauman *et al.,* 2002, Thakur *et al.,* 2003, Van den Bleek *et al.,* 1996). Thus, issues such as very diffusive adsorption front could be remedied thereby minimising the perturbation across the gas channel.

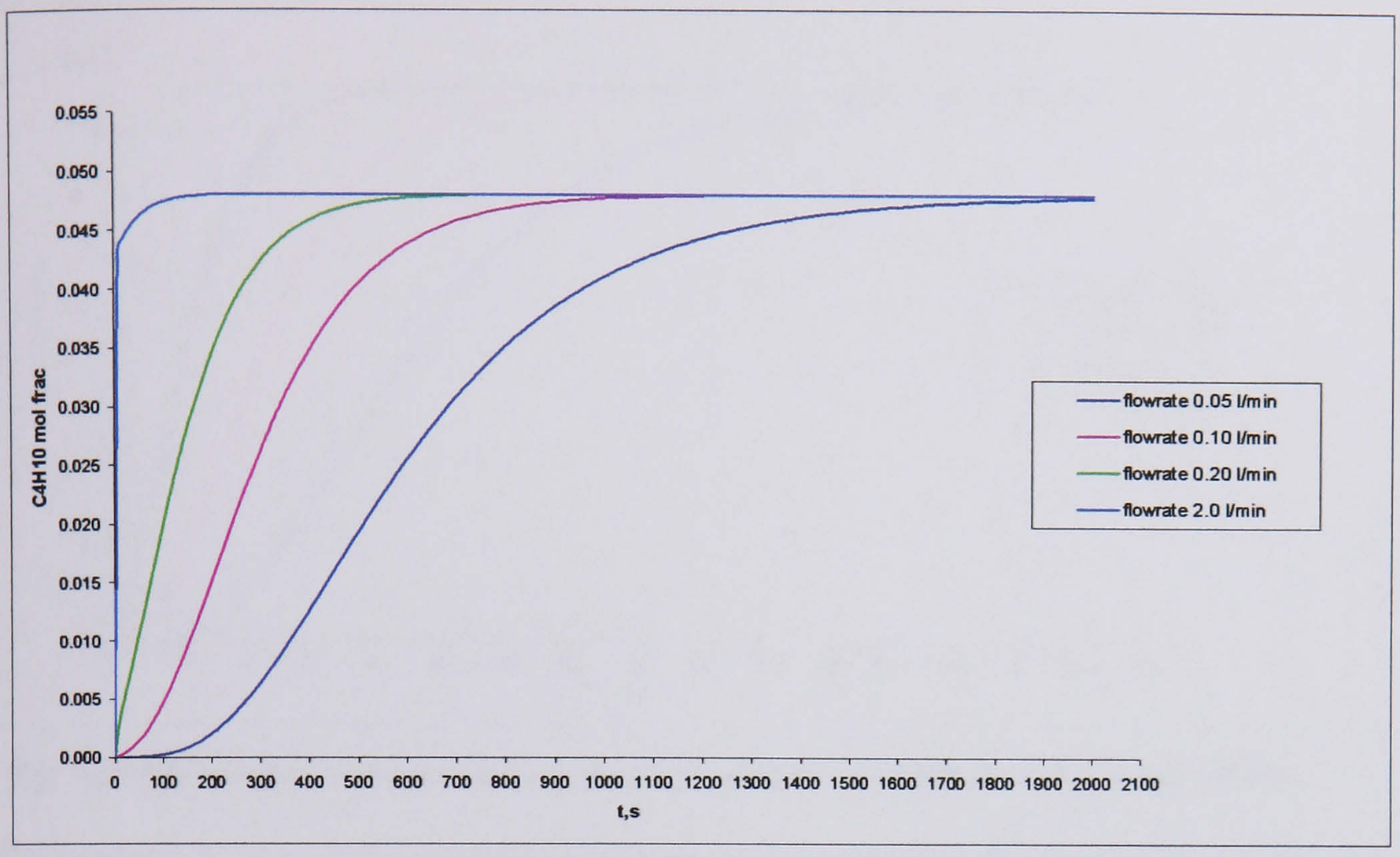


Fig. 7.4 SAR isobutane adsorption breakthrough profiles at 4 different flow rates, T=600K

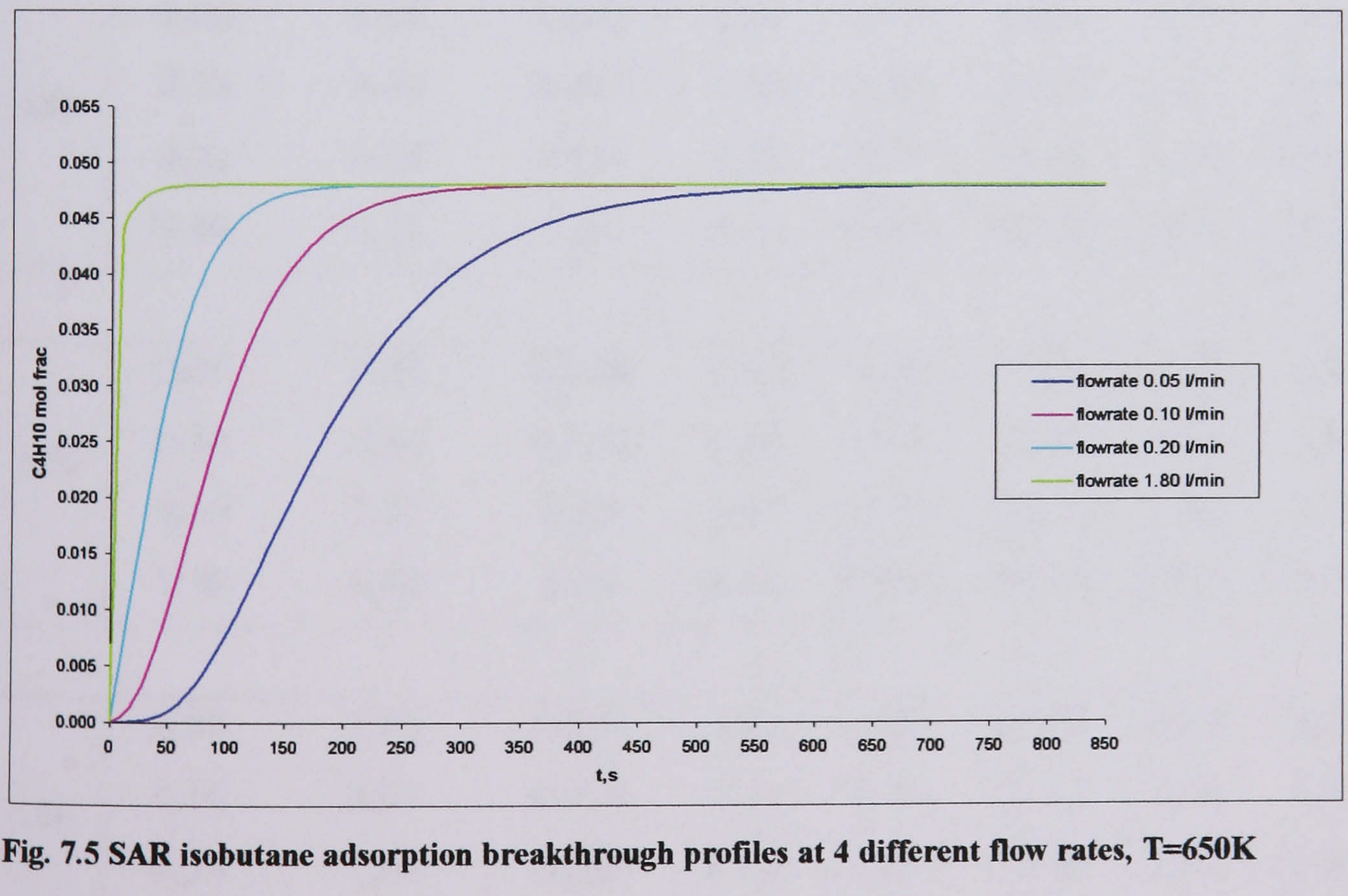


Fig. 7.5 SAR isobutane adsorption breakthrough profiles at 4 different flow rates, T=650K

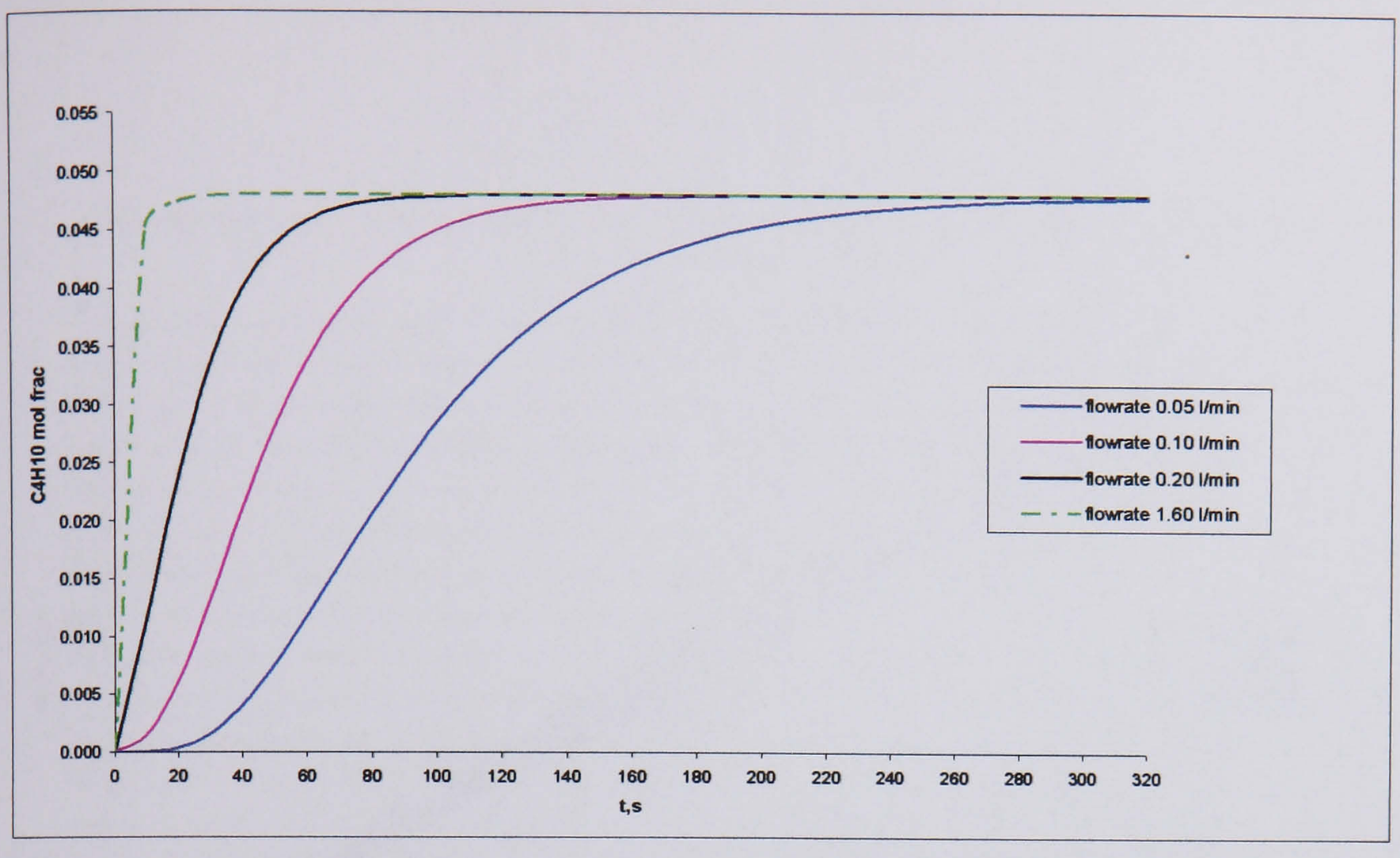


Fig. 7.6 SAR isobutane adsorption breakthrough profiles at 4 different flow rates, T=700K

T,K	flow rates		v	τ, s		N_{Re}		ΔP/L, Pa m^{-1}	
	l min^{-1}	$10^{-6} m^3 s^{-1}$	m s^{-1}	SAR	PFR	SAR	PFR	SAR	PFR
600	0.05	1.68	0.033	2.10	1.57	24.84	0.55	1.35	6.91×10^2
	0.10	3.36	0.067	1.40	1.05	49.68	1.11	2.71	1.38×10^3
	0.20	6.71	0.134	1.05	0.79	99.36	2.21	5.42	2.77×10^3
	2.00	6.71	1.34	0.11	0.090	993.55	22.11	54.15	2.76×10^4
650	0.05	1.82	0.036	1.94	1.45	27.64	0.62	1.43	7.90×10^2
	0.10	3.64	0.072	1.29	0.97	55.27	1.23	2.86	1.58×10^3
	0.20	7.27	0.15	0.97	0.73	110.54	2.46	5.71	3.16×10^3
	1.80	6.54	1.30	0.11	0.081	994.89	22.14	51.41	2.84×10^4
700	0.05	1.96	0.039	1.80	1.35	30.52	0.68	1.50	8.93×10^2
	0.10	3.91	0.078	1.20	0.90	61.05	1.36	3.00	1.78×10^3
	0.20	7.83	0.16	0.90	0.67	122.09	2.72	6.00	3.57×10^3
	1.60	6.26	1.25	0.11	0.084	976.74	21.73	47.98	2.86×10^4

Table 7.2 Summary of flow rates at each temperature along with its Reynolds number, N_{Re} and estimated pressure drop, ΔP/L

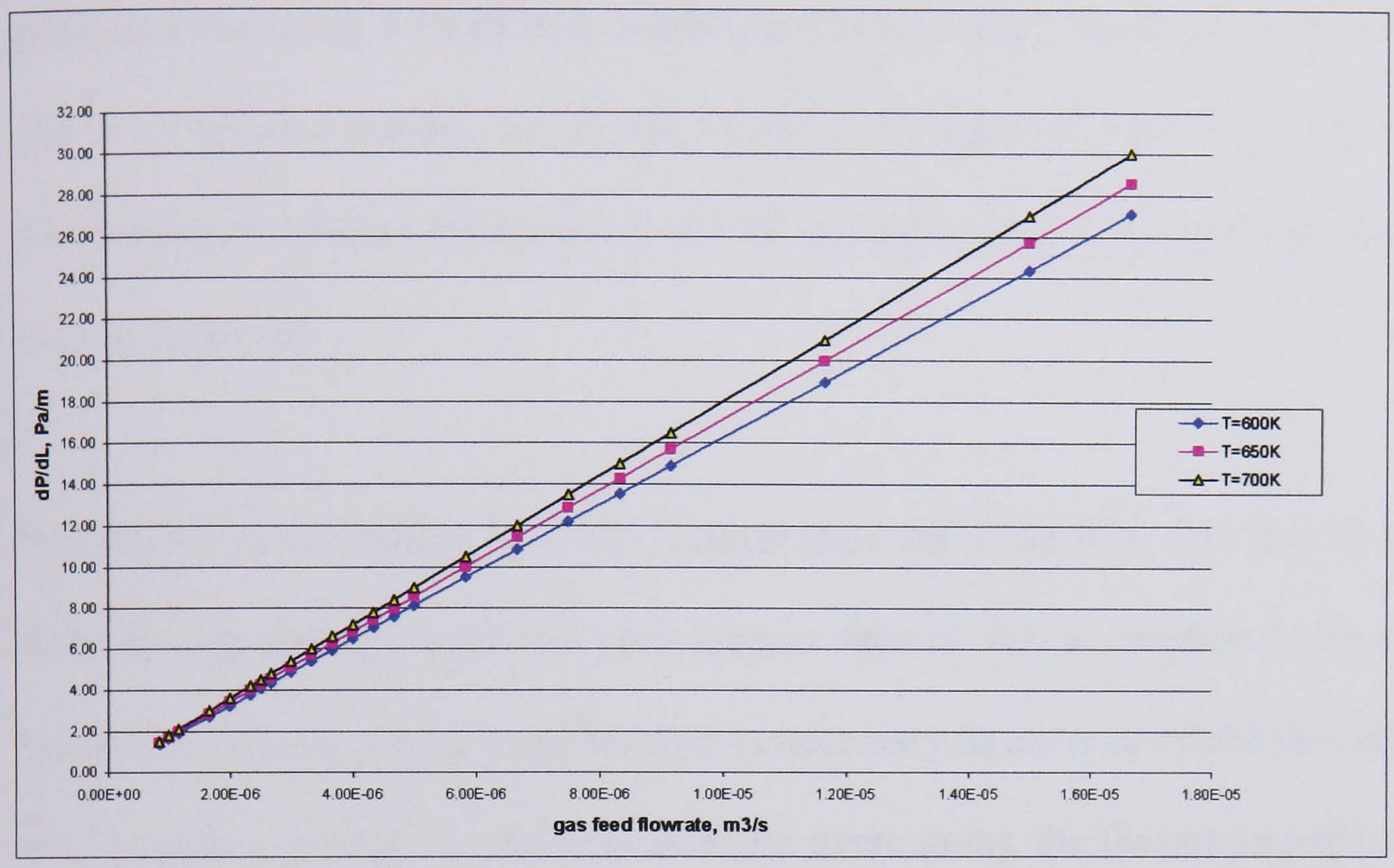


Fig. 7.7 Estimated pressure drop across the gas channel of SAR at increasing feed flow rates

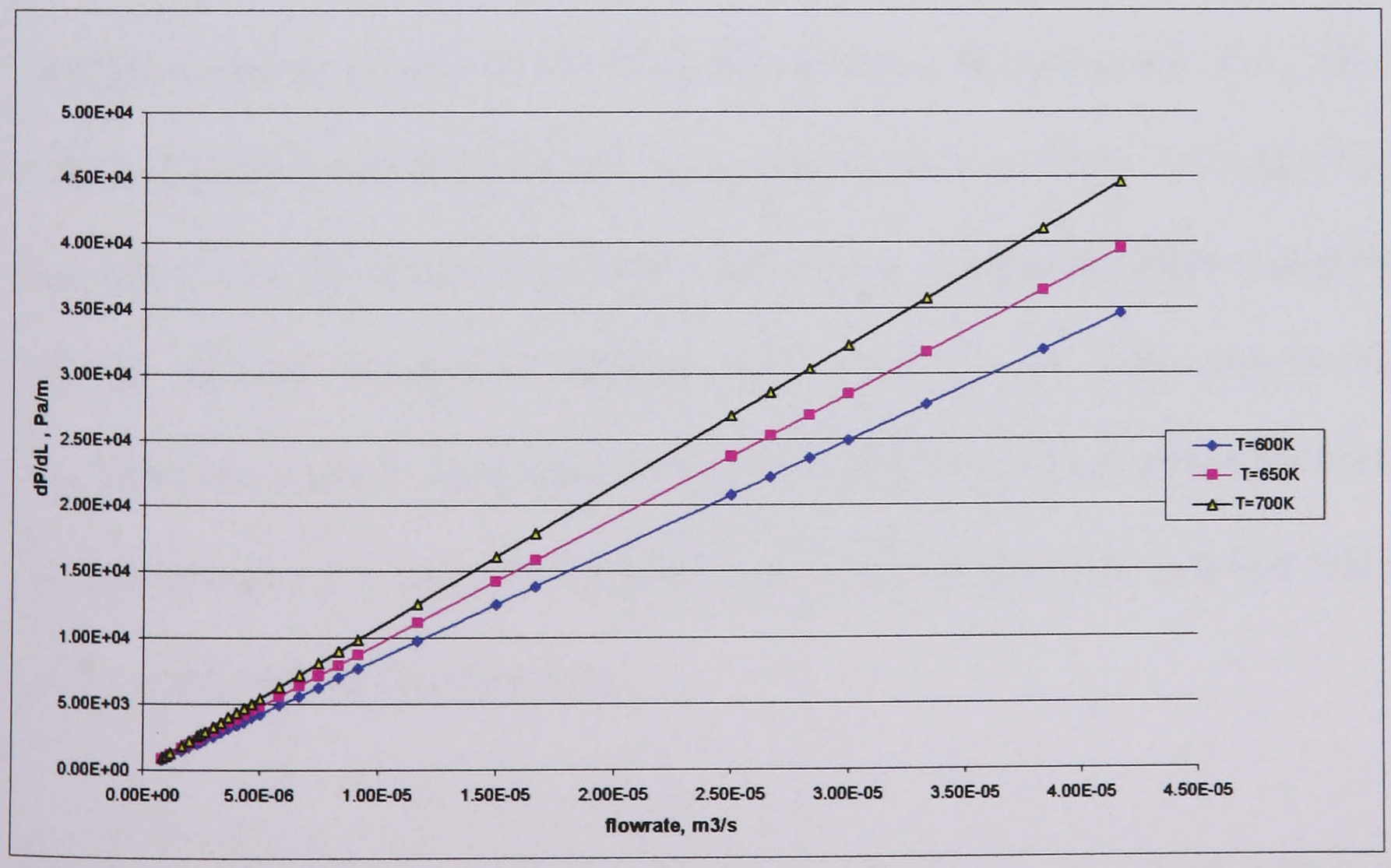


Fig. 7.8 Estimated pressure drop across PFR bed at increasing feed flow rates

7.3.2 Conversion enhancement effect

The direct local removal of the desired product has been exploited through the traditional configuration using a fixed bed, random packing reactor. Such a hybrid reactor concept has shown promising results yet at the expense of high pressure drop. By incorporating the advantages of such a concept using a SAR configuration, a low pressure drop operation may well be achieved.

The choice of a suitable operating temperature and feed flow rate has to be a compromise between adsorption equilibria and kinetic factors for a combined, in situ reaction and separation process. Such consideration is necessary in order to establish a selective separation of the desired product by adsorption while overcoming the thermodynamic limitations of the catalytic reversible reaction.

The effect of temperature for the adsorption enhancement of isobutane dehydrogenation reaction is shown in fig.7.9. At 600 K, and a relatively high space time, isobutene yield is low, but the relatively low temperature increases adsorption affinity and capacity for isobutene. On the other hand, the catalyst performs much better at relatively higher temperature, but because of the reduced adsorption affinity and capacity, the enhancement effect is reduced. Nevertheless, a nearly comparable isobutane equilibrium conversion for both SAR and PFR at all temperatures is observed, suggesting that dehydrogenation reaction takes place regardless of the solid packing configurations.

It can also be seen that it takes a longer time for E (t) $_{SAR}$, the enhancement factor for SAR system to approach zero at 600K, which implies slow adsorbate breakthrough. This is due to the longer reactor residence time, which allows relatively higher amount of feed gas to diffuse

to the solid zone from the empty central gas channel. In addition, the low temperature condition promotes a higher interaction between adsorption and reaction process as there is higher isobutene retention and its subsequent influence in the local reaction kinetics and equilibria (Ding and Alpay, 2000). Subsequently, adsorbent capacity is increased at negligible axial dispersion effect across the annular bed where molecular diffusion predominates. The feed gas in the PFR on the other hand, has relatively lower gas-solid contact time due to the axial dispersion effect along the random bed packing. The diffusional path is increased causing greater intraparticle mass transfer resistance and hence, reduced conversion enhancement effect.

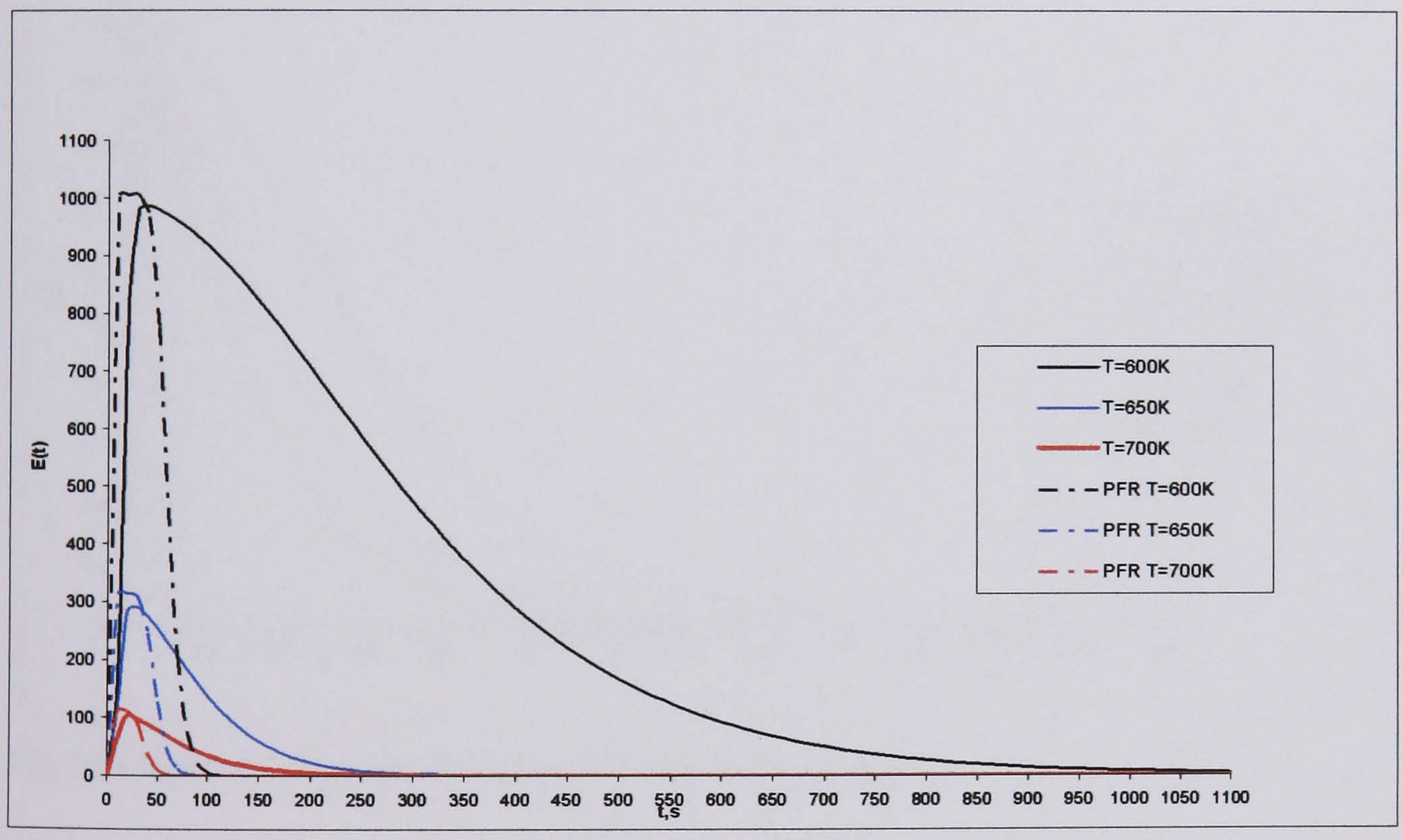


Fig. 7.9 Adsorption enhancement effect at three different temperatures; flow rate= 0.10 l min^{-1}

Evidently, lower feed flow rate also shows a pronounced effect on achieving a substantial conversion enhancement effect. Such a phenomenon is illustrated in fig. 7.10 whereby the shorter E (t) $_{SAR}$ peak coincides with the faster equilibration time as the feed flow rate increased from 0.10 l min^{-1} to 0.20 l min^{-1}. Due to the fact that the flow transport in the SAR

packing arrangement is dominated by molecular diffusion, increasing the flow rate in the SAR would reduce its enhancement potential as a result of lower residence time. The flow rate effect produces somewhat the opposite in the case of PFR. Even though the equilibration time becomes shorter at higher flow rate, the E (t) $_{PFR}$ curves at different flow rate are not much different from one another. This may be due to the greater, more profuse solid-gas contact in the PFR bed particularly on the catalyst, despite the decreasing adsorbent capacity. Also, the axial dispersion effect becomes more dominant at higher flow rates but since the flow is still well within laminar region (see table 7.2), this could offset the possibility to achieve conversion enhancement effect even at increasing intraparticle diffusional resistance.

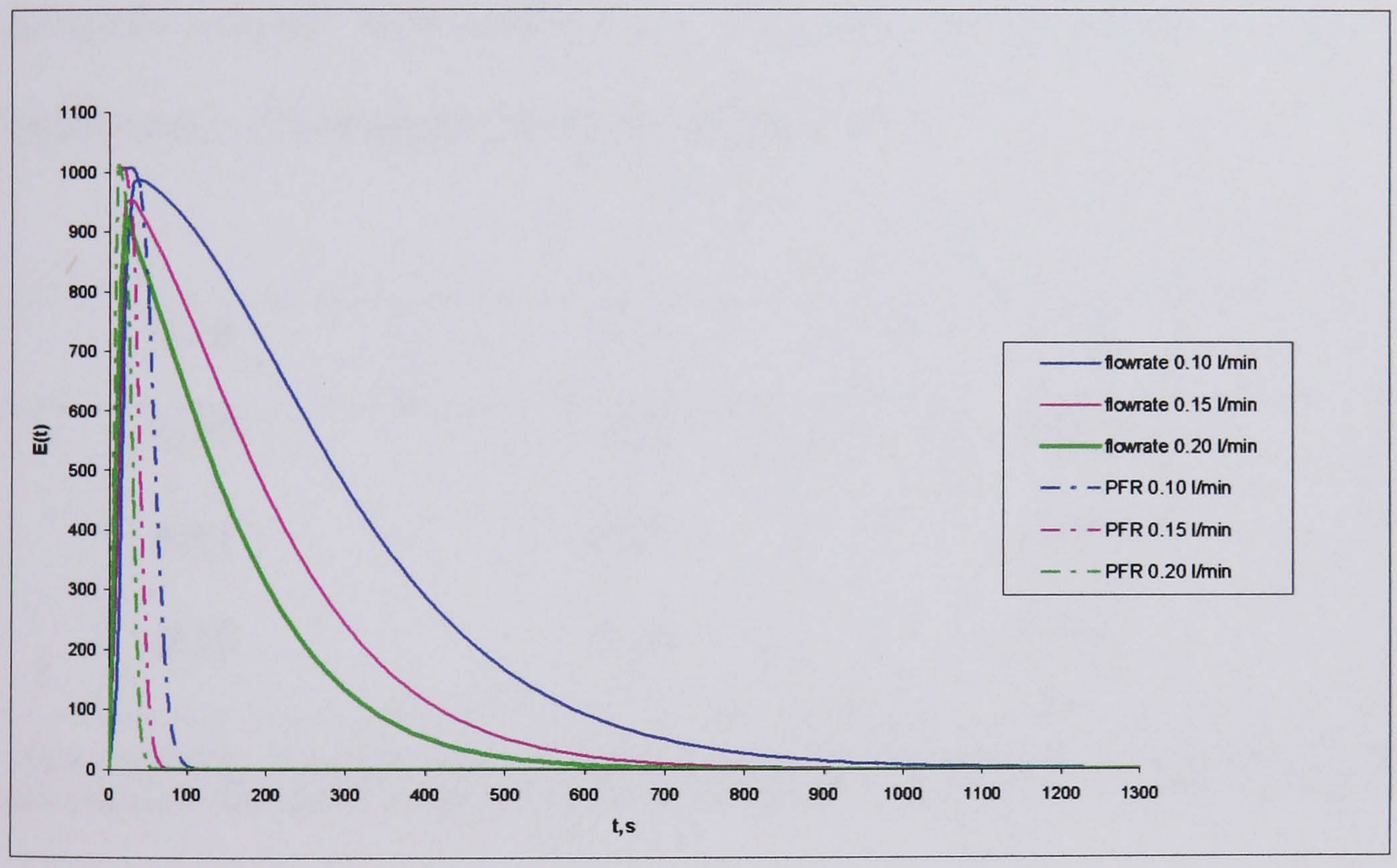


Fig. 7.10 Flow rate effect on adsorption enhancement; T=600K

With reference to table 7.3, the advantage of coupling the adsorption and reaction process in the SAR may be intensified if an appropriate reactor length is used. Evidently, the intrinsic behaviour of adsorption process capitalizes on changes with time as well as with positions in the bed. If the bed is too long, the adsorption time could be extended at increasing mass transfer resistance resulting in less than half of the adsorbent capacity could be utilised. On the

other hand, very short reactor length may also inhibit complete separation of the feed components due to inadequate amount of adsorbent and hence, inefficient bed utilisation. Such phenomena are illustrated in fig.7.11 in which the effect of using longer reactor length, represented by longer E (t) $_{SAR}$ curve, may not contribute to the conversion enhancement effect. This is due to increasing diffusional path, which leads to increasing intraparticle diffusion resistance along the mass transfer zone and hence, slower breakthrough. The amount of isobutene adsorbed per mass of adsorbent remains unchanged at longer length even at relatively higher residence time denoted by higher space time in table 7.3. Thus, conversion enhancement effect would only become more substantial if the beneficial effects of local isobutene removal were realised at a reasonable reactor length in order to overcome the disadvantage of incomplete adsorbent utilisation.

L, m	**τ , s**	**X_{ad}**	**X_{nad}**
0.07	**1.05**	**0.089**	**0.089**
0.14	**2.10**	**0.090**	**0.090**
0.21	**3.15**	**0.090**	**0.090**

Table 7.3 Effect of varying reactor length on corresponding equilibrium conversion, X with (ad) and without incorporation of adsorbent (nad) for SAR at three different reactor lengths, T=600K, flow rate = 0.10 l min^{-1}

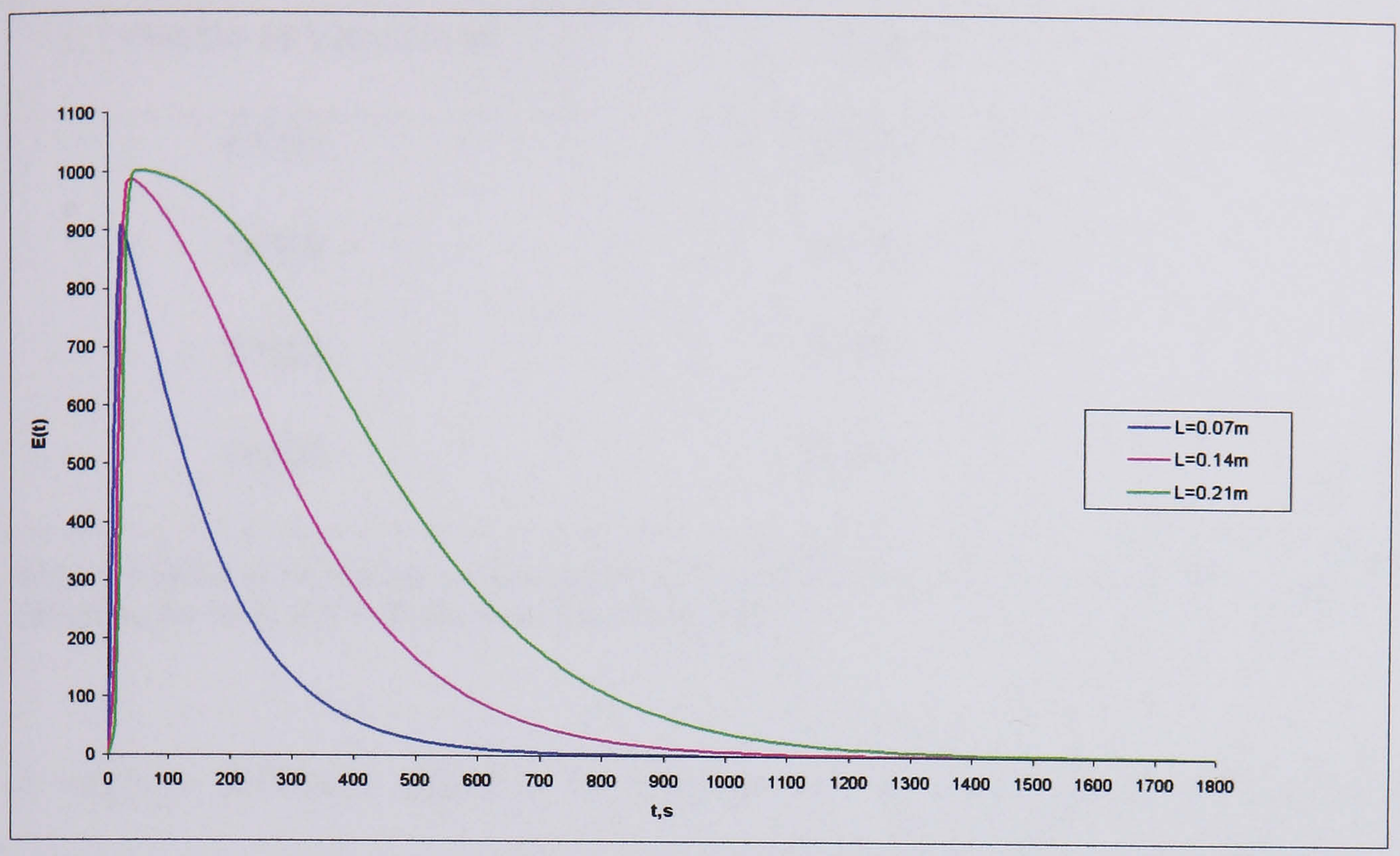


Fig. 7.11 SAR axial effect on adsorption enhancement; T=600K, flow rate= 0.10 l min^{-1}, R1 and R2 are 0.004 m and 0.014 m respectively

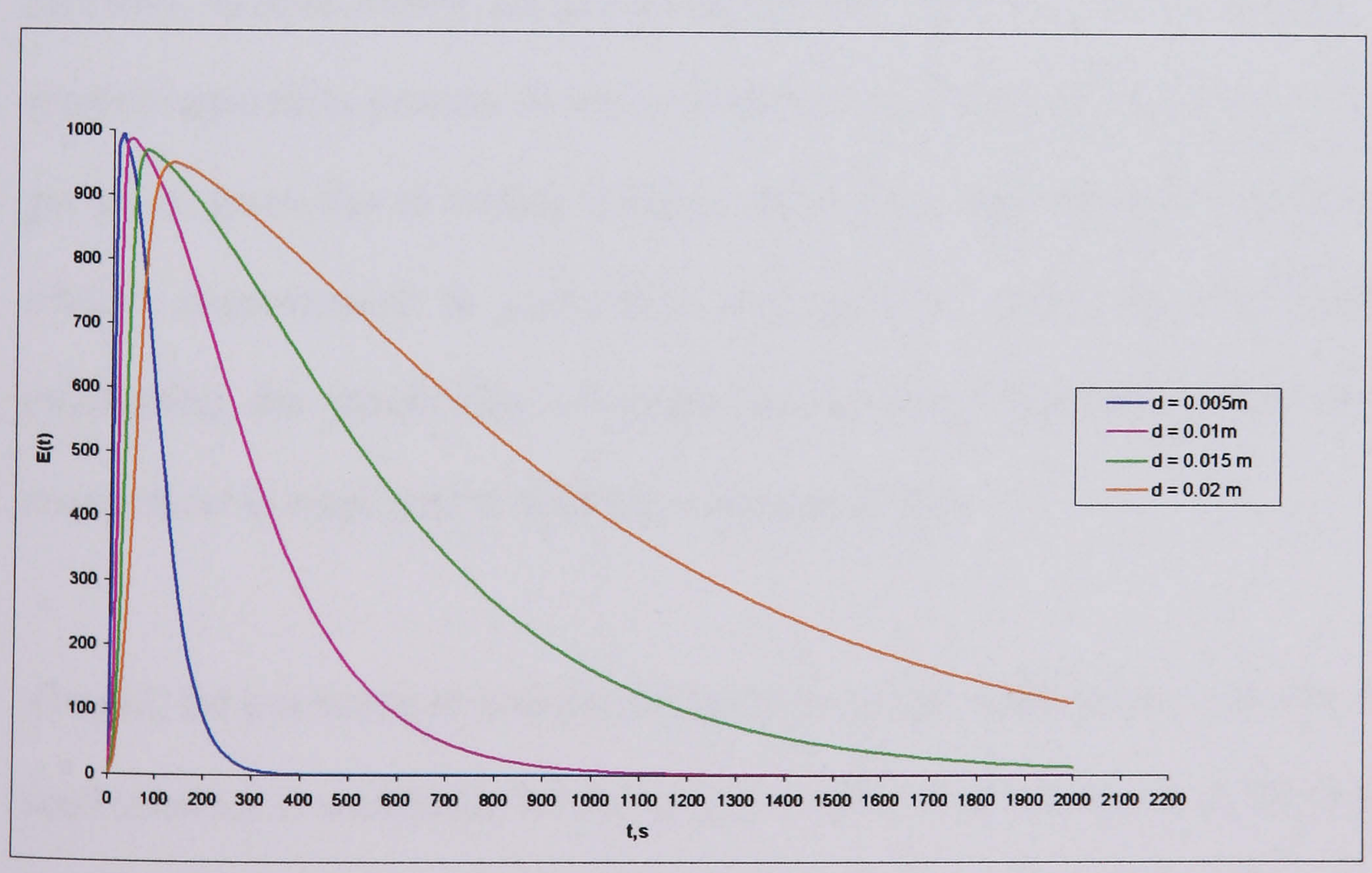


Fig. 7.12 SAR annular thickness effect on adsorption enhancement; T=600K, flow rate= 0.10 l min^{-1}, reactor length, L= 0.14 m, d denotes δ, the annular thickness

δ, annular thickness, m	X_{ad}	X_{nad}
0.005	0.090	0.090
0.010	0.090	0.090
0.015	0.101	0.090
0.020	0.191	0.090

Table 7.4 Effect of increasing annular thickness on equilibrium conversion with (ad) or without (nad) incorporation of adsorbent for SAR at T = 600K, flow rate = 0.10 l min^{-1}

A slightly different situation is observed if the SAR annular thickness is increased (see fig.7.12). At a similar base case reactor length and feed flow rate, the space time is unchanged but intraparticle mass transfer resistance decreases substantially due to the reduced distance of diffusional path in the thicker annular bed packing. As the result, the equilibrium conversion increases because higher amount of isobutene could be adsorbed during the simultaneous reaction-separation process in situ (see table 7.4). Thus, the depletion of isobutene from the gas phase gives rise to further shifting the reaction equilibrium for product formation. This marked improvement in conversion enhancement effect provides further insights into establishing the practicality of employing in situ adsorption if thicker annular packing arrangement is employed at relatively high space time.

Overall, the governing molecular diffusion transport, which arises from the structured packing configuration, is central in determining the adsorption efficiency in the SAR. At practically very low pressure drop estimated across the bed, such reactor applications may be limited to lower feed flow rates as the SAR performance is more effective when operated at high residence time within laminar flow region. Such criteria are critical towards improving the conversion enhancement effect if an appropriate reactor length and/or thicker annular packing

section are employed at low reaction temperature. In addition to low pressure drop characteristic, this reactor configuration may still be operated at reasonably higher flow rates if static mixers are incorporated in the gas channel to incite the axial and radial mixing at minimum perturbation.

7.3.3 Cyclic process

The SAR, like any other adsorptive reactors, undergoes an in situ periodic regeneration to remove the adsorbate upon equilibration of the adsorbent in a single bed operation. At very low adsorbate concentration, the adsorbent bed is regenerated by passing in the inert hot purge gas during the desorption step to reduce the partial pressure of the adsorbate. Nitrogen is selected as the non-adsorbable gas and is fed into the reactor at the same reaction temperature (for e.g. T = 600K). The adsorbate is periodically removed from the adsorbent bed and is carried off by the purge gas towards the reactor outlet. Such dynamic operation is utilised to generate a favourable condition for a continuous adsorption-enhanced reaction-separation process.

In this work, the periodic adsorptive process of the SAR is investigated using cyclic steady state (CSS) approach. It is where the periodic boundary conditions are imposed such that it embodies a CSS system whereby the conditions at the end of each subsequent cycle is the same as the first cycle for both gas and solid phase. The CSS convergence based on simultaneous discretisation of both axial and radial domain using BFDM method is checked for three consecutive cycles mirroring the behaviour of the first cycle. The simulation results are compared to its equivalent PFR. In each case, the cycle profiles of an adsorption-only

process are also plotted for each temperature as a mean to draw the attention to the effect of synergetic behaviour of the hybrid process.

The CSS periodic adsorptive process is first observed at 600K as shown in figs.7.13 and 7.14 for the SAR and PFR. The cyclic behaviour of each of the adsorptive reactors is identical to the adsorption-only process. Combined in situ reaction-separation process occurs during adsorption step. Due to the fact that the fluid transport mechanism in the SAR is governed by molecular diffusion at relatively high space time and relatively higher annular volume, the time it takes to complete one cycle in the SAR is significantly longer than the PFR. The molecular diffusion transport allows for relatively greater bed utilisation and thus, relatively higher isobutene retention resulting in the longer time to regenerate the adsorbent bed in the SAR.

The cycle time decreases as the temperature increases and such phenomenon is shown in figs.7.15 and 7.17. Catalytic isobutane dehydrogenation reaction is essentially endothermic and favours higher temperature to overcome thermodynamic limitations. However, the adsorption process is intrinsically exothermic and favours lower temperature operations. Operating at high temperature would reduce the adsorbent capacity to retain isobutene and this affect the conversion enhancement effect, despite achieving higher CSS conversion. On the other hand, desorption performs better at higher temperature due to its endothermic nature. The time taken to regenerate the adsorbent bed is thus reduced considerably.

The temperature influence on the physical property of the bulk gas causes increased gas velocity. In as much as the fluid transport is dominated by molecular diffusion across the annular packing, the increasing axial convective transport along the central gas channel as the

result of high temperature may reduce the amount of reactant gas to come into contact with the solid material. This also magnifies the axial dispersion effect in the PFR bed (see figs 7.16 and 7.18). Subsequently, this adds to lower local adsorbates removal at reduced residence time across the reactor. Therefore, the adsorption enhancement effect becomes less significant at high temperatures.

Table 7.5 summarises the effect of varying temperature on the CSS process for each reactor studied. The estimated energy input is similar for each type of reactor. This suggests that at isothermal condition, the heat carried by the bulk gas (i.e. nitrogen) mainly provides the energy required for the endothermic reaction as well as during regeneration. Also, the cyclic steady state conversion for each reactor is slightly higher than the corresponding equilibrium conversion, indicating negligible isobutane concentration and mass accumulation effects over a cycle.

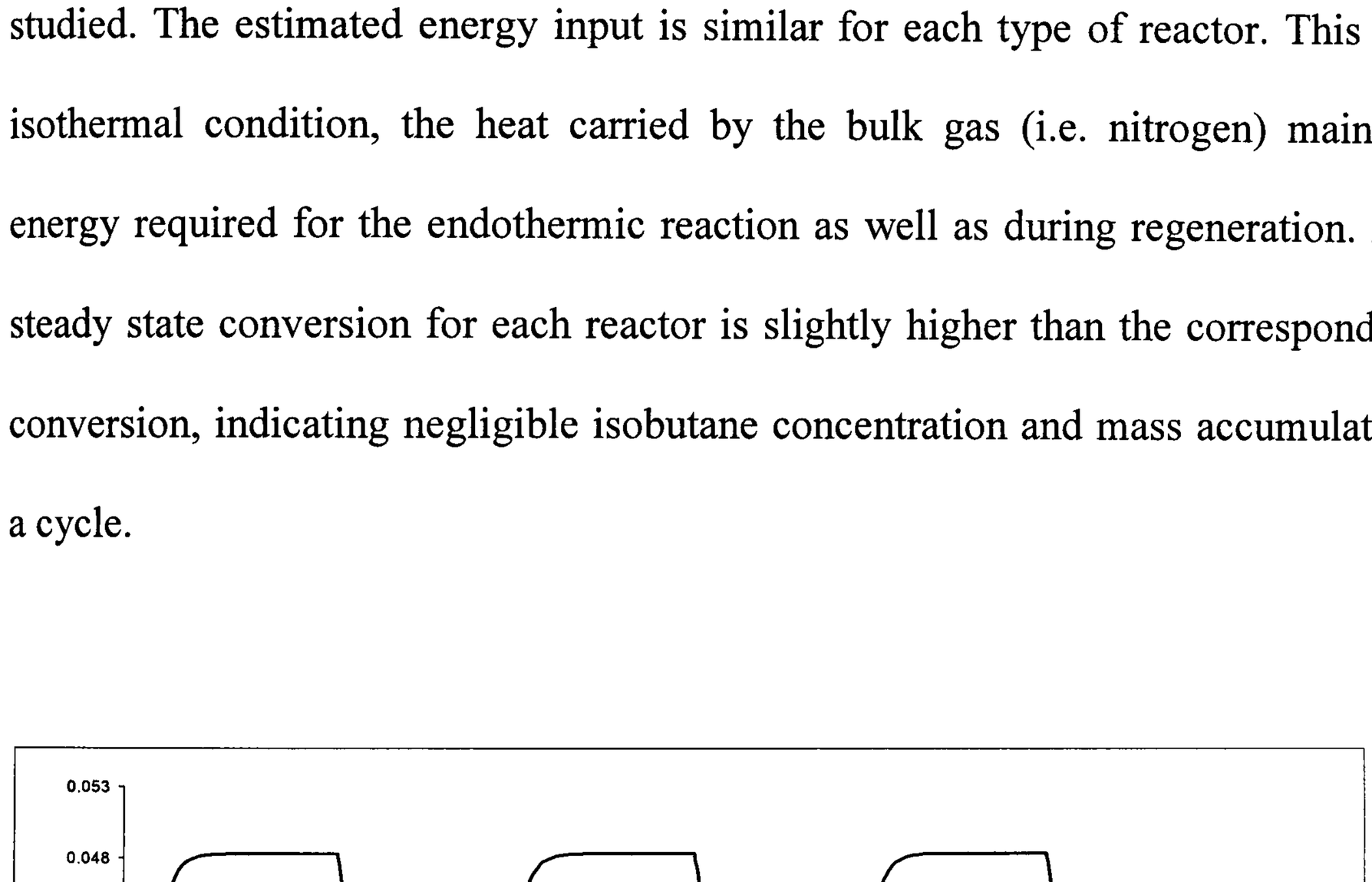


Fig. 7.13 SAR isobutane dynamic cyclic process for adsorption only and combined reaction-separation process at T= 600K, flow rate= 0.10 l min^{-1}. Adsorption cycle time= 2000s; desorption cycle time=1500s; ads = adsorbent ; admix = admixture

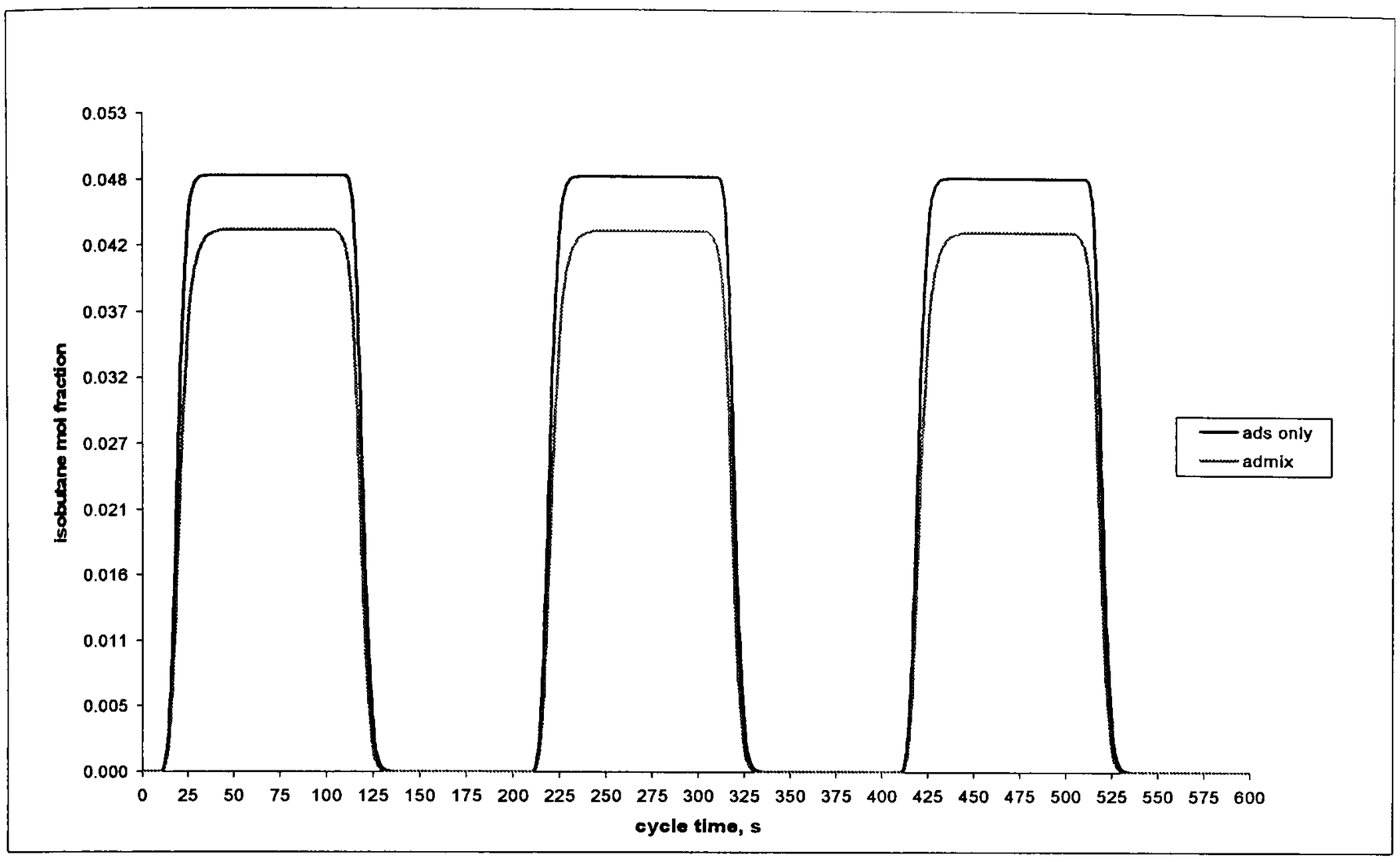


Fig. 7.14 PFR isobutane dynamic cyclic process for adsorption only and combined reaction-separation process at T= 600K, flow rate= 0.10 l min^{-1}. Adsorption cycle time= 100s; desorption cycle time=100s; ads = adsorbent ; admix = admixture

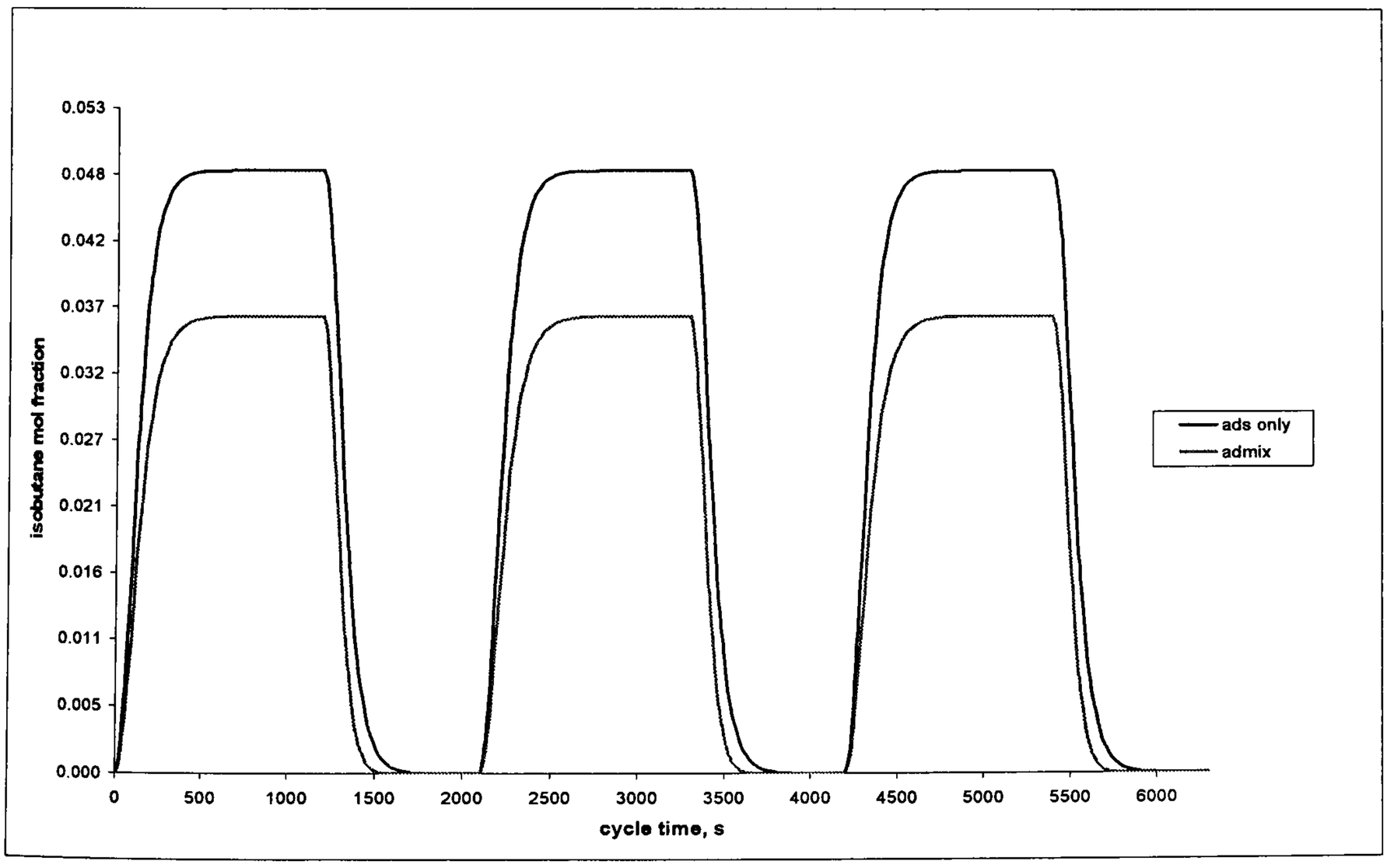


Fig. 7.15 SAR isobutane dynamic cyclic process for adsorption only and combined reaction-separation process at T= 650K, flow rate= 0.10 l min^{-1}. Adsorption cycle time= 1200s; desorption cycle time=900s; ads = adsorbent ; admix = admixture

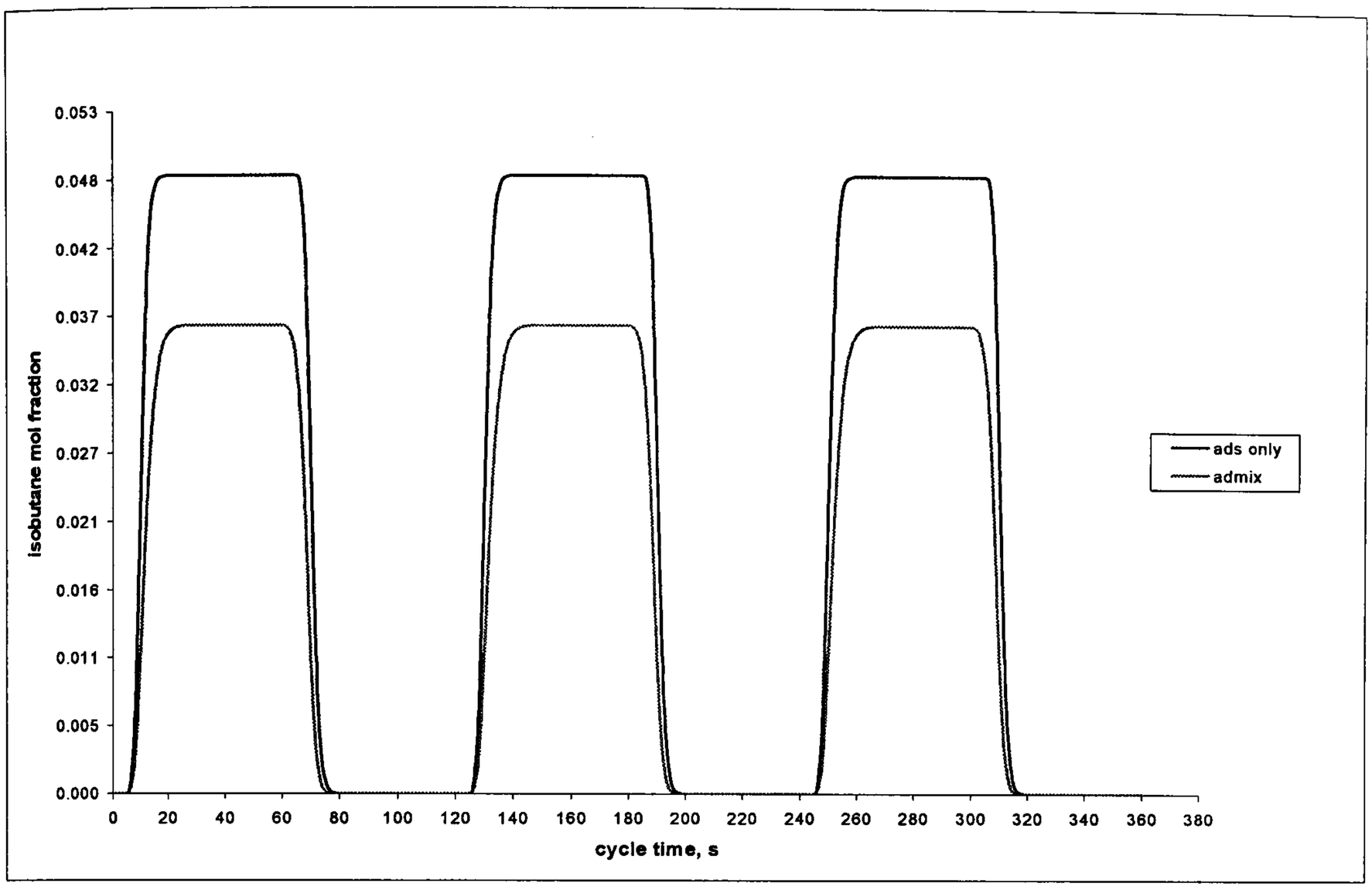


Fig.7.16. PFR isobutane dynamic cyclic process for adsorption only and combined reaction-separation process at T= 650K, flow rate= 0.10 l min^{-1}. Adsorption cycle time= 60s; desorption cycle time=60s; ads = adsorbent ; admix = admixture

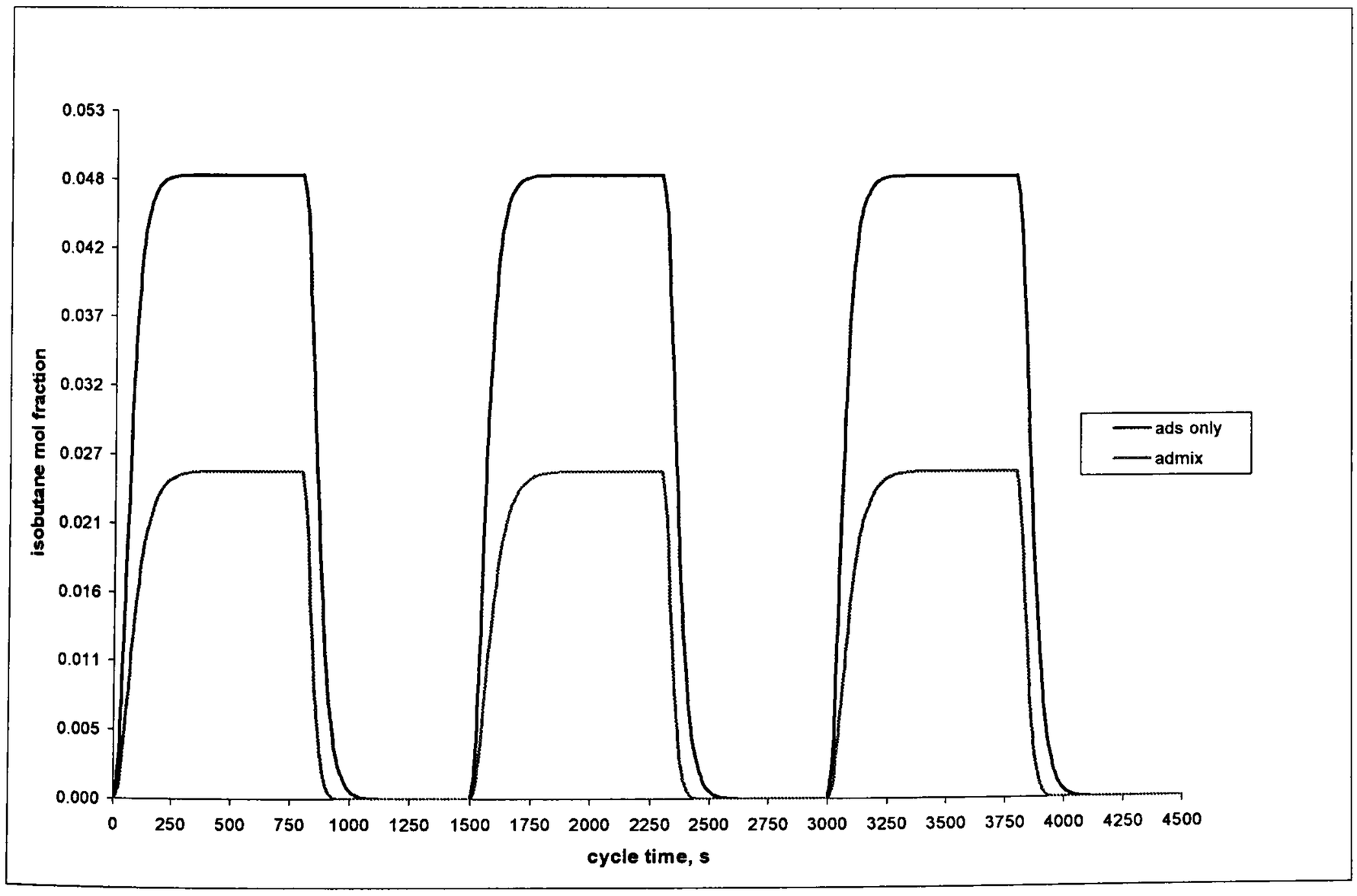


Fig.7.17. SAR isobutane dynamic cyclic process for adsorption only and combined reaction-separation process at T= 700K, flow rate= 0.10 l min^{-1}. Adsorption cycle time= 800s; desorption cycle time=700s; ads = adsorbent ; admix = admixture

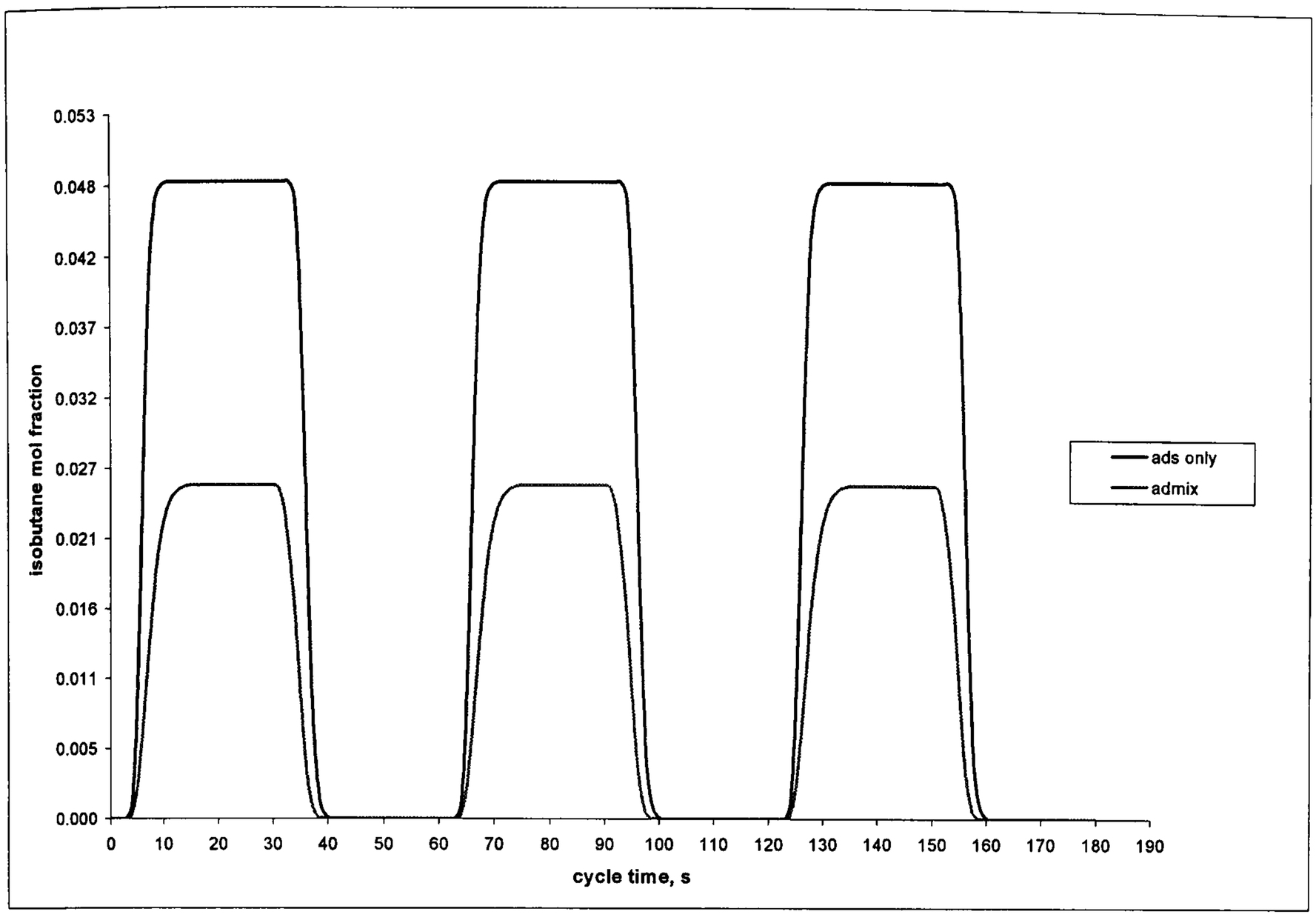


Fig.7.18. PFR isobutane dynamic cyclic process for adsorption only and combined reaction-separation process at T= 700K, flow rate= 0.10 l min^{-1}. Adsorption cycle time= 30s; desorption cycle time=30s; ads = adsorbent ; admix = admixture

T, K	v, m s^{-1}	τ, s		Energy input, J s^{-1}	cycle time, s				conversion			
					SAR		PFR		X_{SAR}		X_{PFR}	
		SAR	PFR		t_{ads}	t_{des}	t_{ads}	t_{des}	CSS	eqm	CSS	eqm
600	0.067	2.10	1.57	0.578	2000	1500	100	100	0.13	0.09	0.11	0.09
650	0.072	1.94	1.45	0.673	1200	900	60	60	0.31	0.26	0.28	0.24
700	0.078	1.80	1.35	0.769	800	700	30	30	0.53	0.47	0.53	0.46

Table 7.5 Summary of energy input, cycle times and equilibrium conversion of SAR and PFR at flow rate = 0.10 l min^{-1}; t_{ads} and t_{des} are reaction-adsorption time and desorption time respectively; eqm = equilibrium; CSS = cyclic steady state

From Table 7.6, the CSS conversion is zero at T = 500K, implying unfeasible operating condition for the dehydrogenation reaction. The local adsorption however is remarkably high and this is represented by a relatively long t_{ads} and t_{des} for similar feed components. Higher amount of gas adsorbed often dictates lower temperature condition and the adsorption

equilibrium tends to be kinetically controlled, implying adsorbate may spend longer time within the pellet due to higher diffusion rate. Such information also provides a possibility to consider running adsorption only experiments at temperatures lower than 500K for adsorption equilibria studies.

From a design configuration point of view, both the SAR and PFR share similar potential of achieving higher isobutane conversions at high temperatures. However, further adsorption enhancement effect becomes rather limited when using the PFR, particularly at higher temperature operations due to increasing adverse effect of axial dispersion which further limits the mass transfer in the bed. Such phenomenon, denoted by dramatic decrease in t_{ads} and t_{des} in table 7.6, obviously does not comply with the intrinsically transient adsorption bed property whereby the physical interaction between the adsorbent and feed components varies with time. On the other hand, molecular diffusion predominates in the absence of any sort of convective transport in the SAR annular packing. Such transport mechanism may contribute to providing in situ adsorbate removal to some extent. Consequently, possible reaction enhancement may still be attained at relatively higher t_{ads} and t_{des} than the PFR at temperatures below 800K.

T,K	v, m s^{-1}	Energy input, J s^{-1}	cycle time				X_e		N_{Re}	
			SAR		PFR		SAR	PFR	SAR	PFR
			t_{ads}	t_{des}	t_{ads}	t_{des}				
500	0.056	0.386	10000	11500	200	200	0	0	39.03	0.868
550	0.061	0.482	6500	5500	150	150	0.030	0.035	44.25	0.98
750	0.083	0.865	600	550	15	10	0.78	0.76	66.97	1.49
800	0.089	0.960	450	400	10	8	0.92	0.89	73.04	1.63
850	0.095	1.056	290	280	8	6	0.96	0.96	79.24	1.76
900	0.100	1.152	240	230	6	4	0.985	0.98	85.58	1.90
950	0.106	1.247	190	180	4	2	0.994	0.9933	92.04	2.05
1000	0.111	1.343	140	130	2	1	0.9975	0.9977	98.63	2.19

Table 7.6 Summary of the temperature dependent parameters and their respective Reynolds number, N_{Re}, at temperatures other than stated previously for an admixed process; feed flow rate= 0.10 litre min^{-1} at T=298K

7.4 Concluding remarks

The potential of SAR as an attractive alternative to the traditional packed bed configuration was theoretically explored by incorporating the experimentally measured adsorption and kinetic parameters within the gPROMS modelling environment. The selected key decision parameters, which included reaction temperatures, feed flow rates (represented in terms of

superficial velocities), as well as reactor annular thickness and length have substantially influenced the transient kinetic and adsorption profiles.

In terms of temperature change, higher isobutane equilibrium conversions were achieved at higher reaction temperature but further adsorption enhancement was difficult. Although high temperature was the principal characteristic to overcome the reaction equilibrium limitations, it could result in relatively low adsorbent capacity and subsequently, low adsorption affinity. Nevertheless, the catalytic dehydrogenation reaction has to be operated within certain temperature ranges to overcome side reactions, coke formation, and catalyst deactivation. Therefore, this has called for a careful temperature range selection, which would offset the benefit of reaction enhancement in particular within the thermodynamic limitations. In addition, this would also imply that optimal temperature exists for maximum enhancement effect.

The increase in feed flow rates would result in a steady decrease of adsorption enhancement effect due to the relatively low space time of gas diffusing across the solid admixture bed. The catalytic dehydrogenation reaction however, seized to exist regardless of the increasing feed flow rates within the laminar region. On the other hand, the benefits of in situ separation became negligible as temperature decreased even though the adsorption affinity for the adsorbates was relatively high. This was due to rather low, if not, negligible dehydrogenation reaction, even at relatively higher space time.

A longer reactor length might improve the reaction enhancement effect. This was owing to the higher adsorbent loading which led to longer adsorption equilibration time yet at relatively higher mass transfer resistance. A larger cross-sectional area as the result of increasing the annular thickness would increase the in situ reaction-separation due to substantially low mass transfer resistance. Therefore, it was of great importance to establish a right geometrical

combination for SAR design while sustaining the low pressure drop advantage over the conventional packed bed tubular reactor.

The dynamic operation of the synergetic coupling of reaction and separation process dictated a suitable periodic regeneration method. In this work, the adsorbent was regenerated using inert gas purge stripping method, which proved to be adequate for a reasonably dilute adsorbate concentration throughout the cyclic operation at isothermal and isobaric conditions.

Chapter 8

Conclusions and Recommendations for Future Work

This thesis has explored a novel multifunctional type of reactor model, in which the structural design benefits of the parallel passage, monolith and annular reactors are combined with adsorptive separation. The work is intended as the first study of its kind to identify and thus, to exploit theoretically and experimentally the potential of conducting a periodic adsorptive process in a novel structured packing configuration. The overall aim of the thesis was principally concerned with establishing an experimentally validated theoretical modelling in order that the proposed mathematical model would be viable in providing the framework for future investigations.

In order to achieve the aim, the work in the thesis involved:

- Mathematical modelling of the SAR
- SAR prototype reactor design
- Catalyst and adsorbent characterisations
- Comparison and analysis of the experimental and theoretical SAR studies
- SAR optimisation studies within the selected design parameters

The conclusions of this work, which include the major original contributions followed by the directions for the future work, are now given.

8.1. Conclusions of this work

Studies of a novel annular-type, structured adsorptive reactor, SAR, have been presented. In particular, this work involved theoretical and experimental studies of the catalytic dehydrogenation of isobutane process.

The SAR is a prototype adsorptive reactor containing a structured annular packing arrangement of zeolite KY adsorbent and platinum-alumina catalyst admixture. The design concept could be viewed as a hybrid between monolith-type and parallel-passage type structures, in which it aimed to provide a low-pressure drop alternative to the conventional adsorptive reactor arrangement.

The theoretical background information related the development of the hybrid SAR has been presented in Chapter 2. Reviews on the adsorptive reactor concept as well as structure reactor packing development have been considered. The latter has thus far shown significant improvement in solid handlings, flow distributions and adsorbent utilization management while achieving low pressure drop across the bed. This has led to alternative means of operating the adsorptive reactor by employing a structured packing configuration in the reactor column.

A two-dimensional mathematical model to account for the process and reactor configuration has been developed. This was presented in Chapter 3. The model equations consisted of gas and solid phase component material balances describing the diffusive transport phenomena in the reactor and a velocity profile representing a fully developed laminar flow condition. An LDF equation according to the Glueckauf and Coates (1947) model along with macropore diffusion equation were embedded in the solid phase equation, which were described by the

parallel mechanism of Knudsen and molecular diffusion. Such diffusion mechanisms were determined by Knudsen's diffusion law and Chapman-Enskog kinetic theory. The boundary conditions were imposed such that the model could be simulated in the manner of a single-step process as well as a cyclic steady state. On applying the BFDM numerical method within the gPROMS software simulator, the convergence based on simultaneous discretisation of the spatial domains was achieved.

In order to accomplish the experimental validation of the proposed mathematical model, the SAR prototype design was constructed. It consisted of a sintered wire screen gauze central gas channel of 0.14m length and 0.008m diameter, surrounded by an annulus of admixed catalyst and adsorbent of 0.01m thickness as illustrated in Chapter 4. The reactor was operated with laminar flow in the central gas channel; reactant contact with admixed particles was achieved through diffusive transport in the direction perpendicular to the convective gas flow. A convective oven was used to carry out the experiments under isothermal condition. Fractions of sample products were collected in a Valco multiposition valve at controlled time intervals and analysed using the FID in a Shimadzu 14B GC.

Chapter 5 gave an account of the catalyst and adsorbent characterisations prior to conducting the sorption-enhance dehydrogenation of isobutane over an admixture of platinum-alumina catalyst and zeolite-KY adsorbent. Step-by-step procedures were carried out to investigate the key adsorbent parameters for zeolite-KY and reaction rate constant using platinum on an alumina support catalyst over selected temperatures (i.e. 600K, 650K and 700K) under isobaric condition. Similar experiments were also conducted using inert material, in this case, carborundum, to indicate a clean bed. The periodic regeneration of adsorbent involved purging

the reactor with an inert gas, which may also be used to supply the necessary reaction heat to the catalyst and to prevent any moisture build-up.

The comparison of the SAR performance with that of an equivalent packed bed arrangement was aimed at identifying and thus characterising the potentials of the SAR at given operating conditions. The key adsorption parameters were obtained by matching the experimental breakthrough curves with the corresponding theoretical curves. Overall, the transient adsorption and kinetic responses obtained from the experiments were in good agreement with the theoretical results. In catalyst-only experiments, the reaction conversions at each selected temperature were the same for both reactors suggesting that the transient kinetic responses were only thermodynamically limited.

The adsorption breakthrough responses for the SAR, on the other hand, were significantly longer than that of the PFR due to the difference in the amount of adsorbent loading and bed packing arrangements. The higher the amount of adsorbent, the more adsorbate could be retained in the case of the SAR at relatively higher gas-solid contact time. In addition, the flow transport in the SAR was governed by molecular diffusion at the absence of convective transport in the solid zone. Thus, it took a longer time for the adsorbate to break through at low intraparticle diffusional resistance.

In Chapter 6, the potentials of the SAR in improving the catalytic reaction performance were investigated and compared with the equivalent packed bed system. The conversion enhancement effect profiles were plotted to compare the magnitude of enhancement attained during the experiment and each curve was tallied with the theoretical results. It could be deduced that conversion enhancement favoured lower temperature operation and lower feed

flow rate to maximise the adsorption potential by ensuring efficient adsorbent utilisation. The governing molecular diffusive transport in the SAR encouraged significant conversion enhancement effect at negligible axial dispersion and low pressure drop across the bed. The purge stripping method was also considered sufficient to regenerate the adsorbent as the adsorption-enhanced processes were operated within Henry's law region at laminar flow condition.

The potentials of the SAR were further investigated theoretically in Chapter 7. For the computational validation purpose, design parameters were appropriately selected, which intrinsically affected the performance of the reaction-separation process. Such key parameters were obtained from the experimental findings as mentioned above. The theoretical results, which were illustrated in transient response breakthrough curves as well as conversion-enhancement effect plots, provided the comparison studies of the effect of the parameters on the reactor configuration. Equivalent conventional packed-bed reactor arrangements were also compared for further validations. Optimisation studies were also demonstrated within the selected design parameters, which were the temperature, gas velocity and geometrical sizes, to further justify such a novel type system.

The SAR theoretical studies showed promising results in achieving a significant conversion enhancement effect at low energy requirement and low pressure drop across the unit operation. This was attributed to the molecular diffusive transport phenomena, which arose from the structured packing arrangement. An optimal reactor length and annular thickness existed which also prompted the enhancement effect.

The SAR performances

Advantages	Disadvantages
Good solid handlings	Only efficient at low gas velocities
Low pressure drop even at high velocity	Relatively longer cyclic steady state operations for adsorption-only and combined in situ reaction-separation processes
High thermal stress for the sintered core gas channel	Highly dependent on axial and radial mixing throughout the core gas channel as well as in the annular packing region
Enables the packing of admixed small particle sizes thus, a flexible reactor	The adsorption performance decreases at relatively higher gas velocities due to the increase in the feed gas bypass which leads to reduced reactor residence time
Low mass transfer resistance across the annular packing region	
Can be utilised for catalyst-only, adsorption-only as well as combined in situ reaction-separation processes	
Isothermal condition could be approached	
Inert purge gas stripping method is possible for complete adsorbate removal when operated within Henry's law region	
Low energy input requirement hence, an economical operation	

Table 8.1 Summary of the SAR performances

The SAR versus the PFR performances

SAR	PFR
Capable of achieving low pressure drop thus minimising any adverse effect due to high pressure drop	More inclined towards high pressure drop operation
Absence of convective transport; the mass transfer mechanism in the annular packing is therefore governed by molecular diffusion	Convective transport exists
Negligible axial dispersion effect hence, improved adsorption separation	Axial dispersion effect must be taken into consideration
Analogous parallel passage-type structure configuration; the solids are not in direct contact with the gas flow	Solids are in direct contact with the gas flow, creating bed interstices which lead to somewhat tortuous flow
Molecular diffusion predominates the reactant gas mass transfer	Intraparticle as well as extraparticle diffusion govern the mass transfer
Longer adsorption-desorption cycle	Relatively shorter adsorption-desorption cycle
Capable of producing higher conversion enhancement effect	Lower conversion enhancement effect depicted by faster adsorbent equilibration time due to axial dispersion effect
The annular section offers larger cross-sectional area, which allows reduced distance of travel for gas flow hence, low mass transfer resistance	Longer diffusional path leads to reduced concentration gradient in the direction of flow hence, relatively higher mass transfer resistance
Relatively higher space time and therefore, higher gas-solid contact time	Relatively lower space time leads to reduced gas-solid contact time
Ability to achieve considerable conversion enhancement effect at relatively higher temperature	The axial dispersion effect, coupled with the lower residence time further reducing the enhancement effect at higher temperature

Table 8.2 Major original contributions for this work

8.2 Directions for future work

In this system, the experimental works have so far considered forward-flow desorption at identical flow rates, one mean particle size, one type of adsorbent and low flow rates, all of which have contributed to the viability of such a reactor model. The future work should then be focused on comparing the performance of the SAR through certain modifications without attempting to modify the reactor design. Therefore, further experimental works recommended to investigate the conversion enhancement effect potential of the SAR are:

- The effect of varying zeolite KY mean particle sizes:
  - The performance of the reactor will be macropore diffusion limited and this will influence the uptake curve shape. Previous works regarding adsorbent particle size effect have been conducted in RPSA and radial flow-RPSA processes (see for example, Alpay *et al.*, 1994, Huang and Chou, 2003). Particle size will influence the gas flow dynamics and mass transfer limitation and hence, the existence of optimum particle size in order to improve the SAR performance. Various particle size ranges could be securely packed in the annulus section since the sintered tube aperture is 1.0 μm in size.
- The effect of using other type of thermally stable zeolites:
  - Alpay *et al.* (1996) have conducted adsorbent characterisation studies at high adsorption temperature to examine the adsorption equilibria properties of commercially available zeolite adsorbents that could be incorporated in the hydrocarbon dehydrogenation reaction. Adsorbents like zeolite NaY, 13X and 10X could be potentially exploited in order to draw comparisons in terms of conversion enhancement effect in the SAR at given operating conditions.

- Forward-flow and reverse-flow purge stripping regeneration:
    - At high adsorption temperatures, TSA may not be feasible. Therefore, the adsorbent regeneration could be improved by purging the bed in the direction of forward-flow (cocurrent) or reverse-flow (countercurrent) at the same feed flow rate or by varying purge gas flow rates. Gelbin *et al.* (1983) advocated that reverse-flow desorption would be a better choice as high separation efficiency could be achieved at shorter cycle time.

Computational validations for the above suggested works should be accompanied as well. The combination for any particular system is also possible in order to optimise the reactor performance.

Using different types of software such as the CFD codes may also provide further scope for fluid dynamic study in terms of varying geometrical sizes effect as well as temperature distribution of such reactor configuration where experimental validations could be challenging. Previously, two proprietary CFD codes have been applied in the application of an annular adsorber based on a 2-D axisymmetric system in order to predict the pressure patterns across the bed (see Tierney *et al.*, 1998). Thus, any improvements in this area could well be achieved without the recourse of experimental works.

References

Agar, D. W. (1999). Multifunctional reactors: old preconceptions and new dimensions. Chemical Engineering Science **54**: 1299-1305.

Alpay, E. (1992). Rapid pressure swing adsorption processes. Cambridge, UK, University of Cambridge.

Alpay, E., Chatsiriwech, D., Kershenbaum, L.S., (1994). Combined reaction and separation in pressure swing processes. Chemical Engineering Science **49**(24B): 5845-5864.

Alpay, E., Haq, N., Kershenbaum, L.S., Kirkby, N.F (1996). Adsorption parameters for strongly adsorbed hydrocarbon vapours on some commercial adsorbents. Gas Separations and Purifications **10,**(1): 25-33.

Alpay, E., Kenney, C.N., Scott,D.M. (1993). Simulation of rapid pressure swing adsorption and reaction processes. Chemical Engineering Science **48**(18): 3173-3186.

Alpay, E., Kershenbaum, L.S. (1995). Pressure correction in the intrepretation of microreactor data. Chemical Engineering Science **50**(6): 1063-1067.

Alpay, E., Scott, D.M. (1992). The linear driving force model for fast-cycle adsorption and desorption in a spherical particle. Chemical Engineering Science **47**(2): 499-502.

Atkins, P., de Paula, J. (2002). Atkins' Physical Chemistry, Oxford University Press.

Beretta, A. (1998). A novel structured catalytic reactor for high space velocity. Chemical Engineering Communications **170**: 39-49.

Beretta, A., Baiardi, P., Prina, D., Forzatti, P. (1998). Development of a catalytic reactor with annular configuration. Preparation of Catalysis VII. B. Delmon, Elsevier Science B.V.

Bhasin, M. M., McCain, J.H., Vora, B.V., Imai, T., Pujado, P.R. (2001). Dehydrogenation and oxydehydrogenation of paraffins to olefins. Applied Catalysis A: General **221**: 397-419.

Bird, R. B., Stewart, W.E., Lightfoot, E.N. (1960). Transport Phenomena. New York, John Wiley and Sons, Inc.

Bjorklund, M. C., Carr, R.W. (1995). The simulated countercurrent moving bed chromatographic reactor: a catalytic and separative reactor. Catalysis Today **25**: 159-168.

Breck, D. W. (1974). Zeolite Molecular Sieves, Wiley.

Bunke, G., Gelbin, D. (1978). Breakthrough curves in the cyclic steady state for adsorption systems with concave isotherms. Chemical Engineering Science **33**: 101-108.

Calis, H. P., Everwijn, T.S., Gerritsen, A.W., Van den Bleek, C.M., Goudriaan, F., Van Dongen, F.G (1994). Mass transfer characteristics of parallel passage reactors. Chemical Engineering Science **49**: 4289-4297.

Caputo, D., Eic, M., Colella, C. (2002). Diffusion and adsorption of hydrocarbons from automotive engine exhaust in zeolitic adsorbents. Studies in Surface Science and Catalysis **142**: 1611-1618.

Carleton, F. B., Kershenbaum, L.S., Wakeham, W.A. (1978). Adsorption in non-isobaric fixed beds. Chemical Engineering Science **33**(9): 1239-1246.

Carta.G. (1993). The linear driving force approximation for cyclic mass transfer in spherical particles. Chemical Engineering Science **48**(3): 622-625.

Carvill, B. T., Hufton, J.R., Anand, M., Sircar, S (1996). Sorption-enhanced reaction process. AIChE Journal **42**(10): 2765-2772.

Casanave, D., Fiaty, K., Dalmon, J.A., Forissier, M. (1999). Kinetics and mechanism studies of the catalytic dehydrogenation of isobutane on platinum-indium catalyst. Reaction Kinetics and The Development of Catalytic Processes Studies in Surface Science and Catalysis **122**: 367-374.

Chahbani, M. H., Tondeur, D. (2000). Mass transfer kinetics in pressure swing adsorption. Separation and Purification Technology **20**: 185-196.

Champagnie, A. M., Tsotsis, T.T., Minet, R.G., Webster, I.A. (1990). A high temperature catalytic membrane reactor for ethane dehydrogenation. Chemical Engineering Science **36**: 2423-2429.

Chatsiriwech, D., Alpay, E., Kershenbaum, L.S.,Hull, C.P. (1994). Enhancement of catalytic reaction by pressure swing adsorption. Catalysis Today **20**: 351-366.

Cheng, Y. S., Alpay, E., Kershenbaum, L.S. (1998). Simulation and optimisation of a rapid pressure swing reactor." Computers and Chemical Engineering **22**: S45-S52.

Chiang, A. S. T., Hong, M.C. (1995). "Radial flow rapid pressure swing adsorption." Adsorption **1**: 153-164.

Choong, T. S. Y., Scott, D.M. (1998). The linear driving force model for cyclic adsorption and desorption: the effect of external fluid-film mass transfer. Chemical Engineering Science **53**(4): 847-851.

Chu, C., Tsang, L.C. (1971). Behavior of a chromatographic reactor. Ind. Eng. Chem. Process Des. Develop **10**(1): 47-53.

Cortright, R. D., Bergene,E., Levin,P., Natal-Santiago,M., Dumesic, J.A (1996). Reactions of isobutane and isobutylene over silica- and L-zeolite-supported Pt/Sn and Pt/Sn/K catalysts. 11th International Congress on Catalysis - 40th anniversary, Elsevier Science.

Cortright, R. D., Dumesic, J.A (1998). Catalyst to dehydrogenate paraffin hydrocarbons. US 5,736,478, USA, Wisconsin Alumni Research Foundation.

Cortright, R. D., Hill ,J.M., Dumesic, J.A. (2000). Selective dehydrogenation of isobutane over supported Pt/Sn catalysts. Catalyst Today **55**: 213-223.

Cortright, R. D., Levin, P.E., Dumesic, J.A. (1998). Kinetic studies of isobutane dehydrogenation and isobutene hydrogenation over Pt/Sn-based catalysts. Industrial & Engineering Chemistry Research **37**: 1717-1723.

Coulson, J. M., Richardson, J.F., Backhurst, J.R., Harker,J.H. (1990). Chemical Engineering Vol 1 Fluid, Heat Transfer and Mass Transfer, Pergamon Press.

Cybulski, A., Moulijn, J.A. (1998). The present and future of structured catalysts- an overview. Structured Catalysts and Reactors. A. Cybulski, Moulijn, J.A., Marcel Dekker, Inc.**:** 1-14.

Dabrowski, A**.** (2001). Adsorption- from theory to practice. Advances in colloid and interface science **93**: 135-224.

Dautzenberg, F. M., Mukherjee, M. (2001). Process intensification using multifunctional reactors. Chemical Engineering Science **56**: 251-267.

Dietrich, W., Lawrence, P.S., Grunewald,M., Agar, D.W. (2005). Theoretical studies on multifunctional catalysts with integrated adsorption sites. Chemical Engineering Journal **107**: 103-111

Ding, Y., Alpay, E. (2000). Adsorption-enhanced steam-methane reforming. Chemical Engineering Science **55**: 3929-3940.

Doong, S. J., Yang, R.T. (1988). The role of pressure drop in pressure swing adsorption. AIChE Symposium Series **84**(264): 145-154.

Dyroff, D. R. (2002). Advances in dehydrogenation catalysis, US 6,417,135, Hunstman petrochemical corporation (Austin,TX)**:** 1-33.

Edwards, M. F., Richardson, J.F. (1968). Gas dispersion in packed beds. Chemical Engineering Science **23**: 109-123.

Elsner, M. P., Dittrich, C., Agar, D.W. (2002). Adsorptive reactors for enhancing equilibrium gas-phase reactions - two case studies. Chemical Engineering Science **57**: 1607-1619.

Eriksson, R. (1979). Fractionating apparatus, US 4,169,715, AGA Aktiebolag**:** 1-5.

Fish, B., Carr, R.W., Aris, R. (1986). The continuous countercurrent moving bed chromatographic reactor. Chemical Engineering Science **41**(4): 661-668.

Fogler, H. S. (1992). Elements of Chemical Reaction Engineering, Prentice Hall.

Gadkaree, K. P. (1998). Carbon honeycomb structures for adsorption applications. Carbon **36**(7): 981-989.

Gelbin, D., Bunke, G., Wolff, H.J., Neinass, J. (1983). Adsorption separation efficiency in the cyclic steady state: A continuous countercurrent analogy and an experimental investigation. Chemical Engineering Science **38**(12): 1993-2001.

Glueckauf, E., Coates, J.I. (1947). Theory of chromatography. part IV. the influence of incomplete equilibrium on the front boundary of chromatograms and on the effectiveness of separation. Journal of Chemical Society **Part 2**: 1315-1321.

Gobina, E., Hou, K., Hughes, R. (1997). A reactor-separator incorporating porous and dense membrane systems. Journal of Chemical Technology & Biotechnology **70**: 74-82.

gPROMS Introductory User's Guide, (1998), Process Systems Enterprise Ltd.

Groppi, G., Ibashi, W., Tronconi, E., Forzatti, P. (2001). Structured reactors for kinetic measurements in catalytic combustion. Chemical Engineering Journal **82**: 57-71.

Gunn, D. J., Thomas, W.J. (1965). Mass transport and chemical reaction in multifunctional catalyst systems. Chemical Engineering Science **20**: 89-100.

Gunn, D. J., England, R. (1971). Dispersion and diffusion in beds of porous particles. Chemical Engineering Science **26**: 1413-1423.

Han, C., Harrison, D.P. (1994). Simultaneous shift reaction and carbon dioxide separation for the direct production of hydrogen. Chemical Engineering Science **49**(24B): 5875-5883.

Handbook of Compressed Gases, (1990), New York, Compressed Gas Association, Inc.,Van Nostrand Reinhold.

Hart, J., Thomas, W.J. (1991). Gas separation by pulsed pressure swing adsorption. Gas Separations and Purifications **5**: 125-133.

Hartley, F. R. (1991). Chemistry of the Platinum group metals, Elsevier Science.

Heggs, P. J., Ellis, D.I., Ismail, M.S. (1994). The modelling of fluid-flow distributions in annular packed beds. Gas Separations and Purifications **8**(4): 257-264.

Heggs, P. J., Ellis, D.I., Ismail, M.S. (1995). "Evaluation of pressure profiles and overall pressure drop for flow through annular packed bed configurations." Gas Separations and Purifications **9**(3): 171-180.

Hill, J. M., Cortright, R.D., Dumesic,J.A. (1998). Silica- and L-zeolite-supported Pt, Pt/Sn and Pt/Sn/K catalysts for isobutane dehydrogenation. Applied Catalysis A: General **168**: 9-21.

Hoebink, J. H. B. J., Marin, G.B. (1998). Modelling of monolithic reactors for automotive exhaust gas treatment, Structured Catalysts and Reactors. Structured Catalysts and Reactors. A. Cybulski, Moulijn, J.A., Marcel Dekker, Inc.: 209-237.

Huang, W. C., Chou, C.T. (2003). "Comparison of radial flow and axial flow rapid pressure swing adsorption processes." Industrial & Engineering Chemistry Research **42**: 1998-2006.

Hufton, J. R., Mayorga,S., Sircar, S. (1999). Sorption-enhanced reaction process for hydrogen production. AIChE Journal **45**(2): 248-256.

Hufton, J. R., Ruthven, D.M., Danner, R.P. (1995). Adsorption and diffusion of hydrocarbons in silicalite at very low concentration: effect of defect sites. Microporous Materials **5**(1995): 39-52.

Imai, T. (1988). Dehydrogenation catalyst composition and paraffin dehydrogenation. US 4,762,960, USA, UOP Inc.

Imai, T., Abrevaya, H. (1989). Dehydrogenation catalyst and process, US 4,880,764, UOP: 1-17.

Ioannides, T., Gavalas, G.R. (1993). Catalytic isobutane dehydrogenation in a dense silica membrane reactor. Journal of Membrane Science **77**: 207-220.

Itoh, N. (1987). A membrane reactor using palladium. AIChE Journal **33**: 1576-1578.

Jones, R. L., Keller, G.E. (1981). Pressure-swing parametric pumping - a new adsorption process. Journal of Separation and Process Technology **2**(3): 17-23.

Karger, J., Ruthven, D.M. (1992). Diffusion in zeolites and other microporous solids, John Wiley & Sons Inc.

Kehat, E., Berkovici, J., Orell, A. (1988). Dynamic Adsorption of SO_2 on an annular bed of molecular sieve 5A. American Chemical Society.

Keller, G. E., Kuo, Chia-Huei.A. (1982). Enhanced gas separation by selective adsorption, US 4,354,859, Union Carbide Corporation: 1-12.

Kershenbaum, L. S., Kohler, M.A. (1984). Adsorption in non-isobaric fixed beds - II. Measurements of rates of adsorption. Chemical Engineering Science **39**(9): 1423-1426.

Kodde, A. J. (2001). Operation of irreversible series reactions in pressure swing reactors, University of Amsterdam.

Langer, G., Roethe,A.,Roethe, K.P., Gelbin,D. (1978). Heat and mass transfer in packed beds -III: axial mass dispersion. International Journal of Heat and Mass Transfer **21**(751-759).

Lee, I. D., Kadlec, R.H. (1989). Effects of adsorbent and catalyst distributions in pressure swing reactors. AIChE Symposium Series **84**: 167-172.

Li, Y. Y., Perera, P., Crittenden, B.D. (1998). Zeolite monoliths for air separation Part 1: Manufacture and Characterization. Trans IChemE **76**(Part A): 921-930.

Li, Y. Y., Perera, P., Crittenden, B.D. (1998). Zeolite Monoliths for air separation Part 2: Oxygen enrichment, pressure drop and pressurization. Trans IChemE **76**(Part A): 931-941.

Li, Y. Y., Perera, P., Crittenden, B.D., Bridgwater, J. (2001). The effect of the binder on the manufacture of a 5A zeolite monolith. Powder Technology **116**: 85-96.

Loc, K. C., Gaidai, N.A., Gudkov, B.S., Kiperman, S.L., Kogan, S.B. (1987). Investigation of the kinetics and mechanism of the dehydrogenation of isobutane on platinum-tin catalysts. Translated from Kinetica i Kataliz **27**(6): 1184-1189.

Loc, K. C., Gaidai, N.A., Gudkov, B.S., Kostyukovskiss, M.M., Kiperman, S.L., Podkletnova, N.M., Kogan, S.B., Bursian, N.R. (1987). Investigations of the kinetics and mechanism of the dehydrogenation of isobutane on platinum and platinum-indium catalysts. Kinetika I Kataliz (translated) **27**(6): 1371-1377.

Magee, E. M. (1963). The course of a reaction in a chromatographic column. Industrial & Engineering Chemistry Fundamentals **2**(1): 32-36.

Matsuda, T., Koike, I., Kubo,N., Kikuchi,E. (1993). Dehydrogenation of isobutane to isobutene in a palladium membrane reactor. Applied Catalysis A: General **96**: 3-13.

Nakao, S., Suzuki, M. (1983). Mass transfer coefficient in cyclic adsorption and desorption. Journal of Chemical Engineering of Japan **16**(2): 114-119.

Nauman, E. B., Kothari, D., Nigam, K.D.P. (2002). Static mixers to promote axial mixing. Trans IChemE **80**(A): 681-685.

Oh, M. (1995). Modelling and simulation of combined lumped and distributed process. Department of Chemical Engineering and Chemical Technology. London, Imperial College London.

Ortiz, A. L., Harrison, D.P. (2001). Hydrogen production using sorption-enhanced reaction. Industrial & Engineering Chemistry Research **40**: 5102-5109.

Papadias, D., Edsberg, L., Bjornbom, P. (2001). Effect of eccentricity and interaction between kinetics and mass transfer on thebehaviour of catalytic annular reactors: a comparison between lumped and distributed models. Chemical Engineering Science **56**: 4863-4878.

Perry, R. H. (1997). Perry's chemical engineer's handbook. New York, McGraw-Hill.

Petroulas, T., Aris, R., Carr, R.W. (1985). Analysis and performance of a countercurrent moving-bed chromatographic reactor. Chemical Engineering Science **40**(12): 2233-2240.
Pritchard, C. L., Simpson, G.K. (1986). Design of an oxygen concentrator using the rapid pressure-swing adsorption principle. Chem. Eng. Res. Des **64**: 467-472.

Pujado, P. R., Vora,B.V. (1984). Production of LPG Olefins by catalytic dehydrogenation. Energy Process **4**(3): 186-191.

Resasco, D. E., Haller, G.L. (1994). Catalytic dehydrogenation of lower alkanes. Catalysis: A Specialist Periodical Report, The Royal Society of Chemistry. **11:** 379-411.

Rodrigues, A. E., Zuping, L., Loureiro,J.M. (1991). Residence time distribution of inert and linearly adsorbed species in a fixed bed containing "large-pore" supports: applications in separation engineering. Chemical Engineering Science **46**(11): 2765-2773.

Roginskii, S. Z., Yanovskii, M.I., Gaziev, G.A. (1961). Intensification of pressure swing adsorption processes. Kinetika i kataliz c/c Kinetics & Catalysis **140**: 771-785.

Rota, R., Wankat, P.C. (1990). Intensification of pressure swing adsorption processes. AIChE Journal **36**(9): 1299-1312.

Rouse, A. J. (2004). Fast cycle low pressure drop systems for the separation of CO_2. Department of Chemical Engineering. London, University College London.

Ruthven, D. M. (1984). Principles of adsorption and adsorption processes, John Wiley & sons Inc.

Ruthven, D. M., Farooq, S., Knaebel, K.S. (1994). Pressure swing adsorption, VCH Publishers

Ruthven, D. M., Thaeron, C. (1997). Performance of a parallel passage adsorbent contactor. Separation and Purification Technology **12**: 43-60.

Seijger, G. B. F., Oudshoorn,O.L., Boeckhorst, A., Van Bekkum,H., Van den Bleek, C.M., Calis, H.P.A. (2001). Selective catalytic reduction of NOx over zeolite-coated structured catalyst packings. Chemical Engineering Science **56**: 849-857.

Sheikh, J. (1999). Rapid Pressure Swing Reaction Processes. Department of Chemical Engineering and Chemical Technology. Imperial College London.

Sheikh, J., Kershenbaum, L.S., Alpay, E. (2001). 1-butene dehydrogenation in rapid pressure swing reaction processes. Chemical Engineering Science **56**(4): 1511-1516.

Shin, H. S., Knaebel, K.S. (1987). Pressure swing adsorption: A theoretical study of diffusion-induced separations. AIChE Journal **33**(4): 654-662.

Shinji, O., Misono, M., Yoneda, Y. (1982). The dehydrogenation of cyclohexane by the use of a porous glass reactor. Bull. Chem. Soc. Japan **55**: 2760-2764.

Sie, S. T., Calis, H.P. (1998). Parallel-passage and Lateral-flow reactors. Structured and Catalyst Reactors. A. Cybulski, Moulijn, J.A., Marcel Dekker, Inc.: 323-354.

Sinnot, R. K. (1993). Chemical Engineering Design. Oxford, Pergamon Press.

Sircar, S. (1994). Adsorption technology: a versatile separation tool. Separation Technology: The Next Ten Years. J. Garside, IChemE UK: 47-72.

Skarstrom, C. W. (1960). Method and apparatus for fractionating gaseous mixtures by adsorption, US 02944627

Sun, Y. M., Khang, S.J. (1988). Catalytic membrane for simultaneous chemical reaction and separation applied to a dehydrogenation reaction. Industrial & Engineering Chemistry Research **27**: 1136-1142.

Suzuki, M. (1990). Adsorption engineering. Tokyo, Elsevier.

Suzuki, T., Sakoda, A., Suzuki, M. (1997). Recovery of carbon dioxide from stack gas by piston-driven ultra-rapid PSA. Journal of Chemical Engineering of Japan **30**(6): 1026-1033.

Thakur, R. K., Vial, Ch., Nigam, K.D.P., Nauman, E.B., Djelveh, G. (2003). Static mixers in the process industries - a review. Trans IChemE **81**(A): 787-826.

Tierney, M., Nasr, A., Quarini, G. (1998). The use of proprietary computational fluid dynamics codes for flows in annular packed beds. Separation and Purification Technology **13**: 97-107.

Tierney, M. J., Saidani Scott, H., Erb, T., Prasertmanukitch, S. (1999). The purification of dilute CO_2/air solutions with an annular bed adsorber: numerical and experimental investigations. Separation and Purification Technology **17**: 159-171.

Treybal, R. E. (1980). Mass transfer operations. New York, McGraw-Hill.

Turnock, P. H., Kadlec, R.H. (1971). Separation of nitrogen and methane via periodic adsorption. AIChE Journal **17**(2): 335-342.

Valdes-Solis, T., Marban, G., Fuertes, A.B. (2001). Preparation of microporous carbon-ceramic cellular monoliths. Microporous and Mesoporous Materials **43**: 113-126.

Van den Bleek, C. M., Calis, H.P.A., Gerritsen, A.W. (1996). Structured reactor packing & method of the manufacturing same. Patent PCT/NL96/00168, WO 96/33017, Delft University of Technology. Netherlands.

Vaporciyan, G. G., Kadlec, R.H. (1987). Equilibrium-limited periodic separating reactors. AIChE Journal **33**(8): 1334-1343.

Vaporciyan, G. G., Kadlec, R.H. (1989). Periodic separating reactors: Experiments and theory. AIChE Journal **35**(5): 831-844.

Wakao, N., Smith, J.M. (1962). Diffusion in catalyst pellets. Chemical Engineering Science **17**: 825-834.

Watson, J. T. R. (1972). Viscosity of gases in metric units ; air, argon, carbon dioxide, helium, hydrogen, krypton, methane, neon, nitrogen, oxygen and xenon at atmospheric pressure in the temperature range 270-2200k.

Westerterp, K. R. (1992). Multifunctional reactors. Chemical Engineering Science **47**(9-11): 2195-2206.

Xiu, G. H., Li,P., Rodrigues, A.E. (2002). Sorption-enhanced reaction process with reactive regeneration. Chemical Engineering Science **57**: 3893-3908.

Yang, R. T. (1987). Gas separation by adsorption processes, Butterworth Publishers.

Yates, M., Blanco, J., Avila, P., Martin, M.P. (2000). Honeycomb monoliths of activated carbons for effluent gas purifications. Microporous and Mesoporous Materials **37**: 201-208.

Yongsunthon, I. (1999). Design of periodic adsorptive reactors for optimal integration of reaction, separation and heat-exchanger. Department of Chemical Engineering and Chemical Technology. London, Imperial College London.

Yongsunthon, I., Alpay, E. (1998). Conversion-temperature trajectories for well-mixed adsorptive reactors. Chemical Engineering Science **53**(4): 691-696.

Yongsunthon, I., Alpay, E. (1999). Design of periodic adsorptive reactors for the optimal integration of reaction, separation and heat exchange. Chemical Engineering Science **54**: 2647-2657.

Yoshida, M., Takeda, T., Maruko, M., Matsumoto, S. (2003). Control of the temperature distribution in two dimensional space of an annular type non-isothermal adsorber. Journal of Process Control **13**.

Ziaka, Z. D., Minet, R.G., Tsotsis, T.T. (1993). Propane dehydrogenation in a packed bed membrane reactor. AIChE Journal **39**: 526-529.

Appendix A

Governing Diffusion Coefficients

A.1 Molecular Diffusion Coefficient

At low Reynolds number, the molecular diffusional transport mechanism predominates in both gas and solid phase across the SAR column. As mentioned previously, there is an absence in convective transport in the annular packing region and the solid materials are essentially surrounded by stagnant gas. At low feed flow rate, the parallel passage analogous structured packing configuration is not in direct contact with the gas stream. The catalytic reaction and adsorption process across the bed packing are thus dependent upon molecular diffusion and subsequently the reaction products diffuse towards the central gas channel through the fine sintered tube wall.

Based on the Chapman-Enskog kinetic theory, at ideal gas law condition, the molecular diffusion, D_m ($m^2\ s^{-1}$) for binary gas mixture, (M_A and M_B) as previously given in section 3.3.2, Chapter 3 is:

$$D_{AB} = 1.8583 \times 10^{-7} \frac{\sqrt{T^3\left(\frac{1}{M_A}+\frac{1}{M_B}\right)}}{P\,\sigma_{AB}^2\,\Omega_{AB}} \qquad (A.1)$$

where T is the reactor temperature (K), M_A , M_B are the molecular weight of species A and B, which in this work represents isobutane (58.124 g mol^{-1}) and nitrogen (28.00 g mol^{-1}), P is the total pressure (atm), σ^2_{AB} is Lennard-Jones collision diameter for A and B (m) and Ω_{AB} is the corresponding dimensionless collision integral. As the process is operated at isobaric condition, D_m is only dependent on temperature change in this work. Methods for evaluating σ^2_{AB} and Ω_{AB} can be found in Bird *et al.* (1960). Table A.1 presents the summary of values of each of the parameters used to calculate D_m.

Parameters	**Values**			**Unit**
Isobutane, M_A	**58.124**			**g mol^{-1}**
Nitrogen, M_B	**28.00**			**g mol^{-1}**
σ_{AB}	**4.53 Å**			**m**
T	**600**	**650**	**700**	**K**
Ω_{AB}	**0.9131**	**0.8952**	**0.8796**	**-**
P	**1.0**			**atm**

Table A.1 Summary of parameters used to calculate D_m

A.2 Axial dispersion coefficient

Axial dispersion coefficient, D_x ($m^2\ s^{-1}$) is only used for PFR system assessment in this work. For a randomly packed bed of porous particles and at low Reynolds number, the axial dispersion arises due to somewhat tortuous fluid-particle transfer process and is principally affected by molecular diffusion, D_m ($m^2\ s^{-1}$) and the distribution of interstitial bed velocity, v ($m\ s^{-1}$) (see Edwards and Richardson, 1968, Gunn and England, 1971).

The axial dispersion coefficient, D_x considered in this work is a simplified form of the Langer *et al.* (1978) correlation (see section 3.4, Chapter 3):

$$D_x = \frac{\varepsilon_b D_m}{\tau_x} + \frac{(v\, d_p)^2}{Pe_\infty \left(v\, d_p + \beta_r \varepsilon_b \frac{D_m}{\tau_x} \right)} \qquad (A.2)$$

where ε_b is the bed particle voidage, τ_x the axial bed tortuosity factor, v the interstitial inert gas velocity ($m\ s^{-1}$), d_p the mean particle pore diameter (m), D_m the molecular diffusion for binary system derived from Chapman-Enskog kinetic theory ($m^2\ s^{-1}$), Pe_∞ is the limiting value of the dimensionless Peclet number and β_r is the radial dispersion factor.

Wicke correlation for axial bed tortuosity factor, τ_x is used as proposed by Langer *et al.* (1978) to account for the effect of radial dispersion in the intermediate region where the effect of D_m and D_x are of importance. The correlation is thus given as:

$$\tau_x = 0.45 + 0.55\ \varepsilon_b \qquad (A.3)$$

For $d_p < 0.0025$ m, the limiting value of Pe_∞ could be assumed as:

$$Pe_\infty = 670\ d_p \qquad (A.4)$$

Typical value of β_r could be taken as ≈ 0.5

Summary of parameters used to determine D_x at any v are summarised below.

Parameters	**Values**	**Unit**
ε_b	**0.35**	**-**
τ_x	**0.64**	**-**
d_p	**1.78×10^{-4}**	**m**
Pe_∞	**0.12**	**-**
β_r	**0.5**	**-**

Table A.2 Summary of parameters for D_x calculation

Appendix B

Mass Transfer Coefficient from LDF Approximation

B.1 Effective intraparticle diffusion coefficient

The adsorption mass transfer coefficient, k_{mass} (s^{-1}) is evaluated from the LDF approximation model of Glueckauf and Coates (1947) based on the simplification of Fick's second law of diffusion (see equation 5.19 and 5.20 of Chapter 5) and assuming linear adsorption isotherm (see equation 3.16). For spherical particles,

$$k_{mass,i} = \frac{15\,D_{e,i}}{r_p^2} \tag{B.1}$$

where r_p is mean particle radius (m) and $\bar{D}_{e,i}$ the modified effective intraparticle diffusion coefficient ($m^2\ s^{-1}$), and is derived from the diffusion equation within adsorbent particle, i.e.

$$\frac{\partial q}{\partial t} = \frac{\bar{D}_{e,i}}{r^2}\frac{\partial}{\partial r}\left(r^2\frac{\partial q}{\partial r}\right) \tag{B.2}$$

and

$$\bar{D}_{e,i} = \frac{\varepsilon_p(1-\varepsilon_b)D_{e,i}}{\rho_b m_i R_{gas} T} \tag{B.3}$$

where ε_p and ε_b are particle and bed voidages, $D_{e,i}$ is the effective intraparticle diffusion coefficient of component i ($m^2\ s^{-1}$), ρ_b the adsorbent bulk density ($kg\ m^{-3}$), R_{gas} the molar gas constant ($J\ mol^{-1}\ K^{-1}$) and T is the operational temperature (K).

B.2 Macropore diffusion

In this work, macropore diffusion is considered the dominant diffusion mechanism in which the particle size distribution will influence the uptake curve shape and is considered as the rate-limiting step. Micropore diffusion is assumed constant whereby the concentration through the individual microparticle is uniform. The former diffusivity is largely dependent on temperature and is determined by the parallel mechanism of Knudsen and molecular diffusion. For zeolite KY adsorbent pore diameter (i.e. $d_{pore} = 1.2 \times 10^{-7}$ m), the application of two macropore diffusion mechanisms are predetermined by the mean free path of gas molecules, γ (m), i.e.

$$\gamma = \frac{1}{\pi \sigma_A^{\,2} \sqrt{2}} \frac{R_{gas}\, T}{P\, N_{AV}} \qquad \text{(B.4)}$$

where $\sigma_A^{\,2}$ is the Lennard-Jones collision diameter for species A (m), P the total pressure (Pa) and N_{AV} is the Avogadro number (6.02×10^{23} molecules mol^{-1}). Treybal (1980) gave the assumption on the apparent dominance of Knudsen diffusivity, D_k or molecular diffusion, D_m, based on the ratio of d_{pore} to mean free path, γ, i.e.

if $\mathbf{d_{pore}/\gamma > 20}$, D_m is said to dominate;

if $\mathbf{d_{pore}/\gamma < 0.2}$, D_k is said to dominate;

if $\mathbf{0.2 \leq d_{pore}/\gamma \leq 20}$, D_k and D_m are of importance (parallel mechanism).

From the calculation using the values tabulated in Table B.1, $\mathbf{d}_{\mathbf{pore}}/\gamma \approx 1.87$ at T = 600K, and hence the parallel mechanism.

Knudsen's diffusion law is represented as:

$$D_K = 48.5\, d_{pore} \sqrt{\frac{T}{M_A}} \qquad (B.5)$$

and D_m can be referred in section 3.3.2, equation (3.17) and Appendix A (equation (A.1)). For a binary gas in porous solid at constant pressure, the molar flux of species A and B becomes equimolar counter-diffusion (see Yang, 1987), and therefore, D_m and D_k are used to determine pore diffusivity, D_p, i.e.

$$\frac{1}{D_P} = \frac{1}{D_K} + \frac{1}{D_m} \qquad (B.6)$$

To account for the actual path on the pore structure for a single pore, the effective diffusivity is related to D_p and is given by

$$D_{e,i} = \frac{\varepsilon_p D_p}{\tau_p} \qquad (B.7)$$

This equation is applied based on the assumption that the bed porosity, ε_p is constant throughout adsorption and desorption; τ_p the particle tortuosity factor can be approximated based from the literature, i.e. $\tau_p \approx 3$ for cylindrical pores and it is independent of either temperature or the nature of the diffusing species (Ruthven, 1984).

Thus, k_{mass} could be determined and the values for three temperatures are shown in Table 5.10, Chapter 5. Table B.1 summarizes the parameters and corresponding values used to determine

both the modified effective intraparticle diffusivity, $\bar{D}_{e,i}$ and ultimately, k_{mass}. The values of adsorption equilibrium isotherm gradient, m_i are shown in Table 5.6, Chapter 5.

Parameters	values	Unit
σ_A	5.393 Å	m
R_{gas}	8.314	J mol^{-1} K^{-1}
P	1.0×10^5	Pa
N_{AV}	6.02×10^{23}	molecules mol^{-1}
d_{pore}	1.2×10^{-7}	m
r_p	89×10^{-6}	m
ε_p	0.62	-
ε_b	0.35	-
τ_p	3	-
ρ_b	500	kg m^{-3}

Table B.1 Summary of parameters used to determine k_{mass}

Appendix C

Gas Chromatography Calibration

C.1 Gas Chromatography Calibration results

The calibration of the gas chromatography model Shimadzu 14B GC with an FID detector equipped with a Graphpac column and using helium as the carrier gas was performed using methane, isobutane and isobutene as described in Chapter 4 (see section 4.4). The results of the calibrations are presented in Figures C.1 to C.3. Each of the calibration readings was repeated for three times.

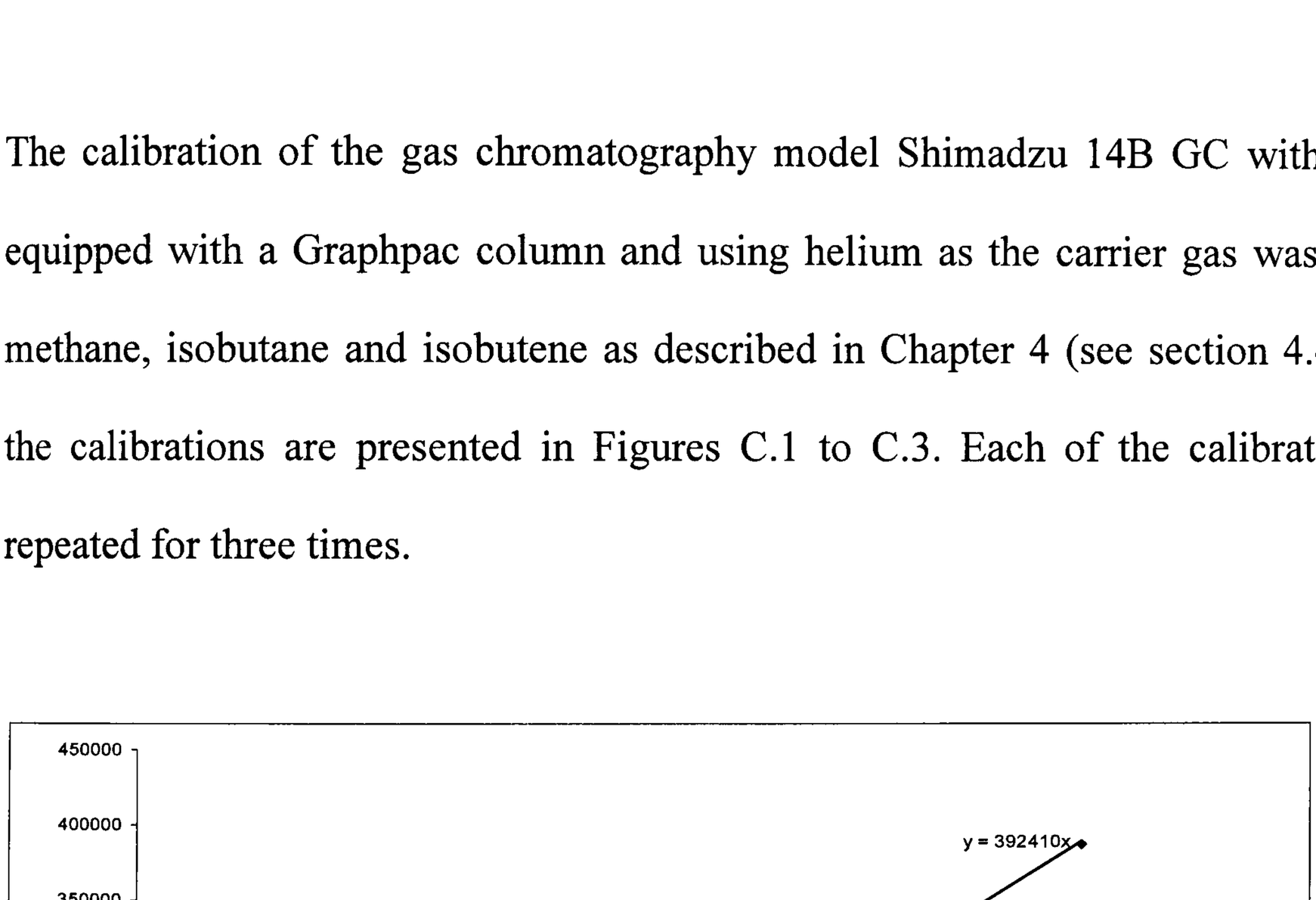


Fig.C.1 Methane calibration

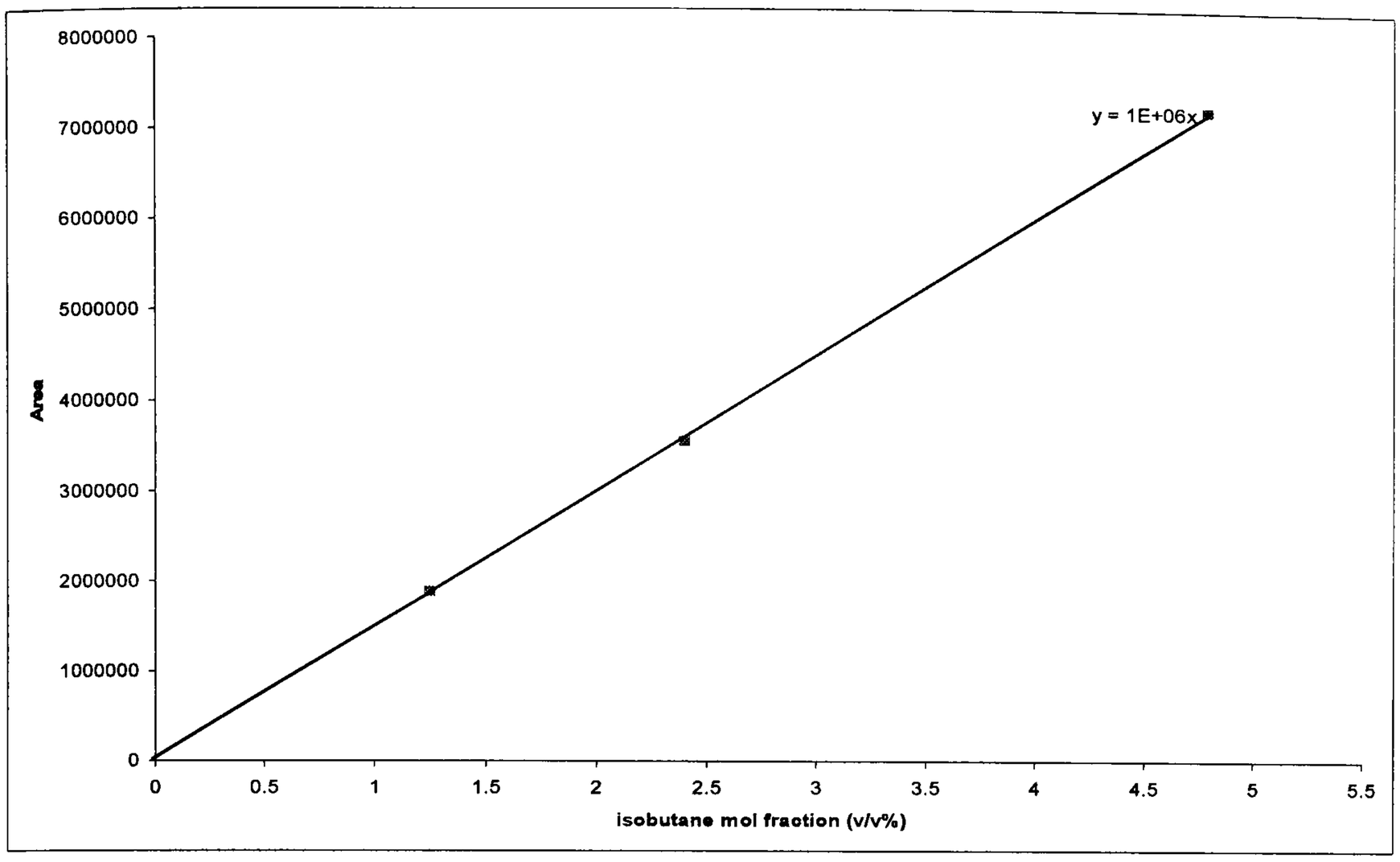


Fig.C.2 Isobutane calibration

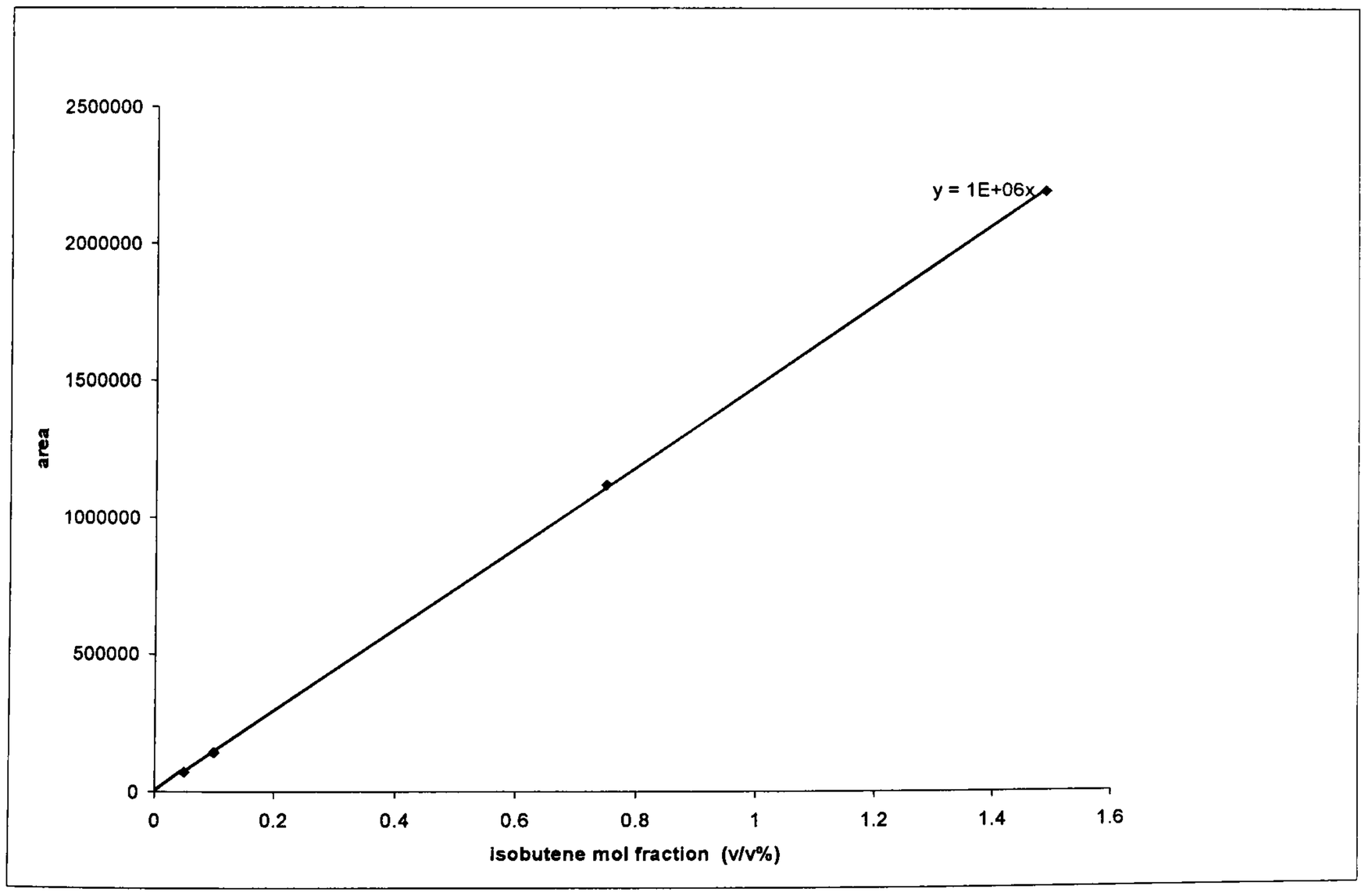


Fig.C.3 Isobutene calibration

Appendix D

Example of Cyclic Steady State SAR Model

```
PARAMETER

  ncomp              AS          INTEGER
  E                  AS          REAL
  Rhobedads          AS          REAL
  rhobedc            AS          REAL
  Rmol               AS          REAL
  nu                 AS          ARRAY(ncomp) OF   INTEGER
  Agas               AS          REAL
  Asolid             AS          REAL
  gasvolf            AS          REAL
  Vsolid             AS          REAL
  yf                 AS          ARRAY(ncomp) of REAL
  Vgas               AS          REAL
  pi                 AS          REAL
  Ptotal             AS          REAL
  cap                AS          REAL
  camb               AS          REAL
  alpha              AS          REAL
  Flow               AS          REAL

DISTRIBUTION_DOMAIN

  axial    AS  (0.0: 1)
  radial   AS  (0.0: 1)


SELECTOR
  cycstep  AS ( feed, desorb)
              DEFAULT feed

VARIABLE
  c          AS    DISTRIBUTION(ncomp,axial,radial) OF  concentration
  v          AS    DISTRIBUTION(radial)  OF velocity
  q          AS    DISTRIBUTION(ncomp, axial,radial) OF  aveadsorb
  qiso       AS    DISTRIBUTION(ncomp, axial,radial) OF equiadsorb
 conv        AS    conversion
  totf1      AS    totalflux
  totf2      AS    totalflux
```

totf3 AS totalflux
yield2 AS notype
yield3 AS notype
prodpure AS notype
regpure AS notype
cycles,totcycles AS notype
nfeed AS DISTRIBUTION(ncomp) OF flow
R1 AS notype
R2 AS notype
L AS length
cin AS notype
creac AS DISTRIBUTION(ncomp) OF notype
Tf AS temperature
D AS DISTRIBUTION(ncomp) OF notype
mgrad AS DISTRIBUTION(ncomp) OF notype
kcon AS rate
Keq AS rate
Kf AS notype
kmass AS DISTRIBUTION(ncomp) OF notype
Energy AS energyinput
totfeed AS notype
tmstep1 AS notype
tmstep2 AS notype
Flowtemp AS velocity
vave AS velocity
miu AS notype
rhogas AS notype

SET

Flow := 1.67e-6;
ncomp := 4;
E := 0.75;
rhobedads := 500;
rhobedc := 1000;
Rmol := 8.314;
Agas := 5.027e-5;
Asolid := 5.65e-4;
gasvolf := 8.546e-7;
Vsolid := 7.9168e-5;
Vgas := 7.0378e-6;
pi := 3.142;
Ptotal := 1.0e5;
cap := 28.442;
ytotal := 1.0;
camb := 40.34;
alpha := 0.50;

```
yf(1)        :=      0.048;
yf(2)        :=      0.001;
yf(3)        :=      0.001;
yf(4)        :=      0.95;


nu(1)        :=      -1;
nu(2)        :=      +1;
nu(3)        :=      +1;
nu(4)        :=      0;


BOUNDARY
 # At axial boundary , where x = 0 and x = L, equation 1

  CASE cycstep OF

   WHEN feed :

   FOR r := 0|+ to alpha| DO

   c(1,0,r) = creac(1);
   c(2,0,r) = creac(2);
   c(3,0,r) = creac(3);
   c(4,0,r) = creac(4);

   END

   FOR i := 1 to ncomp DO

   FOR r := 0|+ to alpha| DO

   partial(c(i,1,r), axial) = 0.0;

 END

 FOR x := 0| to 1| DO

  partial(c(i,x,0), radial) = 0.0 ;

  END

  FOR x := 0|+ to 1|- DO

   partial(c(i,x,1),radial) = 0.0;
```

```
 END
FOR r := alpha|+ to 1| DO

 partial(c(i,0,r),axial) = 0.0;

 partial(c(i,1,r),axial) = 0.0;

 END
 END
WHEN desorb :


 FOR r := 0|+ to alpha| DO

 c(1,0,r) = 0.0;
 c(2,0,r) = 0.0;
 c(3,0,r) = 0.0;
 c(4,0,r) = cin;

 END

 FOR i := 1 to ncomp DO

  FOR r := 0|+ to alpha| DO

  partial(c(i,1,r), axial) = 0.0;

  END

   FOR x := 0| to 1| DO

partial(c(i,x,0), radial) = 0.0 ;

END

FOR x := 0|+ to 1|- DO

 partial(c(i,x,1),radial) = 0.0;

 END

FOR r := alpha|+ to 1| DO

 partial(c(i,0,r),axial) = 0.0;

 partial(c(i,1,r),axial) = 0.0;
```

END

END

END

EQUATION

```
miu =(SQRT(Tf))/(0.57956129 + (2.8474859*(100/Tf)) - (13.23249*((100/Tf)^2)) +
(37.106107*((100/Tf)^3)) - (37.549675*((100/Tf)^4))) * 0.000001;

rhogas = 1.25 *(Tf/273);

Flowtemp = Flow * (Tf/298.15);

 vave = Flowtemp / Agas;

 cin = Ptotal/ (Rmol * Tf);

  creac(1) = yf(1) * cin;
  creac(2) = yf(2) * cin;
  creac(3) = yf(3) * cin;
  creac(4) = yf(4) * cin;


kcon = 0.517 * exp((-34866)/ (Rmol * Tf));

Keq = (1.472e-14) *exp ( ((-13118)*( 1/Tf - 1/298.15)) + (5.39 * log(Tf/298.15)) -
        (0.0057145*(Tf - 298.15))   + (1.327e-6 *( Tf^2 - ((298.15)^2))) - (1.223e-10*( Tf^3
        - ((298.15)^3))));

Kf = Keq * cin ;

mgrad(1) = (7.30e-10) * exp((42570.17)/(Rmol * Tf));

mgrad(2) = (7.1e-10) * exp((46298.17)/(Rmol * Tf));

mgrad(3) = 0.0;

mgrad(4) = 0.0;
```

```
kmass(1) = 1.8937e9 * ((0.403 * (0.183 * (1/ (1/(2.28e-9 * sqrt(Tf^3)) + 1/(7.63e-7 *
sqrt(Tf))))) )/ ( rhobedads * Tf * Rmol * ((7.30e-10) * exp((42570.17)/(Rmol * Tf)))));

kmass(2) = 1.8937e9 * ((0.403 * (0.183 * (1/ (1/(2.28e-9 * sqrt(Tf^3)) + 1/(7.63e-7 *
sqrt(Tf))))) )/ ( rhobedads * Tf * Rmol * ((7.1e-10) * exp((46298.17)/(Rmol * Tf)))));

kmass(3) = 0;#1.8937e9 * DEM(3);

kmass(4) = 0;#1.8937e9 * DEM(4);
```

```
# Equation 1 = Component mass balance in the gas phase


 FOR i := 1 to ncomp DO
 FOR  x := 0|+ to 1|- DO
 FOR  r := 0|+ to alpha| DO


  $c(i,x,r) = -v(r) * partial(c(i,x,r),axial)   + D(i)*partial(c(i,x,r),axial,axial)/L^2
          + (D(i)/(r/R2))  *partial(( (r/R2) * partial(c(i,x,r),radial)),radial)/R2^2 ;


END
```

```
  END

  END


# Equation 2 =  Component mass balance  in the solid phase


  FOR i := 1 to ncomp DO
  FOR x := 0|+ to 1|- DO
  FOR r := alpha|+ to 1|- DO

E * $c(i,x,r) =   D(i) * partial (c(i,x,r),axial,axial) /L^2
              + (D(i)/(r/R2))  * partial (( (r/R2) * partial(c(i,x,r),radial)),radial)/R2^2
                    + rhobedc * nu(i) * kcon * (c(1,x,r) - ((c(2,x,r) * c(3,x,r))/ Kf))
                    - rhobedads * kmass(i) * (qiso(i,x,r) - q(i,x,r)) ;


END
END
```

```
#Rate of Adsorption


FOR x := 0| to 1| DO
FOR r := alpha| to 1| DO

$q(i,x,r) = kmass(i) * (qiso(i,x,r) - q(i,x,r)) ;
  qiso(i,x,r) = mgrad(i) * c(i,x,r) * Rmol * Tf;


END

 FOR r := 0| to alpha|- DO

  $q(i,x,r) = 0.0;
  qiso(i,x,r) = 0.0;


END

END

 END

# velocity profile


 FOR r := 0| to alpha| DO


 v(r) = 8* vave * (alpha^2 - ((r*R2)^2))/ (4 * alpha^2);

 END

FOR r := alpha|+ to 1| DO

 v(r) = 0.0;

 END
```

```
CASE cycstep OF

    WHEN feed:

    $nfeed(1) = creac(1)* sigma(v(0:alpha));
    $nfeed(2) = creac(2) * sigma (v(0:alpha));
    $nfeed(3) = creac(3) *sigma( v(0:alpha)) ;
    $nfeed(4) = creac(4) * sigma(v(0:alpha));
    totfeed = nfeed(1) + nfeed(2) + nfeed(3) + nfeed(4) ;
    prodpure = 0.0;
    regpure  = 0.0;
    $totf1 = sigma(c(1,1,0:alpha) * v(0:alpha)) ;
    nfeed(1) *conv = nfeed(1) - totf1;
    $totf2 = sigma(c(2,1,0:alpha) * v(0:alpha)) ;
    $totf3 = sigma(c(3,1,0:alpha) * v(0:alpha)) ;
    nfeed(1)*  yield2 = totf2;
    nfeed(1)* yield3 = totf3;
    Energy = ((Agas*cap* Ptotal * vave)/(Rmol*Tf))* ( ( Tf- 298.15) );


    WHEN desorb:

    $nfeed(1) = 0.0;
    $nfeed(2) = 0.0;
    $nfeed(3) = 0.0 ;
     $nfeed(4) = cin * sigma(v(0:alpha));
     totfeed = nfeed(1) + nfeed(2) + nfeed(3) + nfeed(4) ;
     prodpure = (totf3)/ ( totf1+ totf2 + totf3 );
     regpure  = (totf2)/ ( totf1 + totf2 + totf3 );
     $totf1 = sigma(c(1,1,0:alpha) * v(0:alpha)); #0.0;
     conv = (nfeed(1) - totf1)/(nfeed(1));
     $totf2 = sigma(c(2,1,0:alpha) * v(0:alpha)) ;
    $totf3 = sigma(c(3,1,0:alpha) * v(0:alpha)) ;
    yield2 = (totf2)/ ( nfeed(1) );
    yield3 = (totf3)/ ( nfeed(1) );
    Energy = ((Agas*cap* Ptotal * vave)/(Rmol*Tf))* ( ( Tf- 298.15) );

END
```

```
#Process

UNIT  cyctemp AS   cyclictemp

SET
 WITHIN cyctemp DO
   axial  :=  [BFDM,1,50];
   radial :=  [BFDM,1,24];


END

ASSIGN
 WITHIN cyctemp DO
  cycles := 1;
  totcycles := 3;
  cyctemp.tmstep1 := 2000;
  cyctemp.tmstep2 := 1500;
  cyctemp.L := 0.14;
  cyctemp.Tf := 600;
  cyctemp.R2 := 0.014;
 cyctemp.R1 := 0.004;


 END

SELECTOR

 WITHIN cyctemp DO

cycstep := feed;

END


INITIAL
 WITHIN  cyctemp DO

      FOR  x := 0|+ to 1|- DO
      FOR  r := 0|+ to alpha|- DO

    c(1,x,r) = 0.0;
    c(2,x,r) = 0.0;
    c(3,x,r) = 0.0;
    c(4,x,r) = camb;
```

```
END
    FOR r := alpha| to 1|- DO

    c(1,x,r) = 0.0;
    c(2,x,r) = 0.0;
    c(3,x,r) = 0.0;
    c(4,x,r) = camb;


    END
    END

    FOR i := 1 to ncomp DO
    FOR  x := 0| to 1| DO
    FOR  r := 0| to alpha|- DO

    q(i,x,r) = 0.0;


    END

    FOR r := alpha| to 1| DO

    q(i,x,r) = 0.0;

        END
        END
        END


    nfeed() = 0.0;
    totf1 = 0.0;
    totf2 = 0.0;
    totf3 = 0.0;

END

SCHEDULE

  WHILE cyctemp.cycles <= cyctemp.totcycles DO

    SEQUENCE

      CONTINUE FOR cyctemp.tmstep1

      SWITCH  cyctemp.cycstep := cyctemp.desorb;
```

```
    END

    CONTINUE FOR cyctemp.tmstep2

    SWITCH cyctemp.cycstep := cyctemp.feed;

    END

  RESET

      cyctemp.cycles := OLD (cyctemp.cycles)+1 ;

      END

REINITIAL

      cyctemp.nfeed(),
      cyctemp.totf1,
      cyctemp.totf2,
      cyctemp.totf3

     WITH

      cyctemp.nfeed() = 0.0;
      cyctemp.totf1 = 0.0;
      cyctemp.totf2 = 0.0;
      cyctemp.totf3 = 0.0;

       END
   END
END
```

Appendix E

Example of a Single Step SAR Model

```
PARAMETER

   vave          AS     REAL
   L             AS     REAL
   R1            AS     REAL
   R2            AS     REAL
   ncomp         AS     INTEGER
   cin           AS     REAL
   E             AS     REAL
   rhogas        AS     REAL
   miu           AS     REAL
   kcon          AS     REAL
   Keq           AS     REAL
   kmass         AS     ARRAY(ncomp) OF  REAL
   rhobedads     AS     REAL
   rhobedc       AS     REAL
   creac         AS     ARRAY(ncomp) OF  REAL
   Rmol          AS     REAL
   T             AS     REAL
   mgrad         AS     ARRAY(ncomp) OF  REAL
   nu            AS     ARRAY(ncomp) OF  INTEGER
   Agas          AS     REAL
   Asolid        AS     REAL
   Vsolid        AS     REAL
   y             AS     ARRAY(ncomp) of REAL
   Vgas          AS     REAL
   pi            AS     REAL

DISTRIBUTION_DOMAIN
   axial         AS     (0.0 : L)
   radial        AS     (0.0 : R2)
```

VARIABLE

c	AS	DISTRIBUTION(ncomp,axial,radial) OF concentration
v	AS	DISTRIBUTION(radial) OF velocity
D	AS	DISTRIBUTION(ncomp) OF notype
q	AS	DISTRIBUTION(ncomp, axial,radial) OF aveadsorb
qiso	AS	DISTRIBUTION(ncomp, axial,radial) OF equiadsorb
conv	AS	conversion
totf1	AS	totalflux
totf2	AS	totalflux
totf3	AS	totalflux
qmin	AS	notype
cgas	AS	notype
csolid	AS	notype
yield2	AS	notype
yield3	AS	notype
nfeed1	AS	notype

SET

vave	:=	0.067;
L	:=	0.14 ;
R1	:=	0.004;
R2	:=	0.014;
ncomp	:=	4;
cin	:=	20.05;
E	:=	0.3 ;
rhogas	:=	2.747;
miu	:=	2.953e-5;
rhobedads	:=	500;
rhobedc	:=	1000;
kmass( )	:=	[215.47,100.97,0,0];
kcon	:=	4.419e-4;
Keq	:=	1.31e-2;
Rmol	:=	8.314;
T	:=	600.0;
mgrad( )	:=	[3.523e-6,7.882e-6,0,0];
Agas	:=	5.027e-5;
Asolid	:=	5.65e-4;
Vsolid	:=	5.938e-5;
Vgas	:=	7.0378e-6;
pi	:=	3.142;

y(1)	:=	0.048;
y(2)	:=	0.001;
y(3)	:=	0.001;
y(4)	:=	0.95;

```
creac(1)      :=      y(1) * cin;
creac(2)      :=      y(2) * cin;
creac(3)      :=      y(3) * cin;
creac(4)      :=      y(4) * cin;

nu(1)         :=       -1;
nu(2)         :=      +1;
nu(3)         :=      +1;
nu(4)         :=       0;
```

EQUATION

At axial boundary , where x = 0 and x = L, equation 1

FOR i:= 1 to ncomp DO

FOR r := 0|+ to R1| DO

c(i,0,r) = creac(i);

partial(c(i,L,r), axial) = 0.0;

END

At radial boundary where r = 0 , r= R1 and r = R2

FOR x := 0| to L| DO

partial(c(i,x,0), radial) = 0.0 ;

END
END

At equation 2,

FOR i := 1 to ncomp DO
FOR x := 0|+ to L|- DO

partial(c(i,x,R2),radial) = 0.0;

END

```
FOR r := R1|+ to R2| DO

partial(c(i,0,r),axial) = 0.0;

partial(c(i,L,r),axial) = 0.0;


END
END
```

```
# Equation 1 = Mass balance of isobutane in the fluid phase

 D( ) = 3.353e-5;


 FOR i := 1 to ncomp DO
 FOR  x := 0|+ to L|- DO
 FOR  r := 0|+ to R1| DO


   $c(i,x,r) = -v(r) * partial(c(i,x,r),axial)   + D(i)*partial(c(i,x,r),axial,axial) +
            D(i)/r * partial((r * partial(c(i,x,r),radial)),radial) ;


 END
 END
 END
 END
```

```
# Mass balance at the catalyst/adsorbent phase, equation 2

 D( ) =   3.353e-5;


 FOR i := 1 to ncomp DO
 FOR x := 0|+ to L|- DO
 FOR r := R1|+ to R2|- DO


 E * $c(i,x,r) =   D(i) * partial (c(i,x,r),axial,axial)
              + D(i)/r * partial ((r * partial(c(i,x,r),radial)),radial)
                       + rhobedc * nu(i) * kcon * (c(1,x,r) - ((c(2,x,r) * c(3,x,r)/ Keq)))
                       - rhobedads * kmass(i) * (qiso(i,x,r) - q(i,x,r)) ;



END
END
```

```
#Rate of Adsorption

 FOR x := 0| to L| DO
 FOR r := R1| to R2| DO

 $q(i,x,r) = kmass(i) * (qiso(i,x,r) - q(i,x,r)) ;



#Simplified Langmuir equation
  qiso(i,x,r) = mgrad(i) * c(i,x,r) * Rmol * T;

END

 FOR r := 0| to R1|- DO

 $q(i,x,r) = 0.0;
 qiso(i,x,r) = 0.0;


END
END
END

# Momentum equation

 # At velocity profile

  FOR r := 0| to R1| DO

  v(r) = 8* vave * (R1^2 - r^2)/ (4 * R1^2);

  END


  FOR r := R1|+ to R2| DO

  v(r) = 0.0;

  END
```

```
# To calculate the conversion for such process, we apply totalflux of velocity and
 # concentration at time, t :

 $totf1 = sigma(c(1,L,0:R1) * v(0:R1)) ;
 $totf2 = sigma(c(2,L,0:R1) * v(0:R1)) ;
 $totf3 = sigma(c(3,L,0:R1) * v(0:R1)) ;
 $nfeed1 = creac(1) * sigma(v(0:R1));


 # Conversion Equation at steady state:

 cgas   = (2/(((R1)^2)*L)) * integral(x := 0|:L|,r := 0|:R1|; r * c(1,x,r));
 csolid = (2/(L*((R2-R1)^2))) * integral(x := 0|:L|,r := R1|:R2|; r* c(1,x,r));
 qmin =  (2/(L*((R2-R1)^2)))* integral( x:= 0|:L|, r := R1|:R2| ; r* q(1,x,r));


# conversion:

 (Agas * nfeed1)*conv =  ((Agas *nfeed1) - (Agas* totf1) - (Vgas * cgas)
       -  (Vsolid * E * csolid)
       - (Vsolid *rhobedads * qmin));

 # yield:

  # 1. Isobutylene yield:

     yield2 = (totf2)/  ( creac(1)* sigma(v(0:R1)) );


  # 2. Hydrogen yield:

     yield3 = (totf3)/ ( creac(1)*sigma(v(0:R1)) );


#process

UNIT  Gen5plat AS   General

SET
 WITHIN Gen5plat DO
   axial  :=   [BFDM,1,50];
   radial :=  [BFDM,1,24];

 END
```

```
INITIAL
 WITHIN  Gen5plat DO

        FOR  x := 0|+ to L|- DO
        FOR  r := 0|+ to R1|- DO


        c(1,x,r) = 0.0;
        c(2,x,r) = 0.0;
        c(3,x,r) = 0.0;
        c(4,x,r) = cin;

        END


        FOR r := R1| to R2|- DO


        c(1,x,r) = 0.0;
        c(2,x,r) = 0.0;
        c(3,x,r) = 0.0;
        c(4,x,r) = cin;

        END
        END


        FOR i := 1 to ncomp DO
        FOR  x := 0| to L| DO
        FOR  r := 0| to R1|- DO

        q(i,x,r) = 0.0;


        END

        FOR r := R1| to R2| DO

        q(i,x,r) = 0.0;

        END
        END
        END
```

```
      nfeed1 = 0.0;
      totf1 = 0.0;
      totf2 = 0.0;
      totf3 = 0.0;



END

SCHEDULE
CONTINUE FOR 1800
```

Appendix F

Example of a Single Step PFR Model

```
PARAMETER

    vave          AS      REAL
    L             AS      REAL
    ncomp         AS      INTEGER
    cin           AS      REAL
    E             AS      REAL
    rhogas        AS      REAL
    miu           AS      REAL
    kmass         AS      ARRAY(ncomp) of REAL
    kcon          AS      REAL
    Keq           AS      REAL
    rhobedads     AS      REAL
    rhobedc       AS      REAL
    creac         AS      ARRAY(ncomp) OF REAL
    Rmol          AS      REAL
    T             AS      REAL
    mgrad         AS      ARRAY(ncomp) OF  REAL
    nu            AS      ARRAY(ncomp) OF INTEGER
    A             AS      REAL
    y             AS      ARRAY(ncomp) OF REAL
    tau           AS      REAL
    Peclet        AS      REAL
    Br            AS      REAL
    dpore          AS     REAL

DISTRIBUTION_DOMAIN
    axial         AS      (0.0 : L)
```

VARIABLE

c	AS	DISTRIBUTION(ncomp,axial) OF concentration
D	AS	DISTRIBUTION(ncomp) OF notype
Da	AS	DISTRIBUTION(ncomp) OF notype
q	AS	DISTRIBUTION(ncomp,axial) OF aveadsorb
qiso	AS	DISTRIBUTION(ncomp,axial) OF equiadsorb
conv	AS	conversion
totf1	AS	totalflux
totf2	AS	totalflux
totf3	AS	totalflux
yield2	AS	notype
yield3	AS	notype
nfeed1	AS	notype

SET

vave	:=	0.067;
L	:=	0.14;
ncomp	:=	4 ;
cin	:=	20.05 ;
E	:=	0.3 ;
rhogas	:=	2.747;
miu	:=	2.953e-5;
rhobedc	:=	1000;
rhobedads	:=	500.0;
kcon	:=	4.419e-4;
kmass( )	:=	[215.47,100.97,0,0];
Keq	:=	1.31e-2;
Rmol	:=	8.314;
T	:=	600.0;
mgrad( )	:=	[3.523e-6,7.882e-6,0,0];
A	:=	5.027e-5;
tau	:=	0.64;
Peclet	:=	0.12;
Br	:=	0.5;
dpore	:=	178e-6;

y(1)	:=	0.048 ;
y(2)	:=	0.001 ;
y(3)	:=	0.001 ;
y(4)	:=	0.95;

creac(1)	:=	y(1) * cin;
creac(2)	:=	y(2) * cin;
creac(3)	:=	y(3) * cin;

```
creac(4)      :=      y(4) * cin;

nu(1)         :=      -1;
nu(2)         :=      +1;
nu(3)         :=      +1;
nu(4)         :=      0;


EQUATION

# At axial boundary , where x = 0 and x = L, equation 1

 FOR i:= 1 to ncomp DO

  c(i,0) = creac(i);

  partial(c(i,L), axial) = 0.0;

  END


# Equation =  component mass balance

  D() = 3.353e-5;

  Da() =( E*D())/tau + (((vave*dpore)^2)/(Peclet*((vave*dpore) + (Br*E*D()/tau))))  ;


FOR i := 1 to ncomp DO
FOR  x := 0|+ to L|- DO


E * $c(i,x) =  -vave * partial(c(i,x),axial) + Da(i) * partial (c(i,x),axial,axial)
               + rhobedc * nu(i) * kcon * (c(1,x) - ((c(2,x) * c(3,x)/ Keq)))
                - rhobedads * kmass(i) * (qiso(i,x) - q(i,x));

 END
 END


#Rate of Adsorption

  FOR i := 1 to ncomp DO
  FOR x := 0| to L| DO

  $q(i,x) = kmass(i) * (qiso(i,x) - q(i,x)) ;

 #Simplified Langmuir equation
```

```
    qiso(i,x) = mgrad(i) * c(i,x) * Rmol * T;

  END
  END
```

```
 # To calculate the conversion for such dynamic process,  we apply totalflux of velocity and
#concentration at time, t :

      $totf1 = sigma(c(1,L) * vave)  ;
      $totf2 = sigma(c(2,L) * vave) ;
      $totf3 = sigma(c(3,L) * vave) ;
      $nfeed1 = creac(1) * vave;

    # Conversion Equation:


    conv = (creac(1)* vave - sigma(c(1,L)*vave))/(creac(1)*vave ) ;
```

```
#process

UNIT  GencatPFR AS   generalpfr

SET
 WITHIN GencatPFR DO
   axial  :=  [BFDM,1,50];

 END


INITIAL
 WITHIN  GencatPFR DO

        FOR  x := 0|+ to L|- DO

        c(1,x) = 0.0;
        c(2,x) = 0.0;
        c(3,x) = 0.0;
        c(4,x) = cin;


END
```

```
FOR i := 1 to ncomp DO
FOR  x := 0| to L| DO

 q(i,x) = 0.0;


 END
 END
```

```
      totf1 = 0.0;
      totf2 = 0.0;
      totf3 = 0.0;
      nfeed1 = 0.0;


END

SCHEDULE

 CONTINUE  FOR  1200
```